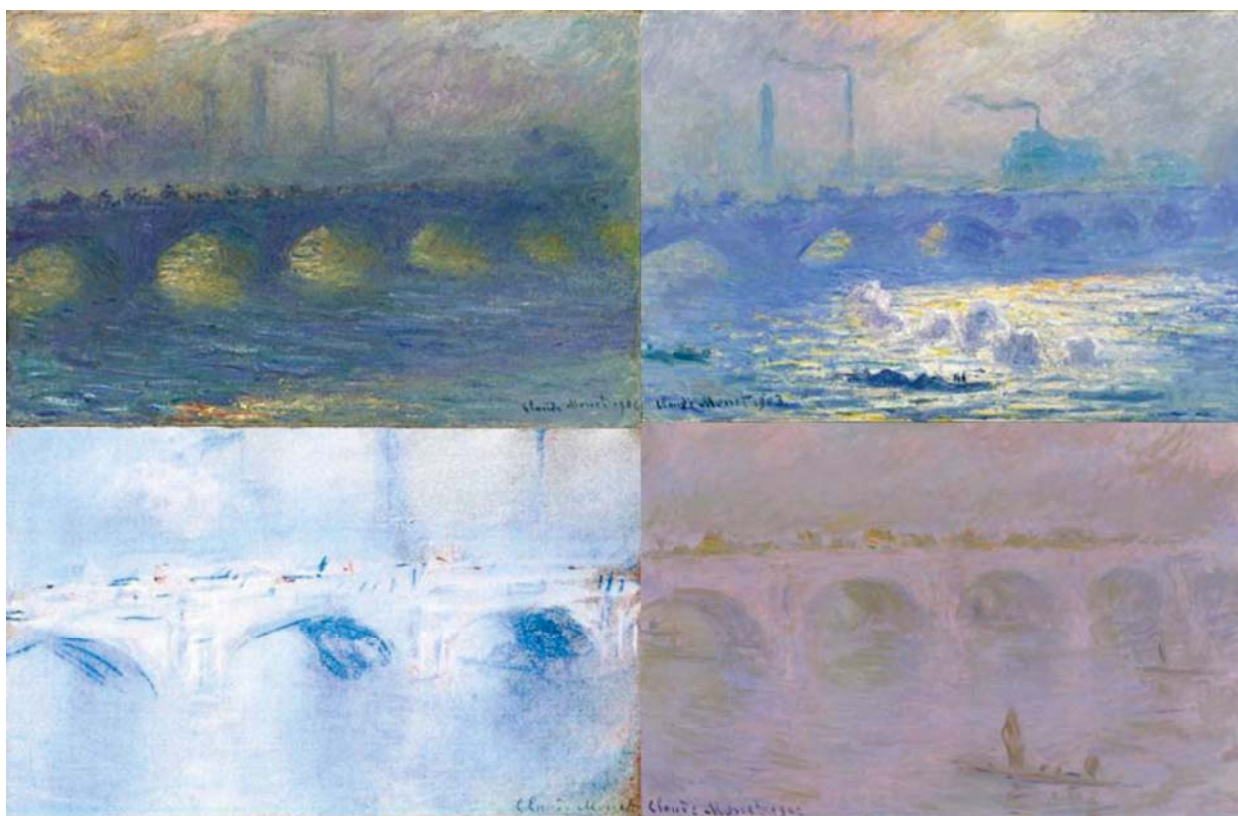




PhD Thesis

Drummond E-Wen McCulloch

Pharmacokinetic and pharmacodynamic evaluation of classical psychedelic substances in the human brain



This thesis has been submitted to the Graduate School of Health and Medical Sciences,
University of Copenhagen on 27th June 2025

Supervisor: Patrick MacDonald Fisher
Co-Supervisor: Gitte Moos Knudsen

Name of department:	Neurobiology Research Unit, Copenhagen University Hospital Rigshospitalet, Denmark
Author:	Drummond E-Wen McCulloch
Title:	Pharmacokinetic and pharmacodynamic evaluation of classical psychedelic substances in the human brain
Institutions:	Faculty of Health and Medical Sciences University of Copenhagen Neurobiology Research Unit, Copenhagen University Hospital Rigshospitalet
Principal supervisor:	Associate Prof. Patrick MacDonald Fisher, Neurobiology Research Unit, Copenhagen University Hospital Rigshospitalet, Denmark
Co-supervisor:	Prof. Gitte Moos Knudsen, Neurobiology Research Unit, Copenhagen University Hospital Rigshospitalet, Denmark
Submitted on:	27th June 2025
Date of defence:	5th September 2025
Assessment committee:	Prof. Anders Fink-Jensen (chair), University of Copenhagen, Denmark Prof. David Nutt, Imperial College London, United Kingdom Prof. Diego Vidaurre Aarhus University, Denmark
Frontpage:	Four paintings from Monet's Waterloo Bridge series (1901-1904)

“I think it’s absurd that we try to examine this phenomenon. That we are scanning my brain to figure out what’s happening. I know that we can’t understand it, that we can’t put an equation on it and figure it out. I feel it is human arrogance, trying to tame all the beauty. I think;
“Scan me then! We won’t get any closer to the truth!” “

– Participant

Preface

The present PhD thesis is based on my work at the Neurobiology Research Unit, Copenhagen University Hospital Rigshospitalet, which commenced on March 17, 2021. My main supervisor is Associate Prof. Patrick MacDonald Fisher, and my co-supervisor is Prof. Gitte Moos Knudsen.

Acknowledgements

I would like to thank my NRU co-firsts, Kristian Larsen and Anders Olsen, for wonderful brainstorming and a serious amount of getting down to it. Thanks to Martin Korsbak for writing the papers that got me into this lab. To the rest of the NRU crew past and present who have made our office such an exciting, engaging, and fun place to work; Annette, Søren, Sophia, Kristoffer, Sara, Kristian, Ruben, Clara, Charlotte, Nakul, Anna, Peter, Maria, Joan, Martin, Pontus, Gjertrud, Vibeke, Brice, and Miriam. Dea, thank you for your constant encouragement and for always being a source of engaging and thoughtful discussions. To the beating heart of the NRU, Arafat, Claus, Peter, Dorte, Lone, Emilie, and Birgit, none of this works without you. Patrick, I am beyond glad we met in New Orleans and shared some PBRs and made this whole thing work. I very literally could not have done any of it without you. I am extremely grateful for the effects of your mentorship on my life, academic and otherwise. Gitte, the opportunities you have provided me with are far beyond what I could have imagined, thank you for your leadership and your support. To the original COMPASS Pathways leadership team, Katya, George and Lars, and Hans for trusting me to do something useful, and to the rest of the COMPASS science team for guiding me through the start of my research journey. To the brave and curious research participants. To my friends Jacob, Philip, Joe, Salman, and Rory back in Scotland, sorry I left, I'm not coming back, thank you for being my friends. To the fellas, Pete and Aaron, for your fellowship. To my parents and Isla, for your boundless and unconditional love and encouragement. To Chainey. To Granny Mabel and Papa Joe, I wish you were still here so I could tell you all about it. To my fiancée and teammate Maja, you're the shining star. To our daughter Idun Mabel and our unborn son, who are now the centre of my connected family universe.

Funding

My PhD salary was supported by an unrestricted grant from COMPASS Pathways PLC, which had no role in designing, analysing, interpreting, or writing the studies.

List of Manuscripts

The thesis is based on the following manuscripts.

1. McCulloch, D.E.-W., Madsen, M.K., Stenbæk, D.S., Kristiansen, S., Ozenne, B., Jensen, P.S., Knudsen, G.M., Fisher, P.M., 2021. **Lasting effects of a single psilocybin dose on resting-state functional connectivity in healthy individuals.** *J. Psychopharmacol. (Oxf.)*
2. McCulloch, D.E.-W., Grzywacz, M.Z., Madsen, M.K., Jensen, P.S., Ozenne, B., Armand, S., Knudsen, G.M., Fisher, P.M., Stenbæk, D.S., 2022. **Psilocybin-Induced Mystical-Type Experiences are Related to Persisting Positive Effects: A Quantitative and Qualitative Report.** *Frontiers in Pharmacology*. 13, 1–17.
3. McCulloch, D.E.-W., Olsen, A.S., Ozenne, B., Stenbæk, D.S., Armand, S., Madsen, M.K., Knudsen, G.M., Fisher, P.M., 2023. **Navigating the chaos of psychedelic neuroimaging: A multi-metric evaluation of acute psilocybin effects on brain entropy.** (*Manuscript submitted to Neuroimage December 2024*)
4. McCulloch, D.E.-W., Larsen, K., Johansen, A., Jensen, K.H.R., Nykjær, C.H., Holze, F., Falck, N., Neufeld, V., Steenstrup, E., Skov-Andersen, P., Spangsgård, A., Geisler, M., Randrup, P.P., Jensen, P.S., Shulganov, V., Johansen, S.S., Nielsen, M.K.K., Andersen, T.L., Stenbæk, D.S., Svarer, C., Fisher, P.M., Knudsen, G.M., 2025. **Molecular, haemodynamic, and functional effects of LSD in the human brain.** (*Manuscript submitted to Nature Neuroscience June 2025*)

Related articles not included in the thesis:

1. McCulloch, D.E.-W., Knudsen, G.M., Barrett, F.S., Doss, M.K., Carhart-Harris, R.L., Rosas, F.E., Deco, G., Kringelbach, M.L., Preller, K.H., Ramaekers, J.G., Mason, N.L., Müller, F., Fisher, P.M., 2022. **Psychedelic resting-state neuroimaging: A review and perspective on balancing replication and novel analyses.** *Neuroscience and Biobehavioural Reviews*.
2. McCulloch, D.E.-W., Liechti, M.E., Kuypers, K.P.C., Nutt, D., Lundberg, J., Stenbæk, D.S., Goodwin, G.M., Gründer, G., Butlen-Ducuing, F., Haberkamp, M., Thirstrup, S., Knudsen, G.M., 2024. **Knowledge gaps in psychedelic medicalisation: Clinical studies and regulatory aspects.** *Neuroscience Applied*
3. McCulloch, D.E.-W., Lopez, J.P., Dalla, C., Castrén, E., Erritzoe, D., Frokjaer, V.G., Lundberg, J., Preller, K.H., Fisher, P., Knudsen, G.M., 2023. **Knowledge gaps in psychedelic medicalisation: Preclinical and neuroimaging mechanisms.** *Neuroscience Applied*.
4. Butlen-Ducuing, F., McCulloch, D.E.-W., Haberkamp, M., Mattila, T., Bałkowiec-Iskra, E., Aislaitner, G., Balabanov, P., Lundberg, J., Stenbæk, D.S., Elferink, A., Knudsen, G.M., Thirstrup, S., 2023. **The therapeutic potential of psychedelics: the European regulatory perspective.** *The Lancet*.

Contents

Preface.....	2
Acknowledgements.....	2
Funding.....	2
List of Manuscripts.....	3
Summary.....	6
Dansk Resumé.....	7
Abbreviations.....	8
Background.....	9
Psychedelics.....	9
Pharmacology and physiological effects of psilocin.....	9
Pharmacology and physiological effects of LSD.....	10
Safety of psychedelics.....	10
Medicalisation of psychedelics.....	11
Magnetic resonance imaging.....	13
Functional MRI.....	13
Previous fMRI work with psychedelics.....	14
The entropic brain hypothesis.....	18
Entropy.....	18
Positron emission tomography imaging.....	18
Simplified Reference Tissue Model.....	19
[¹¹ C]Cimbi-36.....	21
Occupancy estimation.....	21
Previous PET work with psychedelics.....	21
Motivation and aims.....	23
Paper 1.....	23
Paper 2.....	23
Paper 3.....	24
Paper 4.....	24
Study designs.....	25
Paper 1.....	25
Paper 2.....	26
Paper 3.....	27
Paper 4.....	30

Methods.....	31
Psychometrics (Papers 1, 2, 3, and 4).....	31
Plasma psilocin and LSD quantification (Papers 1, 2, 3, and 4).....	31
Structural MRI acquisition (Papers 1, 3, and 4).....	31
Functional MRI acquisition (Papers 1, 3, and 4).....	32
Functional MRI processing and denoising (Papers 1, 3, and 4).....	32
Functional MRI metrics (Papers 1, 3, and 4).....	34
Relation between GCOR and other imaging metrics (Paper 4).....	38
PET acquisition and processing (Papers 1 and 4).....	38
Language analyses (Paper 2).....	38
Mandala drawing (Papers 2 and 4).....	38
Statistical analyses (Papers 1, 2, 3, and 4).....	38
Ethical approvals (Papers 1, 2, 3, and 4).....	39
Results.....	41
Paper 1.....	41
Paper 2.....	43
Paper 3.....	50
Paper 4.....	55
Discussions.....	63
Paper 1.....	63
Paper 2.....	64
Paper 3.....	65
Paper 4.....	67
Conclusions and future research.....	70
References.....	73
Appendix.....	89

Summary

Psychedelic drugs, including LSD and psilocybin, produce a wide range of scientifically intriguing acute and persisting behavioural effects. These include transient mystical, meaningful, and ineffable experiences as well as lasting reductions in symptom severity across a range of psychiatric disorders or increases in wellbeing in healthy individuals. The present PhD thesis seeks to develop our understanding of the neurological underpinnings of these acute and lasting effects using functional magnetic resonance imaging (fMRI) and Positron Emission Tomography (PET), and by evaluating the relation between the acute mystical-type effects and persisting effects in healthy people.

Paper 1 evaluated the persisting effects of a single dose of psilocybin on fMRI-derived brain-network connectivity in healthy individuals. Paper 2 evaluated the relation between psilocybin induced mystical-type experiences, measured using the Mystical Experiences Questionnaire (MEQ), and persisting positive effects in healthy people and provided a qualitative description of these mystical-type experiences. Paper 3 built on previous hypothesis-generating research that suggested psychedelics increase fMRI-measured brain-entropy, testing these hypotheses in an independent and larger cohort and presenting a toolbox resource for future researchers. Paper 4 evaluated the relation between plasma LSD levels, acute subjective effects, functional brain effects using fMRI, and occupancy at the serotonin 2A receptor (5-HT_{2A}R) using [¹¹C]Cimbi-36 PET.

Paper 1 showed a network-wide decrease in functional connectivity in the executive control network, which was associated with increases in self-reported mindful-attention and awareness, highlighting a potential neural mechanism through which psilocybin may have its persisting behavioural effects. Paper 2 found that the subscales *mystical* and *positive mood* of the MEQ were significantly related to persisting positive effects, but that the subscales *ineffability* and *transcendence of time and space* were not. Natural-language processing revealed themes exclusive to mystical-type experiences, such as feelings of unity with the universe, familial love, and profound aesthetic experiences. Paper 3 identified that previously reported measures of fMRI brain entropy were distinct and uncorrelated. Despite this, three of the thirteen metrics evaluated were significantly correlated with acute psychedelic effects and are thus candidate biomarkers for acute neural effects of psychedelics. These included increases in the distribution of connectivity paths across the brain, the distribution of connectivity strengths over time, and the unpredictability of the signal across several brain areas. Paper 4 showed a close relation between plasma LSD levels and occupancy at the 5-HT_{2A}R, which can inform future dosing strategies. fMRI analyses showed decreases in the global connectivity of the cortex, which was correlated with 5-HT_{2A}R occupancy.

In conclusion, the present work constitutes a wide knowledge base describing the acute and lasting effects of psychedelics both behaviourally and neurologically. These findings can be used to design future studies, highlighting candidate biomarkers that can be used to develop our understanding of altered states of consciousness. These data show that measuring psychedelic effects using plasma drug level measurements and behavioural questionnaires in combination with fMRI and PET imaging can assist in our understanding of the brain and the eventual development of future therapeutics.

Dansk Resumé

Psykedeliske stoffer, herunder LSD og psilocybin, inducerer et bredt spektrum af videnskabeligt interessante akutte og vedvarende adfærdsmæssige effekter. Disse omfatter forbigående mystiske, meningsfulde og ubeskrivelige oplevelser samt varige reduktioner i symptomsværhedsgrad på tværs af en række psykiatriske lidelser eller stigninger i velbefindende hos raske individer. Denne ph.d.-afhandling søger at udvikle vores forståelse af de neurologiske grundlag for disse akutte og varige effekter ved hjælp af funktionel magnetisk resonans billeddannelse (fMRI) og Positron Emissions Tomografi (PET), samt ved at evaluere forholdet mellem de akutte mystiske effekter og vedvarende effekter hos raske individer.

Artikel 1 evaluerede de vedvarende effekter af en enkelt dosis psilocybin på fMRI-afledt hjernenetværkskonnektivitet hos raske individer. Artikel 2 evaluerede forholdet mellem psilocybin-inducerede mystiske oplevelser, målt ved hjælp af Mystical Experiences Questionnaire (MEQ), og vedvarende positive effekter hos raske individer og gav en kvalitativ beskrivelse af disse mystiske oplevelser. Artikel 3 byggede på tidligere hypotesegenererende forskning, der antydede, at psykedelika øger fMRI-målt hjerneentropi, og testede disse hypoteser i en uafhængig og større kohorte og præsenterede en toolbox ressource til fremtidige forskere. Artikel 4 evaluerede forholdet mellem plasma koncentrationer af LSD, akutte subjektive effekter, funktionelle hjerneeffekter ved hjælp af fMRI og okkupans af serotonin 2A-receptoren (5-HT2AR) ved hjælp af [¹¹C]Cimbi-36 PET.

Artikel 1 viste et netværksomfattende fald i funktionel konnektivitet i det eksekutive kontrolnetværk, hvilket var associeret med stigninger i selvrapporteret bevidst nærvær og opmærksomhed, hvilket fremhæver en potentiel neural mekanisme, hvorigennem psilocybin kan have sine vedvarende adfærdsmæssige effekter. Artikel 2 fandt, at underskalaerne *mystical* og *positive mood* i MEQ var signifikant relateret til vedvarende positive effekter, men at underskalaerne *ineffability* og *transcendence of time and space* ikke var det. Sprogteknologi afslørede temaer, der var eksklusive for mystiske oplevelser, såsom følelser af enhed med universet, familiær kærlighed og dybe æstetiske oplevelser. Artikel 3 identificerede, at tidligere rapporterede mål for fMRI-hjerneentropi var forskellige og ukorrelerede. På trods af dette var tre af de tretten evaluerede målinger signifikant korreleret med akutte psykedeliske effekter og er således kandidatbiomarkører for akutte neurale effekter af psykedelika. Disse omfattede stigninger i fordelingen af konnektivitsveje på tværs af hjernen, fordelingen af konnektivitsstyrker over tid og signalets uforudsigelighed på tværs af flere hjerneområder. Artikel 4 viste et tæt forhold mellem plasma koncentrationer af LSD og okkupans af 5-HT2AR, hvilket kan danne grundlag for fremtidige doseringsstrategier. fMRI-analyser viste et fald i den globale konnektivitet af hjernebarken, hvilket var korreleret med okkupans af 5-HT2AR.

Afslutningsvis udgør dette arbejde et bredt vidensgrundlag, der beskriver de akutte og varige effekter af psykedelika både adfærdsmæssigt og neurologisk. Disse fund kan bruges til at designe fremtidige studier og fremhæver kandidatbiomarkører, der kan bruges til at udvikle vores forståelse af ændrede bevidsthedstilstande. Disse data viser, at måling af psykedeliske effekter ved hjælp af plasma koncentrationer og adfærdsmæssige spørgeskemaer i kombination med fMRI- og PET-billeddannelse kan hjælpe vores forståelse af hjernen samt den eventuelle udvikling af fremtidige terapeutiske midler.

Abbreviations

5-HT - 5-hydroxytryptamine (serotonin)
5-HT2AR - Serotonin 2A receptor
BOLD - Blood Oxygen Level Dependent
BP_{ND} - Non-displaceable binding potential
CBF - Cerebral blood flow
CM - Connectivity matrix
CME - Complete Mystical Experience
CopBET - Copenhagen Brain Entropy Toolbox
DCC - Dynamic Conditional Correlation
DMN - Default Mode Network
ECN - Executive Control Network
ED₅₀ - Effective dose producing 50% effect
EEG - Electroencephalography
FDG - Fluorodeoxyglucose
fMRI - Functional magnetic resonance imaging
GCOR - Global Correlation
IC₅₀ - Inhibitory concentration producing 50% effect
LSD - Lysergic acid diethylamide
LVM - Latent variable model
LZc - Lempel-Ziv complexity
MAAS - Mindful Attention and Awareness Scale
MDMA - 3,4-methylenedioxymethamphetamine
MEG - Magnetoencephalography
MEQ - Mystical Experience Questionnaire

MTE - Mystical-type experience
N,N-DMT - N, N-dimethyltryptamine
NSC - Normalised Spatial Complexity
NVC - Neurovascular coupling
Occ_{2A} - Estimated 5-HT2A receptor occupancy
Occ_{max} - Maximum occupancy
PEQ - Persisting Effects Questionnaire
PET - Positron Emission Tomography
PLD - Path-length distribution
PLL - Plasma LSD level
PPL - Plasma psilocin level
PPE_{LV} - Persisting Positive Effects Latent Variable
PsiFx - Collective term for PPL, SDI, and Occ2A
ROI - Region of interest
SDI - Subjective drug intensity
SERT - Serotonin transporter
SNR - Signal-to-noise ratio
SRTM - Simplified Reference Tissue Model
SSRI - Selective serotonin reuptake inhibitor
TAC - Time-activity curve
TCOR - Thalamic Correlation
tf-idf - Term frequency-inverse document frequency
WNC - Within-network connectivity

Background

Psychedelics

Psychedelic drugs are a family of naturally occurring and synthetic compounds. These include lysergic acid diethylamide (LSD), first synthesised from ergot fungus alkaloids by Albert Hoffman in Switzerland in 1938 (Hofmann, 1992); psilocin, the active metabolite of psilocybin, which is naturally occurring in many fungal species (most notably but not exclusively from the *psilocybe* genus (Gotvaldová et al., 2022)); mescaline, which naturally occurs in hundreds of species of cactus, most notably the peyote (*Lophophora williamsii*) and san pedro (*Echinopsis pachanoi*) cacti (Shulgin and Shulgin, 1991); and dimethyltryptamine (N, N-dimethyltryptamine), which is widely found in the plant kingdom, most notably in the leaves of *Psychotria viridis*, which is used in the preparation of ayahuasca (Shulgin and Shulgin, 1997).

Psychedelics are typically defined in terms of their behavioural effects. The set of these has been proposed to include, among others, alterations in sensory perception (e.g., open- and closed-eye simple and complex visual effects, auditory and synesthetic effects), affect (e.g., both positive, negative and susceptibility to perturbation), a range of cognitive domains (e.g., theory of mind, metacognitive capacity, long-term memory recall) and the nebulous concept of “consciousness expansion/increase” (Preller and Vollenweider, 2018; Studerus et al., 2010). Despite many psychedelics also being referred to as “hallucinogens,” true hallucinations (i.e., sensory appearances indistinguishable from reality) are rarely reported following ingestion of psychedelics (Sacks, 2012). Certain drugs from other pharmacological classes, including the NMDA receptor antagonist phencyclidine and the muscarinic agonist scopolamine, do produce true hallucinations (Bey and Patel, 2007; Warburton et al., 1985). The term “hallucinogen” is used throughout this thesis only when referencing previous work using this term to refer to psychedelics, e.g., Hallucinogen Perception Persisting Disorder. There is hitherto no consensus on the precise set of behavioural effects considered both necessary and sufficient for a compound to be considered “psychedelic.”

Another way psychedelics may be defined is that they are centrally-acting partial agonists at the serotonin (5-HT) subtype 2A receptor (5-HT_{2A}R). Most, if not all, the subjective effects of LSD and psilocybin are blocked by administration of 5-HT_{2A}R antagonists (Becker et al., 2023; Holze et al., 2022b; Preller et al., 2017). The potency of compounds to produce these effects is closely related to their affinity at this receptor (Glennon et al., 1984; Halberstadt et al., 2017; Wallach et al., 2023), occupancy of psilocin at the 5-HT_{2A}R is related to intensity of subjective effects (Madsen et al., 2019), and compounds selective for the 5-HT_{2A}R have been reported to produce psychedelic behavioural effects (Bersani et al., 2014; Rickli et al., 2015; Shulgin and Shulgin, 1991). The categorisation of a drug as a psychedelic is not informed by the effect on functional brain activity as measured using in vivo clinical neuroimaging. As future work reveals specific neural signatures of psychedelic drug effects and the next wave of derivative compounds become available for clinical use, such effects will become relevant, e.g., as it becomes important for regulators and political bodies to classify whether drugs are psychedelics or not.

Pharmacology and physiological effects of psilocin

As well as binding to 5-HT_{2A}R, psilocin is a partial agonist at several other serotonergic receptors, including subtypes 1A, 1D, 2C, and 7. Psilocin may also inhibit the serotonin transporter SERT at higher concentrations (Halberstadt and Geyer, 2011; Rickli et al., 2016). Following oral administration, psilocybin is rapidly dephosphorylated to psilocin by alkaline phosphatase enzymes (Horita and Weber, 1961); plasma psilocin levels (PPL) peak after approximately 2.5 hours and are metabolised with a half-life of

approximately 2.5 hours (Holze et al., 2022b). Psilocin is primarily metabolised by monoamine oxidase A to 4-HIA and subsequently to 4-HIAA and 4-HTP, neither of which are active at 5-HT receptors (Thomann et al., 2024). It is also metabolised to its glucuronide by UDP-glucuronosyltransferase 1A10 (Manevski et al., 2010). Psilocin may also be metabolised by the enzyme CYP2D6, but to a much lesser degree than the aforementioned metabolic pathways (Thomann et al., 2024). Psilocin produces dose-dependent psychedelic behavioural effects as detailed above; roughly, a low dose is around 5-10 mg, and a high dose is around 30-40 mg (Liechti and Holze, 2022). At a moderate dose, subjective effects typically onset in 1 hour, peak around 2 hours, and dissipate after 5-6 hours.

Pharmacology and physiological effects of LSD

LSD is more pharmacologically promiscuous than psilocin, binding to most serotonin receptors with nanomolar affinity, as well as alpha-2 adrenergic receptors and dopamine D2, D3, and D4 receptors (Marona-Lewicka and Nichols, 1995; Nichols et al., 2002); though, unlike psilocin, it does not appear to inhibit monoamine transporters. Following oral administration, plasma LSD levels peak after 1.5 hours. Curiously, subjective effects peak around an hour later, indicating either slow brain penetrance, slow kinetics at the 5-HT_{2A}R, or slow second-messenger signalling (Holze et al., 2021). The plasma half-life is approximately 4 hours, and LSD is metabolised via a wide range of metabolic pathways, but primarily it is metabolised to nor-LSD, which has a receptor binding profile similar to LSD, and O-H-LSD, and by several cytochrome P450 enzymes (Luethi et al., 2019). Individuals who are genetically classified as poor CYP2D6 metabolisers tend to metabolise LSD more slowly (Vizeli et al., 2021), and inhibition of CYP2D6 also increases the half-life of LSD (Straumann et al., 2023). A low dose of LSD is around 20 µg, and a high dose is around 200 µg (Liechti and Holze, 2022).

Safety of psychedelics

Physiological effects of psilocybin include dose-dependent mild increases in heart rate (8 bpm @ 30 mg p.o.) and body temperature (0.8 °C), and moderate increases in blood pressure (15/11 mmHg systolic/diastolic) and mydriasis (0.8mm) (Holze et al., 2022b). LSD has similar physiological effects, including dose-dependent moderate increases in heart rate (16 bpm @ 200 µg p.o.) and body temperature (0.4 °C), and mild increases in blood pressure (10/5 mmHg systolic/diastolic) and mydriasis (0.9mm) (ibid.). Although case reports of hospitalisation due to overdoses of LSD and psilocybin are rare (Nichols and Grob, 2018), overdoses of a class of highly 5-HT_{2A}R selective psychedelics known as NBOMes (N-benzylmethoxy derivatives of mescaline (Halberstadt, 2017)) have been reported to have caused significant adverse effects resulting in death, seizures and severe prolonged agitation (Suzuki et al., 2015). The mechanism through which NBOMes produce their toxic effects is unresolved, but may include rhabdomyolysis secondary to vasoconstriction and hyperthermia (Halberstadt, 2017).

Hallucinogen use disorder is defined by the Diagnostic and Statistical Manual of Mental Disorders V (DSM-V) according to several criteria including “Craving or a strong desire or urge to use the hallucinogen” and “Recurrent hallucinogen use resulting in a failure to fulfil major role obligations at work, school or home” (*Diagnostic and statistical manual of mental disorders*, 2013). Use of LSD or psilocybin is rarely associated with the development of this disorder (Shalit et al., 2019). Psilocybin has been determined to have a low, but not zero, abuse potential according to the eight factors of the Controlled Substances Act (Johnson et al., 2018). Expert panels from the UK, Australia, and the EU have also ranked LSD and psilocybin among the least dangerous drugs using a multi-criterion decision analysis (Bonomo et al., 2019; Nutt et al., 2010; van Amsterdam et al., 2015).

Despite their general low risk for abuse, dependency, or acute toxicity, psychedelics can produce acute and lasting adverse effects. The most common adverse effects are known colloquially as “bad trips”; this refers to acute drug effects characterised by fear, confusion, paranoia, or dysphoria. In one trial in healthy volunteers, 7 out of 18 reported extreme fear, fear of insanity, or feeling trapped at some point during their experience (Griffiths et al., 2011). In a survey study, 39% reported that their most challenging psychedelic experience was among the top 5 most challenging experiences of their lifetime (Carbonaro et al., 2016). Although anxiety does occur at some point during the psychedelic effects in 20-30% of participants, it rarely lasts for the entire experience (Holze et al., 2021). The same participants often also report extremely positive effects during the course of the drug effects. Although some early trials indicated that “difficult” experiences were associated with positive lasting outcomes (Carbonaro et al., 2016; Griffiths et al., 2006), more recent work suggests that positively valenced acute drug effects are positively related to reductions in clinical symptoms (Goodwin et al., 2025; Roseman et al., 2018; von Rotz et al., 2023).

Hallucinogen Perception Persisting Disorder (HPPD) is a mental disorder defined by the DSM-V according to three criteria: The persistence of visual effects that were experienced during the acute effects of psychedelics, after the other acute effects have ended; that those visual effects are distressing or limit normal function; and that are not attributable to another medical condition (*Diagnostic and statistical manual of mental disorders*, 2013). An online study of psychedelic users found that 60% of respondents experienced psychedelic-like visual effects in the absence of acute drug intake, an effect that was associated with lifetime LSD use. Additionally, 4.2% of respondents experienced persisting visual effects following psychedelic use that they found distressing (Baggot et al., 2011). Another more recent online prospective survey study found that over 30% of psychedelic uses were associated with visual effects persisting up to 4 weeks after use, but less than 1% of the sample found them distressing (Zhou et al., 2025). Therefore, persisting visual effects following psychedelic use are relatively common, but rarely distressing enough to warrant medical attention.

Although extremely rare relative to the number of psychedelic administrations that occur in recreational and clinical settings, there have been several case reports of prolonged psychoses following psychedelic administration (Cohen, 1960; dos Santos et al., 2017; McGlothlin and Arnold, 1971). In the aforementioned survey of challenging experiences, 3 out of 1993 respondents experienced lasting psychotic symptoms. In most cases, the patient was directly related to someone with a psychotic disorder, and as such, this is a recommended exclusion criterion in modern clinical research (Johnson et al., 2008). No prolonged psychosis reactions have been reported in the modern age of clinical research (Johnson et al., 2008; Schlag et al., 2022). Hospital admissions attributed to psychedelic use are relatively rare, especially compared to alcohol or cannabis. One study of emergency department visits in California in the year 2022 reported 3467 hallucinogen-associated emergency department visits and 3965 hospitalisations (Garel et al., 2024). For comparison, in the same year, there were 267,729 alcohol-associated emergency department visits and 227,165 hospitalisations. The criteria “hallucinogen-associated” included hospitalisations for MDMA, phencyclidine (PCP), and ketamine-related issues as well, and thus, the actual number of admissions related to psychedelics as defined above must be substantially lower.

Medicalisation of psychedelics

Following the discovery of its subjective effects, LSD was first considered a “psychotomimetic” (i.e., mimicking psychosis) and distributed under the brand name ‘Delysid’ to psychiatrists to “gain insights into the world of mental patients” (Hofmann, 2022). LSD was also attempted to be weaponized in government projects such as MK-Ultra in the USA (“Project MKULTRA, the CIA’s Program of Research in Behavioral

Modification,” 1977), Project Coast in South Africa (Truth and Reconciliation Commission of South Africa, 1998) and Project Moneybags in the UK (“LSD Experiments,” 1995). Simultaneously, work began investigating the potential for using LSD in combination with psychotherapy for the treatment of psychiatric disorders such as alcohol addiction and anxiety in palliative care (Krebs and Johansen, 2012; Liechti, 2017), and over 1000 research articles were published in this period (Nutt et al., 2013). Following widespread public use of LSD, it was made illegal in the early 1970s, forcing research into the therapeutic potential to stop worldwide, although limited clinical work continued in Switzerland through their ‘restricted medical program’ from the 1970s until today (Oehen and Gasser, 2022).

In the 21st century, psychedelics have re-emerged as novel treatments for several psychiatric and headache conditions. To date, phase 2a trials have been conducted in a wide range of disorders including psilocybin for nicotine addiction (Johnson et al., 2017), alcohol use disorder (Bogenschutz et al., 2022), AIDS associated demoralisation (Anderson et al., 2020), major depressive disorder (Carhart-Harris et al., 2016; Davis et al., 2020; Sloshower et al., 2023; von Rotz et al., 2023), cluster headache (Madsen et al., 2022; Schindler et al., 2022), body dysmorphic disorder (Schneier et al., 2023), obsessive compulsive disorder (Moreno et al., 2006), depression associated with cancer (Agrawal et al., 2024), and anxiety associated with end of life (Griffiths et al., 2016). There has also been a phase 1 trial of psilocybin in anorexia nervosa patients, indicating safety and potential efficacy (Peck et al., 2023) and a pilot study in Parkinson’s Disease patients showing improvements in both motor and non-motor symptoms (Bradley et al., 2025). LSD has shown safety and efficacy in the treatment of anxiety disorders (Gasser et al., 2015; Holze et al., 2022a) and major depressive disorder (Müller et al., 2025). Dimethyltryptamine has shown efficacy in the treatment of depression (Falchi-Carvalho et al., 2025), and a phase 1/2 trial of inhaled 5-Methoxy-DMT has shown efficacy in reducing depressive symptoms in treatment-resistant depression (Reckweg et al., 2023). Each of these trials has shown significant efficacy in the treatment of its respective disorder. There has been one trial showing that low doses of LSD were not effective for the treatment of ADHD (Mueller et al., 2025). Three phase 2b trials have been conducted evaluating psilocybin as a treatment for treatment-resistant and major depressive disorders (Carhart-Harris et al., 2021; Goodwin et al., 2022; Raison et al., 2023), each showing significant antidepressant effects.

Although psychedelics target the serotonin system in common with current first-line treatments such as fluoxetine and escitalopram, if approved, they will represent a significant paradigm shift in psychiatry, as they target a novel mechanism as 5-HT_{2A}R agonists. They produce acute effects that are currently deemed to require psychological preparation before, support during the session, and integration sessions afterwards (Johnson et al., 2008); though the effect of each of these on the safety and efficacy of treatment has not been tested in comparative trials (McCulloch et al., 2024). Most importantly, psychedelics are characterised by their ability to produce rapid therapeutic benefits following relatively brief acute effects, with these beneficial changes persisting long after the drug has been fully cleared from the system—a fundamentally different temporal profile from conventional antidepressants, which can require weeks of continuous administration to achieve lasting effects (Cipriani et al., 2018). There is also evidence that although psychedelics are at least as effective as SSRIs at reducing depressive symptoms, they may be superior for improving other patient outcomes such as self-reported quality of life and wellbeing (Carhart-Harris et al., 2021).

Pivotal phase 3 trials of psychedelics for the treatment of major depressive disorder and generalised anxiety disorder are underway. Despite the lack of formal approval from regulatory agencies, psychedelics are available to be used as medications in at least three countries. Medical professionals in Switzerland can apply

for an “exception authorisation for limited medical use of MDMA, LSD and psilocybin”; 450 such licenses were issued in 2024 (Elçi, 2025). Health Canada has begun to allow select practitioners to apply for licenses to administer psychedelics with life-threatening conditions (Schlag et al., 2022), and the Australian Therapeutic Goods Administration has approved the use of psilocybin for the treatment of treatment-resistant depression (Nutt et al., 2024).

Magnetic resonance imaging

Magnetic resonance imaging (MRI) leverages the magnetic properties of atoms to non-invasively produce structural and functional images. The MRI scanner includes a large magnet which produces a strong, uniform B₀ field, this is commonly 1.5 or 3 Tesla in strength. This field causes the net magnetisation direction of the protons in the object placed in the scanner to go from being uniformly distributed to becoming aligned. The precession frequency of the magnetic moment of the proton is known as the Larmor frequency and can be expressed as the gyromagnetic ratio multiplied by the magnetic field strength experienced by that particle. It is possible to selectively perturb this net magnetisation by applying a radio-frequency (RF) pulse that matches the Larmor frequency. Thus, to image a single “slice”, a magnetic field gradient is applied on top of the B₀ field. The protons of that slice can then be selectively perturbed as they have a different Larmor frequency from the surrounding protons. The thickness of the slice can be determined by the bandwidth of the RF pulse. Once perturbed, the protons begin to relax to their previous configuration in two different ways. The T₁ relaxation is the relaxation of the net magnetisation of the protons back to alignment with the B₀ field. The T₂ relaxation is the desynchronisation of the precessions of protons, after they have become synchronised by the RF pulse. The observed T₂ relaxation is known as the T₂* relaxation and includes both dephasing from spin-spin interactions and additional dephasing from local magnetic field inhomogeneities, resulting in faster signal decay. Next, a phase-encoding gradient is applied, causing protons along the gradient to precess at different frequencies while the gradient is applied. This is then switched off, and a readout or frequency encoding gradient is applied. The receiver coil can then detect the precessions of protons, with the specific frequencies providing spatial information (McRobbie et al., 2006).

Functional MRI

Neural activity requires a supply of oxygen from blood to support the energetic demands of neurotransmission. When a region of the brain is metabolically active, blood flow overshoots in the region, increasing the ratio of oxyhaemoglobin to deoxyhaemoglobin (Drew, 2022). Deoxyhaemoglobin is paramagnetic, meaning that it has small magnetic fields induced in it by the B₀ field, which cause magnetic field inhomogeneities. These inhomogeneities cause the T₂* dephasing to happen faster. Oxyhaemoglobin, by contrast, is diamagnetic, and so the local magnetic field in the area is more homogenous and the T₂* dephasing happens relatively slower (Ogawa et al., 1990). Thus, neural activity, by increasing the ratio of oxyhaemoglobin, causes the T₂* to decay more slowly, causing an increase in the signal in regions, and this is known as the Blood Oxygen Level Dependent (BOLD) signal (Ogawa et al., 1990). Utilising a rapid imaging sequence known as Echo Planar Imaging (EPI), it is possible to acquire whole-brain images with a temporal resolution of 500 to 2000 milliseconds and spatial resolution of 1.5 to 3mm isotropic voxels. Scans are typically 5 to 20 minutes in length, meaning that the resultant data are a 4D matrix of several hundred 3D images of the brain with intensity values at each voxel. This is known now as BOLD functional MRI (fMRI).

Historically, fMRI research was primarily concerned with mapping which areas of the brain responded (i.e., had an increase in BOLD signal) during specific tasks presented in a block design where the participant would be repeatedly exposed to a stimulus e.g., a picture of an angry face, interspersed with a control

condition e.g., a fixation cross or a neutral face. This allowed researchers to conclude, e.g., that the amygdala was involved in the perception of emotion (Hariri et al., 2002). In 1995, Biswal and colleagues began to evaluate instead the correlation between the BOLD signals in distinct regions, a phenomenon now known as functional connectivity (Biswal et al., 1995). Subsequent work then revealed that even in the absence of tasks, the BOLD signal is highly correlated across certain groups of anatomically distinct regions, which have become known as functional brain networks, including the Default-Mode (Raichle et al., 2001) and Fronto-Parietal Networks (Fox et al., 2005), among others. Our understanding of the network structure of the brain has gradually expanded, and modern analyses now use population-level atlases of brain networks to evaluate drug and population effects (Raichle, 2015; Shen et al., 2013; Yeo et al., 2011).

Previous fMRI work with psychedelics

In 2022, we published a review and consensus paper with almost all labs performing fMRI research in the context of psychedelic administration, either evaluating acute or persisting effects on functional brain activity using fMRI in the absence of an explicit task. We identified 42 published studies between 2012 and 2021 and presented a summary of their methodologies as well as proposing consensus guidelines for alignment in future research (McCulloch et al., 2022). A more recent update in July 2024 using the same search methodology has identified that 81 papers analysing data from 25 datasets have been published evaluating acute and persisting effects of psychedelics using fMRI (Figure 1). Fifteen of the datasets and 67 of the published studies evaluated acute effects, and 11 of the datasets and 14 studies evaluated persisting effects (**Fig. 1**). One study evaluated both acute and persistent effects.

Six major groups of analysis strategies have been applied: seed-to-voxel connectivity (how a specific brain region connects to the rest of the brain), whole-brain connectivity (the structure of the entire functional connectome), network-based static connectivity (the structure of communities of functional connectivity), dynamic connectivity (how connectivity changes over time), effective connectivity (the structure of directed connectivity), amplitude (the power of fluctuations in the BOLD signal) and "entropy" based (see **Fig. 2** for more detail). Additionally, some categories of analysis strategy have only been sparsely utilised, which are collected in Figure 2 as "Exploratory Methods". Despite this large corpus of data and thematic alignment in analysis strategy, almost all specific methodologies have only been applied to a single dataset. This lack of independent replication limits our ability to make definitive claims about the effects of psychedelics on functional brain activity. Despite this, some broad hypotheses have gained popularity as explanatory models of psychedelic brain action (Doss et al., 2021). These include alterations in thalamo-cortical connectivity (Delli Pizzi et al., 2023), relaxation of the network structure of the brain (Madsen et al., 2021), changes in global connectivity (Preller et al., 2020, 2018), and increases in information-entropy (Carhart-Harris et al., 2014). At the time of writing, these hypotheses can be considered to be in "phase 1", to borrow nomenclature from clinical drug development. They are promising and insightful, but as yet without evaluation of their specificity for psychedelic effects, and have not been replicated in large, hypothesis-driven studies.

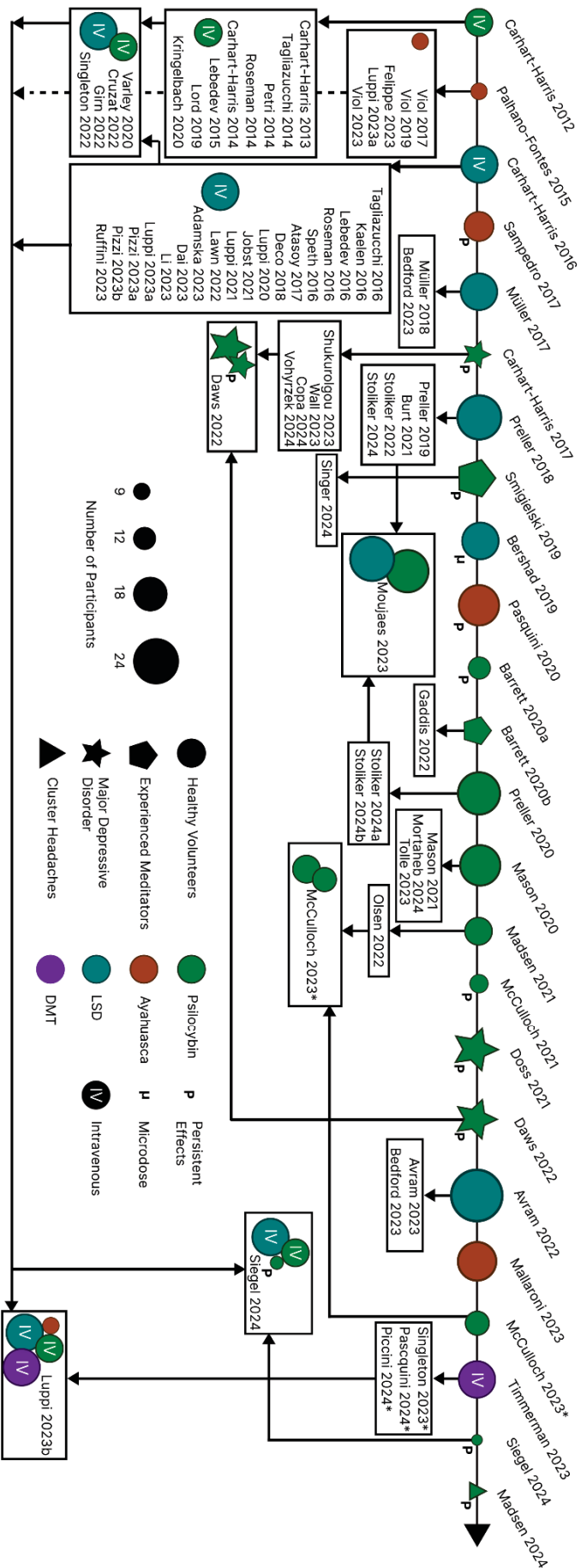


Figure 1 | Graphical timeline detailing all resting-state functional MRI studies in the context of psychedelics. Each coloured shape on the timeline represents a dataset, ordered chronologically from left to right. The size of the shape is proportional to the sample size, the colour illustrates the drug used, and the shape indicates the cohort evaluated. The name and year on top of each shape refers to the first publication in which the dataset was described, and labels below refer to subsequent reanalyses of that data. In some cases, analyses pooled data across multiple datasets, and these are shown in boxes linked with arrows to the datasets. Subscript ‘p’ denotes those datasets evaluating persisting effects (NB. Siegel 2024 evaluates both acute and persisting effects). Subscript ‘μ’ denotes those datasets evaluating ‘microdoses’ of psychedelics, i.e., producing no or only mild subjective effects. All other studies evaluated moderate or greater doses. Asterix beside names denotes articles that are only available on preprint servers. Uppercase ‘IV’ within an icon denotes that the psychedelic was administered intravenously; otherwise, they are administered orally.

Analysis Methods

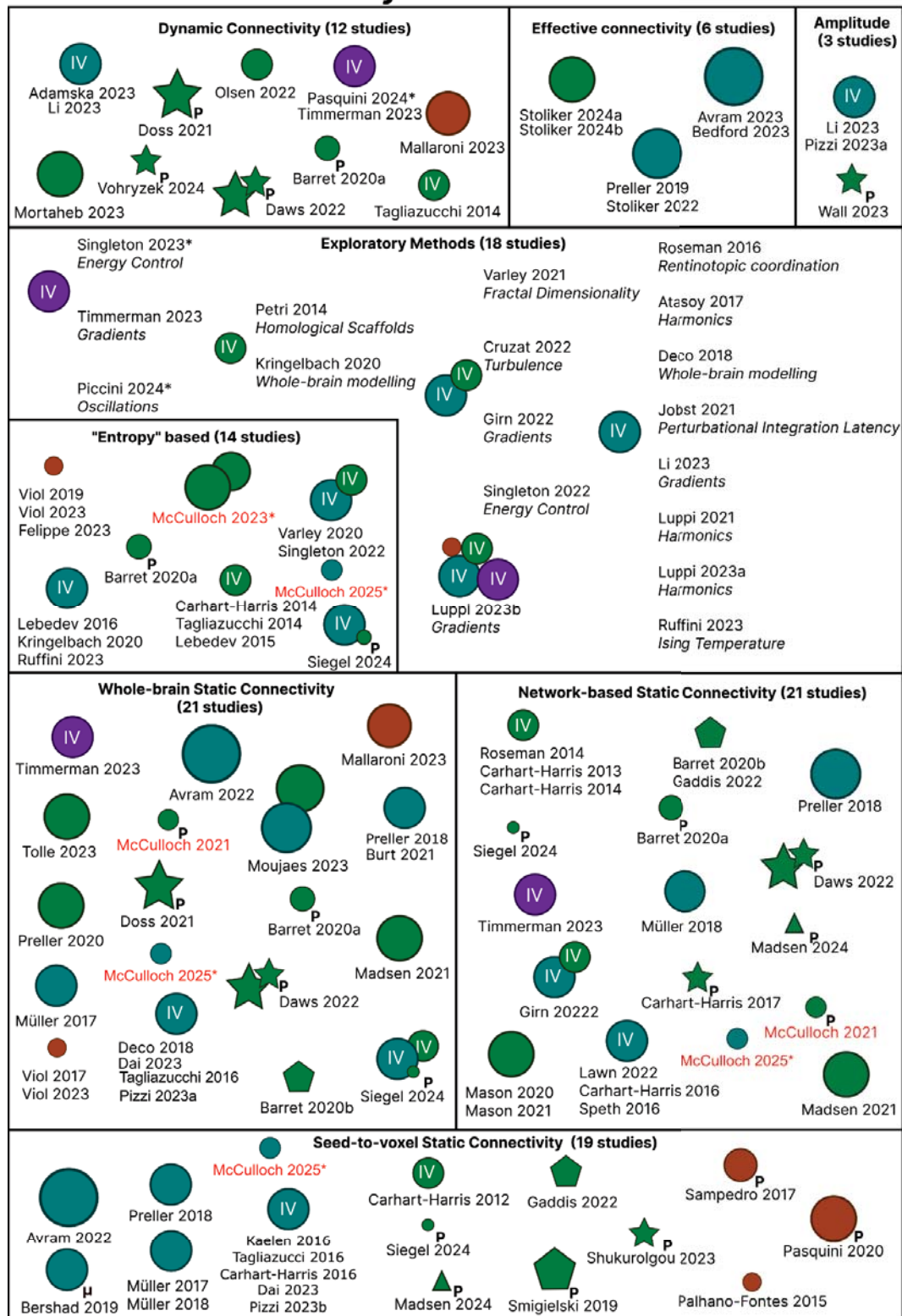


Figure 2 | Methodological overview of resting-state fMRI studies in the context of psychedelics. Symbols represent unique datasets as described in Figure 1 above. Names underneath studies represent analyses or re-analyses of that dataset according to the methodological category described in each box. Papers discussed in this thesis are denoted by red text.

The entropic brain hypothesis

The entropic brain hypothesis was first described by Robin Carhart-Harris and colleagues in 2014 (Carhart-Harris et al., 2014). They propose that “the ‘qualia’ or subjective quality of any given conscious state, and specifically the ‘richness’ of its content, can be indexed by a quantitative measure of the magnitude of entropy (in the information theoretic sense) in a given parameter of spontaneous brain activity” (Carhart-Harris, 2018). Furthermore, they postulate that psychedelics induce a so-called “primary state” which is characterised by increased brain entropy, among other things. In the aforementioned review of psychedelic effects on functional brain activity, we observed that 12 publications had quantified brain entropy, with eight reporting some increase in the psychedelic state, two reporting no change, and two not directly reporting an effect on entropy (Barrett et al., 2020; Carhart-Harris et al., 2014; Felipe et al., 2021; Kringelbach et al., 2020; Lebedev et al., 2016, 2015; Luppi et al., 2021; Singleton et al., 2022; Tagliazucchi et al., 2014; Varley et al., 2020; Viol et al., 2019, 2017). Since then, one additional paper has shown increases in brain-entropy following psilocybin intake (Siegel et al., 2024). Upon closer inspection, we revealed that each of the 13 papers had in fact used a distinct method for quantifying brain-entropy and that no findings had been replicated across sites or datasets. Advancing our understanding of this hypothesis is the focus of paper 3 in the present thesis.

Entropy

The quantification of information into “bits” was first proposed by Claude Shannon in his pivotal 1948 paper “A Mathematical Theory of Communication”, kicking off the field of information theory (Shannon, 1948). Here, he proposed that the information density, or entropy, of a system can be explained as the sum of the probabilities of each event multiplied by the inverse log of the probability of that event. This effectively measures the width of a probability histogram. Such a quantification can be applied to systems with discrete states (e.g., rolls of a die) or systems with continuous states once these have been binned into discrete states (e.g., temperature to the nearest whole degree). This formulation became known as “Shannon Entropy” and is widely used as a means of describing the complexity, unpredictability, or diversity of a system. Since then, other forms of measuring entropy have emerged. One of the most widely applied is known as Lempel-Ziv complexity, developed by Nobel laureates Abraham Lempel and Jacob Ziv, which measures the degree to which a system can be described as a reduced codebook without losing any information (Lempel and Ziv, 1976). In biological time-series analysis, a metric known as “sample entropy” (SampEn), an improved version of approximate entropy, was described in the year 2000 by Richman and Moorman (Richman and Moorman, 2000). By identifying patterns in the data and the degree to which they are maintained over longer time-scales, SampEn measures the irregularity of a sequence.

Positron emission tomography imaging

Positron Emission Tomography (PET) is an in vivo imaging method based on measuring the locations of radioactive decay events. Certain radioisotopes, such as [^{11}C] and [^{18}F], decay by beta-plus decay, releasing a positron which travels a very short distance before colliding with an electron. This annihilation subsequently releases two photons that travel in approximately opposite directions and can be detected by gamma ray detectors as (roughly) coincident detection events (Ter-Pogossian et al., 1975). To utilise this phenomenon to evaluate biological systems, radioisotopes can be attached to molecules with known pharmacokinetic and pharmacodynamic properties. A relevant example to the work presented here is to radio-label (i.e., add a radioisotope to) a drug with specific affinity for a target of interest, creating what is known as a “radiotracer”. Radiotracers are typically administered intravenously, they then travel to the tissue of interest and cross into that organ, e.g., via the blood-brain-barrier into the brain. Once in the tissue of interest, the radiotracer can

exist either as free, i.e., in the interstitial space, specifically bound, i.e., bound to the tissue of interest, or non-specifically bound, i.e., bound to a protein that is not the tissue of interest (Innis et al., 2007). PET scans last for several minutes to hours, resulting in a timeseries for each 2-4 mm isotropic voxel within the field of view. These data are then preprocessed, steps of which typically include summarising time-periods into frames, realigning these frames to a single reference frame to correct for participant motion, and co-registering the PET image to a high resolution T1-weighted MR image for delineation of anatomical structures (Nørgaard et al., 2020; Svarer et al., 2005). This process results in the generation of “Time-Activity Curves” (TACs) for each brain-region. There are degrees of freedom in each preprocessing step that can meaningfully affect results (Nørgaard et al., 2020).

Simplified Reference Tissue Model

The properties of the tracer binding in each region can then be mathematically modelled using kinetic modelling. Different kinetic models provide different outcome measures. The two-tissue compartment model (2TCM) typically estimates the volume of distribution (V_T), which represents the total binding capacity in the tissue. In contrast, models utilising a reference tissue like the Reference Tissue Model and its simplified version (RTM, SRTM) provide the binding potential (BP_{ND}), which specifically quantifies the ratio of specifically bound to non-displaceable tracer, effectively isolating the signal of interest from non-specific binding (Lammertsma and Hume, 1996). This model is based on considering a brain region that contains the target of interest and a similar brain region that does not contain the target of interest but does have similar non-specific binding properties (Figure 3). SRTM has the benefit over other kinetic modelling strategies of not requiring an arterial input function, therefore alleviating the requirement for regular arterial blood sampling during the PET scan, which can cause discomfort for participants.

SRTM is a simplification of the reference tissue model (Hume et al., 1992; Lammertsma et al., 1996), which describes the following four compartments and six rate constants (See figure 3).

- C_p is the concentration of tracer in blood.
- C_r is the concentration of free and non-specifically bound tracer in the reference tissue
- C_f is the concentration of free and non-specifically bound tracer in the target tissue
- C_b is the concentration of tracer bound to the specific target in the target tissue
- K_1 is the rate constant for the movement of tracer from C_p to C_f
- k_2 is the rate constant for C_f to C_p
- k_3 is the rate constant from C_f to C_b
- k_4 is the rate constant from C_b to C_f
- K'_1 is the rate constant for C_p to C_r
- k'_2 is the rate constant for the movement of C_r to C_p

Through a series of assumptions, including the lack of specific binding in the reference tissue and that the volume of distribution is the same in both target and reference tissues, the four compartments and six rate parameters can be simplified to two compartments and three parameters. This is known as SRTM.

- C_t is the concentration of tracer in the target tissue
- C_r is the concentration of tracer in the reference tissue
- R_1 is the ratio between the delivery from blood to the target tissue (K_1) and the reference tissue (K'_1)
- k_{2a} is the rate constant for the transfer of tracer from the target tissue to the plasma ($k_2/(1+BP)$)
- BP_{ND} is the ratio of specifically bound to free ligand in the target tissue (k_3 / k_4)

The operational equation is then written:

$$C_t(t) = R_1 C_r(t) + [k_{2a} - R_1 k_{2a} / (1 + BP_{ND})] C_r(t) \otimes \exp[-k_{2a} t / (1 + BP_{ND})]$$

Where \otimes represents the convolution operator.

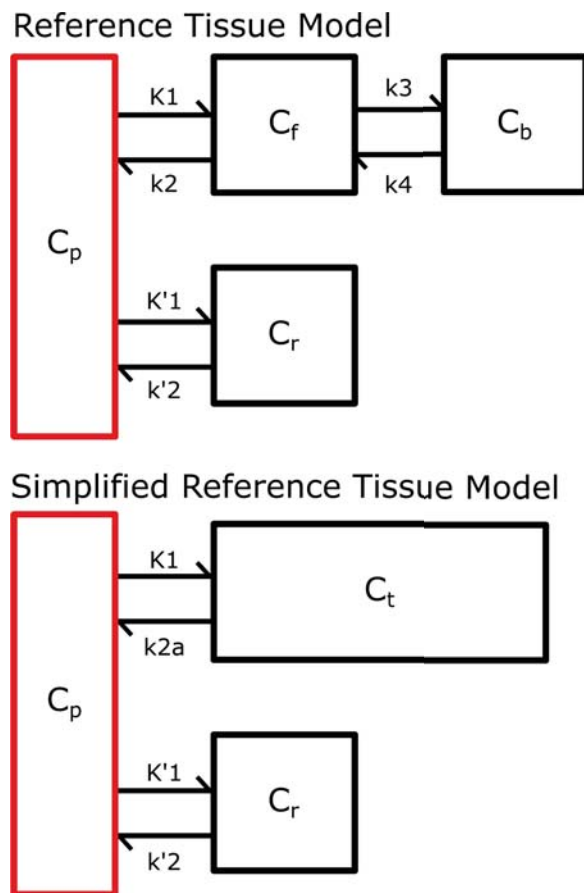


Figure 3 | Compartmental models used in PET. Top: Compartmental model showing the kinetic relationships between plasma (C_p), reference tissue (C_r), and target tissue compartments as characterised in the Reference Tissue Model. The target tissue includes free/non-specifically bound (C_f) and specifically bound (C_b) tracer concentrations. Rate constants K_1 , k_2 , k_3 , k_4 govern target tissue kinetics, while K'_1 and k'_2 describe reference tissue kinetics. Bottom: Compartmental model showing compartments described by the Simplified Reference Tissue Model, where the target tissue compartments, C_f and C_b , are combined into a single compartment C_t . Rate constant k_{2a} represents the apparent efflux rate from the combined target tissue compartment.

[¹¹C]Cimbi-36

[¹¹C]Cimbi-36 is a radiotracer produced by labelling the phenethylamine psychedelic 25B-NBOMe at the methoxy in the 2-position on the N-benzyl ring (Ettrup et al., 2011). It is an agonist, meaning that it binds preferentially to the G-protein-coupled conformational state of the receptor. It is selective for 5-HT_{2A}R (K_i (nM): 5-HT_{2A}R = 0.5; 5-HT_{2B}R = 100; 5-HT_{2C}R = 6.2) with some lower affinity for H₁ receptors (K_i (nM) = 80) (Rickli et al., 2015). Cimbi-36 was first evaluated in pigs (Ettrup et al., 2011) and then shown not to produce behavioural effects in rats at tracer doses (Ettrup et al., 2013). [¹¹C]Cimbi-36 was then evaluated in non-human primates, wherein the two-tissue compartment model (2TCM) and SRTM with cerebellar reference region were both shown to adequately describe the tracer kinetics. Additionally, binding was shown to be related to the distribution of 5-HT_{2A}R in the cortex and 5-HT_{2C}R in the choroid plexus and subcortical regions (Finnema et al., 2014). It was then evaluated in humans, showing a relation between V_T estimates from 2TCM and BP_{ND} estimates from SRTM, and showing that binding could be displaced by preadministration with the 5-HT_{2A/2C}R antagonist ketanserin (Ettrup et al., 2014). [¹¹C]Cimbi-36 forms mostly glucuronide radio-metabolites which do not cross the blood-brain barrier (Johansen et al., 2018), and has an effective dose of 5.5 µSv/MBq, indicating that it is safe to administer several scans within a year (Johansen et al., 2019). A test-retest study and comparison with the antagonist radiotracer [¹⁸F]altanserin showed less than 5% test-retest variability and strong correlation between the BP_{ND}s estimated with each tracer, except within the choroid plexus and hippocampus, likely due to 5-HT_{2C}R binding (Ettrup et al., 2016). [¹¹C]Cimbi-36 has been shown to be sensitive to fenfluramine-mediated 5-HT release in the pig and non-human primate brains (Jørgensen et al., 2017; Yang et al., 2017) but not to citalopram mediated (smaller) 5-HT release or acute tryptophan depletion in humans (da Cunha-Bang et al., 2019).

Occupancy estimation

A primary utility of PET in drug development is the estimation of the relation between plasma drug levels and occupancy of the target receptor, i.e., determination of the plasma concentration producing 50% occupancy (IC₅₀) and maximum occupancy (Occ_{max}) for the drug-receptor pair (Laurell et al., 2022). The typical study design includes a baseline scan to determine the receptor availability in the absence of drug, followed by a re-scan wherein the radiotracer is administered shortly after administration of the drug of interest. During this 2nd scan, plasma samples are taken to determine the plasma concentration of the drug during the scan ([DRUG]). If binding can be quantified using any appropriate metric (e.g., BP_{ND} from reference tissue methods, V_T from compartmental modelling), one can then determine the occupancy as the percentage reduction in that binding metric between the baseline and block scans. Once this has been determined across a range of plasma concentrations, one can then determine IC₅₀ and Occ_{max} using the Hill-Langmuir, or E_{max} model (See **Fig. 4** for an example):

$$Occupancy = Occmax \frac{[Drug]}{IC50 + [Drug]}$$

Previous PET work with psychedelics

Four previous studies have applied PET imaging to investigate the neuromolecular effects of psychedelics in humans, all of which analysed the effects of psilocybin. The first of these investigated the acute change in neural metabolic rate using the radiotracer [¹⁸F]fluorodeoxyglucose (FDG). This study reported global increases in neural metabolic rate, with the largest effects seen as increases of 20-25% in frontal regions (Vollenweider et al., 1997). The same group later investigated the effect of psilocybin on the binding potential of [¹¹C]raclopride, a radiotracer for dopamine type 2 receptors (D₂) (Vollenweider et al., 1999).

They observed a 20% decrease in BP_{ND} , interpreted as being caused by occupancy of the receptors by psilocybin-stimulated endogenous dopamine release, as psilocybin has low direct affinity for D2 receptors ($K_i = 3700\text{nM}$) relative to 5-HT_{2A}R ($K_i = 49\text{ nM}$) (Rickli et al., 2016). One study investigated the relation between PPL and receptor occupancy at the 5-HT_{2A}R using [¹¹C]Cimbi-36, showing an IC_{50} of 1.95 $\mu\text{g/L}$ (10 nM) and an Occ_{max} of 76.6% (Figure 4) (Madsen et al., 2019). Finally, a study investigated whether there were lasting changes in 5-HT_{2A}R binding potential one week after psilocybin administration in healthy volunteers, showing no group difference but a linear relation between decreases in [¹¹C]Cimbi-36 BP_{ND} and increases in self-reported mindful-attention and awareness (Madsen et al., 2020).

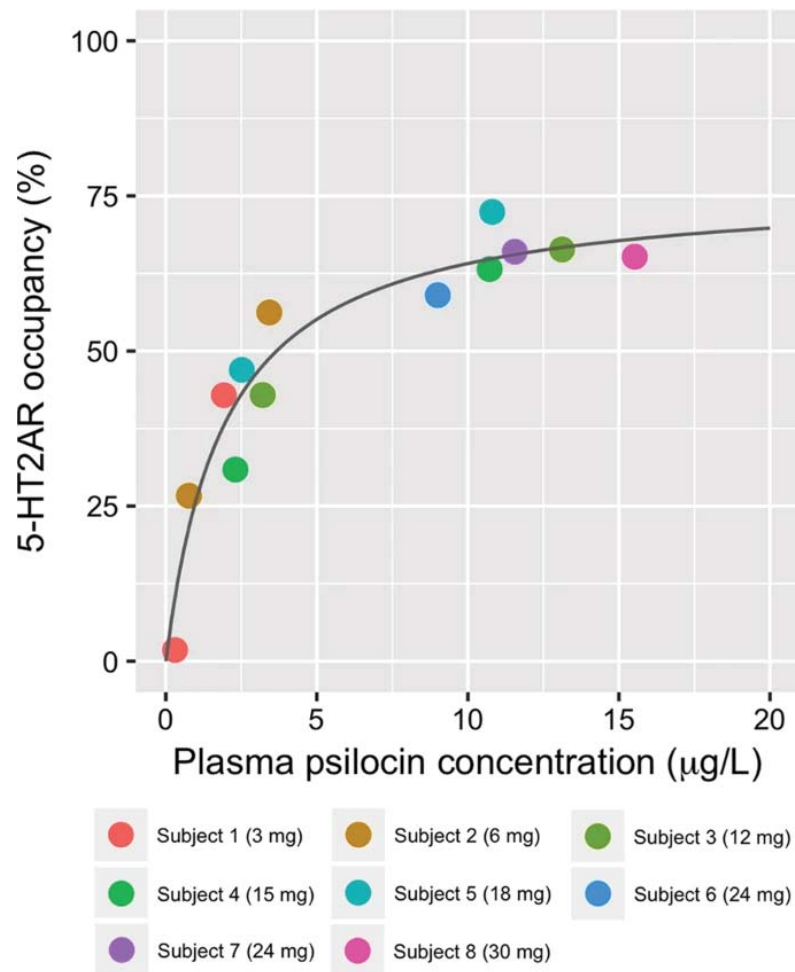


Figure 4 | 5-HT_{2A}R occupancy of psilocybin from Madsen et al., 2019. Each coloured point represents an estimated occupancy for a PET scan in one individual; the colours represent the individuals who each received a different dose. The x-axis value denotes the plasma concentration of psilocin during each PET scan, and the y-axis denotes the occupancy. The curve is a fitted Hill-Langmuir model indicating that psilocin binds to the 5-HT_{2A}R with an IC_{50} of 1.95 $\mu\text{g/L}$ (10 nM) and an Occ_{max} of 77%.

Motivation and aims

Paper 1

Arguably, the most medically intriguing property of psychedelics is their apparent capacity to produce lasting positive changes in behaviour for weeks or even months after the acute psychedelic effects have subsided. At the time we published this paper, only one paper had investigated the persisting effects of psychedelics on functional brain activity more than 24 hours after administration. In this paper, we sought to characterise alterations in network- and region-level connectivity one week and three months after psilocybin administration in healthy volunteers. Following identification of a candidate connectivity change, we also evaluated the relation between this and previously reported alterations in 5-HT_{2A}R availability, self-reported change in mindful awareness, personality, and persisting positive effects. Finally, we evaluated whether findings from the only prior analysis of this kind could be replicated in our sample using the same atlas and analysis method. This constituted only the second replication effort in the field of functional brain imaging with psychedelics.

Paper 2

Lasting positive effects on wellbeing and behaviour have even been reported in healthy people. Previous studies have reported associations between the acute effects of psychedelics and their lasting effects, particularly those effects described as “mystical”, characterised using the “Mystical Experience Questionnaire” (MEQ). In this paper, we first aimed to replicate previous findings in a new population of healthy Danish individuals and expand on previous findings by delving into which components of the MEQ were most closely related to persisting positive effects. We collected qualitative “trip reports” from all individuals and, using natural language processing, identified themes that characterised mystical-type experiences (MTE) in participants’ own words, and present quotes from participants alongside their drawings to provide a more comprehensive overview of how MTE manifest in healthy individuals.

Paper 3

The Entropic Brain Hypothesis states that "the 'qualia' or subjective quality of any given conscious state, and specifically the 'richness' of its content, can be indexed by a quantitative measure of the magnitude of entropy (in the information theoretic sense) in a given parameter of spontaneous brain activity". It also states that psychedelics increase the richness of content of consciousness, and therefore should also produce increases in brain entropy. At the time of writing this paper, 12 papers had evaluated psychedelic effects on the fMRI entropy, yet each had used a distinct quantification of entropy. In this project, we sought to apply each of the previously used methods to fMRI data collected from individuals administered a high dose of psilocybin. We aimed to determine whether there was any relation between each distinct entropy metric and whether any of these were associated with acute psychedelic effects.

Paper 4

Lysergic acid diethylamide (LSD) is a prototypical psychedelic and is in clinical development for the treatment of several psychiatric and neurological conditions, including anxiety and migraine. The clinical benefits of LSD are purported to be due to agonism at the 5-HT_{2A}R. No previous target-engagement studies have been performed to evaluate the relation between plasma LSD levels and occupancy at the 5-HT_{2A}R, and no previous evaluations of the acute neurological effects of LSD have concurrently measured receptor occupancy. In this project, we characterised the baseline 5HT_{2A}R binding and functional brain activity using [¹¹C]Cimbi-36 in a simultaneous PET and MRI scanner in healthy volunteers. We then administered a range of doses of LSD (25 to 200µg) and rescanned participants during peak drug effects to determine the occupancy at peak and changes in functional brain activity.

Study designs

Paper 1

The data collection study design of paper 1 is shown in **Fig. 5**. Ten healthy participants were included. At baseline, each participant received a resting-state fMRI scan in a 3T Siemens scanner. They also received a [¹¹C]Cimbi-36 PET scan and completed the Mindful Attention and Awareness Scale (MAAS). On a separate day, they received a single dose of 0.2-0.3mg/kg of psilocybin in a comfortable room with two psychological support staff and music. Both one week and three months later, participants received another fMRI and PET scan. After the three-month scan, participants also filled out the MAAS and the Persisting Effects Questionnaire (PEQ), which measures lasting positive and negative changes across a range of domains that the participant attributes to the psychedelic experience. fMRI data were pre-processed and denoised to derive region-to-region connectivity matrices from which within- and between-network connectivity was estimated. Whether the observed change in network connectivity was related to changes in MAAS or PEQ score was evaluated using linear mixed models.

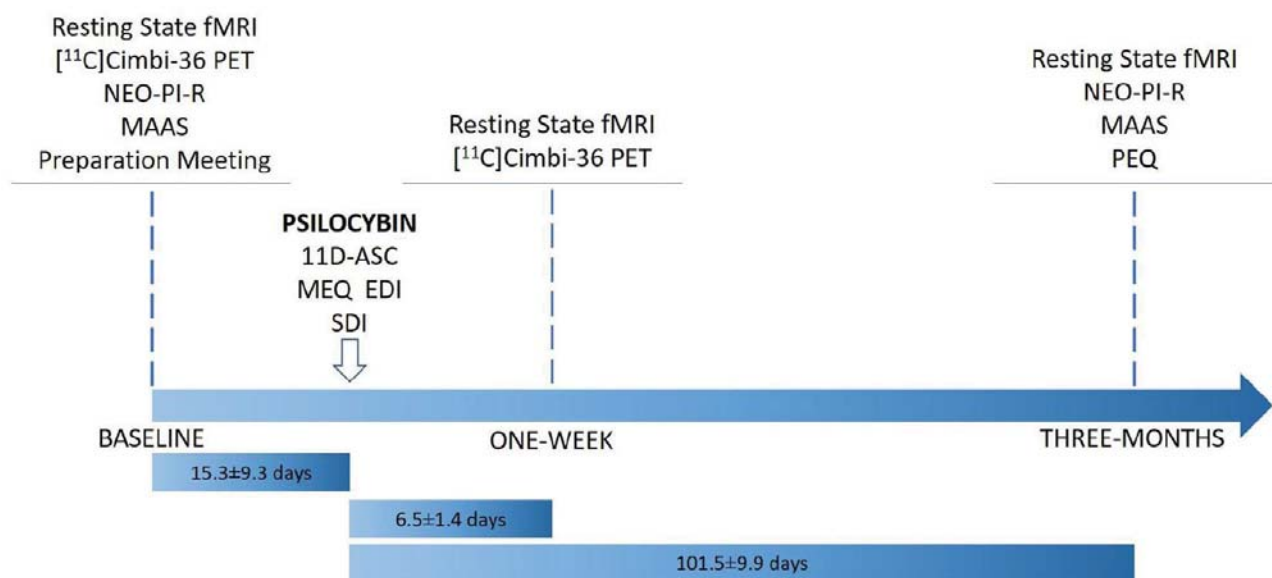


Figure 5 | Study overview for paper 1. NEO-PI-R: NEO Personality Inventory-Revised, MAAS: Mindful Attention Awareness Scale, 11D-ASC: 11-Dimensional Altered States of Consciousness Scale, MEQ: Mystical Experience Questionnaire, EDI: Ego Dissolution Inventory, SDI: Subjective Drug Intensity, fMRI: functional Magnetic Resonance Imaging.

Paper 2

The data collection study design of paper 2 is shown in **Fig. 6**. Twenty-eight healthy participants (12 female) were included and administered 0.19-0.31 mg/kg psilocybin in a range of settings, seven participants underwent two sessions in different settings, so there were a total of 35 sessions included. When subjective drug effects had subsided, participants filled out the MEQ, provided an open-ended qualitative description of their experience, and provided a drawing of their experience in coloured pencil. Three months later, participants filled out the PEQ. Associations between MEQ total or subscale scores and PEQ were evaluated using a latent variable model (LVM). Words used exclusively to describe so-called “complete mystical experiences” were determined by tf-idf analysis of the preprocessed qualitative reports, and post-hoc, representative quotes were extracted that contextualised these themes and paired with relevant drawings.

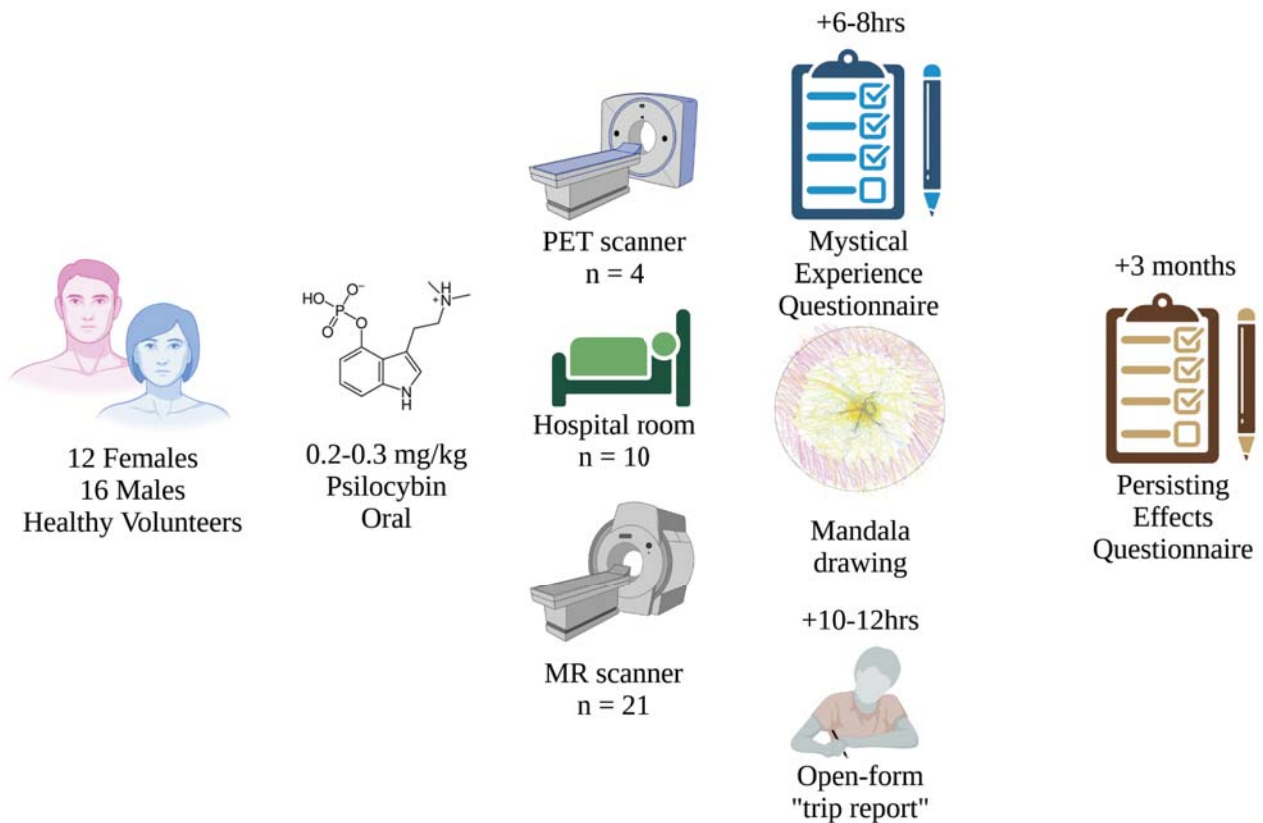


Figure 6 | Study design for paper 2. PET: Positron Emission Tomography, MR: Magnetic Resonance.

Paper 3

The data collection study design of paper 3 is shown in **Fig. 7**. 27 healthy young adults were included. On the dosing day, participants were scanned using a BOLD fMRI sequence in the morning before drug administration. They were then administered between 0.2 and 0.3mg/kg of psilocybin orally before being rescanned up to four times at +50, 90, 140, and 300 minutes. Following each scan, participants were asked to rate their subjective drug intensity (SDI) on a scale from 0-10, and a plasma sample was taken, which was used for quantification of PPL. Following the identification of manuscripts that evaluated task-free fMRI brain entropy in the context of psychedelics, we mathematically determined and coded each study's entropy quantification method into a MATLAB toolbox (the Copenhagen Brain Entropy Toolbox, or CopBET). Each quantification method was then sent to the original authors to determine whether the methods were the same as previously applied. For a summary of the 13 methods applied, see **Fig. 8**. Each of these methods was then applied to the fMRI data from this sample, and the relation between SDI, PPL, and estimated occupancy of the 5-HT_{2A}R based on PPL (Occ_{2A}) was evaluated using mixed-effect models. Then, to evaluate the metrics, the intercorrelation between them, the effect of different fMRI denoising pipelines, and the effects on the two different scanners on the relation with drug effects were each evaluated.

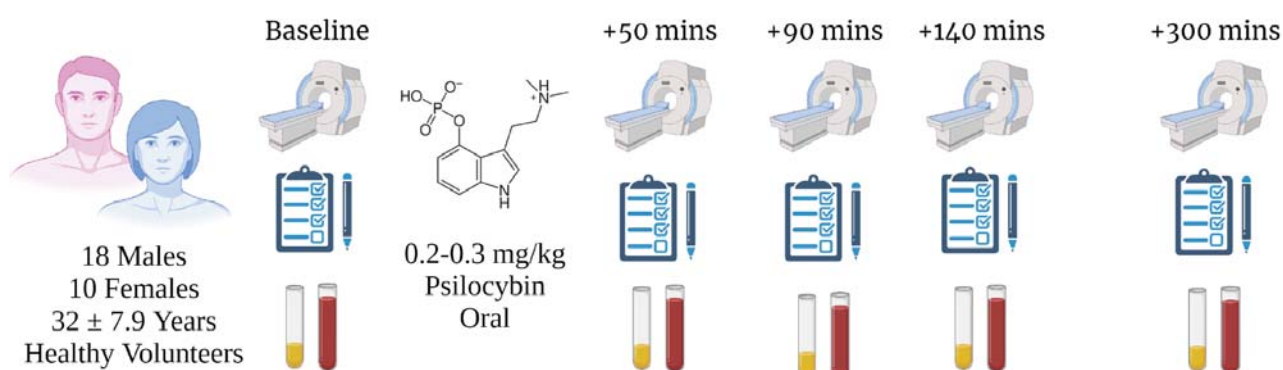
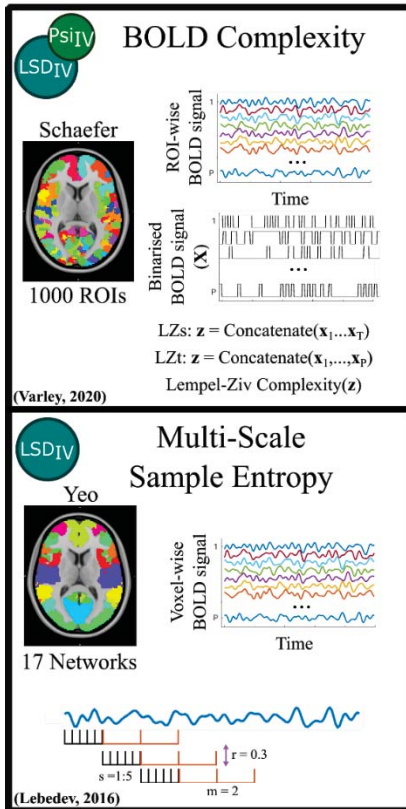
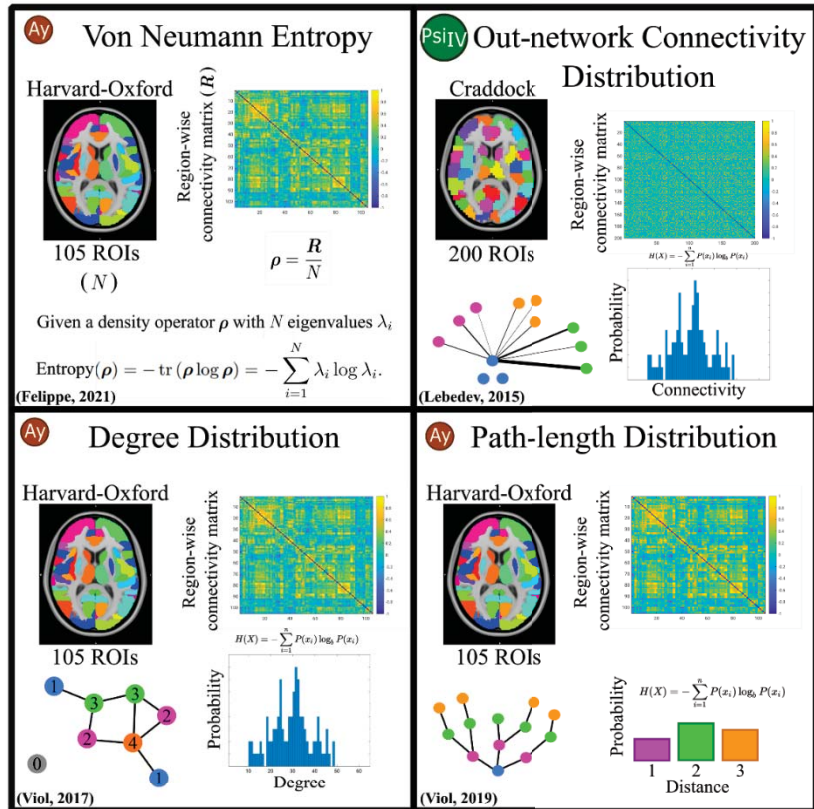


Figure 7 | Study design for paper 3. Scanner icons represent fMRI BOLD scans, the clipboard represents a measure of subjective drug intensity, and the vials of blood represent a plasma blood sample that was drawn and used to quantify plasma psilocin levels. Times are approximate and vary between participants.

Dynamic Activity



Static Connectivity



Dynamic Connectivity

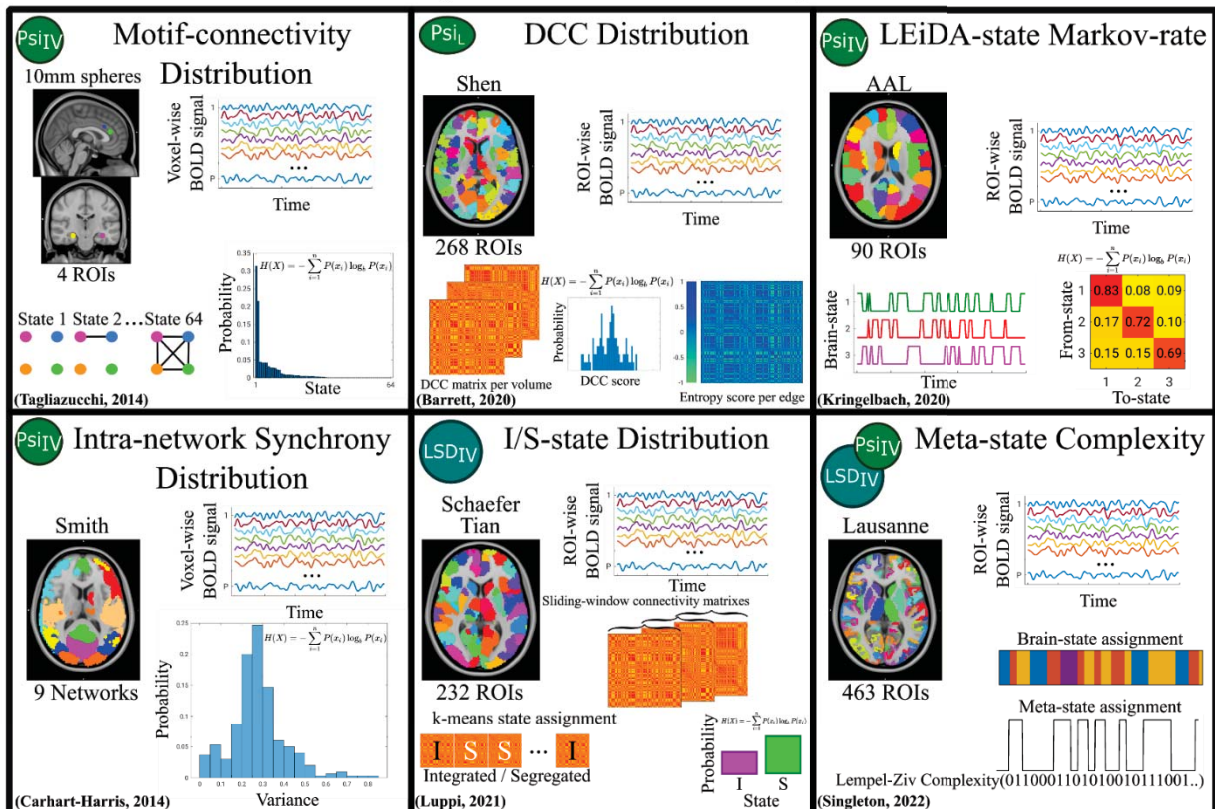


Figure 8 | Data analysis overview for paper 3. Each square represents a method of quantification of “brain-entropy” as previously reported in the literature. They are grouped into three categories: “Dynamic Activity”, “Static Connectivity”, and “Dynamic Connectivity”. Each square contains details of the method. In the top left, a symbol describes the dataset upon which the method was first described in the field of psychedelic fMRI. Psi_{IV} : Intravenous psilocybin, LSD_{IV} : Intravenous LSD, Ay: Oral ayahuasca, Psi_{L} : lasting effects of oral psilocybin. To the left, below the metric name, there is a description of the spatial parcellation used. To the right is a representation of the input to the function (i.e., regional or voxel-wise timeseries, or region-to-region connectivity matrix). Below that is a graphical description of the method, and in the bottom left corner is a citation for the paper that originally described the method.

Paper 4

The study design of paper 4 is shown in **Fig. 9**. Eleven healthy adults were included. At baseline, participants received a 2-hour simultaneous PET/MR scan. The PET scan was a dynamic PET acquisition using [^{11}C]Cimbi-36. The MR scans acquired during the PET scan included multi-band multi-echo BOLD sequences. BP_{ND} was determined for the neocortex using SRTM, with the cerebellum as reference tissue. Occupancy was determined as the relative difference in BP_{ND} , and the relation between occupancy and plasma drug level was determined using the Hill-Langmuir model. fMRI data were preprocessed and denoised, and regional timeseries were extracted. Global, thalamic, and network connectivity were evaluated, and several measures of brain entropy were quantified using CopBET. Comparing pre- and post-LSD scans, effect sizes are reported for each fMRI metric.

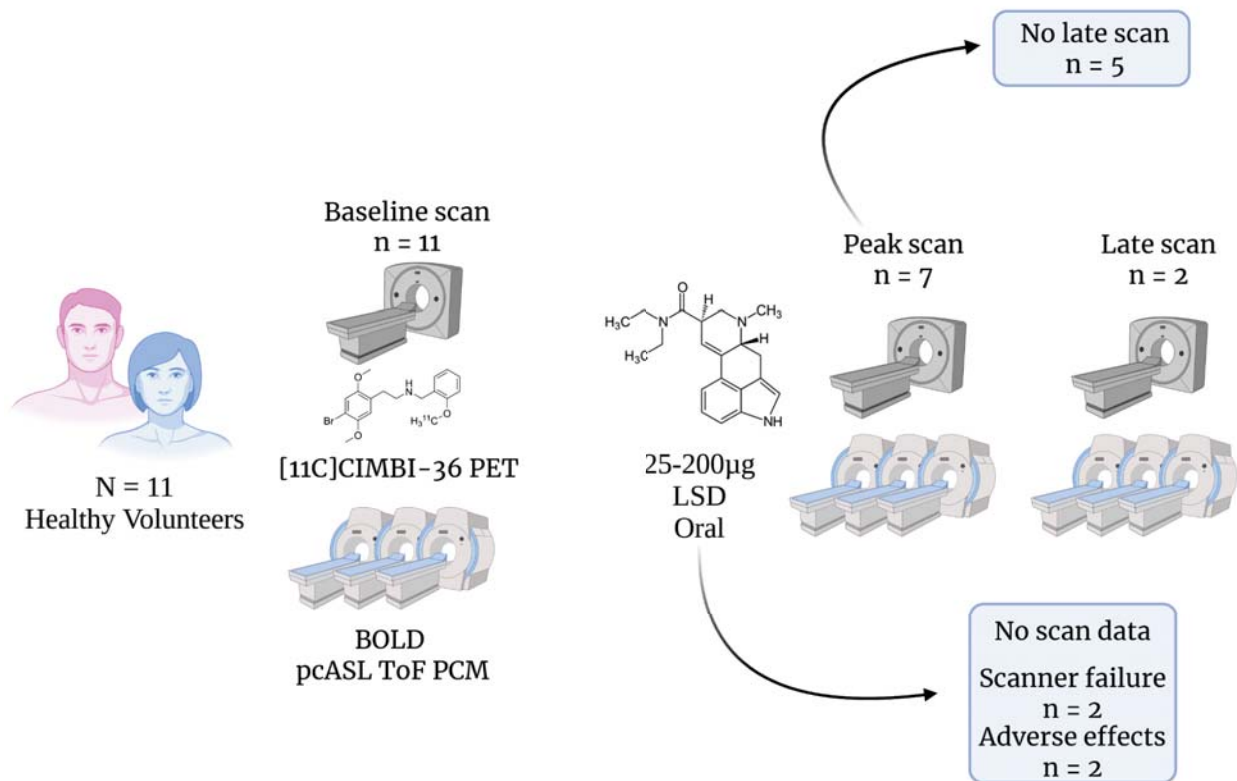


Figure 9 | Study design for paper 3. PET: Positron Emission Tomography, BOLD: Blood-oxygen Level Dependent functional magnetic resonance imaging, pcASL: pseudocontinuous Arterial Spin Labelling, ToF: Time-of-flight, PCM: Phase-Contrast Mapping.

Methods

Psychometrics (Papers 1, 2, 3, and 4)

The subjective intensity of drug effects was assessed during the acute drug effects by regularly asking participants, “How intense are your effects right now?” on a Likert scale from 0 to 10, where 0 represented “not at all” and 10 represented “very much”. This was used in papers 3 and 4. A retrospective evaluation of acute drug effects was also performed using the 30-item Mystical Experience Questionnaire (Barrett et al., 2015), which is a self-report scale with four subscales, “mysticality”, “positive mood”, “transcendence of time and space”, and “ineffability”. In paper 1, participants were asked to fill out the 15-item Mindful Attention and Awareness Scale (MAAS), which measures self-reported degree of mindful attention to the present moment. In papers 1 and 2, participants were asked three months after their psilocybin session to fill out the Persisting Effects Questionnaire (PEQ) (Griffiths et al., 2006), which asks about “persisting effects that they evaluate to be the result of their intervention or their subsequent reflection over their experience”. This contained twelve subscales: positive or negative effects on behaviour, attitudes about life, mood, attitudes about self, social effects, and spirituality. In paper 2, participants were asked to provide a circular drawing and a free-form written description of their psychedelic experience on the evening of their experience. These were used for natural language processing and qualitative analyses. In paper 4, participants were asked to rate their emotional response to the music they listened to during the scans using the Geneva Emotional Music Scale (Zentner et al., 2008).

Plasma psilocin and LSD quantification (Papers 1, 2, 3, and 4)

At regular intervals following either psilocybin or LSD administration, blood samples were drawn using a venous antecubital catheter. Samples were stored on ice until centrifugation. Plasma was extracted and stored at -20°C. Quantification of psilocin or LSD was performed by the Section of Forensic Chemistry, Department of Forensic Medicine, Faculty of Health and Medical Science, University of Copenhagen, using ultra-performance liquid chromatography and tandem mass spectrometry on EDTA-stabilised plasma samples. In paper 3, PPL were converted into estimated occupancies using an IC_{50} of 1.95 $\mu\text{g/L}$ and B_{max} of 76.6% (Madsen et al., 2019).

Structural MRI acquisition (Papers 1, 3, and 4)

In papers 1, 3, and 4, T1 and T2-weighted images were acquired at the start of each imaging session. These images were used for the identification of single-subject grey and white matter maps as well as for the co-registration of the functional images. T1-weighted structural images were acquired across three studies using MPRAGE sequences. Paper 1 used a 64-channel head coil with parameters: TR = 1900 ms, TE = 2.58 ms, TI = 900 ms, flip angle = 9°, FOV = 256 × 256 mm, matrix size = 256 × 256, voxel size = 0.9 × 0.9 × 0.9 mm, 224 slices, no gap. Paper 3 collected data on two scanners: Scanner A used parameters identical to those of Paper 1. Scanner B employed a 32-channel head coil with parameters: TR = 1810 ms, TE = 2.41 ms, TI = 920 ms, flip angle = 9°, matrix size = 288 × 288, voxel size = 0.8 × 0.8 × 0.8 mm, 224 slices. Paper 4 also used a 32-channel head coil but with parameters: TR = 2300 ms, TE = 2.26 ms, TI = 900 ms, flip angle = 8°, FOV = 256 × 256 mm, matrix size = 256 × 256, voxel size = 1 × 1 × 1 mm, 176 sagittal slices, and GRAPPA parallel imaging with acceleration factor = 3.

Functional MRI acquisition (Papers 1, 3, and 4)

BOLD functional images were acquired across studies using echo-planar imaging (EPI) sequences. Paper 1 used a 64-channel head coil with parameters: TR = 2000 ms, TE = 30 ms, flip angle = 90°, FOV = 230.4 × 230.4 mm, matrix size = 64 × 64, voxel size = 3.6 × 3.6 × 3.0 mm, 32 slices, slice gap = 0.75 mm, GRAPPA acceleration factor = 2. Paper 3 collected data on two scanners: Scanner A used identical parameters to Paper 1. Scanner B employed a 32-channel head coil with parameters: TR = 800 ms, TE = 37 ms, flip angle = 52°, matrix size = 104 × 104, voxel size = 2 × 2 × 2 mm, 72 slices, no gap, multi-band acceleration factor = 8, collecting either 750 volumes (n = 5) or 375 volumes (n = 8) over 10 minutes. Paper 4 used a multi-echo, multi-band EPI sequence with parameters: TR = 1117 ms, TEs = 15.0/33.68/52.36 ms, flip angle = 70°, FOV = 204 × 204 mm, matrix size = 68 × 68, voxel size = 3 × 3 × 3 mm, 42 axial slices, multi-band acceleration factor = 3, GRAPPA acceleration factor = 2.

Functional MRI processing and denoising (Papers 1, 3, and 4)

In paper 1, fMRI data were preprocessed using SPM12 (Penny et al., 2007). fMRI data were first realigned and distortion-corrected using a spin-echo field map, then slice-time corrected. The structural T1-weighted image was co-registered to the functional data and segmented to derive single-subject grey matter (GM), white matter (WM) and cerebrospinal fluid (CSF) masks. Functional data were co-registered to the T1-weighted image, and transformation parameters from the T1 to MNI space were applied. Functional data were then smoothed using an 8mm full-width half-maximum (FWHM) Gaussian kernel. Functional data were then de-noised using the CONN toolbox for SPM (Whitfield-Gabrieli and Nieto-Castanon, 2012) wherein the first 5 principal components and their first derivative of the signal from WM and CSF were regressed as well as the 6-motion parameters from the realignment step, and their first derivatives and flagged volumes as identified using the Artifact Detection Tools (ART) toolbox with global variance threshold = 4 and composite motion threshold = 2. Data were linearly detrended and bandpass filtered (0.008 to 0.09 Hz). Denoised data were then parcellated into 36 regions using the Raichle atlas (Raichle, 2011) as well as 268 regions using the Shen atlas (Shen et al., 2013). An illustration showing the Executive Control Network (ECN) from the Raichle atlas is shown in **Fig. 10**.

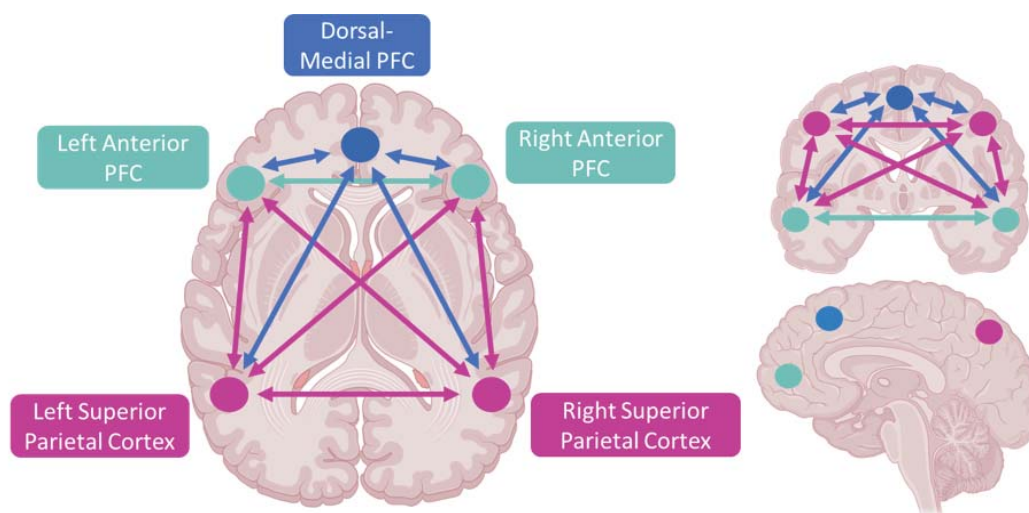


Figure 10 | Executive control network as defined by the Raichle atlas. Illustration showing axial (left), coronal (top right), and sagittal (bottom right) projections of the regions included in the executive control network as defined by Raichle.

In paper 3, fMRI data from both scanners were preprocessed and denoised in the same way as paper 1, except that a 6mm FWHM smoothing kernel was used, and data from scanner B were not slice-time corrected. After denoising, data from scanner B were downsampled to match the temporal resolution of scanner A (TR = 2000ms). Data were parcellated using eleven different atlases to match those utilised in the original publications, as well as a separate atlas, common across all metrics, to evaluate the effect of parcellation.

- Schaefer-1000 regions (Schaefer et al., 2018)
- Yeo-17 Networks (Yeo et al., 2011)
- Harvard-Oxford 105 regions (Desikan et al., 2006)
- Craddock-200 regions (Craddock et al., 2012)
- 4 x 10mm ROI spheres at bilateral anterior cingulate cortices and hippocampi (Tagliazucchi et al., 2014)
- Shen-268 regions (Shen et al., 2013)
- Automated Anatomical Labelling-90 regions (Tzourio-Mazoyer et al., 2002)
- Smith 9 Networks (Smith et al., 2009)
- Schaefer-200 cortical regions + Tian-32 subcortical regions (Tian et al., 2020)
- Lausanne-463 regions (Hagmann et al., 2008)
- Schaefer-100 cortical regions + Tian-16 subcortical regions (common atlas)

Additionally, as a post-hoc analysis, six different preprocessing pipelines were applied, and in each case, the common atlas was used.

- Including global-signal regression
- Removal of the low-pass filter
- Applying a narrower bandpass filter (0.03-0.07 Hz)
- Regression 24- instead of 12- motion parameters (i.e., the squares of the motion and derivatives)
- Omitting scrubbing
- Stricter scrubbing ($z > 3SDs$, motion $> 0.5mm$)

In paper 4, fMRI data were preprocessed using the Configurable Pipeline for the Analysis of Connectomes (C-PAC; version 1.8.7.Dev1). T1-weighted and functional data were preprocessed using FSL, AFNI, and ANTs. Processing began with brain extraction of T1-weighted images using FSL's Brain Extraction Tool (robust setting), followed by tissue segmentation with FSL FAST. Segmentation masks were generated using a 0.9 probability threshold. For functional data, preprocessing included slice-timing correction, motion correction (AFNI 3dvolreg), and distortion correction using fieldmap unwarping. AFNI masking was applied to the functional images, followed by intensity normalisation. Spatial normalisation was performed by registering T1 images to MNI152 space using ANTs, while functional images were first co-registered to T1 space using FSL FLIRT with boundary-based registration before transformation to MNI space. Denoising was performed in native space and included ICA-AROMA (non-aggressive option), regression of 24 motion parameters (6 parameters plus derivatives, squares, and squared derivatives), the first 5 principal components from white matter and CSF, mean CSF signal, and linear/quadratic trends. Finally, a bandpass filter was applied (0.01-0.1 Hz). Data were then parcellated into Schaefer-200 cortical regions + Tian-32 subcortical regions.

Functional MRI metrics (Papers 1, 3, and 4)

fMRI metrics are described fully within the methods sections of the relevant publications, but are described in brief below. Code is publicly available for the computation of each metric on the following two GitHub repositories: <https://github.com/Pneumaethylamine>, <https://github.com/anders-s-olsen/CopBET>.

Several analyses used connectivity matrices (CM) calculated as the Fisher-transformed r-to-z Pearson's correlation between each region pair. "Edge" refers to the correlation between one region-of-interest (ROI) and another. Several analyses ultimately quantify the Shannon entropy of a specific feature as described in the background section.

In paper 4, baseline estimates for each metric were determined as the mean across 2 (n=3) or 3 (n=4) baseline scans.

Network connectivity (Papers 1 and 4)

This method used the CM as input. Regions were assigned to networks based on the parcellation of interest. Within-network connectivity (WNC) is defined as the mean (paper 1) or median (paper 4) of all of the correlations that link the nodes that belong to the same network. Between-network correlation is defined similarly, but for all edges connecting regions from one network to another.

ROI-to-ROI edge strength (Paper 1)

This method used the CM as input. First, a one-sample t-test is applied to all correlations to retain only those with significantly non-zero connectivity after Bonferroni correction for the number of edges (i.e., the strongest edges). Then, uncorrected paired t-tests were performed for each surviving edge between conditions.

Out-network connectivity distribution (Paper 3)

This method used the CM as input. A community detection algorithm was applied to the CM, assigning a community affiliation to each ROI. The Shannon entropy of the connectivity from any ROI to all ROIs assigned to different communities was then calculated, returning an Out-network Connectivity Distribution score for each region. This method was applied as described in (Lebedev et al., 2015).

Degree distribution (Paper 3)

This method used the CM as input, taking the absolute edge strengths. Degree is defined as the number of super-threshold edges that an ROI has. First, the edges were thresholded with both a one-sample t-test and then with a dynamic threshold that produced a given mean-degree across all ROIs (e.g., on average, each ROI is connected to 27 others). The Shannon entropy of the number of edges that each ROI has was then calculated, resulting in a single whole-brain score describing the width of the distribution of edge-numbers. This method was applied as described in (Viol et al., 2017).

Path-length distribution (Papers 3 and 4)

This method used the CM as input, taking the absolute edge strengths. "Path length" is the shortest set of edges that must be crossed to get from any ROI to another. First, a path-length matrix was calculated representing the shortest paths between each ROI pair. Then the Shannon entropy of these matrix values was calculated. This method was applied as described in (Viol et al., 2019).

Von Neumann entropy (Paper 3)

This method used the Pearson's CM as input. The Von Neumann entropy is calculated as :

$$S(\rho) = - \sum_{i=1}^N \lambda_i \log \lambda_i$$

Where λ are the eigenvalues of the scaled correlation matrix $\rho = R/N$, where R is the CM and N is the number of regions. This method was applied as described in (Felippe et al., 2021).

Intra-network synchrony distribution (Paper 3)

This method used voxel-wise time series as input. Within each region, at each timepoint, the variance across voxel intensities was evaluated. Then the Shannon entropy of this variance over time was calculated. This method was applied as described in (Carhart-Harris et al., 2014).

Motif-connectivity distribution (Paper 3)

This method used time series data from 4 regions of interest (ROIs) - bilateral hippocampi and anterior cingulate cortices - each defined as 10mm diameter spheres. Using sliding windows of 15-150 seconds, partial correlation matrices were calculated between all ROI pairs in each window, controlling for other regions and motion. The standardised correlations were binarised using a significance threshold of $p=0.0083$ (0.05/6 pairs). This generated a probability distribution across all 64 possible network configurations, from which Shannon entropy was calculated. This method was applied as described in (Tagliazucchi et al., 2014).

LEiDA-state Markov-rate (Paper 3)

This method used regional time series as input. The method computed phase coherence matrices using the Hilbert transform to find phase differences between regions. These matrices were decomposed using eigenvalue decomposition, retaining the first eigenvector at each timepoint. K-means clustering (K=3) was applied to these eigenvectors. Transition probabilities between states were calculated, and the entropy rate was computed as

$$S_i = - p(i) \sum_{j=1}^K p(i, j) \log P(i, j)$$

Where p is the leading eigenvector of the transition matrix P. The final entropy was normalised as

$$S = \sum_{j=1}^K S_i / \log 2(K)$$

This method was applied as described in (Kringelbach et al., 2020).

Dynamic conditional correlation distribution (Papers 3 and 4)

This method used regional time series as input. Dynamic Conditional Correlation (DCC) was used to calculate framewise correlation coefficients between all region pairs (Lindquist et al., 2014). The Shannon entropy was calculated from the probability distribution of each edge's DCC strengths across time. Bin widths for entropy calculation were determined automatically using MATLAB's built-in *histcounts* function. ROIs were assigned to networks. The mean entropy was calculated for each network-to-network pair. This method was applied as described in (Barrett et al., 2020).

Meta-state complexity (Paper 3)

This method used regional time series as input. K-means clustering (K=4) was applied to BOLD time series using Pearson correlation distance, with 200 random initialisations to find the optimal solution. The four states were condensed into two meta-states based on sign symmetry. Each volume was labelled as meta-state 0 or 1, and the Lempel-Ziv complexity was calculated from this binary sequence using the LZ76 exhaustive algorithm (Lempel and Ziv, 1976). This method was applied as described in (Singleton et al., 2022).

Integration/Segregation-state distribution (Paper 3)

This method used regional time series as input. A sliding window correlation analysis was performed using a 44-second window convolved with a Gaussian kernel (FWHM = 3s). For each window, the correlation matrix was calculated, and the Louvain modularity algorithm was applied to compute module degree z-scores and participation coefficients. K-means clustering (K=2, 500 repetitions) was applied to the cartographic profile of these measures using correlation distance. The Shannon entropy was calculated from the probability distribution of state occurrences (i.e., segregated or integrated). This method was applied as described in (Luppi et al., 2021).

Multi-scale sample entropy (Papers 3 and 4)

This method used voxel-wise time series as input. For each voxel, sample entropy was calculated by examining the probability that signal patterns similar at length $m=2$ remain similar when extended to length $m = 3$, with similarity defined by Chebyshev difference less than 0.3. Specifically, it counts matching patterns of both lengths and takes the negative log of their ratio. To examine multiple timescales, the time series was first coarse-grained by averaging over non-overlapping windows of different lengths (scales 2-5). Sample entropy was then calculated on each of these coarse-grained signals to quantify pattern predictability across different temporal resolutions. The entropy value for each region was then calculated as the mean entropy across all voxels belonging to that region. This method was applied as described in (Lebedev et al., 2016) and as originally described in (Richman and Moorman, 2000).

Lempel-Ziv complexity (Papers 3 and 4)

This method used regional time series as input. The analysis begins by applying the Hilbert transform to extract amplitude information from each regional signal. These amplitude time series are then simplified into binary sequences by marking timepoints as 1 if they exceed that region's mean amplitude, and 0 if they fall below it. This creates a matrix where each row represents a time point and each column represents a region's binary state. From this binary matrix, two different types of complexity can be measured using the Lempel-Ziv algorithm (LZ78) (Ziv and Lempel, 1978). Temporal Lempel-Ziv complexity (LZc-temporal) examines how patterns in brain activity change over time by concatenating complete regional time series. Spatial complexity (LZc-spatial) instead looks at how complex the patterns of activity are across brain regions at each moment by concatenating time-adjacent "region-series". This method was applied as described in (Varley et al., 2020).

Normalised spatial complexity (Paper 4)

This method used voxel-wise time series as input. First, a PCA is performed on the time x voxel matrix. The resultant eigenvalues are then normalised by the sum of all eigenvalues. The normalised spatial complexity is then calculated as

$$NSC = - \sum_{i=1}^m \frac{\lambda_i' * \log(\lambda_i')}{\ln(m)}$$

This is analogous to the Shannon entropy of the eigenvalues, normalised by $\ln(m)$ to ensure values fall between 0 and 1. To calculate a global score, all voxels are included, and for regional scores, only voxels from the given region are included. This method was applied as described in (Siegel et al., 2024).

Global correlation (Paper 4)

This method used voxel-wise time series as input. The correlations between each voxel's timeseries and all other voxels within a cortical and subcortical mask were calculated. The median correlation value was assigned as the Global Correlation (GCOR) score for each voxel.

Thalamo-cortical correlation (Paper 4)

This method used voxel-wise time series as input. The correlation between a thalamus seed's time series and every other voxel in a cortical mask was calculated. The median correlation value was assigned as the TCOR (Thalamic Correlation) score for each voxel.

Modularity (Paper 4)

This method used the Pearson's CM as input. Modularity was calculated using the *community_louvain* function from the Brain Connectivity Toolbox (BCT) (Rubinov and Sporns, 2010), with $\gamma = 1$ and asymmetric treatment of negative weights applied to the weighted, undirected Pearson's correlation matrix for each scan. This calculation was repeated 100 times, with the maximum value retained as the absolute modularity. One hundred null graphs were then generated using the BCT's *null_model_und_sign* function. For each null graph, the same modularity calculation procedure was performed, taking the maximum of 100 repetitions of the *community_louvain* function. The observed modularity underwent normalisation relative to the mean modularity of these null models, expressed as: $\text{normalised_modularity} = \text{absolute_modularity} / \text{null_modularity}$.

Small-worldness (Paper 4)

This method used the Pearson's CM as input, retaining only positively weighted edges. The mean clustering coefficient (C) across all regions was calculated using the BCT function *clustering_coef_wu*. The average path length (L) was computed using the BCT function *distance_we_floyd('log')*, determined as the mean of the non-infinite, non-zero path lengths. One hundred null graphs were generated using the BCT function *null_model_und_sign* on the unthresholded matrix, which was subsequently thresholded to retain only positive edges. C and L were calculated for each null graph, and the observed small-worldness underwent normalisation according to: $\text{normalised_smallworldness} = (C / \text{mean}(C_{\text{null}})) / (L / \text{mean}(L_{\text{null}}))$, where C_{null} and L_{null} represent the C and L values calculated on null graphs.

Relation between GCOR and other imaging metrics (Paper 4)

To evaluate the relation between distinct neural effects of LSD, maps describing the change in GCOR (LSD minus baseline) were parcellated using the AAL3 atlas (Rolls et al., 2020) and regional values were compared with regional values for change in cerebral blood flow or neocortical occupancy using Spearman's rank correlation. This created a regional correlation estimate for each region.

PET acquisition and processing (Papers 1 and 4)

PET images in paper 1 were collected on a high-resolution research tomograph (HRRT) PET scanner (CTI/Siemens, Knoxville, TN, USA). PET images in paper 4 were collected on one of two identical 3T Siemens Biograph mMR scanners (Siemens Healthcare, Erlangen, Germany). Data were attenuation corrected using an MR-based attenuation correction method, reconstructed, and framed using a protocol of 6x10s, 6x20s, 6x60s, 8x120s, 19x300s, and then realigned and coregistered to session-specific T1- and T2-weighted MR images. Segmentation maps were created using the T1- and T2-weighted MR images, which were used to delineate grey-matter voxels. Regions of interest were defined using Pvelab (Svarer et al., 2005), and regional time-activity curves were extracted for use in SRTM to determine BP_{ND} in the neocortex, defined as an average across cortical regions. The cerebellum was chosen as the reference region due to the absence of 5-HT_{2A}R (Ettrup et al., 2016, 2014; Spies et al., 2020).

Language analyses (Paper 2)

Natural language processing analyses were performed on qualitative reports by first lemmatising all words (e.g., “swimming” and “swam” were transformed to “swim”) using the Python package *lemmy* (v2.1.0). Then these reports were split by whether participants had a Complete Mystical-Experience (CME), defined as a score greater than 60% on all four subscales of the MEQ. The lemmatised reports from CME and non-CME were then compared using a term-frequency inverse-document frequency (tf-idf) analysis using the R package *tidytext* (Silge and Robinson, 2016), which evaluates the relative frequency of word use across documents. Reports containing the top 5 terms identified in the tf-idf analyses were then qualitatively analysed, and representative quotes were extracted.

Mandala drawing (Papers 2 and 4)

On the day of dosing, after the psychoactive effects had ceased, participants were asked to provide a drawing of their experience in a circle. Where relevant, these are presented with the accompanying quote.

Statistical analyses (Papers 1, 2, 3, and 4)

Paper 1 evaluated differences in connectivity using paired t-tests and reported p-values with and without correction for multiple comparisons using the Bonferroni-Holm method (Salkind, 2012). We also report effect sizes for network-connectivity as Cohen's d_z , i.e., the mean difference divided by the standard deviation of the differences. Correlations between PET and MRI outcomes with various psychometrics were evaluated using Pearson's correlations. The “Positive” subscales of the PEQ were evaluated together using an LVM that captures the shared covariance within each subscale into a single variable (PPE_{LV}) using the R package *lava* (v.1.8.0); this approach was also used in paper 2. See **Fig. 11** for an illustration of the structure of the LVM. P-values were corrected for multiple comparisons using the Bonferroni-Holm method (P_{FWE}) (Holm, 1979).

Paper 2 evaluated the association between the total score and individual subscales of the MEQ and the PPE_{LV} . P-values were corrected for multiple comparisons using the Bonferroni method (P_{corr}) (Dunn, 1961).

Paper 3 evaluated each entropy metric for each scan as described above. The relation between PPL, SDI, and estimated 5-HT_{2A} occupancy (Occ_{2A}) with each entropy metric was evaluated using linear mixed effects models using the R packages *predictmeans* (v1.0.6), *lme4* (v1.1.30), *nlme* (v3.1.157), *lmerTest* (v3.1.3) and *LMMstar* (v0.7.6). We specified a subject-specific random intercept and adjustment for motion (i.e., Framewise Displacement (FD) estimated using Artifact Detection Tools), age, sex and scanner. We controlled the family-wise error rate within each metric across regions (e.g., across the 17 networks for scale-1 sample entropy) but not across metrics nor across SDI, PPL and Occ_{2A}. This was done using the maxT test method using a permutation framework (p_{FWER}) (Lee et al., 2012; Westfall and Troendle, 2008). Metrics without regions (e.g., BOLD complexity) were evaluated using only permutation testing (p_{perm}), applying 10000 permutations. Findings were considered statistically significant if they were associated with all three metrics (collectively termed “PsiFx”) at p_{perm} < 0.05 or p_{FWER} < 0.05 for regional metrics. Effect sizes are reported as Pearson’s correlation coefficients between the partial residuals of the entropy metrics adjusted for the above covariates and each of PsiFx. The effect of the scanner on the estimated relation between PPL and entropy was evaluated by a separate model including a scanner-x-PPL interaction as an additional covariate. The relations between all non-regional entropy metrics plus motion were evaluated using Pearson’s correlations.

Paper 4 used PET data from baseline and LSD sessions to estimate the occupancy of LSD at the 5-HT_{2A} for each participant as $100 \times (\text{baseline BP}_{\text{ND}} - \text{LSD scan BP}_{\text{ND}}) / \text{baseline BP}_{\text{ND}}$. The across-participants relation between plasma LSD levels during the scans and occupancy was then modelled using a single-site binding model, i.e., $\text{Occupancy} = (\text{Occ}_{\text{max}} \times [\text{LSD}]) / (\text{IC}_{50} + [\text{LSD}])$, where Occ_{max} is the maximal occupancy of LSD and IC₅₀ is the estimated concentration at which half of the binding of [¹¹C]Cimbi-36 is blocked, i.e., half of the receptors are occupied. This was estimated using a nonlinear least squares regression from the R package *stats* (v4.3.1). Confidence intervals were determined using a residuals bootstrap. Effect sizes comparing baseline and LSD fMRI metrics (GCOR and brain-entropy metrics) were calculated using Cohen's dz.

Ethical approvals (Papers 1, 2, 3, and 4)

Papers 1, 2, and 3 were based on data collected in a study approved by the Danish Medicines Agency (EudraCT ID: 2016-004000-61, amendments: 2017014166, 2017082837, 2018023295) and by the ethics committee for the capital region of Copenhagen (journal ID: H-16028698, with amendments). The study was preregistered at ClinicalTrials.gov (identifier: NCT03289949).

Paper 4 was based on a study approved by the ethics committee of the Capital Region of Denmark (H-21060056) and the Danish Medicines Agency (EudraCT no.: 2021-002633-42; CTIS: 2024-519564-41-00). The study was preregistered at clinicaltrials.gov (NCT05953038) and aspredicted.com (<https://aspredicted.org/gn3un.pdf>).

In both studies, participants were given information packs including an overview of their rights and the use of their data following telephone screening and before signing the consent forms. All research procedures were conducted in accordance with the Declaration of Helsinki (World Medical Association, 2025).

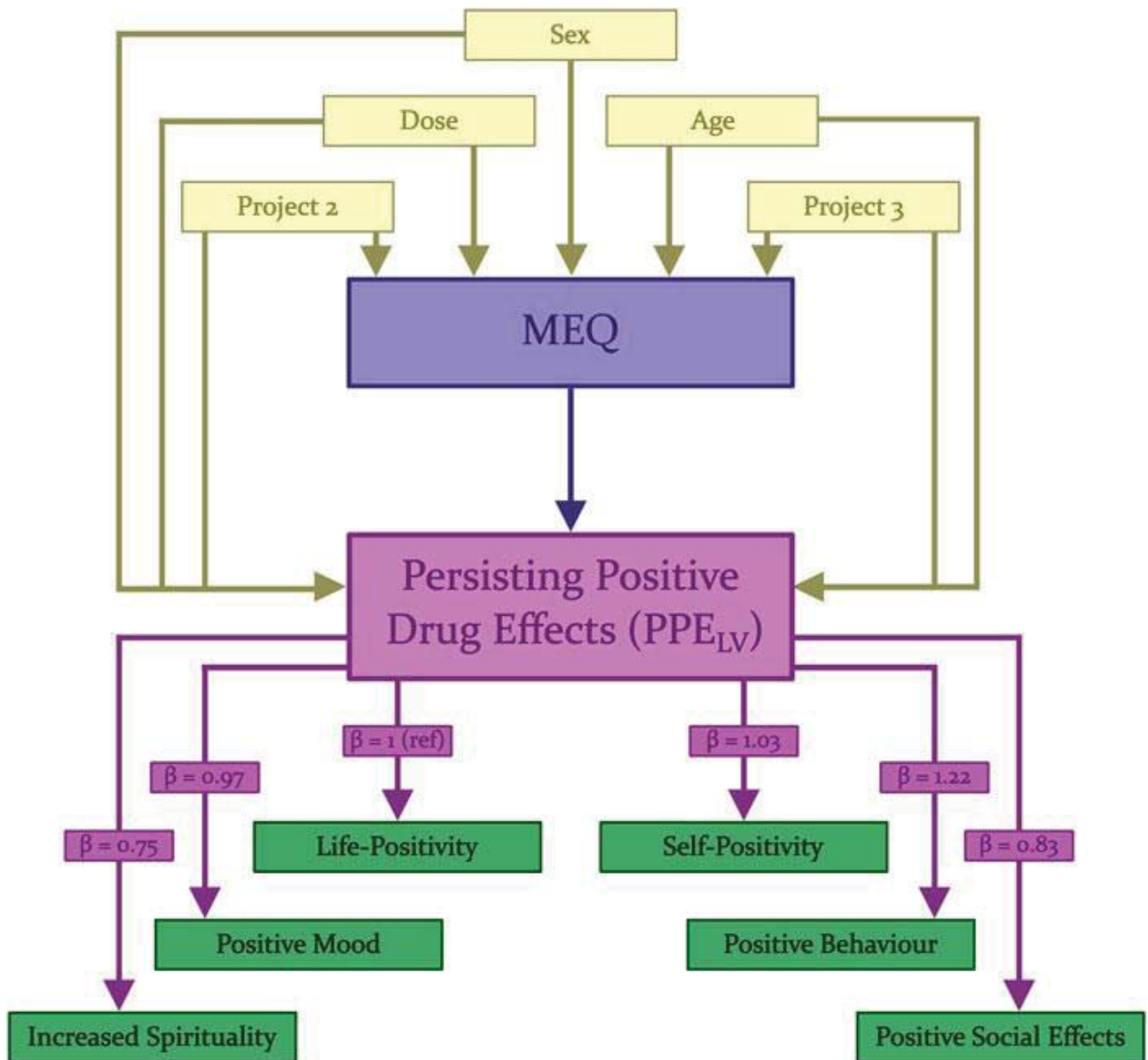


Figure 11 | Latent variable model applied in paper 2. Subscales of the persisting effects questionnaire (green boxes) are shown to load onto the latent variable PPE_{LV} by estimates shown in the boxes on the connecting lines. The effect of covariates (yellow boxes) on PPE_{LV} are assessed both directly and indirectly via modulation of MEQ (blue box). MEQ represents one of five inputs, each applied separately, the total MEQ score and each of the four subscales.

Results

In the following sections, a summary of the main results from papers 1-4 is presented. Full details are provided in each of the manuscripts (see Appendix).

Paper 1

In paper 1, we aimed to quantify the lasting effects of psilocybin on functional brain connectivity in 10 healthy individuals administered psilocybin in a comfortable research setting. We then evaluated whether these functional brain changes were associated with behavioural outcomes.

Baseline network functional connectivity was as expected, with high within-network connectivity and relatively lower between-network connectivity. At one-week follow-up scan, within-network connectivity (WNC) was reduced in the Executive Control Network (ECN) ($p_{FWE} = 0.010$, Cohen's $d_z = -1.73$). Further investigation revealed that ECN WNC was reduced in 9/10 participants, and across participants was reduced in 9/10 of the “edges” (Region-to-region connections) that make up the ECN. At three-month follow up this effect had largely returned to baseline ($p_{FWE} = 1$, Cohen's $d_z = -0.4$). No other network-connectivity estimates were statistically significantly affected at one-week or three-month follow-up (**Fig. 12**).

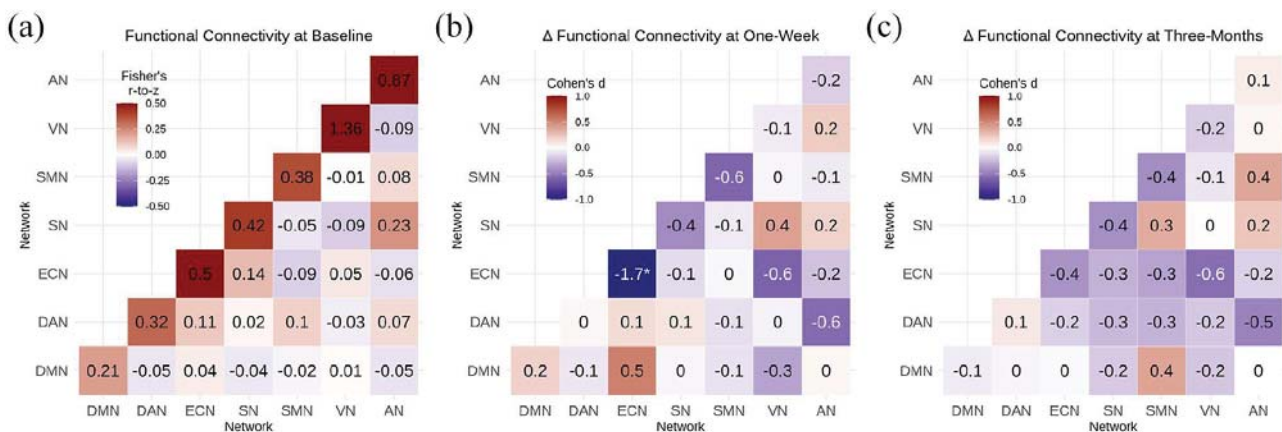


Figure 12 | Lasting effects of psilocybin on network connectivity. Three heatmaps showing within- (diagonal) and between- (off-diagonal) network connectivity scores, a) Connectivity scores (Fisher's r-to-z) during the baseline scan showing clear network structure. b) Cohen's d_z for the comparison between baseline and 1-week follow-up, c) Cohen's d_z for the comparison between baseline and three-month follow-up.

Our exploratory correlation analyses did not find any significant relationship between changes in ECN WNC and measures of the acute psychedelic experience. Participants who showed larger reductions in ECN WNC after one week demonstrated greater increases in mindfulness awareness (MAAS) scores at three months (r [95% CI] = -0.65 [$-0.91, -0.04$], $p_{\text{unc}} = 0.04$). Conversely, those with smaller reductions at the three-month mark also had greater MAAS increases (r [95% CI] = 0.71 [$0.15, 0.93$], $p_{\text{unc}} = 0.02$) (**Fig. 13**). We observed a trend suggesting that greater decreases in ECN WNC at one week were associated with higher positively valenced Persisting Effects Questionnaire (PEQ) scores at three months, though this did not reach statistical significance (Beta = -19.9 [$-41.7, 1.93$]; $p = 0.07$; units: change in Life Positivity PEQ per 0.1-unit change in ECN RSFC). Additionally, ECN disintegration measured at three months correlated with change in neocortex 5-HT_{2A}R binding at one-week compared to baseline (r [95% CI] = -0.67 [$-0.91, -0.06$], $p_{\text{unc}} = 0.01$).

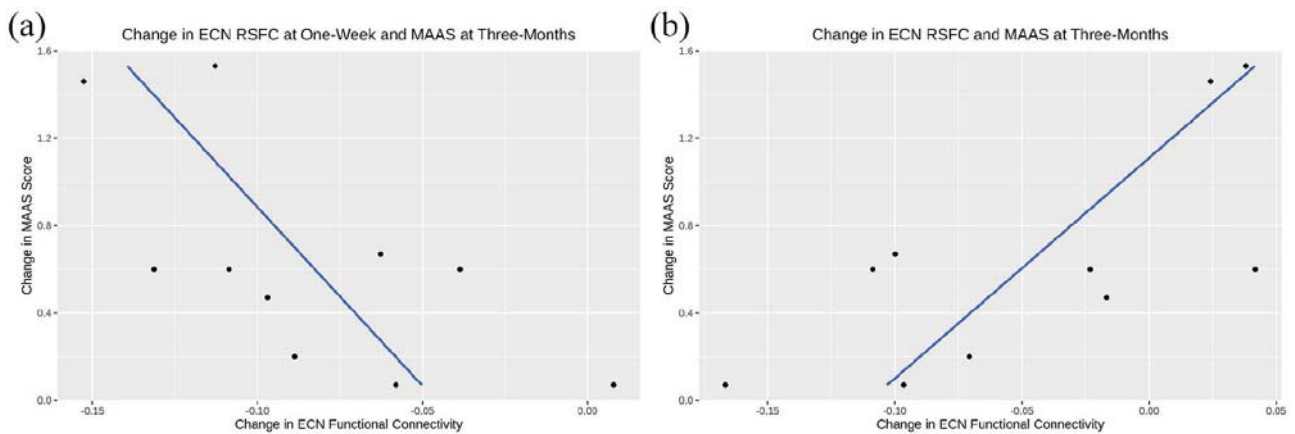


Figure 13 | Correlations between Executive Control Network functional connectivity changes and mindful attention and awareness scores. Correlations between ECN-WNC changes and MAAS score changes at three months post-intervention. (a) Negative correlation between ECN-WNC reduction at 1-week and increased MAAS scores at 3-months ($r = -0.65$ [95% CI: $-0.91, -0.04$], $p_{\text{unc}} = 0.04$). (b) Positive correlation between ECN-WNC changes and MAAS score increases at three months ($r = 0.71$ [95% CI: $0.15, 0.93$], $p_{\text{unc}} = 0.02$). ECN-WNC, Executive control network within-network connectivity; MAAS, mindful attention and awareness scale.

Paper 2

In paper 2, we evaluated the associations between psilocybin-induced MTE measured on the day of the experience with the MEQ and lasting behavioural outcomes as measured using a LVM of the PEQ (PPE_{LV}), measured at three-month follow-up. We also provide qualitative descriptions of these experiences. Participants received 19.4 ± 3.7 mg of psilocybin. 21 of the 35 experiences analysed met the threshold for complete mystical experiences (CME), i.e., scored more than 60% on all four subscales of the MEQ.

First, we compared those participants who had MTE vs those who did not meet the criteria. We found no effect of sex, age, baseline depression, stress or sleep-quality scores. We did not observe an effect of peak PPL on MTE or PPE_{LV} (Table 1).

Measure	All	CME	Non-CME	p value
Participants (no.)	28	16*	12*	NA
Psilocybin sessions (no.)	35	21	14	NA
Project 1 (PET) (no.)	4	1	3	0.31
Project 2 (no.)	10	7	3	0.21
Project 3 (MRI) (no.)	21	13	8	0.28
Female (%)	15 (43%)	8 (38%)	7 (50%)	0.50
Mean age (SD) (years)	31.7 (7.0)	30.8 (4.9)	33.1 (9.4)	0.45
Mean weight (SD) (kg)	72.4 (12.2)	75.5 (11.9)	72.7 (12.7)	0.44
Psychedelic Naïve (no. (%))	23 (66%)	14 (67%)	9 (64%)	0.89
Mean dose (SD) (mg)	19.4 (3.7)	19.3 (3.5)	19.5 (4.2)	0.80
Mean dose (SD) (mg/kg)	0.26 (0.04)	0.26 (0.04)	0.27 (0.04)	0.34
Mean baseline MDI	4.2 (2.4)	4.1 (2.6)	4.3 (2.2)	0.94
Mean baseline PSS	6.8 (3.8)	6.7 (3.6)	7.1 (4.1)	0.70
Mean baseline PSQI	3.7 (1.7)	3.3 (1.5)	4.3 (1.9)	0.18

Table 1 | Descriptive statistics for participants from paper 2. Data are presented as an overall cohort and split between those who had a complete mystical experience (CME) and those who did not. SD: Standard deviation, MDI: Major Depressive Inventory, PSQI: Pittsburgh Sleep Quality Index, PSS: Perceived Stress Scale, PET: Positron emission tomography, MRI: Magnetic resonance imaging, CME: Complete mystical experience.

Secondly, we showed a significant positive association between MEQ total score and PPE_{LV} ($\beta = 14.8$, $95\%CI = 8.66:20.96$, $p_{unc} = 3 \times 10^{-5}$) where β represents the increase in PPE_{LV} (rated from 0-100) per unit MEQ score (rated from 0-5). When examining individual MEQ subscales, we found significant positive associations between PPE_{LV} and both Positive Mood ($\beta = 14.5$, $95\% CI = 7.90:21.11$, $p_{corr} = 4.1 \times 10^{-4}$) and Mysticality ($\beta = 10.8$, $95\% CI = 6.14:15.51$, $p_{corr} = 2.0 \times 10^{-4}$). However, no significant associations were observed for the subscales Transcendence of Time and Space ($\beta = 9.4$, $95\% CI = -1.72:20.56$, $p_{corr} = 0.38$) or Ineffability ($\beta = 11.2$, $95\% CI = -2.75:25.14$, $p_{corr} = 0.45$) (**Fig. 14, Table 2**).

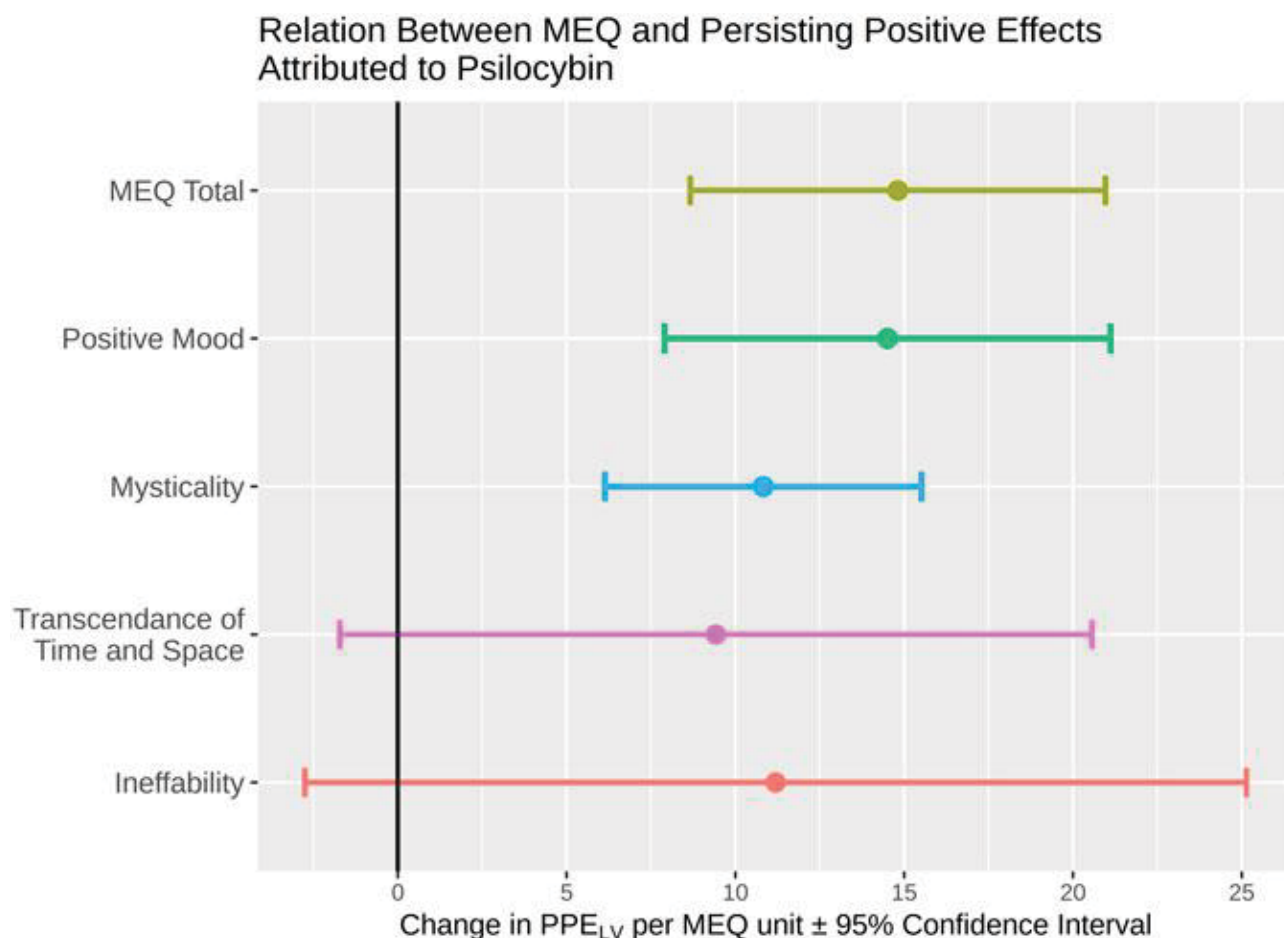


Figure 14 | Estimates of the relation between MEQ and Persisting Positive Effects. Each y-axis value represents either the Mystical Experience Questionnaire total score or each of the four subscales. The x-axis value represents the estimate for the relation between that scale and the latent variable PPE_{LV}, which represents the self-reported persisting positive effects of psilocybin measured three months after administration. MEQ, Mystical Experiences Questionnaire; PPE_{LV}, Persisting Positive Effects Latent Variable.

Variable	β	95% CI	p-value	p-value (corrected)
MEQ total	14.8	8.66:20.96	3.0×10^{-5}	3.0×10^{-5}
Positive Mood	14.5	7.90:21.11	1.0×10^{-4}	4.1×10^{-4}
Mysticality	10.8	6.14:15.51	5.1×10^{-5}	2.0×10^{-4}
Transcendence of Time and Space	9.4	-1.72:20.56	0.094	0.377
Ineffability	11.2	-2.75:25.14	0.111	0.446

β and 95% CI indicate effect size and 95% confidence interval in units of the latent variable PPE_{LV} which represents persisting positive effects attributable to the drug experience as a % of maximum possible score.

Table 2 | Statistical description of the associations between MEQ and PPE_{LV}. Descriptive text is directly from the original publication.

The natural language processing of open-form reports revealed that the most frequently used words unique to CME were “Universe”, “dad”, “MR” (Magnetic Resonance), “beautiful”, “simultaneous”, “infinite”, “purple”, “in relation to”, “ray”, “happy”, and “brother” (**Fig. 15**). Manual searching confirmed that these were not driven by a single report in any case. The most frequently used words unique to non-CME reports were “gloomy”, “cycle”, “evil”, “cold” and “need”; most of these, except “gloomy”, were driven by one or two reports only.

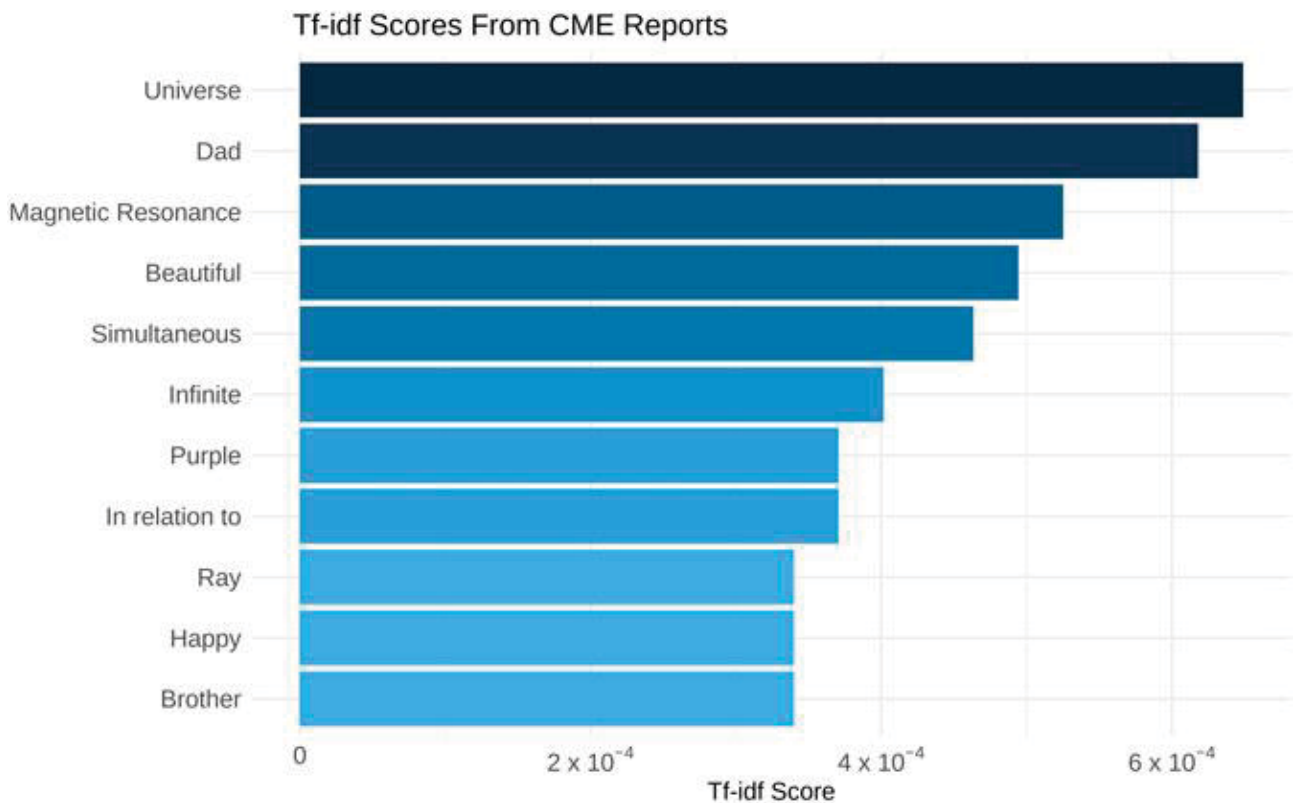


Figure 15 | Natural-language processing results from complete mystical experiences. The x-axis value indicates the term-frequency inverse document frequency score for each word, for reports from complete mystical experiences.

In context, the word “Universe” referred to feelings of connectedness, aligning with MEQ item 14 “, Freedom from the limitations of your personal self and feeling a unity or bond with what was felt to be greater than your personal self”

The light of love brings clarity to everything. I get a deep feeling of purity and feel that everything is beautiful, and that love is what makes up the world and the universe and connects everything like a network of roots.

Report 22, female, CME, MEQ total 3.9 (out of 5)

The word “Dad” was used to describe connectedness and love for the participants’ fathers, as in the below quote and accompanying drawing. The word “mother” was present in both CME and non-CME reports, but the word “father” was not found in non-CME reports. There are no allusions to feelings of connection to family in the MEQ.

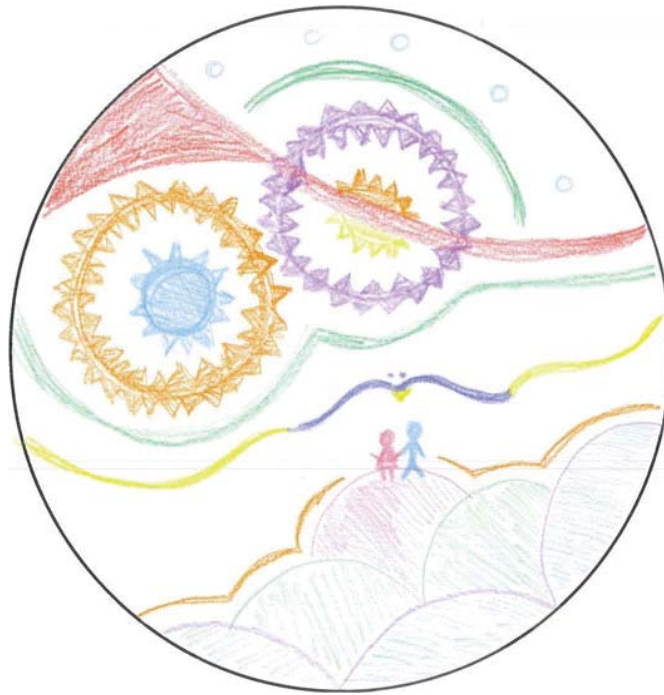


Figure 16 | Participant’s drawing of their experience - Report 6

I had the feeling that I was experiencing the world through myself as a little girl holding her dad’s hand. My dad and I were observing what was happening around us. I think we saw something that resembled beautiful nature and charming castles.

Report 6, female, CME, MEQ total 3.9

21 of the 35 experiences were largely undertaken within an MRI scanner. One participant reported synesthetic experience due to the MR sounds, and several described a feeling of connectedness with the scanner echoing MEQ item 6, “Experience of oneness or unity with objects and/or persons perceived in your surroundings.”

The sounds from the MR scanner each cast a specific hue, with high-frequency tones giving a yellowish tinge and low-frequency tones having a purple tinge.

Report 22, female, CME, MEQ total 3.9



Figure 17 | Participant’s drawing of their experience - Report 32

I felt a sense of no longer being connected to my own body. The MRI scanner and I stepped into a different reality together. With colours, and shapes, and figures.

Report 32, female, CME, MEQ total 4.7, see Figure 6

The word “beauty” referred in several cases to perceptual effects which are not captured by the MEQ but also to reflections on human nature and the depths and complexities of human conscious experience. In some cases, these echo MEQ item 27, “sense of awe or awesomeness”.



Figure 18 | Participant’s drawing of their experience - Report 15

My inner vision became the universe, filled with colourful waterfalls, glistening like stars, not bound by gravity. They floated in the air and folded around each other. Totally quiet. The streams were infinite and beautiful.

Report 15, female, CME, MEQ total 3.5

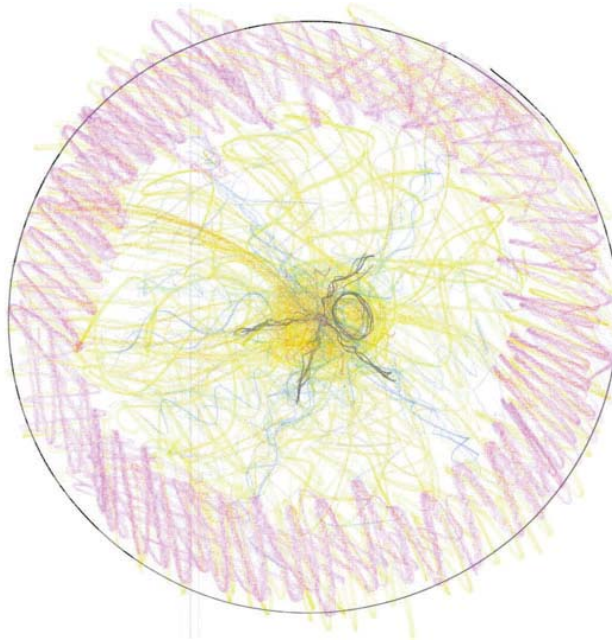


Figure 19 | Participant's drawing of their experience - Report 3

The feeling of joy and love was the energy in the universe, completely intense and multiplied by 100. It was like taking those two emotions and concentrating them, to have them in their purest form without any worries or other troubles that can come with everyday reality. Everything else ceased to matter while those two emotions were so pure—they made everything incredibly beautiful. When I was soaring through the soundwaves with this energy, I could see all the people close to me in my life appear. My partner, my sister and her boyfriend and their new-born son, my mother, my amazing friends. I felt immensely privileged to be part of this universe/community, to be able to feel those feelings in such a pure form, to have such deep emotions in my body—and I was overwhelmed with gratitude for this world. That everything simply is. And with that I was overtaken by a desire to protect it all, to show the world how beautiful it is and to take care of it.

Report 3, female, CME, MEQ total 3.9

The word “simultaneous” frequently reflects that some participants felt like they had several experiences occurring at the same time, sometimes complementary and sometimes contradictory.

In my thoughts, mentally, physically, and bodily. I desire the togetherness of being a pair, but simultaneously I feel a togetherness with the whole world and all people.

Report 12, male, CME, MEQ total 4.9

From the non-CME reports, the word “gloomy” was often in reference to their dislike of certain songs that were played during their experience.

The physical insecurities I have about myself and the gloomy music made me feel uneasy.

Report 7, female, non-CME, MEQ total 2.8

Paper 3

In paper 3, we evaluated the acute brain effects of psilocybin in healthy volunteers using functional MRI. Analyses focused on 13 metrics of brain-entropy that had previously been reported in the context of psychedelic administration.

The previous metrics can be considered as belonging to one of three groups. Group A metrics evaluate the entropy of the static connectivity matrix. Three of these, Out-Network Connectivity Distribution, Degree Distribution and Von Neumann Entropy, were not associated with PsiFx (**Fig. 24**). Path-length distribution, a measure of the distribution of path-lengths across the whole brain, was significantly positively weak-to-moderately associated with PsiFx at the a priori defined threshold producing a mean degree of 27 (Pearson's $\rho = 0.39, 0.27$, and 0.23 for PPL, Occ_{2A} and SDI, respectively) as well as exploratory extra degrees from 22 to 38 inclusive.

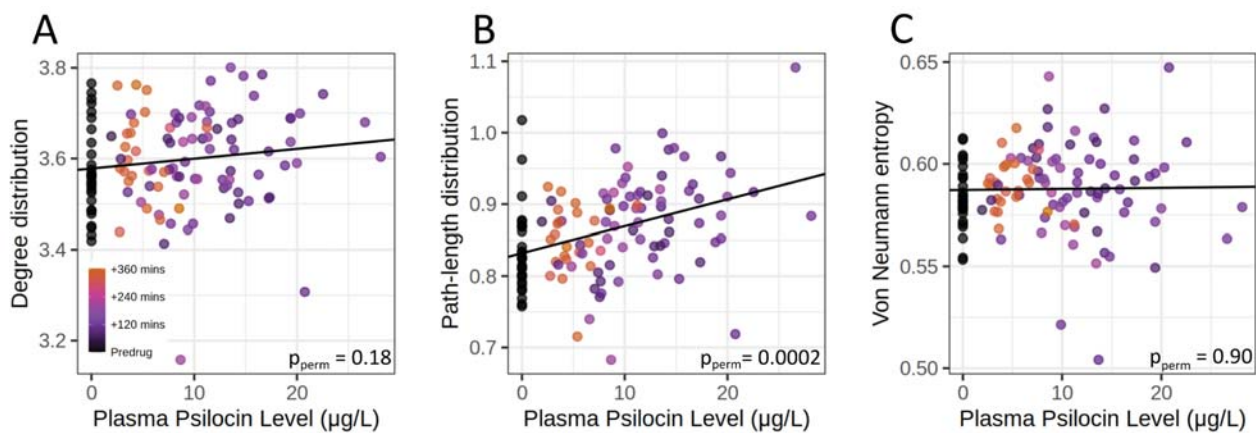


Figure 20 | Relations between plasma psilocin levels and whole-brain static connectivity entropy measures. Points are coloured according to time after administration such that black dots represent pre-drug scans, purple represent upslope and peak drug scans, and orange represent scans once participants were mostly sober again. Y-axis values are adjusted for covariates: subject, age, sex, scanner, and motion. P_{perm} values refer to the correlation with PPL.

Group B metrics evaluate the entropy of dynamic or time-varying connectivity. Four of these, Intra-network Synchrony Distribution, Motif-connectivity Distribution, LEiDA-state Markov-rate and Integration/Segregation-state Distribution, were not significantly associated with PsiFx (**Fig. 21**). Meta-state Complexity, a measure of the complexity of the timeseries of brain-states, was weakly associated with Occ_{2A} and SDI, but not PPL (Pearson's $\rho = 0.22, 0.33$, and 0.20 , respectively). DCC Distribution, a measure of the width of distribution of connectivity strengths across time within and between given network edges (e.g., Default-Mode to Frontoparietal Networks), was positively moderate-to-strongly associated with PsiFx across 35/36 network edges (Rho range: 0.35 to 0.78 ; $18/36$ $p_{\text{FWER}} < 0.0001$, $29/36$ $p_{\text{FWER}} < 0.001$, $35/36$ $p_{\text{FWER}} < 0.05$) (**Fig. 22**).

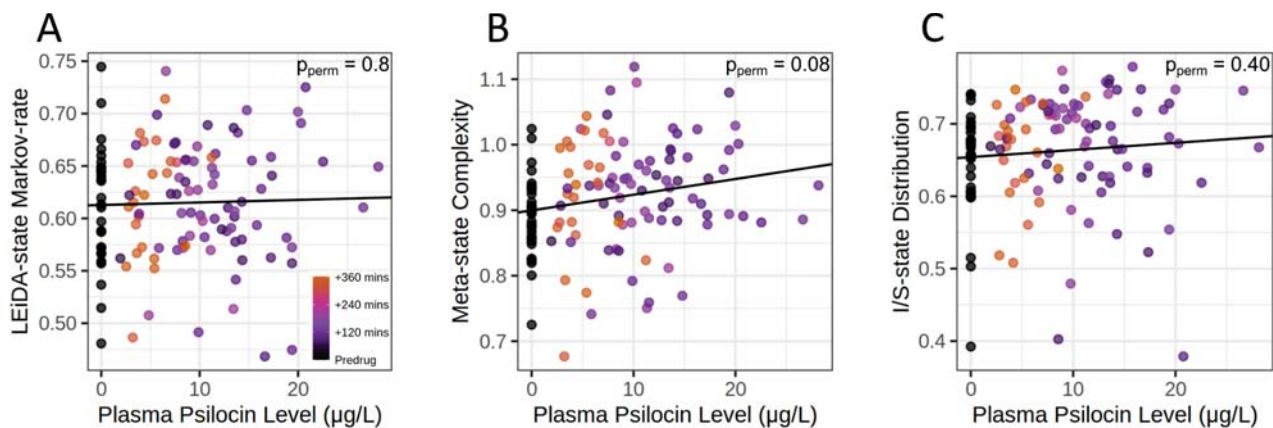


Figure 21 | Relations between plasma psilocin levels and whole-brain dynamic connectivity entropy measures. Points are coloured according to time after administration such that black dots represent pre-drug scans, purple represent upslope and peak drug scans, and orange represent scans once participants were mostly sober again. Y-axis values are adjusted for covariates: subject, age, sex, scanner, and motion. P_{perm} values refer to the correlation with PPL.

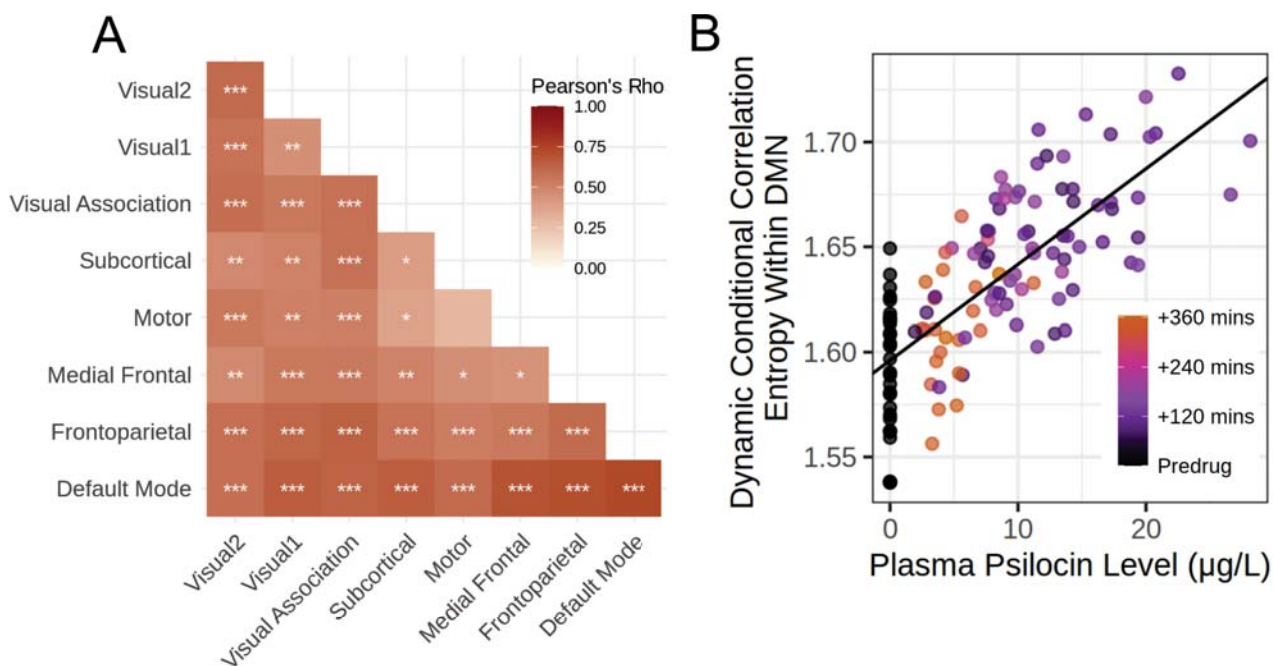


Figure 22 | Relation between plasma psilocin level and dynamic conditional correlation distribution. A) Heatmap of Pearson's correlation values for each within and between network pair *** represents $p_{FWER} < 0.0001$, ** $p_{FWER} < 0.001$, and * $p_{FWER} < 0.05$ for associations with PPL. B) A scatter plot showing the relation between DCC distribution and plasma psilocin level for one of the strongest network edges, which was within the default-mode network. (Rho = 0.74). Y-axis values are adjusted for subject, age, sex, MR scanner and motion.

Group C metrics evaluate the entropy of the timeseries themselves. Sample entropy is a measure of the regularity of a timeseries. We evaluated sample entropy across five scales by down-sampling the timeseries by taking the mean across non-overlapping windows of length s . At $s = 1$ (not downsampled), sample entropy was positively associated with PsiFx across most networks, with $P_{\text{FWER}} < 0.05$ in 7/17 networks. At $s = 2, 3$, and 4, there was no association with PsiFx, but at $s = 5$, sample entropy was significantly negatively associated with PsiFx in 14/17 networks. Scale 1 associations were weak to moderate (Rho range: 0.26 to 0.47), as were Scale 5 associations (Pearson's rho range: -0.27 to -0.49) (**Fig. 23**). Lempel-Ziv complexity is evaluated either by concatenating the regional time-series end-to-end (LZc-temporal) or across all regions at each timepoint (LZc-spatial). LZc-spatial was not associated with PsiFx. LZc-temporal, a measure of the complexity of the BOLD signal across time, was significantly but weakly associated with Occ_{2A} (Rho = 0.23) and SDI (Rho = 0.3) but not PPL ($p_{\text{perm}} = 0.14$) (**Fig. 24**).

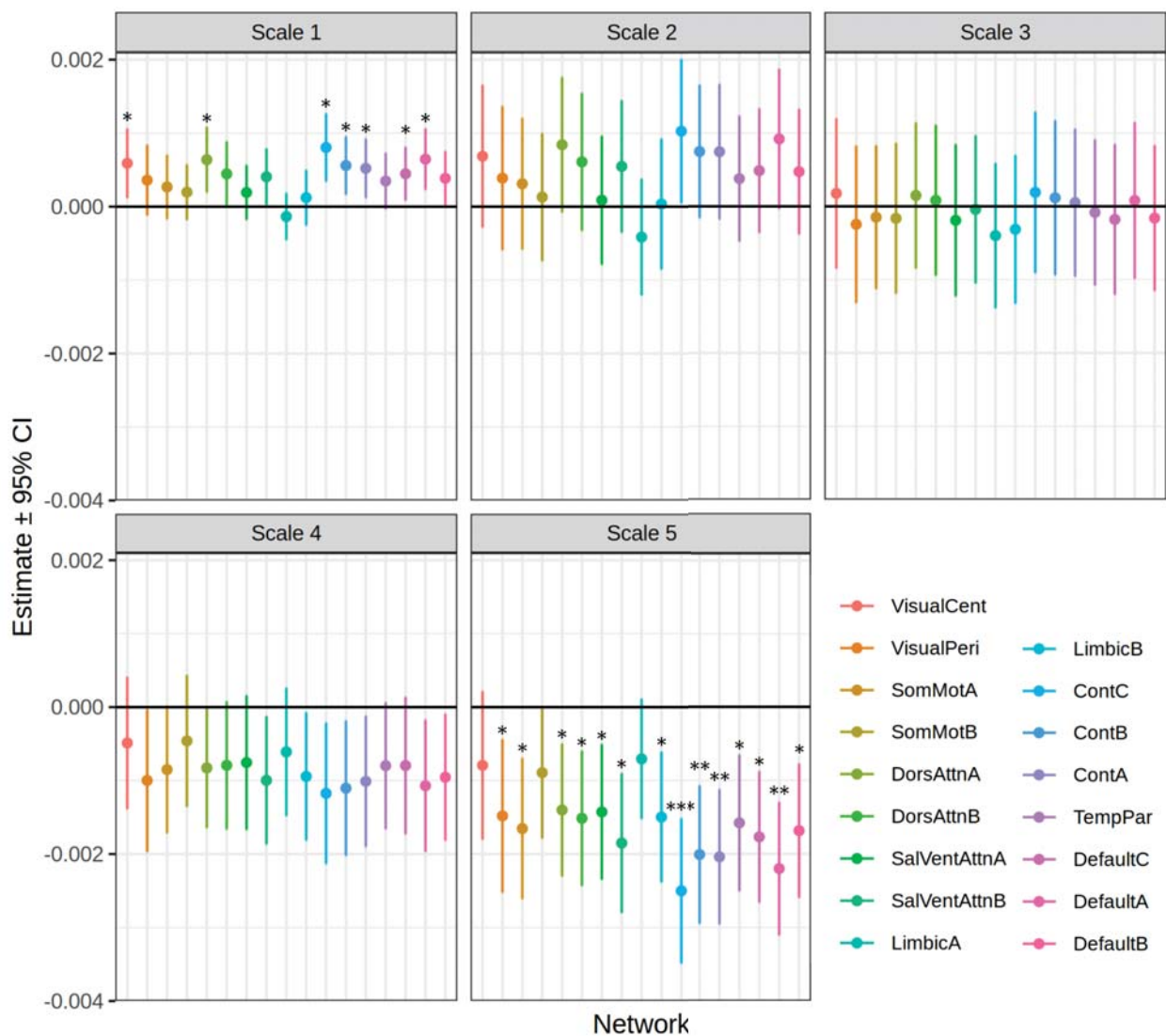


Figure 23 | Relation between plasma psilocin and multi-scale sample entropy. Forest plots describing the estimate and 95% confidence intervals for the relation between sample entropy and plasma psilocin level. Colours represent brain networks from the Yeo atlas, and each subplot represents a different temporal scale from 1-5. *** $p_{\text{FWER}} < 0.0001$, ** $p_{\text{FWER}} < 0.001$ and * $p_{\text{FWER}} < 0.05$ for associations with PPL.

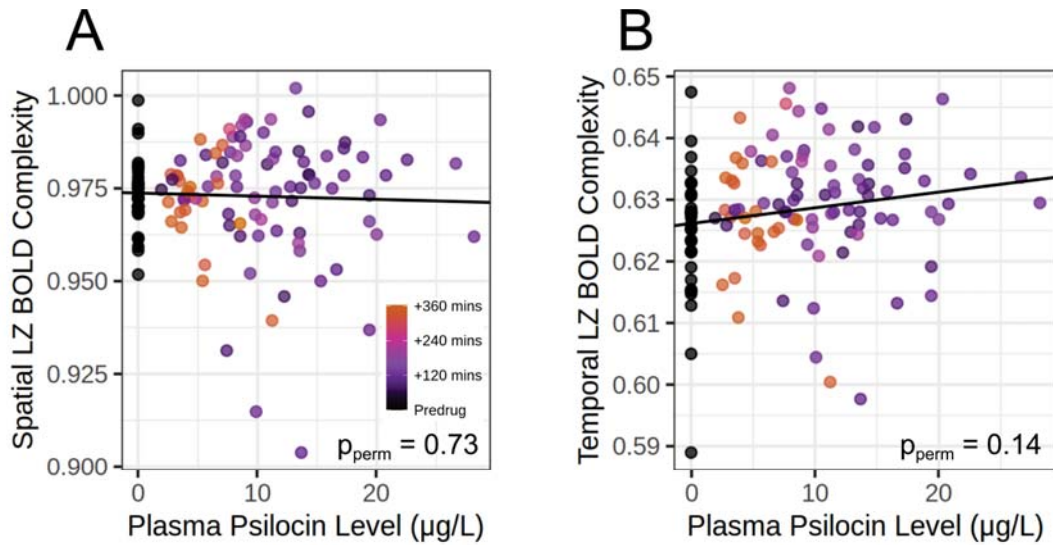


Figure 24 | Relations between plasma psilocin levels and whole-brain Lempel-Ziv complexity measures. Points are coloured according to time after administration such that black dots represent pre-drug scans, purple represent upslope and peak drug scans, and orange represent scans once participants were mostly sober again. Y-axis values are adjusted for covariates: subject, age, sex, scanner, and motion. P_{perm} values refer to the correlation with PPL.

All entropy metrics presented above were evaluated using the same parcellation as in the original paper that evaluated their effects in the context of psychedelics. To evaluate the effect of parcellation, all metrics were reevaluated using a common parcellation, i.e., 100 cortical regions from the Schaefer parcellation (divided into 7 networks) combined with 16 subcortical regions from the Tian atlas. Consistent with previous results, we observed significant associations with PsiFx for path-length distribution (mean degrees 31-38), DCC distribution across most network edges, and sample entropy without downscaling.

To explore the effect of different preprocessing strategies on each entropy metric, the analyses were re-run across six different pipelines, using the common atlas. These included adding global-signal regression (GSR), removal of the lowpass (0.09Hz) filter, narrowing the bandpass filter (0.03-0.07 Hz), increasing the number of motion parameter regressors from 12 to 24, omitting scrubbing, and increasing the strictness of the scrubbing threshold from $z > 4$ SDs, motion > 2 mm to $z > 3$ SDs, motion > 0.5 mm. With regard to the relation with PsiFx, path-length distribution was unaffected across most pipelines except when adding GSR. DCC was also consistent across most pipelines except those related to alterations in the filtering strategy. Specifically, the narrow bandpass filter removed any association with PsiFx, and the removal of the lowpass filter flipped the sign to a weak negative association in a few sparse network pairs. Sample entropy was consistent across variations in scrubbing, but the effect was largely eradicated following GSR, alterations in filtering and the addition of extra motion regressors.

As the data in this experiment were collected on two different scanners with different scanning parameters, we constructed additional models to evaluate the effect of scanner on the interaction between each entropy metric and PsiFx. There was a significant effect of scanner on the relation between path-length distribution and PsiFx, such that the effect for one scanner was strong, and close to zero for the other. There was also an

effect for sample entropy at scale 5, but for both scanners, there were still a significant negative association. There was no moderating effect of scanner for DCC entropy.

To evaluate the relation between these entropy measures, the correlation across all whole-brain metrics was estimated, as well as their relation to motion. After correction for multiple comparisons, certain entropy quantification pairs showed significant relations, but there was no clear theme across metrics. Positive associations were found between Motif Connectivity Distribution with a window length of 100 & Von-Neumann, LEiDA state & Von-Neumann, Path-length distribution & Degree-distribution, LZc-spatial & Von Neumann, and LZc-spatial & LZc-temporal. Negative relationships were observed between Degree-distribution & Von Neumann, Degree-distribution & LEiDA state, Path-length distribution & Von-Neumann, and Path-length distribution & LEiDA state. Additionally, LZc-spatial was significantly negatively associated with motion (**Fig. 25**).

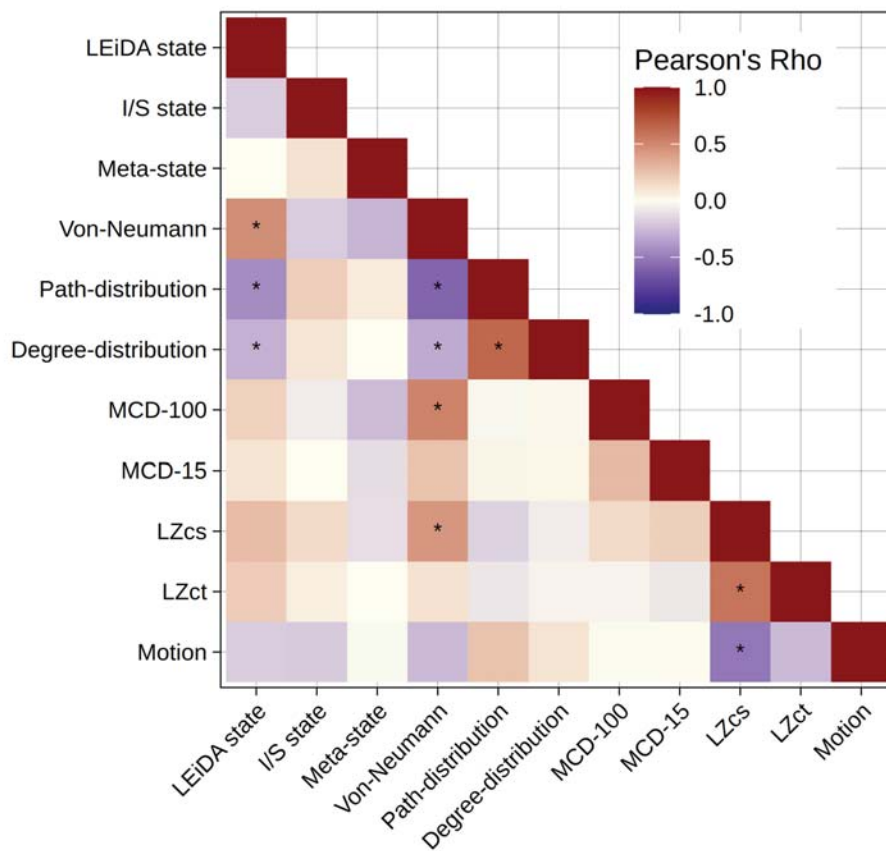


Figure 25 | Relation between brain-entropy metrics. Heatmap showing Pearson's Rho correlations between each of the whole-brain entropy metrics and motion. *, $P_{FWE} < 0.05$.

Paper 4

In paper 4, we aimed to evaluate the occupancy of LSD at the 5-HT_{2A}R using [¹¹C]Cimbi-36 PET imaging, while simultaneously assessing functional brain effects using BOLD fMRI and hemodynamic effects using arterial spin-labelling and time-of-flight angiography. For the purpose of this thesis, I will omit detailed reporting of the hemodynamic effects (i.e., cerebral blood-flow and internal carotid artery diameter and flow), as they were mostly performed by my co-first author, Kristian Larsen.

Eleven healthy volunteers were administered a single oral dose of LSD between 25 and 200 µg freebase equivalent. Participants generally tolerated LSD well, with no severe adverse effects. One participant experienced nausea throughout the session and thus did not undergo any intervention scans. One other participant experienced significant anxiety during their intervention scan, and thus, the scan was terminated before data could be collected. Furthermore, scanner malfunctions resulted in data from one peak scan and one late scan being lost. Therefore, we ultimately collected 11 scans at baseline, seven during peak LSD effects two of whom also received scans during late-phase LSD effects. Plasma LSD levels peaked approximately 90 minutes after administration (**Fig. 26A**) and subjective drug intensity ratings peaked 30 minutes after that (**Fig. 26B**). By plotting concurrent SDI against PPL over time on a single-subject level (**Fig. 26C**) we were able to observe a clear anti-clockwise hysteresis effect in 10/11 participants such that during the early phase, SDI ratings were relatively lower for a given PPL than during the post-peak phase.

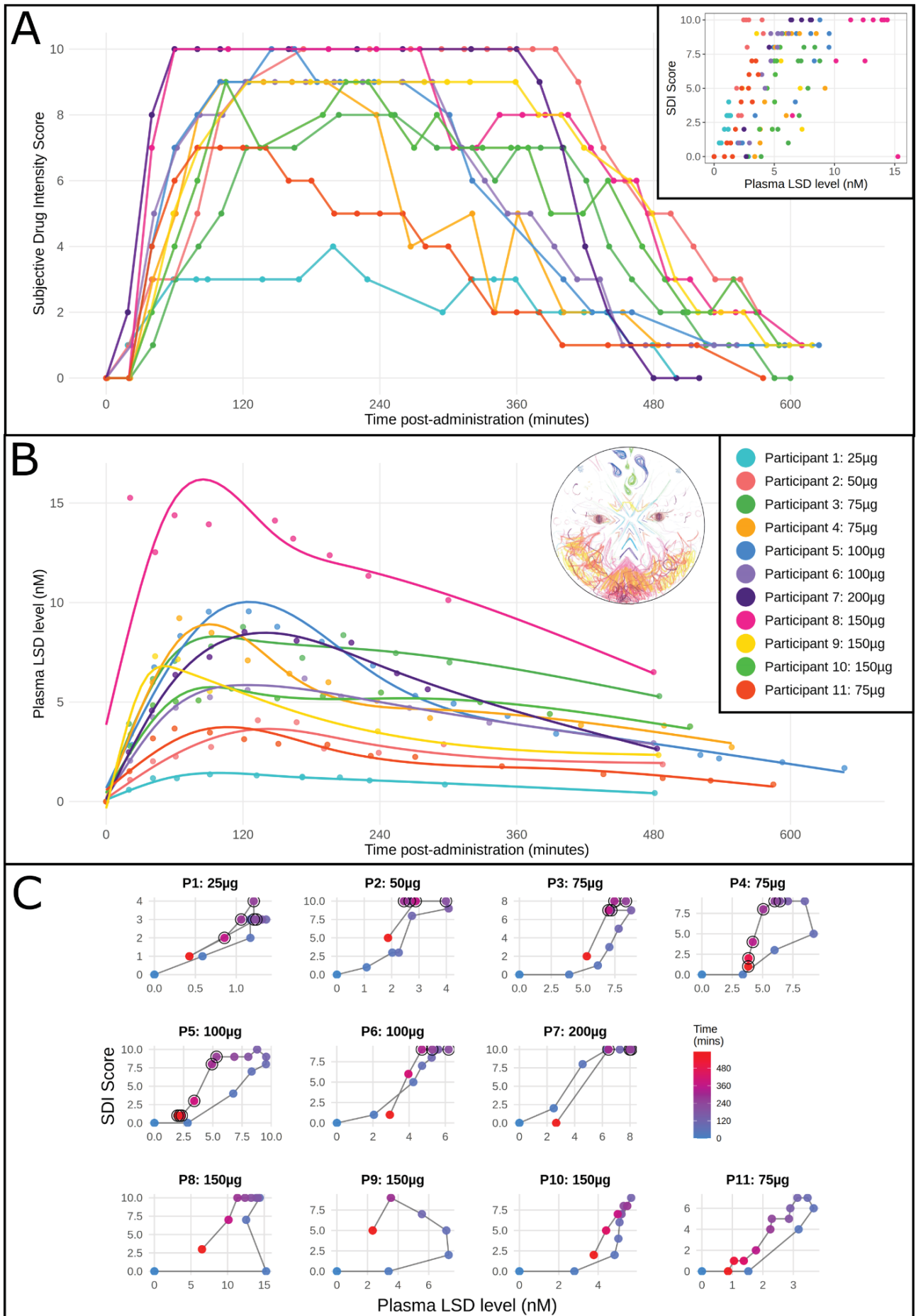


Figure 26 | Subjective and Pharmacokinetic Effects of LSD A) Temporal profile of Subjective Drug Intensity (SDI) ratings (scale 0-10) from individual participants following LSD administration (25-200µg). The inset graph shows the relation between concurrent SDI and plasma LSD concentration measures. B) Plasma LSD concentration measurements over time after administration (t=0), with spline curve fitting. Inset features a representative illustration of the LSD experience drawn by participant 8. C) Individual subject SDI versus plasma LSD concentration (PPL) hysteresis plots. Thin black lines chronologically connect data points, which are colour-coded by time (minutes after LSD intake). Black-outlined circles indicate measurements taken during PET scanning. Participants 4 and 5 underwent two PET scans during LSD effects. All participants except P7 demonstrate an anticlockwise hysteresis pattern.

All participants had normal [¹¹C]Cimbi-36 BP_{ND} values during the baseline scan (mean ± SD = 1.11 ± 0.26). For representative baseline and intervention images from the highest and lowest administered doses, see **Fig. 27A**. Observed reductions in BP_{ND} following LSD were converted to receptor occupancy percentages (Table 3). We fit a Hill-Langmuir (E_{max}) model to the occupancy and average plasma LSD level from during each scan and calculated confidence intervals on the parameters using a bootstrap technique. This model described the data well (R² = 0.60) and estimated an IC₅₀ (the plasma concentration at which we estimate 50% occupancy at the 5-HT_{2A}R) of 1.93 nM (95% CI: 0.53-2.79 nM) and maximum occupancy (Occ_{max}) of 97.4% (95% CI: 75.3-100%) (**Fig. 27B**). When evaluating a similar model comparing body-weight adjusted dose with occupancy the model also fit the data well (R² = 0.75), with an ED₅₀ (the dose at which we estimate 50% occupancy of the 5-HT_{2A}R) of 0.41 µg/kg (95% CI: 0.17-0.54 µg/kg) and Occ_{max} of 98.7% (95% CI: 80.3-100%). Using a sigmoidal fit, we show a relation between peak occupancy and within-scan SDI ratings (**Fig. 27C**, R² = 0.87).

	LSD dose μg	Cmax nM	Peak Scan				Late Scan			
			Time post-dose min	[LSD] nM	SDI a.u.	Occupancy	Time post-dose min	[LSD] nM	SDI a.u.	Occupancy
1	25	1.37	175	1.23	3.0	48%				
2	50	4.08	164	3.32	10.0	42%				
3	75	8.77	175	7.22	7.5	75%				
4	75	9.21	161	6.43	8.5	85%	420	3.84	1.5	74%
5	100	9.56	271	5.31	8.0	67%	522	2.25	1.0	12%
6	100	6.19	167	6.19	9.0	73%				
7	200	8.52	168	8.08	10.0	83%				
8	150	15.26								
9	150	7.30								
10	150	5.67								
11	75	3.67								

Table 3 | LSD pharmacokinetics and 5-HT_{2A}R occupancy. LSD dose, plasma concentrations, PET scan timing, subjective drug intensity (SDI), and receptor occupancy data for each participant. Peak and late timepoint measurements are shown where available. No intervention PET scans were collected for Participants P8-11. SDI rated 0-10 (no effects to very strong effects). Receptor occupancy measured using [¹¹C]Cimbi-36 PET. Time post-LSD indicates minutes between administration and radiotracer injection.

Two participants received late scans. One participant was administered 75 μg and received scans starting 161 minutes (peak scan) and 420 minutes (late scan) after LSD administration. At peak, we observed 84% receptor occupancy, 6.43 nM plasma LSD, and they rated an average of 8.5/10 SDI. At the late scan, we observed 74% receptor occupancy, 3.84 nM plasma LSD and an average of 1.5/10 SDI. This scan implies continued receptor occupancy in the absence of subjective drug effects. The other participant received 100 μg of LSD with scans starting 271 minutes (peak) and 522 minutes (late scan) after LSD administration. At peak scan, we observed 67% receptor occupancy, 5.31 nM plasma LSD and an average rating of 8.5/10 SDI. At late scan, we observed 12% receptor occupancy, 2.25 nM plasma LSD, and minimal subjective effects (SDI rating: 1/10). This scan suggests that receptor binding eventually returns to near-baseline levels (**Table 3**).

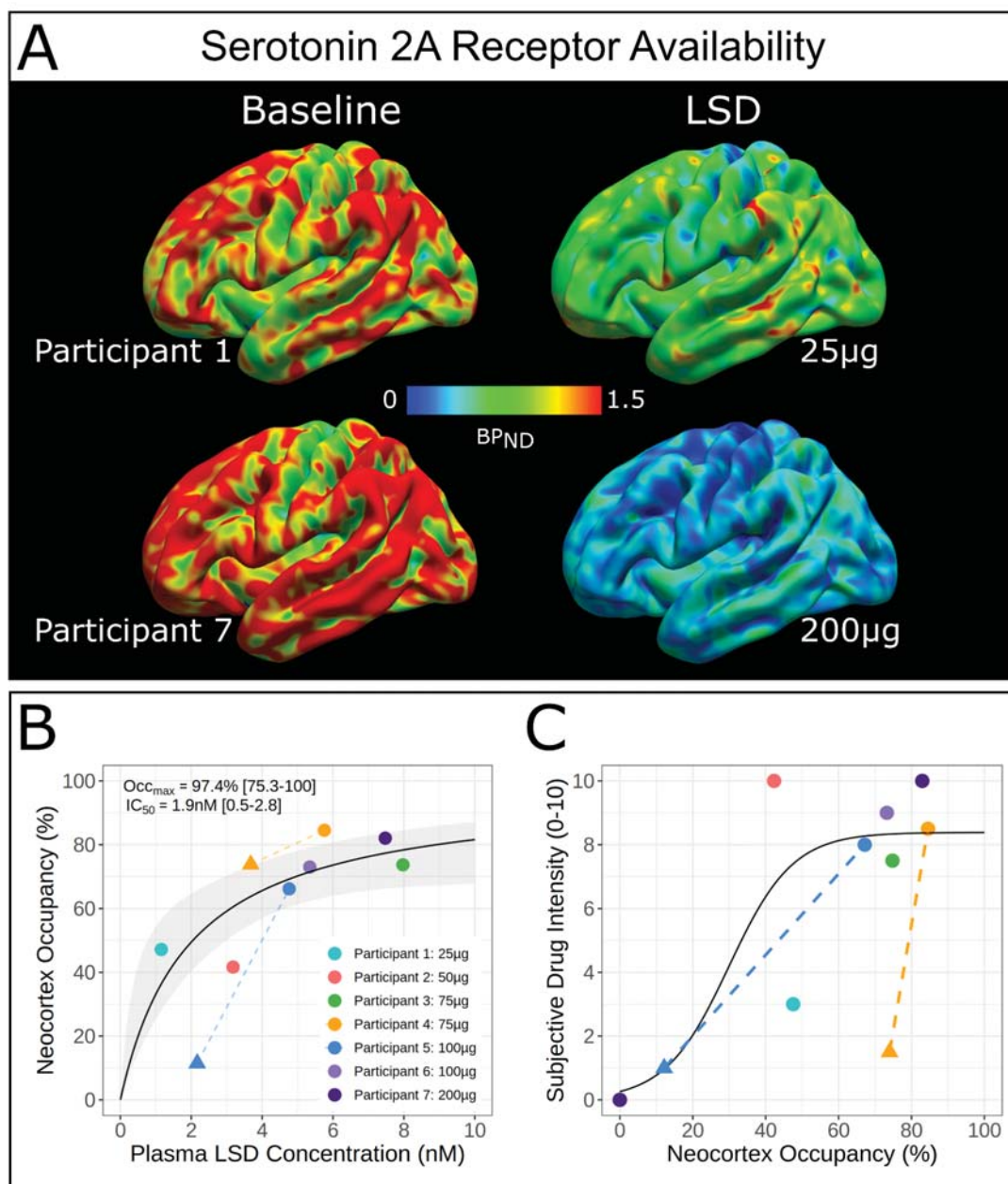


Figure 27 | Serotonin 2A receptor occupancy by LSD measured with [¹¹C]Cimbi-36 PET.

A) Cortical [¹¹C]Cimbi-36 nondisplaceable binding potential (BP_{ND}) maps at baseline and peak LSD for 25 μ g (top) and 200 μ g (bottom) doses. B) Plasma LSD concentration versus receptor occupancy with Hill-Langmuir model fit (95% confidence intervals in grey). Circles show peak scans; triangles show late scans. C) Receptor occupancy versus subjective drug intensity with sigmoid function fit. Colours represent individual participants (n=7 for peak scans, n = 2 for late scans). Models in B and C are fit using peak scans only.

Comparing the LSD scan to the mean baseline global correlation (GCOR) map revealed decreases in GCOR across most of the cortex, with numerically decreased GCOR in all brain networks defined by the Yeo-17 network parcellation. The areas defined by the Schaefer-Tian atlas with the largest effect sizes were in regions assigned to the central and peripheral visual cortex networks (Average effect size of regions assigned to Central: Cohen's $d_z = -0.43$, Peripheral: $d_z = -0.40$) and in regions assigned to dorsal-attention B (Average $d_z = -0.53$), temporal-parietal (Average $d_z = -0.64$) and default-mode networks A and C (Average A: $d_z = -0.48$; C: $d_z = -0.43$) (**Fig. 28A**). Changes in regional GCOR scores following LSD were negatively associated with both regional changes in cerebral-blood flow following LSD (**Fig. 29A, C**), and neocortical occupancy across most of the cortex (**Fig. 29A, D**). Effects on thalamocortical connectivity were more limited except a bilateral increase in connectivity with primary somatomotor regions (**Fig. 28B**). Effects on static network connectivity showed no consistent effect on within-network connectivity but a general decrease in between-network connectivity especially between the two visual networks and the rest of the brain (**Fig. 28C**). DCC distribution showed negligible to small increases across most network edges (**Fig. 28D**). Sample entropy was increased with a large effect size in visual (central: $d_z = 1.02$; peripheral: $d_z = 0.94$), control (B: $d_z = 0.97$; C: $d_z = 0.96$) and dorsal attention networks (A: $d_z = 1.02$) (**Fig. 28E**). We also evaluated the effect on sample entropy on temporally downsampled signals but effect sizes tended towards zero as scale increased. Similarly, Normalised Spatial Complexity was moderately increased in control A and B ($d_z = 0.77$; $d_z = 0.72$) and limbic A and B networks ($d_z = 0.75$; $d_z = 0.67$) as well as globally ($d_z = 0.55$) (**Fig. 28F, G**). LZc-temporal showed only a small increase ($d_z = 0.40$), and the geodesic (path-length) distribution was very slightly decreased ($d_z = -0.12$). Graph-theory measures were negligibly affected with slight increases in small-worldness ($d_z = 0.22$) and decreases in modularity ($d_z = -0.13$) (**Fig. 28G**).

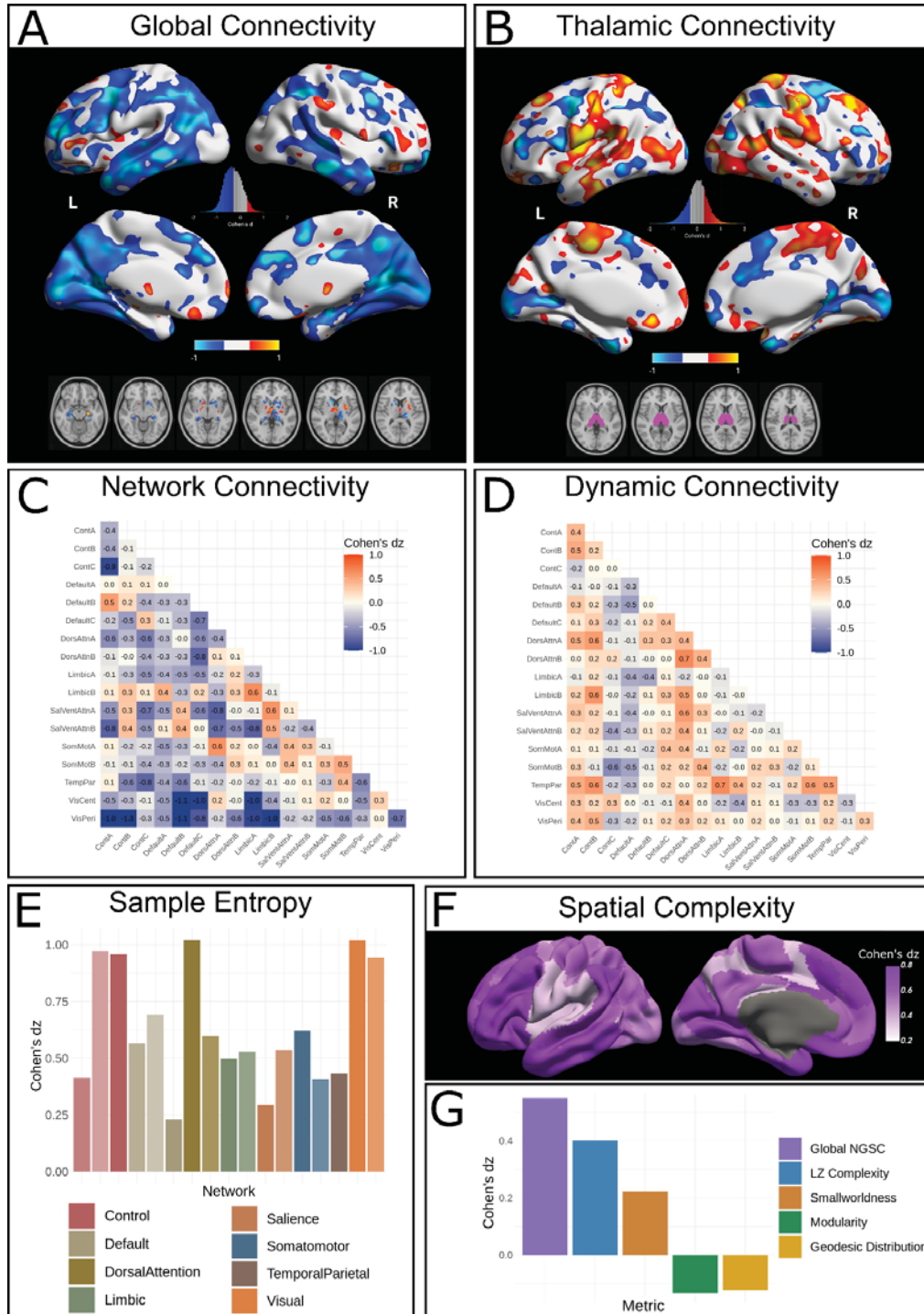


Figure 28 | fMRI-measured brain effects of LSD. A) A surface projection of voxel-wise global connectivity changes (blue=decreased, orange=increased) with subcortical effects below. B) A surface projection of voxel-wise thalamo-cortical connectivity alterations with the seed region highlighted in pink. C) Static network-to-network connectivity effect sizes across Yeo 17 networks. D) Dynamic correlation distribution changes within and between networks. E) Sample entropy alterations within individual brain networks. F) Normalised Spatial complexity changes across the cortex. G) Effect sizes of global metrics including temporal Lempel-Ziv complexity, small-worldness, modularity, and geodesic distribution (n=7).

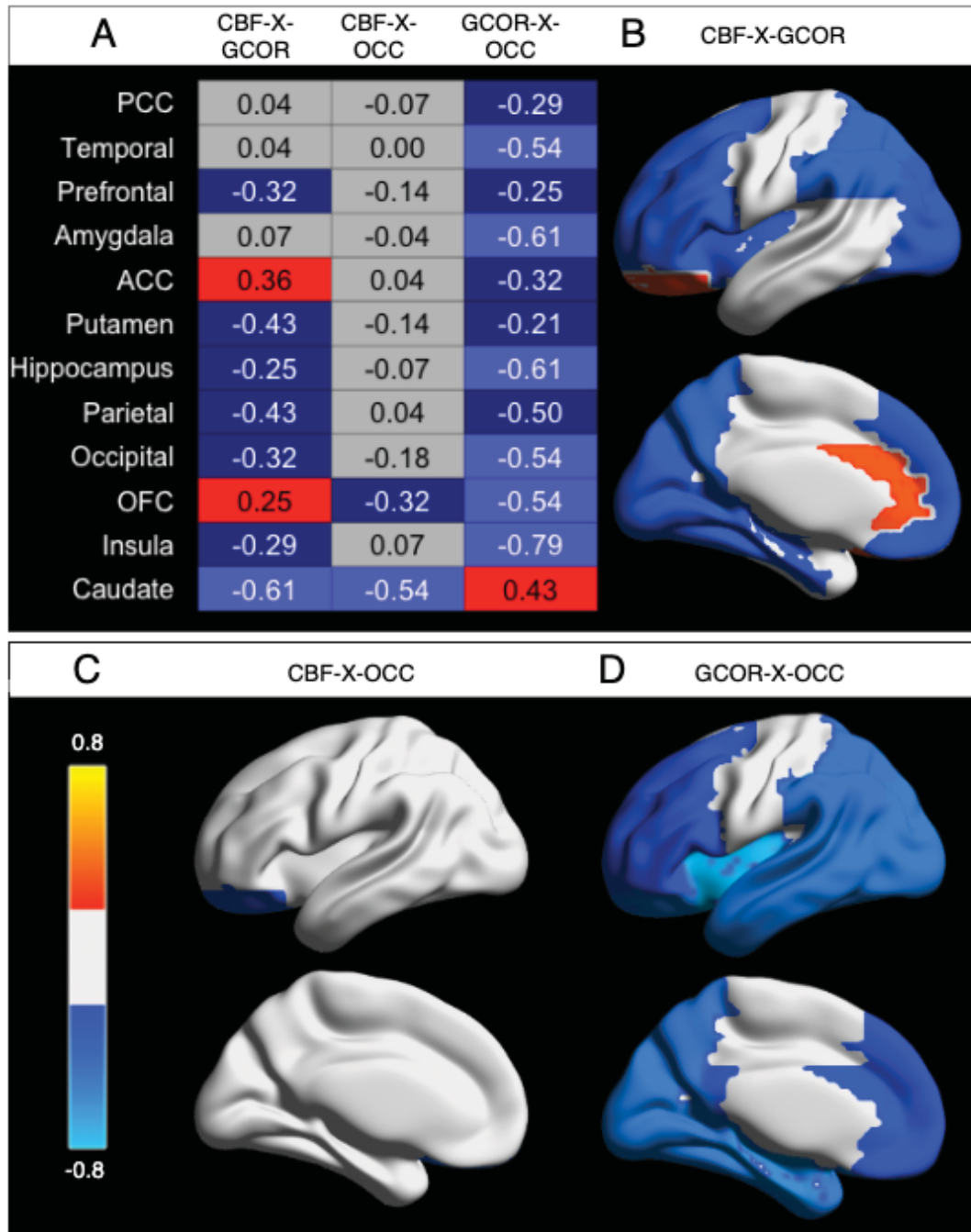


Figure 29 | Correlations between changes in neocortical occupancy, blood flow, and connectivity following LSD. A) Correlation matrix showing Spearman's rank values for CBF (cerebral blood flow)-GCOR (global connectivity across brain regions), CBF-OCC (neocortical occupancy), and GCOR-OCC across 12 regions. B-D) BrainNet visualisation of correlations, thresholded at 0.2. red-yellow = positive correlation, blue = negative correlation. PCC = posterior cingulate cortex; OFC = orbitofrontal cortex; ACC = anterior cingulate cortex.

Discussions

Paper 1

In this paper, we evaluated the persisting effects of psilocybin on resting-state functional connectivity one week and three months after administration in healthy individuals, and their associations with changes in mindfulness and other lasting behavioural effects. At the time, this paper represented only the second investigation of effects lasting more than 48 hours. One subsequent paper has not directly evaluated ECN WNC but reported global decreases in modularity and an association between ECN dynamic network flexibility and change in depression (Daws et al., 2022). We report reductions in within-network connectivity of the executive control network (ECN) with a very large effect size at one-week, that returned to baseline at three-month follow-up. This effect was apparent in 9 out of 10 participants and was distributed across 9 out of 10 of the connections of the ECN, supporting the notion that such an effect was both generalisable and network-wide. The ECN is a group of spatially incoherent brain regions that are associated with so-called executive functions, including sustained attention, cognitive flexibility, and goal-related behaviour (Niendam et al., 2012). Psychedelics have been reported to produce lasting beneficial effects on self-reported mindful attention and awareness (Søndergaard et al., 2022), notably that study included participants from paper 1. Psilocybin has also been reported qualitatively to improve feelings of attentional control and goal setting in addictive disorders (Nielson et al., 2018; Noorani et al., 2018). Therefore, our findings make thematic sense relative to our understanding of the persisting behavioural effects of psychedelics. We report relatively small effect sizes on all other network-to-network connections, including WNC of the default-mode network, which has received substantial attention, especially within evaluations of the acute effects of psychedelics (Carhart-Harris and Friston, 2019; Pasquini et al., 2020; Smigielski et al., 2019).

In further analyses, we demonstrate that greater ECN disintegration at one-week, and lesser ECN disintegration at three-months was associated with increased self-reported mindful-awareness and attention at three-months. This indicates that the process of ECN disintegration followed by reintegration is mechanistically related to lasting effects on attention. We also show a trend-level association between change in ECN connectivity at one-week and positive subscale scores from the persisting effects questionnaire, which evaluates positively felt changes across a range of domains, including positivity about life, positivity about the self, positive mood, and positive behaviours (Griffiths et al., 2011). Importantly, such changes relate only to those changes that the participants believe were due to their psychedelic experience and reflection thereon.

This paper represented a hypothesis-generating investigation of psychedelic effects on ECN connectivity, especially relating to the associations with behavioural scales. We present data from a single preprocessing strategy and a single a priori atlas of the ECN, as well as being from a study powered for a PET-related question, and thus small for the evaluation of fMRI effects. We only evaluate static network connectivity and do not evaluate dynamic brain connectivity effects. We also do not evaluate a control group and did not pre-register any hypotheses or analysis pipelines. Our cohort was young, healthy individuals, and thus may not translate to patient cohorts. We also do not directly measure executive functions like working memory and attention, though a subsequently published paper has shown increases in cognitive flexibility in depression patients post-psilocybin (Doss et al., 2021). Therefore, this paper represents a small, incremental step towards understanding the persisting effects of psychedelics on functional brain activity. We report effect sizes and correlation coefficients so as to inform future research, which may include larger studies, including those in major depression or addiction-disorder patients.

Paper 2

In this paper, we evaluated the association between psilocybin-induced mystical-type experiences and persisting positive effects three months later. Previous work has shown a qualitative relation between these (Belser et al., 2017; Nielson et al., 2018; Noorani et al., 2018; Swift et al., 2017) as well as some quantitative explorations (Davis et al., 2020; Ross et al., 2016; Schmid and Liechti, 2018). We expand upon this previous research by evaluating the subscales of the MEQ and providing data-driven qualitative descriptions of complete mystical experiences (CME) in a novel cohort of healthy individuals administered psilocybin across three different environments (i.e., PET scan, comfortable room, MRI scan).

We first showed that the overall score on the MEQ was related to an LVM representing positive PEQ scores (PPE_{LV}), aligning with previous findings. Next, we showed that the subscales “Positive Mood” (e.g., MEQ item 17 “Experience of ecstasy”) and “Mysticality” (e.g., MEQ item 28 “Experience of unity with ultimate reality”) were significantly related to PPE_{LV} . The subscales “Transcendence of time and space” (e.g., MEQ item 7 “Loss of your usual sense of space”) and “Ineffability” (e.g., MEQ item 10 “Feeling that you could not do justice to your experience by describing it in words”) were not significantly associated with PPE_{LV} . Notably, the estimates for these relations were similar across subscales, but the confidence intervals were much wider for the latter two. We observe no association between peak PPL and PPE_{LV} . These data suggest that the nature of the experience is relevant for the lasting positive effects of psychedelics. This runs contrary to an emerging idea that the subjective effects of psychedelics are only epiphenomenologically related to lasting positive effects, and that the positive effects are mediated by a distinct, sub-perceptual molecular pathway (Hibicke et al., 2020; Olson, 2021). Psychedelic-induced subjective effects are strongly influenced by participant frame-of-mind coming into the session, commonly referred to as “set” (Vizeli et al., 2024), and the setting in which the session takes place (Hartogsohn, 2017). Our results suggest that to optimise the lasting positive effects of psychedelic administration, it may be prudent to facilitate a set and setting conducive to “positive mood” and “mysticism” style experiences, as well as choice of dose, and potentially also drug selection. One recent study has shown in a phase 2b trial that the Five-Dimensional Altered States of Consciousness questionnaire subscale “Oceanic Boundlessness” was significantly associated with observed antidepressant effects (Goodwin et al., 2025). Although this study did not employ the MEQ directly, this subscale is thematically similar to the “Mystical” subscale of the MEQ, sharing themes of connectedness and positive mood (Studerus et al., 2010).

We further investigated the character of the so-called CME by performing natural language processing and thematic analysis of qualitative reports. We showed that words exclusively used to describe CME included “universe”, “dad”, “magnetic resonance”, “beautiful”, and “simultaneous”. We showed that some of these themes, e.g., connection with the Universe, were captured by the MEQ (i.e., “Experience of the fusion of your personal self into a larger whole” (MEQ item 26). Whereas other prominent themes, like familial love and the sense of having several contradictory feelings at once, were not described by the MEQ.

There has been some controversy around the investigation of psychedelic drug effects through the lens of “Mystical-type experiences” (Sanders and Zijlmans, 2021). Broadly, critics express concerns around biasing researchers, participants, and patients to interpret the effects through a spiritual or otherwise non-scientific lens, which they may not have otherwise done. Relatedly, the “Comforting Delusion Objection” postulates that it can be problematic for patients to draw comfort from conclusions drawn during psychedelic experiences, which may not be empirically verifiable. These conclusions may be more likely to manifest if experiences are considered mystical or beyond the scope of science. A full description and reasoned

objections were made by Letheby (Letheby, 2021). It is, nevertheless, empirically valid that psychedelics induce the sort of experiences wherein people rate statements such as “Certainty of encounter with ultimate reality” (MEQ item 9) and “Sense of being at a spiritual height” (MEQ item 15) as accurately describing something about their experience. Therefore, we consider the framework of “mystical-type experiences” as a useful scientific tool for investigating a cluster of similar experiences without attributing any epistemic weight to the claims made by the participants.

There are several ways in which this study may be improved upon in future research. Despite the application of statistical methods to control our type-1 error at the nominal level (Ozenne et al., 2020), small samples limit statistical power and the reliability of our findings. Thus, replication in much larger samples is required for further testing of the claims made in this paper. Further, we did not employ a placebo or measure expectancy effects, which likely influence at least the lasting effects of psychedelics (Muthukumaraswamy et al., 2021). Curiously, although we show similar PEQ scores to similar healthy-volunteer studies in Switzerland (Schmid and Liechti, 2018), they are lower than those from comparable studies in the USA; in fact, they are more similar to the scores from the placebo arm (Griffiths et al., 2011). This indicates that differences in participant cohorts, or set and setting, may be responsible for at least as much variation in PEQ scores as the intervention itself. Future studies could employ a multi-site strategy to account for such differences. We were limited in our capacity to describe non-CME qualitatively by the wide heterogeneity in qualitative reports; larger samples may help to resolve this. It may simply be that CME experiences are more generally aligned than non-CME experiences (e.g., comparing descriptions of a day where you went to the zoo vs a day where you did *not* go to the zoo). We present quotes that we felt best described the themes identified in reviewing the qualitative reports; although we used a data-driven method to first identify the themes, there is undoubtedly bias in the selection of which quotes were presented, as in all qualitative analyses (Galdas, 2017). We were furthermore limited in our capacity to apply more nuanced or advanced natural-language process methodologies to this cohort due to the small sample (e.g, n-gram analysis, further subgroup divisions).

Paper 3

In this paper, we presented the largest and most comprehensive evaluation of psychedelic effects on fMRI-measured brain-entropy and established the publicly available Copenhagen Brain Entropy Toolbox (CopBET), which can be easily applied to future datasets wishing to evaluate each of these measures.

We observe significant correlations with PPL, subjective drug intensity, and estimated occupancy (collectively: PsiFx) with three entropy metrics: path-length distribution, sample entropy, and dynamic conditional correlation (DCC) distribution. We also show correlations with some PsiFx for two Lempel-Ziv complexity-based measures: meta-state complexity and temporal LZ complexity of the BOLD series. We do not find significant associations with 8 of 13 metrics previously reported, and we do not observe any clear correlation pattern between the 13 entropy metrics. Overall, we identify potential neural biomarkers for psychedelic effects and highlight the problematic heterogeneity in the field, even among theoretically aligned analyses.

Path-length distribution is a measure of the width of the distribution of the path-lengths across the whole brain, where path-length represents the number of region-to-region functional connectivity edges that must be traversed to get from one region to another. We observe weak-to-moderately positive associations with all PsiFx, replicating previous research that showed significantly higher PLD following ayahuasca ingestion (Viol et al., 2019). It is encouraging that our results were consistent with those of Viol and colleagues, as they

administered a distinct psychedelic compound and employed relatively dissimilar scanning parameters. No other pharmaco-fMRI studies have evaluated the effects of path-length distribution, so the specificity of these effects for psychedelics is unresolved.

DCC distribution is an index of the width of the distribution of instantaneous connectivity estimates over the duration of the scan. We observe a moderate-to-strong positive association with PsiFx across most within- and between-network connections, indicating increased diversity of connectivity across time in the psychedelic state across the whole brain connectome (i.e., Pearson's rho with PPL > 0.7 for three edges, and Pearson's rho > 0.5 for 28/36 network edges). This is one of the strongest correlations reported in pharmaco-fMRI, and we demonstrate that this association was robust to scanner sequence and across most preprocessing pipelines. Therefore, DCC distribution represents a strong candidate biomarker. The previous paper evaluating this metric showed no persisting effect one week or one month following oral psilocybin administration, indicating that this is only a candidate biomarker for the *acute* effects (Barrett et al., 2020). However, this also means that this represents the first evaluation of DCC distribution in the context of acute psychedelic administration, necessitating independent replication.

Sample entropy is an index of the regularity of a signal. We evaluate it across timescales by temporally downsampling the signal such that we can observe the regularity of the signal on a 2s to 10s timescale. We observed weak to moderate positive associations with PsiFx at scale 1 in 7 out of 17 networks and negative associations at scale 5 in 14 out of 17 networks. These associations were relatively robust to the preprocessing pipeline and between scanners. This indicates that following psilocybin administration, the BOLD signal becomes more irregular at the 2-second scale but more regular at the 10-second scale, compared to the sober state. This pattern replicates the results from the previous investigation applying this method (Lebedev et al., 2016); furthermore, a similar pattern of sample entropy (higher short-scale, lower long-scale) has been shown to be associated with the positive symptoms of schizophrenia, e.g., thought-disorder and hallucinations (Yang et al., 2015). Sample entropy has also been applied to fMRI in the context of sleep, which was associated with decreases at scale 1 (Kung et al., 2022) and following caffeine intake, wherein it increases across much of the brain (Chang et al., 2018). Together, these indicate that increases in sample entropy may simply reflect increases in wakefulness, and not be specific to psychedelic effects, though this is yet to be resolved empirically. Sample entropy requires the selection of at least two hyperparameters i.e., the length of the sequences compared and the similarity threshold, each of which can meaningfully affect the interpretation of results (Wang et al., 2014). Furthermore, the interpretation of the time-scale of the effects is contingent on the TR of the imaging sequence. As we aimed to directly replicate previous methods, we did not explore this parameter space in this study, but future research may wish to do so.

Psychedelic effects on brain entropy have been evaluated using alternative neuroimaging methods, magneto- and electroencephalography (Murray et al., 2024; Pallavicini et al., 2021; Schartner et al., 2017; Timmermann et al., 2023, 2019), each showing increases in LZc of the time-series. Though notably, one of these showed increases in LZc from sub-perceptual doses of LSD, indicating a potential epiphenomenon (Murray et al., 2024). In this study, two LZc measures showed potential as biomarkers of acute psychedelic effects: LZc-temporal (associated with all PsiFx in select pre-processing pipelines) and meta-state complexity (associated with at least one PsiFx in all but one pipeline). Future work using simultaneous MRI-EEG may resolve whether there are correlations between the LZc of fMRI and EEG-derived signals.

Of the 13 metrics evaluated here, eight did not show any effect with PsiFx despite four of these having been previously reported to increase following psychedelic intake (Carhart-Harris et al., 2014; Lebedev et al., 2015; Tagliazucchi et al., 2014; Viol et al., 2017). We apply a distinct statistical method to all previous

studies, evaluating the correlation with plasma drug levels and subjective effect ratings, whereas previous studies have compared drug vs. pre-drug or placebo scans. This is the first study to evaluate brain-entropy effects of psychedelics following oral psilocybin administration. Although this somewhat limits comparison with previous studies that administered psilocybin or LSD intravenously or ayahuasca (a mixture of MAO inhibitors and N,N-DMT), oral psilocybin is the psychedelic formulation that has the most data supporting its efficacy in psychiatric disorders and is thus the most clinically relevant to examine. Further, if effects are specific to LSD or ayahuasca, then they do not represent useful biomarkers of *psychedelic* drug effects.

We do not observe a clear correlation pattern across metrics, except that the two metrics based on a graph-theory representation of the static connectome and the two direct Lempel-Ziv metrics formed pairs. We also observe four pairs of anti-correlated metrics. This highlights that future studies must be specific in the description of their hypotheses and analyses, as simply describing “entropy” is insufficiently specific to be of utility.

An article by Mallaroni et al. has recently become available on a preprint server, wherein they evaluated the effects of oral psilocybin and the phenethylamine psychedelic 2C-B on four of the entropy measures described here, namely, sample entropy, PLD, DCC distribution, and LZc-temporal (Mallaroni et al., 2024). The authors utilised CopBET, ensuring analysis methods replicated previous work, though resting-state data were collected with eyes open, and preprocessing strategies were distinct. The authors report a positive effect of both drugs on LZc-temporal and sample entropy, aligning with our findings, but no significant effect on PLD or DCC distribution, drawing into question their utility as biomarkers.

Data in this study were collected using two different scanners, each of which utilised a different scanning sequence. To ensure comparability, especially regarding the dynamic analyses, data from that scanner with a faster TR were downsampled to match the TR of the other, unfortunately necessitating data loss. However, each participant was only scanned on one scanner, allowing us to statistically model each individual’s response to PsiFx independent of the scanner. We do not use a placebo comparison; instead, we use pre-drug scans as comparators. This may be a superior strategy due to the high inter-day variability in fMRI signal (Noble et al., 2019). However, the test-retest reliability of these metrics is yet to be established, which could have been resolved using a placebo group. PPL was significantly associated with increased motion in the scanner, which may bias our results. We attempted to account for this by realigning scans and applying movement parameters as regressors in the denoising and in the statistical models, though it is not possible to fully remove this as a potential confounder. Our scans were either ten or five minutes long, which is relatively short compared to current guidelines for maximising reliability of functional connectivity estimates (Birn et al., 2013); the effect of scan length on entropy measures has not been evaluated.

Paper 4

In this paper, we present the first ever demonstration and quantification of occupancy characteristics of LSD at the 5-HT_{2A}R in humans, as well as providing effect size estimates for the neural effects of LSD across a wide range of fMRI analysis strategies.

Modern clinical trials using LSD administer patients between 5 and 200 µg, whereas historical clinical trials administered doses as high as 800 µg (Fuentes et al., 2019). We estimate the IC₅₀ and ED₅₀ for LSD at the 5-HT_{2A}R to be 1.9nM and 0.41 µg/kg, respectively, and observe 85% occupancy in a participant administered only 75 µg of LSD. These together suggest historical doses substantially exceeded the maximum dose required for near-maximal occupancy at the 5-HT_{2A}R, and any potential differences in drug effects may be mediated by off-target effects. Furthermore, our reported parameters can be used in subsequent research to convert plasma LSD levels to estimated occupancies. This will allow mechanistic

work to more closely investigate correlations between drug levels and behavioural or neuroimaging outcomes, accounting for the non-linear relation between plasma drug levels and their effects. This study further validates [¹¹C]Cimbi-36 occupancy studies as a method for evaluating target engagement in the living human brain. Future drug development efforts, especially forthcoming 5-HT_{2A}R agonists that are putatively non-psychedelic, e.g., tabernanthalogue (Cameron et al., 2021), will benefit from such measurement of target engagement to select dosages in clinical trials, as no indication of target engagement can be estimated from behavioural effects. Furthermore, despite the overall positive association between occupancy and subjective drug effects, we observe significant variation across participants. One subject rated 10/10 SDI despite only 42% receptor occupancy, whereas another participant reported only 1.5/10 SDI despite 72% receptor occupancy during a late scan. Thus, even in the development of psychoactive 5-HT_{2A}R agonists, receptor occupancy can not be reliably estimated from self-report measures of drug intensity and therefore requires molecular imaging studies.

Several 5-HT_{2A}R agonists, including 5-MeO-DMT (NCT05800860, NCT05839509) and N,N-DMT (NCT06094907, NCT05553691) are in clinical development despite the absence of target engagement studies. The R enantiomer of MDMA is an agonist at 5-HT_{2A}R (Nash et al., 1994; Straumann et al., 2024), and some of its clinically relevant behavioural effects are blocked by pre-administration with a 5-HT_{2A}R antagonist (Liechti et al., 2000). MDMA has recently been rejected by the FDA despite positive results from phase 3 studies, and understanding the degree to which MDMA induces occupancy of 5-HT_{2A}R either by direct action or by induced 5-HT release will be highly informative in determining the safety profile and mechanism of action. The only other psychedelic to have its occupancy described at the 5-HT_{2A}R in humans so far is psilocin (Madsen et al., 2019).

We observed a clear anti-clockwise hysteresis pattern between plasma LSD levels and subjective drug intensity ratings, such that there is an approximately 30-minute delay between the increase in plasma LSD levels and their resultant behavioural effects. There may be several reasons for this delay. Although one may hypothesise that the delay is psychological in nature, i.e., that it takes some time for participants to notice the psychedelic effects, the same delay is not observed with psilocybin, which has almost indistinguishable subjective effects (Holze et al., 2022b). It could be due to low brain penetrance resulting in a slow accumulation in the brain; however, LSD has biochemical properties that favour blood-brain barrier penetrance (i.e., molecular weight 323.4 g/mol; XLogP₃ = 3; pK_a = 7.8) (Kim et al., 2021), rendering this relatively unlikely. This hypothesis could be tested if radiolabelled [¹¹C]LSD PET became available as a tracer. As a result of unique hydrogen-bond interactions between LSD and the 5-HT_{2A}R, LSD has an extremely long residence time at the receptor compared to related psychedelics like mescaline and psilocin (Gumpper et al., 2025). This implies that following brain penetrance, LSD gradually accumulates at the 5-HT_{2A}R, explaining the delayed onset of subjective effects. In the preregistration of this study, we aimed to measure LSD occupancy during the downslope of effects to evaluate whether we observed residual occupancy despite decreases in peripheral PLL. Due to adverse effects, scanner malfunctions, and issues with radiotracer availability, we were unable to quantitatively evaluate this effect, and thus it remains an outstanding question for future research.

LSD may function as a prodrug for nor-LSD, which has been shown to be an agonist at 5-HT_{2A}R with a K_i of 6.1 nM *in vitro* (Luethi et al., 2019). As this is relatively similar to the K_i of LSD, this would not directly explain the delayed effects. However, we did not account for plasma nor-LSD concentration when modelling our PET data, which may improve model fits and should be quantified in future research.

We observe moderate decreases in global connectivity across the entire neocortex, with the strongest decreases observed in the occipital and temporal cortices. Previous work has also reported decreases in visual cortex GCOR (Avram et al., 2024; Preller et al., 2018), but these studies also report increases in frontal and parietal cortex GCOR that we do not observe (Tagliazucchi et al., 2016). We do not observe widespread alterations in thalamo-cortical connectivity as have been previously reported, except moderate to large bilateral increases with the primary motor cortex (Avram et al., 2021; Preller et al., 2018). We evaluated several brain-entropy metrics using the Copenhagen Brain Entropy Toolbox described in paper 3. Sample entropy showed a concurrent effect with previous reports, i.e., moderate-to-large increases at short scale (Lebedev et al., 2016). Normalised global complexity (a measure of signal heterogeneity in a region added to CopBET since the release of paper 3) also showed moderate increases, aligning with a previous report in a similarly sized cohort (Siegel et al., 2024). We show negligible effects on LZc-temporal and path-length entropy and only small effects on DCC distribution, despite each of these emerging as candidate biomarkers in paper 3. We evaluate two graph-theory measures, namely small-worldness and modularity. Modularity has been shown to be reduced several weeks after psilocybin intervention in major depressive disorder patients (Daws et al., 2022); acute effects have not been evaluated, but our results here suggest that effects are small. Finally, we evaluated effects on static brain network connectivity. We do not observe the decreased within-network connectivity and increased between-network connectivity that has been observed across psilocybin, N,N-DMT, and LSD (Madsen et al., 2021; Müller et al., 2018; Timmermann et al., 2023). Instead, our network-connectivity findings complement our GCOR findings, showing that the decreased GCOR from the visual and attention networks are distributed across most of the brain and not driven by a specific network-network edge.

This study was designed with the PET measures as primary outcome measures and thus has a small sample compared to most other fMRI studies evaluating psychedelics. Furthermore, participants were administered one of a range of doses. Thus, we are limited in our ability to draw statistical significance from the fMRI results. Nevertheless, we report effect sizes across a wide range of analyses that can be used in forthcoming meta-analyses and to inform which fMRI metrics may be deserving of greatest focus in future research (Botvinik-Nezer et al., 2020; Taylor et al., 2025). This study was the first to evaluate relations between fMRI changes and occupancy at the 5-HT_{2A}R, wherein we show that the decreases in GCOR are negatively associated with occupancy, suggesting that the effects are 5-HT_{2A}R-related.

Related, although not considered in the thesis, we also evaluated changes in cerebral blood flow (CBF) following LSD, showing that LSD increased CBF by 19.3%. Regional increases in CBF were associated with decreases in GCOR across most of the neocortex (**Fig. 29**). Neural activity drives overcompensatory increases in cerebral blood flow to a region, resulting in a relative decrease in the paramagnetic deoxyhemoglobin, increasing the T₂* relaxation time and the BOLD signal (Drew, 2022). The BOLD signal is considered a measure of neural activity contingent on this effect, known as neurovascular coupling (NVC) (Liu, 2013). Hypercapnia increases CBF without affecting cerebral oxidative metabolism and has been shown to decrease the amplitude and functional connectivity of the BOLD signal, likely by reducing the signal-to-noise ratio (SNR) (Biswal et al., 1997; Chen and Pike, 2010; Jain et al., 2011). Assuming that the entropy of noise is higher than that of signal, decreases in SNR would increase measures of entropy. Therefore, it may be the case that our observed decreases in GCOR and increases in information-entropy are driven by SNR reductions due to increases in CBF, which disrupt NVC, rather than alterations in neural activity.

Conclusions and future research

The present thesis evaluates the effects of psilocybin and LSD in healthy volunteers. The four studies describe 1) lasting effects of psychedelics on functional brain network connectivity, 2) the relation between acute mystical-type experiences and persisting positive behavioural effects, as well as the nature of those mystical-type experiences, 3) acute psilocybin effects on fMRI-measured brain-entropy, and 4) 5-HT_{2A}R occupancy and acute functional brain effects of LSD.

Paper 1 was among the first studies to evaluate the persisting effects of psychedelics on functional brain activity. Although a small study that employed relatively simple analyses, we identified a key hypothesis in the space, i.e., that persisting reductions in executive-control network connectivity were related to the lasting positive effects of psychedelics and provided effect sizes for other network connectivity alterations that can be used to power future studies. Subsequent work has evaluated persisting effects on functional connectivity in patient cohorts (Daws et al., 2022; Doss et al., 2021), representing an essential step forward in the field. However, these were still small, hypothesis-generating studies. Future studies looking to establish our understanding of the persisting effects of psychedelics on functional brain activity may look towards the implementation of naturalistic task designs such as movie watching, which have been shown to be more closely associated with cognition and wellbeing (Finn et al., 2020; Finn and Bandettini, 2021). They may also evaluate tasks which specifically investigate known persisting behavioural effects of psychedelics, such as a focused-attention task (Dickenson et al., 2013) to probe neural circuits related to mindful attention and awareness, which has been shown to increase following psilocybin (Søndergaard et al., 2022). Studies can also look to characterise neural activity beyond effects on network-connectivity, such as information-entropy measures described in paper 3, or graph-theory measures of the functional connectome, such as small-worldness or modularity (Sporns, 2018). Finally, future studies should strive to balance hypothesis-generating research with replication of previously reported observations in larger cohorts. These include the change in executive-control network connectivity reported here, the reduction in modularity described by Daws et al., and increased dynamic functional connectivity between the anterior and posterior cingulate cortices reported by Doss et al. (Daws et al., 2022; Doss et al., 2021).

Paper 2 evaluated the association between mystical-type experiences and persisting positive effects in healthy people and provided qualitative descriptions of those mystical-type experiences. Subsequent work has already built on this research, evaluating the relation between features of the acute experience and persisting effects in patient groups (Goodwin et al., 2025). However, whether the psychedelic effects mediated by 5-HT_{2A}R agonism are necessary for producing persisting effects remains unclear. No studies to date have reported the persisting effects of a psychedelic coadministered with a 5-HT_{2A}R antagonist to block the subjective effects. A single case report describes a patient from a depression trial who was taking trazodone, a 2A antagonist. They reported a dramatic reduction in depressive symptoms despite the patient experiencing no subjective effects of the psilocybin (Rosenblat et al., 2023). Future trials evaluating this are planned, including co-administration with risperidone (also a 5-HT_{2A}R antagonist) (Husain et al., 2023). Regarding the nature of the psychedelic effects, there are many other ways of measuring the quality of the acute psychedelic experience, including the widely applied 5-dimensions of altered states of consciousness scale (Studerus et al., 2010), ego-dissolution inventory (Nour et al., 2016) and psychological insight questionnaire (Davis et al., 2021) each of which may represent distinct features of the psychedelic experience. Furthermore, there are many ways of evaluating the positive persisting effects of psychedelics, be they reductions in clinical symptoms, increases in flourishing, or alterations in health behaviours. The relation

between features of the psychedelic experience and different lasting effects can be resolved in future studies or by data pooling across sites. Paper 2 also provided qualitative descriptions of mystical-type experiences, but we were limited in our capacity to provide qualitative descriptions of non-mystical experiences. As psychedelics move closer to medicalisation, it will become increasingly important for practitioners to develop a qualitative understanding of the full range of psychedelic experiences. Future qualitative research could focus on describing experiences characterised by anxiety, paranoia, and other neutral-to-negative effects, as well as further characterising the range of positive or mystical-type experiences.

Paper 3 evaluated the relation between the acute effects of psilocybin and fMRI-measured indexes of brain-entropy. Specifically, we attempted to replicate psychedelic effects on 13 previously reported entropy measures, as no replication efforts had been performed at the time. Another new entropy metric has since been evaluated in the context of psychedelics, normalised global spatial complexity (Siegel et al., 2024), and this has now been added to the Copenhagen Brain Entropy Toolbox (CopBET). Future research will hopefully apply CopBET to larger and pooled datasets to provide more evidence for or against their utility as neural correlates of the psychedelic experiences. An essential next step will be for these metrics to be evaluated in the context of other non-psychedelic compounds such as caffeine, amphetamine, alcohol, and benzodiazepines, and in other altered states of consciousness, such as REM sleep, to determine their specificity for psychedelic effects. Psychedelic effects on the Lempel-Ziv complexity of EEG signals have been reported across several datasets (Pallavicini et al., 2021; Timmermann et al., 2023, 2019). One of which reported increases in the absence of subjective effects (Murray et al., 2024). The relation between this and the Lempel-Ziv complexity of the BOLD signal, or other entropy measures, has not been evaluated and could be done so using simultaneous fMRI-EEG. We also present a multi-verse analysis evaluating the effect of a range of common pre-processing strategies on the relation between each entropy metric and psychedelic effects. Future work developing entropy metrics as useful medical technologies may wish to evaluate the impact of preprocessing strategies on each metric in large normative datasets, such as the Human Connectome Project (Glasser, 2016) or UK Biobank (Miller et al., 2016).

Paper 4 evaluated the relation between LSD administration and occupancy at the 5-HT_{2A}R, and functional brain effects. As the first study to administer psychedelics in a simultaneous PET/MR scanner, this study establishes a framework for simultaneously evaluating the target engagement and functional effects for the many 5-HT_{2A}R ligands currently in clinical development. We observe evidence for slow receptor kinetics at the 5-HT_{2A}R, aligning with previous *in vitro* work. However, due to technical failures, we were unable to resolve whether there is prolonged occupancy using PET. Future studies measuring occupancy at different timepoints will help to resolve the intriguing temporal dynamics of LSD in the human brain. We provide initial evidence that changes in BOLD connectivity may be related to alterations in CBF, indicating an effect on NVC. Future studies can help shed light on the potential confounding effect by measuring the effects of LSD (increasing CBF) or psilocybin (decreasing CBF (Larsen et al., 2025; Rieser et al., 2023)) on neural activity, and potential effects on neurovascular coupling.

In summary, psychedelic neuroimaging with fMRI has to-date generated several intriguing hypotheses in a range of small cohorts and using diverse mathematical modelling techniques. In order for the field to mature and converge upon replicable and specific biomarkers for the acute and lasting effects of psychedelics on functional brain activity researchers must begin testing these hypotheses using identical methodologies on larger datasets, determine the specificity of these effects using positive and negative controls, and determine the extent to which confounding variables such as neurovascular effects bias outcomes. This thesis presents

estimates of lasting effects that can be used to power future studies, evidence that mystical-type experiences, particularly those characterised by positive mood and mysticality, are associated with lasting positive effects, a toolbox that can be widely applied to allow researchers to attempt to replicate psychedelic effects on brain-entropy, data-driven dosing recommendations for LSD, effect sizes for acute effects on a wide range of functional metrics, and evidence for a potential neurovascular confounding effect. Each of these will hopefully contribute to the maturation of the field and eventual convergence on reliable psychedelic effects on functional brain activity.

References

- Agrawal, M., Richards, W., Beaussant, Y., Shnayder, S., Ameli, R., Roddy, K., Stevens, N., Richards, B., Schor, N., Honstein, H., Jenkins, B., Bates, M., Thambi, P., 2024. Psilocybin-assisted group therapy in patients with cancer diagnosed with a major depressive disorder. *Cancer* 130, 1137–1146. <https://doi.org/10.1002/cncr.35010>
- Anderson, B.T., Danforth, A., Daroff, P.R., Stauffer, C., Ekman, E., Agin-Liebes, G., Trope, A., Boden, M.T., Dilley, P.J., Mitchell, J., Woolley, J., 2020. Psilocybin-assisted group therapy for demoralized older long-term AIDS survivor men: An open-label safety and feasibility pilot study. *EClinicalMedicine* 27, 100538. <https://doi.org/10.1016/j.eclinm.2020.100538>
- Avram, M., Fortea, L., Wollner, L., Coenen, R., Korda, A., Rogg, H., Holze, F., Vizeli, P., Ley, L., Radua, J., Müller, F., Liechti, M.E., Borgwardt, S., 2024. Large-scale brain connectivity changes following the administration of lysergic acid diethylamide, d-amphetamine, and 3,4-methylenedioxymphetamine. *Mol. Psychiatry* 1–11. <https://doi.org/10.1038/s41380-024-02734-y>
- Avram, M., Rogg, H., Korda, A., Andreou, C., Müller, F., Borgwardt, S., 2021. Bridging the Gap? Altered Thalamocortical Connectivity in Psychotic and Psychedelic States. *Front. Psychiatry* 12. <https://doi.org/10.3389/fpsy.2021.706017>
- Baggot, M., Coyle, J., Erowid, E., Erowid, F., Robertson, L., 2011. Abnormal visual experiences in individuals with histories of hallucinogen use: a Web-based questionnaire. *Drug Alcohol Depend.* 114. <https://doi.org/10.1016/j.drugalcdep.2010.09.006>
- Barrett, F.S., Doss, M.K., Sepeda, N.D., Pekar, J.J., Griffiths, R.R., 2020. Emotions and brain function are altered up to one month after a single high dose of psilocybin. *Sci. Rep.* 10, 1–14. <https://doi.org/10.1038/s41598-020-59282-y>
- Barrett, F.S., Johnson, M.W., Griffiths, R.R., 2015. Validation of the revised Mystical Experience Questionnaire in experimental sessions with psilocybin. *J. Psychopharmacol. (Oxf.)* 29, 1182–1190. <https://doi.org/10.1177/0269881115609019>
- Becker, A.M., Klaiber, A., Holze, F., Istampoulouoglou, I., Duthaler, U., Varghese, N., Eckert, A., Liechti, M.E., 2023. Ketanserin Reverses the Acute Response to LSD in a Randomized, Double-Blind, Placebo-Controlled, Crossover Study in Healthy Participants. *Int. J. Neuropsychopharmacol.* 26, 97–106. <https://doi.org/10.1093/ijnp/pyac075>
- Belser, A.B., Agin-Liebes, G., Swift, T.C., Terrana, S., Devenot, N., Friedman, H.L., Guss, J., Bossis, A., Ross, S., 2017. Patient Experiences of Psilocybin-Assisted Psychotherapy: An Interpretative Phenomenological Analysis. *J. Humanist. Psychol.* 57, 354–388. <https://doi.org/10.1177/0022167817706884>
- Bersani, F.S., Corazza, O., Albano, G., Valeriani, G., Santacroce, R., Bolzan Mariotti Posocco, F., Cinosi, E., Simonato, P., Martinotti, G., Bersani, G., Schifano, F., 2014. 25C-NBOMe: Preliminary Data on Pharmacology, Psychoactive Effects, and Toxicity of a New Potent and Dangerous Hallucinogenic Drug. *BioMed Res. Int.* 2014, 734749. <https://doi.org/10.1155/2014/734749>
- Bey, T., Patel, A., 2007. Phencyclidine Intoxication and Adverse Effects: A Clinical and Pharmacological Review of an Illicit Drug. *Calif. J. Emerg. Med.* 8, 9.
- Birn, R.M., Molloy, E.K., Patriat, R., Parker, T., Meier, T.B., Kirk, G.R., Nair, V.A., Meyerand, M.E., Prabhakaran, V., 2013. The effect of scan length on the reliability of resting-state fMRI connectivity estimates. *NeuroImage* 83, 550–558. <https://doi.org/10.1016/j.neuroimage.2013.05.099>
- Biswal, B., Hudetz, A.G., Yetkin, F.Z., Haughton, V.M., Hyde, J.S., 1997. Hypercapnia reversibly suppresses low-frequency fluctuations in the human motor cortex during rest using echo-planar MRI. *J. Cereb. Blood Flow Metab. Off. J. Int. Soc. Cereb. Blood Flow Metab.* 17, 301–308. <https://doi.org/10.1097/00004647-199703000-00007>
- Biswal, B., Yetkin, F.Z., Haughton, V.M., Hyde, J.S., 1995. Functional connectivity in the motor cortex of resting human brain using echo-planar MRI. *Magn. Reson. Med.* 34, 537–541. <https://doi.org/10.1002/mrm.1910340409>

- Bogenschutz, M.P., Ross, S., Bhatt, S., Baron, T., Forcehimes, A.A., Laska, E., Mennenga, S.E., O'Donnell, K., Owens, L.T., Podrebarac, S., Rotrosen, J., Tonigan, J.S., Worth, L., 2022. Percentage of Heavy Drinking Days Following Psilocybin-Assisted Psychotherapy vs Placebo in the Treatment of Adult Patients With Alcohol Use Disorder. *JAMA Psychiatry* 79, 953.
<https://doi.org/10.1001/jamapsychiatry.2022.2096>
- Bonomo, Y., Norman, A., Biondo, S., Bruno, R., Daglish, M., Dawe, S., Egerton-Warburton, D., Karro, J., Kim, C., Lenton, S., Lubman, D.I., Pastor, A., Rundle, J., Ryan, J., Gordon, P., Sharry, P., Nutt, D., Castle, D., 2019. The Australian drug harms ranking study. *J. Psychopharmacol. (Oxf.)* 33, 759–768.
<https://doi.org/10.1177/0269881119841569>
- Botvinik-Nezer, R., Holzmeister, F., Camerer, C.F., Dreber, A., Huber, J., Johannesson, M., Kirchler, M., Iwanir, R., Mumford, J.A., Adcock, R.A., Avesani, P., Baczowski, B.M., Bajracharya, A., Bakst, L., Ball, S., Barilari, M., Bault, N., Beaton, D., Beitner, J., Benoit, R.G., Berkers, R.M.W.J., Bhanji, J.P., Biswal, B.B., Bobadilla-Suarez, S., Bortolini, T., Bottenhorn, K.L., Bowring, A., Braem, S., Brooks, H.R., Brudner, E.G., Calderon, C.B., Camilleri, J.A., Castrellon, J.J., Cecchetti, L., Cieslik, E.C., Cole, Z.J., Collignon, O., Cox, R.W., Cunningham, W.A., Czoschke, S., Dadi, K., Davis, C.P., Luca, A.D., Delgado, M.R., Demetriou, L., Dennison, J.B., Di, X., Dickie, E.W., Dobryakova, E., Donnat, C.L., Dukart, J., Duncan, N.W., Durnez, J., Eed, A., Eickhoff, S.B., Erhart, A., Fontanesi, L., Fricke, G.M., Fu, S., Galván, A., Gau, R., Genon, S., Glatard, T., Glerean, E., Goeman, J.J., Golowin, S.A.E., González-García, C., Gorgolewski, K.J., Grady, C.L., Green, M.A., Guassi Moreira, J.F., Guest, O., Hakimi, S., Hamilton, J.P., Hancock, R., Handjaras, G., Harry, B.B., Hawco, C., Herholz, P., Herman, G., Heunis, S., Hoffstaedter, F., Hogeveen, J., Holmes, S., Hu, C.-P., Huettel, S.A., Hughes, M.E., Iacovella, V., Iordan, A.D., Isager, P.M., Isik, A.I., Jahn, A., Johnson, M.R., Johnstone, T., Joseph, M.J.E., Juliano, A.C., Kable, J.W., Kassinosopoulos, M., Koba, C., Kong, X.-Z., Kosciuk, T.R., Kucukboyaci, N.E., Kuhl, B.A., Kupek, S., Laird, A.R., Lamm, C., Langner, R., Lauharatanahirun, N., Lee, H., Lee, S., Leemans, A., Leo, A., Lesage, E., Li, F., Li, M.Y.C., Lim, P.C., Lintz, E.N., Liphardt, S.W., Losecaat Vermeer, A.B., Love, B.C., Mack, M.L., Malpica, N., Marins, T., Maumet, C., McDonald, K., McGuire, J.T., Melero, H., Méndez Leal, A.S., Meyer, B., Meyer, K.N., Mihai, G., Mitsis, G.D., Moll, J., Nielson, D.M., Nilsson, G., Notter, M.P., Olivetti, E., Onicas, A.I., Papale, P., Patil, K.R., Peelle, J.E., Pérez, A., Pischke, D., Poline, J.-B., Prystauka, Y., Ray, S., Reuter-Lorenz, P.A., Reynolds, R.C., Ricciardi, E., Rieck, J.R., Rodriguez-Thompson, A.M., Romy, A., Salo, T., Samanez-Larkin, G.R., Sanz-Morales, E., Schlichting, M.L., Schultz, D.H., Shen, Q., Sheridan, M.A., Silvers, J.A., Skagerlund, K., Smith, A., Smith, D.V., Sokol-Hessner, P., Steinkamp, S.R., Tashjian, S.M., Thirion, B., Thorp, J.N., Tinghög, G., Tisdall, L., Tompson, S.H., Toro-Serey, C., Torre Tresols, J.J., Tozzi, L., Truong, V., Turella, L., van 't Veer, A.E., Verguts, T., Vettel, J.M., Vijayarajah, S., Vo, K., Wall, M.B., Weeda, W.D., Weis, S., White, D.J., Wisniewski, D., Xifra-Porxas, A., Yearling, E.A., Yoon, S., Yuan, R., Yuen, K.S.L., Zhang, L., Zhang, X., Zosky, J.E., Nichols, T.E., Poldrack, R.A., Schonberg, T., 2020. Variability in the analysis of a single neuroimaging dataset by many teams. *Nature* 582, 84–88.
<https://doi.org/10.1038/s41586-020-2314-9>
- Bradley, E.R., Sakai, K., Fernandes-Osterhold, G., Szegedi, B., Ludwig, C., Ostrem, J.L., Tanner, C.M., Bock, M.A., Llerena, K., Finley, P.R., O'Donovan, A., Zuzuarregui, J.R.P., Busby, Z., McKernan, A., Penn, A.D., Wang, A.C.C., Rosen, R.C., Woolley, J.D., 2025. Psilocybin therapy for mood dysfunction in Parkinson's disease: an open-label pilot trial. *Neuropsychopharmacol. Off. Publ. Am. Coll. Neuropsychopharmacol.* 50, 1200–1209. <https://doi.org/10.1038/s41386-025-02097-0>
- Cameron, L.P., Tombari, R.J., Lu, J., Pell, A.J., Hurley, Z.Q., Ehinger, Y., Vargas, M.V., McCarroll, M.N., Taylor, J.C., Myers-Turnbull, D., Liu, T., Yaghoobi, B., Laskowski, L.J., Anderson, E.I., Zhang, G., Viswanathan, J., Brown, B.M., Tjia, M., Dunlap, L.E., Rabow, Z.T., Fiehn, O., Wulff, H., McCorvy, J.D., Lein, P.J., Kokel, D., Ron, D., Peters, J., Zuo, Y., Olson, D.E., 2021. A non-hallucinogenic psychedelic analogue with therapeutic potential. *Nature* 589, 474–479.
<https://doi.org/10.1038/s41586-020-3008-z>

- Carbonaro, T.M., Bradstreet, M.P., Barrett, F.S., MacLean, K.A., Jesse, R., Johnson, M.W., Griffiths, R.R., 2016. Survey study of challenging experiences after ingesting psilocybin mushrooms: Acute and enduring positive and negative consequences. *J. Psychopharmacol. (Oxf.)* 30, 1268–1278. <https://doi.org/10.1177/0269881116662634>
- Carhart-Harris, R., Giribaldi, B., Watts, R., Baker-Jones, M., Murphy-Beiner, A., Murphy, R., Martell, J., Blemings, A., Erritzoe, D., Nutt, D.J., 2021. Trial of Psilocybin versus Escitalopram for Depression. *N. Engl. J. Med.* 384, 1402–1411. <https://doi.org/10.1056/NEJMoa2032994>
- Carhart-Harris, R.L., 2018. The entropic brain - revisited. *Neuropharmacology* 142, 167–178. <https://doi.org/10.1016/j.neuropharm.2018.03.010>
- Carhart-Harris, R.L., Bolstridge, M., Rucker, J., Day, C.M.J., Erritzoe, D., Kaelen, M., Bloomfield, M., Rickard, J.A., Forbes, B., Feilding, A., Taylor, D., Pilling, S., Curran, V.H., Nutt, D.J., 2016. Psilocybin with psychological support for treatment-resistant depression: an open-label feasibility study. *Lancet Psychiatry* 3, 619–627. [https://doi.org/10.1016/S2215-0366\(16\)30065-7](https://doi.org/10.1016/S2215-0366(16)30065-7)
- Carhart-Harris, R.L., Friston, K.J., 2019. REBUS and the anarchic brain: Toward a unified model of the brain action of psychedelics. *Pharmacol. Rev.* <https://doi.org/10.1124/pr.118.017160>
- Carhart-Harris, R.L., Leech, R., Hellyer, P.J., Shanahan, M., Feilding, A., Tagliazucchi, E., Chialvo, D.R., Nutt, D., 2014. The entropic brain: A theory of conscious states informed by neuroimaging research with psychedelic drugs. *Front. Hum. Neurosci.* 8, 1–22. <https://doi.org/10.3389/fnhum.2014.00020>
- Chang, D., Song, D., Zhang, J., Shang, Y., Ge, Q., Wang, Z., 2018. Caffeine Caused a Widespread Increase of Resting Brain Entropy. *Sci. Rep.* 8, 2700. <https://doi.org/10.1038/s41598-018-21008-6>
- Chen, J.J., Pike, G.B., 2010. Global cerebral oxidative metabolism during hypercapnia and hypocapnia in humans: implications for BOLD fMRI. *J. Cereb. Blood Flow Metab. Off. J. Int. Soc. Cereb. Blood Flow Metab.* 30, 1094–1099. <https://doi.org/10.1038/jcbfm.2010.42>
- Cipriani, A., Furukawa, T.A., Salanti, G., Chaimani, A., Atkinson, L.Z., Ogawa, Y., Leucht, S., Ruhe, H.G., Turner, E.H., Higgins, J.P.T., Egger, M., Takeshima, N., Hayasaka, Y., Imai, H., Shinohara, K., Tajika, A., Ioannidis, J.P.A., Geddes, J.R., 2018. Comparative efficacy and acceptability of 21 antidepressant drugs for the acute treatment of adults with major depressive disorder: a systematic review and network meta-analysis. *Lancet Lond. Engl.* 391, 1357–1366. [https://doi.org/10.1016/S0140-6736\(17\)32802-7](https://doi.org/10.1016/S0140-6736(17)32802-7)
- Cohen, S., 1960. LYSERGIC ACID DIETHYLAMIDE: SIDE EFFECTS AND COMPLICATIONS. *J. Nerv. Ment. Dis.* 130, 30.
- Craddock, R.C., James, G.A., Holtzheimer, P.E., Hu, X.P., Mayberg, H.S., 2012. A whole brain fMRI atlas generated via spatially constrained spectral clustering. *Hum. Brain Mapp.* <https://doi.org/10.1002/hbm.21333>
- da Cunha-Bang, S., Ettrup, A., Mc Mahon, B., Skibsted, A.P., Schain, M., Lehel, S., Dyssegaard, A., Jørgensen, L.M., Møller, K., Gillings, N., Svarer, C., Knudsen, G.M., 2019. Measuring endogenous changes in serotonergic neurotransmission with [¹¹C]Cimbi-36 positron emission tomography in humans. *Transl. Psychiatry* 9, 134. <https://doi.org/10.1038/s41398-019-0468-8>
- Davis, A.K., Barrett, F.S., May, D.G., Cosimano, M.P., Sepeda, N.D., Johnson, M.W., Finan, P.H., Griffiths, R.R., 2020. Effects of Psilocybin-Assisted Therapy on Major Depressive Disorder A Randomized Clinical Trial. *JAMA Psychiatry* Published, 1–9. <https://doi.org/10.1001/jamapsychiatry.2020.3285>
- Davis, A.K., Barrett, F.S., So, S., Gukasyan, N., Swift, T.C., Griffiths, R.R., 2021. Development of the Psychological Insight Questionnaire among a sample of people who have consumed psilocybin or LSD. *J. Psychopharmacol. Oxf. Engl.* 35, 437–446. <https://doi.org/10.1177/0269881120967878>
- Daws, R.E., Timmermann, C., Giribaldi, B., Sexton, J.D., Wall, M.B., Erritzoe, D., Roseman, L., Nutt, D., Carhart-Harris, R., 2022. Increased global integration in the brain after psilocybin therapy for depression. *Nat. Med.* 28, 844–851. <https://doi.org/10.1038/s41591-022-01744-z>
- Delli Pizzi, S., Chiacchiarretta, P., Sestieri, C., Ferretti, A., Tullo, M.G., Della Penna, S., Martinotti, G., Onofri, M., Roseman, L., Timmermann, C., Nutt, D.J., Carhart-Harris, R.L., Sensi, S.L., 2023. LSD-induced changes in the functional connectivity of distinct thalamic nuclei. *NeuroImage* 283,

120414. <https://doi.org/10.1016/j.neuroimage.2023.120414>
- Desikan, R.S., Ségonne, F., Fischl, B., Quinn, B.T., Dickerson, B.C., Blacker, D., Buckner, R.L., Dale, A.M., Maguire, R.P., Hyman, B.T., Albert, M.S., Killiany, R.J., 2006. An automated labeling system for subdividing the human cerebral cortex on MRI scans into gyral based regions of interest. *NeuroImage*. <https://doi.org/10.1016/j.neuroimage.2006.01.021>
- Diagnostic and statistical manual of mental disorders: DSM-5™, 5th ed, 2013. , Diagnostic and statistical manual of mental disorders: DSM-5™, 5th ed. American Psychiatric Publishing, Inc., Arlington, VA, US. <https://doi.org/10.1176/appi.books.9780890425596>
- Dickenson, J., Berkman, E.T., Arch, J., Lieberman, M.D., 2013. Neural correlates of focused attention during a brief mindfulness induction. *Soc. Cogn. Affect. Neurosci.* 8, 40–47. <https://doi.org/10.1093/scan/nss030>
- dos Santos, R.G., Bouso, J.C., Hallak, J.E.C., 2017. Ayahuasca, dimethyltryptamine, and psychosis: a systematic review of human studies. *Ther. Adv. Psychopharmacol.* 7, 141–157. <https://doi.org/10.1177/2045125316689030>
- Doss, Manoj K, Madden, M.B., Gaddis, A., Nebel, M.B., Griffiths, R.R., Mathur, B.N., Barrett, F.S., 2021. Models of psychedelic drug action: modulation of cortical-subcortical circuits. *Brain*. <https://doi.org/10.1093/brain/awab406>
- Doss, Manoj K., Považan, M., Rosenberg, M.D., Sepeda, N.D., Davis, A.K., Finan, P.H., Smith, G.S., Pekar, J.J., Barker, P.B., Griffiths, R.R., Barrett, F.S., 2021. Psilocybin therapy increases cognitive and neural flexibility in patients with major depressive disorder. *Transl. Psychiatry* 11, 574. <https://doi.org/10.1038/s41398-021-01706-y>
- Drew, P.J., 2022. Neurovascular coupling: Motive unknown. *Trends Neurosci.* 45, 809–819. <https://doi.org/10.1016/j.tins.2022.08.004>
- Dunn, O.J., 1961. Multiple Comparisons among Means. *J. Am. Stat. Assoc.* 56, 52–64. <https://doi.org/10.1080/01621459.1961.10482090>
- Elçi, A., 2025. Switzerland is home to Europe’s only psychedelics treatment. SWI Swissinfo.ch. URL <https://www.swissinfo.ch/eng/multinational-companies/switzerland-is-home-to-europes-only-psychedelics-treatment/89195943> (accessed 6.11.25).
- Ettrup, A., Da Cunha-Bang, S., McMahon, B., Lehel, S., Dyssegaard, A., Skibsted, A.W., Jørgensen, L.M., Hansen, M., Baandrup, A.O., Bache, S., Svarer, C., Kristensen, J.L., Gillings, N., Madsen, J., Knudsen, G.M., 2014. Serotonin 2A receptor agonist binding in the human brain with [11 C]Cimbi-36. *J. Cereb. Blood Flow Metab.* <https://doi.org/10.1038/jcbfm.2014.68>
- Ettrup, A., Hansen, M., Santini, M.A., Paine, J., Gillings, N., Palner, M., Lehel, S., Herth, M.M., Madsen, J., Kristensen, J., Begtrup, M., Knudsen, G.M., 2011. Radiosynthesis and in vivo evaluation of a series of substituted 11C-phenethylamines as 5-HT (2A) agonist PET tracers. *Eur. J. Nucl. Med. Mol. Imaging* 38, 681–693. <https://doi.org/10.1007/s00259-010-1686-8>
- Ettrup, A., Holm, S., Hansen, M., Wasim, M., Santini, M.A., Palner, M., Madsen, J., Svarer, C., Kristensen, J.L., Knudsen, G.M., 2013. Preclinical safety assessment of the 5-HT2A receptor agonist PET radioligand [11C]Cimbi-36. *Mol. Imaging Biol.* 15, 376–383. <https://doi.org/10.1007/s11307-012-0609-4>
- Ettrup, A., Svarer, C., McMahon, B., da Cunha-Bang, S., Lehel, S., Møller, K., Dyssegaard, A., Ganz, M., Beliveau, V., Jørgensen, L.M., Gillings, N., Knudsen, G.M., 2016. Serotonin 2A receptor agonist binding in the human brain with [11C]Cimbi-36: Test-retest reproducibility and head-to-head comparison with the antagonist [18F]altanserin. *NeuroImage*. <https://doi.org/10.1016/j.neuroimage.2016.02.001>
- Falchi-Carvalho, M., Palhano-Fontes, F., Wießner, I., Barros, H., Bolcont, R., Laborde, S., Ruschi B Silva, S., Montanini, D., C Barbosa, D., Teixeira, E., Florence-Vilela, R., Almeida, R., K A de Macedo, R., Arichelle, F., J Pantrigo, É., V Costa-Macedo, J., da Cruz Nunes, J.A., de Araújo Costa Neto, L.A., Nunes Ferreira, L.F., Dantas Corrêa, L., da Costa Bezerra, R.B., Arcoverde, E., Galvão-Coelho, N., B Araujo, D., 2025. Rapid and sustained antidepressant effects of vaporized

- N,N-dimethyltryptamine: a phase 2a clinical trial in treatment-resistant depression. *Neuropsychopharmacol. Off. Publ. Am. Coll. Neuropsychopharmacol.* 50, 895–903. <https://doi.org/10.1038/s41386-025-02091-6>
- Felippe, H., Viol, A., Araujo, D., Luz, M.D., F, Palhano-Fontes, Onias, H., Raposo, E., Viswanathan, G., 2021. The von Neumann entropy for the Pearson correlation matrix: A test of the entropic brain hypothesis.
- Finn, E.S., Bandettini, P.A., 2021. Movie-watching outperforms rest for functional connectivity-based prediction of behavior. *NeuroImage* 235, 117963. <https://doi.org/10.1016/j.neuroimage.2021.117963>
- Finn, E.S., Glerean, E., Khojandi, A.Y., Nielson, D., Molfese, P.J., Handwerker, D.A., Bandettini, P.A., 2020. Idiosynchrony: From shared responses to individual differences during naturalistic neuroimaging. *NeuroImage* 215, 116828. <https://doi.org/10.1016/j.neuroimage.2020.116828>
- Finnema, S.J., Stepanov, V., Ettrup, A., Nakao, R., Amini, N., Svedberg, M., Lehmann, C., Hansen, M., Knudsen, G.M., Halldin, C., 2014. Characterization of [11C]Cimbi-36 as an agonist PET radioligand for the 5-HT_{2A} and 5-HT_{2C} receptors in the nonhuman primate brain. *NeuroImage*. <https://doi.org/10.1016/j.neuroimage.2013.08.035>
- Fox, M.D., Snyder, A.Z., Vincent, J.L., Corbetta, M., Van Essen, D.C., Raichle, M.E., 2005. The human brain is intrinsically organized into dynamic, anticorrelated functional networks. *Proc. Natl. Acad. Sci. U. S. A.* <https://doi.org/10.1073/pnas.0504136102>
- Fuentes, J.J., Fonseca, F., Elices, M., Farré, M., Torrens, M., 2019. Therapeutic Use of LSD in Psychiatry: A Systematic Review of Randomized-Controlled Clinical Trials. *Front. Psychiatry* 10, 943. <https://doi.org/10.3389/fpsy.2019.00943>
- Galdas, P., 2017. Revisiting Bias in Qualitative Research. *Int. J. Qual. Methods* 16, 160940691774899. <https://doi.org/10.1177/1609406917748992>
- Garel, N., Tate, S., Nash, K., Lembke, A., 2024. Trends in hallucinogen-associated emergency department visits and hospitalizations in California, USA, from 2016 to 2022. *Addiction* 119, 960–964. <https://doi.org/10.1111/add.16432>
- Gasser, P., Kirchner, K., Passie, T., 2015. LSD-assisted psychotherapy for anxiety associated with a life-threatening disease: A qualitative study of acute and sustained subjective effects. *J. Psychopharmacol. (Oxf.)* 29, 57–68. <https://doi.org/10.1177/0269881114555249>
- Glasser, M., 2016. The Human Connectome Project: Progress and Prospects. *Cerebrum Dana Forum Brain Sci.*
- Glennon, R.A., Titeler, M., McKenney, J.D., 1984. Evidence for 5-HT₂ involvement in the mechanism of action of hallucinogenic agents. *Life Sci.* 35, 2505–2511. [https://doi.org/10.1016/0024-3205\(84\)90436-3](https://doi.org/10.1016/0024-3205(84)90436-3)
- Goodwin, G.M., Aaronson, S.T., Alvarez, O., Arden, P.C., Baker, A., Bennett, J.C., Bird, C., Blom, R.E., Brennan, C., Brusch, D., Burke, L., Campbell-Coker, K., Carhart-Harris, R., Cattell, J., Daniel, A., DeBattista, C., Dunlop, B.W., Eisen, K., Feifel, D., Forbes, M., Haumann, H.M., Hellerstein, D.J., Hoppe, A.I., Husain, M.I., Jelen, L.A., Kamphuis, J., Kawasaki, J., Kelly, J.R., Key, R.E., Kishon, R., Peck, S.K., Knight, G., Koolen, M.H.B., Lean, M., Licht, R.W., Maples-Keller, J.L., Mars, J., Marwood, L., McElhiney, M.C., Miller, T.L., Mirow, A., Mistry, S., Mletzko-Crowe, T., Modlin, L.N., Nielsen, R.E., Nielson, E.M., Offerhaus, S.R., O’Keane, V., Páleníček, T., Printz, D., Rademaker, M.C., Reemst, A. van, Reinholdt, F., Repantis, D., Rucker, J., Rudow, S., Ruffell, S., Rush, A.J., Schoevers, R.A., Seynaeve, M., Shao, S., Soares, J.C., Somers, M., Stansfield, S.C., Sterling, D., Strockis, A., Tsai, J., Visser, L., Wahba, M., Williams, S., Young, A.H., Ywema, P., Zisook, S., Malievskaia, E., 2022. Single-Dose Psilocybin for a Treatment-Resistant Episode of Major Depression. *N. Engl. J. Med.* 387, 1637–1648. <https://doi.org/10.1056/NEJMoa2206443>
- Goodwin, G.M., Aaronson, S.T., Alvarez, O., Carhart-Harris, R., Chai-Rees, J., Croal, M., DeBattista, C., Dunlop, B.W., Feifel, D., Hellerstein, D.J., Husain, M.I., Kelly, J.R., Kirlic, N., Licht, R.W., Marwood, L., Meyer, T.D., Mistry, S., Nowakowska, A., Páleníček, T., Repantis, D., Schoevers, R.A., Simmons, H., Somers, M., Teoh, E., Tsai, J., Wahba, M., Williams, S., Young, A.H., Young,

- M.B., Zisook, S., Malievskaia, E., 2025. The role of the psychedelic experience in psilocybin treatment for treatment-resistant depression. *J. Affect. Disord.* 372, 523–532. <https://doi.org/10.1016/j.jad.2024.12.061>
- Gotvaldová, K., Borovička, J., Hájková, K., Cihlářová, P., Rockefeller, A., Kuchař, M., 2022. Extensive Collection of Psychotropic Mushrooms with Determination of Their Tryptamine Alkaloids. *J. Mol. Sci.* 23, 14068. <https://doi.org/10.3390/ijms232214068>
- Griffiths, R.R., Johnson, M.W., Carducci, M.A., Umbricht, A., Richards, W.A., Richards, B.D., Cosimano, M.P., Klinedinst, M.A., 2016. Psilocybin produces substantial and sustained decreases in depression and anxiety in patients with life-threatening cancer: A randomized double-blind trial. *J. Psychopharmacol. (Oxf.)* 30, 1181–1197. <https://doi.org/10.1177/0269881116675513>
- Griffiths, R.R., Johnson, M.W., Richards, W.A., Richards, B.D., McCann, U., Jesse, R., 2011. Psilocybin occasioned mystical-type experiences: Immediate and persisting dose-related effects. *Psychopharmacology (Berl.)* 218, 649–665. <https://doi.org/10.1007/s00213-011-2358-5>
- Griffiths, R.R., Richards, W.A., McCann, U., Jesse, R., 2006. Psilocybin can occasion mystical-type experiences having substantial and sustained personal meaning and spiritual significance. *Psychopharmacology (Berl.)* 187, 268–283. <https://doi.org/10.1007/s00213-006-0457-5>
- Gumpper, R.H., Jain, M.K., Kim, K., Sun, R., Sun, N., Xu, Z., DiBerto, J.F., Krumm, B.E., Kapolka, N.J., Kaniskan, H.Ü., Nichols, D.E., Jin, J., Fay, J.F., Roth, B.L., 2025. The structural diversity of psychedelic drug actions revealed. *Nat. Commun.* 16, 2734. <https://doi.org/10.1038/s41467-025-57956-7>
- Hagmann, P., Cammoun, L., Gigandet, X., Meuli, R., Honey, C.J., Wedeen, V.J., Sporns, O., 2008. Mapping the Structural Core of Human Cerebral Cortex. *PLOS Biol.* 6, e159. <https://doi.org/10.1371/journal.pbio.0060159>
- Halberstadt, A.L., 2017. Pharmacology and Toxicology of N-Benzylphenethylamine (“NBOMe”) Hallucinogens. *Curr. Top. Behav. Neurosci.* 32, 283–311. https://doi.org/10.1007/7854_2016_64
- Halberstadt, A.L., Geyer, M.A., 2011. Multiple receptors contribute to the behavioral effects of indoleamine hallucinogens. *Neuropharmacology* 61, 364–381. <https://doi.org/10.1016/j.neuropharm.2011.01.017>
- Halberstadt, A.L., Nichols, D.E., Vollenweider, F.X., 2017. Behavioral Neurobiology of Psychedelic Drugs.
- Hariri, A.R., Tessitore, A., Mattay, V.S., Fera, F., Weinberger, D.R., 2002. The amygdala response to emotional stimuli: a comparison of faces and scenes. *NeuroImage* 17, 317–323. <https://doi.org/10.1006/nimg.2002.1179>
- Hartogsohn, I., 2017. Constructing drug effects: A history of set and setting. *Drug Sci. Policy Law* 3, 205032451668332. <https://doi.org/10.1177/2050324516683325>
- Hibicke, M., Landry, A.N., Kramer, H.M., Talman, Z.K., Nichols, C.D., 2020. Psychedelics, but Not Ketamine, Produce Persistent Antidepressant-like Effects in a Rodent Experimental System for the Study of Depression. *ACS Chem. Neurosci.* 11, 864–871. <https://doi.org/10.1021/acscchemneuro.9b00493>
- Hofmann, A., 2022. LSD My Problem Child (4th Edition): Reflections on Sacred Drugs, Mysticism and Science. Multidisciplinary Association for Psychedelic Studies.
- Hofmann, A., 1906-2008, 1992. LSD, my problem child : reflections on sacred drugs, mysticism, and science. Mt. View, Calif. : Wiretap, [1992?].
- Holm, S., 1979. A simple sequentially rejective multiple test procedure. *Scand. J. Stat.*
- Holze, F., Gasser, P., Müller, F., Dolder, P.C., Liechti, M.E., 2022a. Lysergic Acid Diethylamide–Assisted Therapy in Patients With Anxiety With and Without a Life-Threatening Illness: A Randomized, Double-Blind, Placebo-Controlled Phase II Study. *Biol. Psychiatry*. <https://doi.org/10.1016/j.biopsych.2022.08.025>
- Holze, F., Ley, L., Müller, F., Becker, A.M., Straumann, I., Vizeli, P., Kuehne, S.S., Roder, M.A., Duthaler, U., Kolaczynska, K.E., Varghese, N., Eckert, A., Liechti, M.E., 2022b. Direct comparison of the acute effects of lysergic acid diethylamide and psilocybin in a double-blind placebo-controlled study in healthy subjects. *Neuropsychopharmacology* 47, 1180–1187.

- <https://doi.org/10.1038/s41386-022-01297-2>
- Holze, F., Vizeli, P., Ley, L., Müller, F., Dolder, P., Stocker, M., Duthaler, U., Varghese, N., Eckert, A., Borgwardt, S., Liechti, M.E., 2021. Acute dose-dependent effects of lysergic acid diethylamide in a double-blind placebo-controlled study in healthy subjects. *Neuropsychopharmacology*. <https://doi.org/10.1038/s41386-020-00883-6>
- Horita, A., Weber, L.J., 1961. Dephosphorylation of psilocybin to psilocin by alkaline phosphatase. *Proc. Soc. Exp. Biol. Med. Soc. Exp. Biol. Med. N. Y.* N 106, 32–34. <https://doi.org/10.3181/00379727-106-26228>
- Hume, S.P., Myers, R., Bloomfield, P.M., Opacka-Juffry, J., Cremer, J.E., Ahier, R.G., Luthra, S.K., Brooks, D.J., Lammertsma, A.A., 1992. Quantitation of carbon-11-labeled raclopride in rat striatum using positron emission tomography. *Synap. N. Y.* N 12, 47–54. <https://doi.org/10.1002/syn.890120106>
- Husain, M.I., Blumberger, D.M., Castle, D.J., Ledwos, N., Fellows, E., Jones, B.D.M., Ortiz, A., Kloiber, S., Wang, W., Rosenblat, J.D., Mulsant, B.H., 2023. Psilocybin for treatment-resistant depression without psychedelic effects: study protocol for a 4-week, double-blind, proof-of-concept randomised controlled trial. *BJPsych Open* 9, e134. <https://doi.org/10.1192/bjo.2023.535>
- Innis, R.B., Cunningham, V.J., Delforge, J., Fujita, M., Gjedde, A., Gunn, R.N., Holden, J., Houle, S., Huang, S.C., Ichise, M., Iida, H., Ito, H., Kimura, Y., Koeppe, R.A., Knudsen, G.M., Knuuti, J., Lammertsma, A.A., Laruelle, M., Logan, J., Maguire, R.P., Mintun, M.A., Morris, E.D., Parsey, R., Price, J.C., Slifstein, M., Sossi, V., Suhara, T., Votaw, J.R., Wong, D.F., Carson, R.E., 2007. Consensus nomenclature for in vivo imaging of reversibly binding radioligands. *J. Cereb. Blood Flow Metab.* <https://doi.org/10.1038/sj.jcbfm.9600493>
- Jain, V., Langham, M.C., Floyd, T.F., Jain, G., Magland, J.F., Wehrli, F.W., 2011. Rapid magnetic resonance measurement of global cerebral metabolic rate of oxygen consumption in humans during rest and hypercapnia. *J. Cereb. Blood Flow Metab. Off. J. Int. Soc. Cereb. Blood Flow Metab.* 31, 1504–1512. <https://doi.org/10.1038/jcbfm.2011.34>
- Johansen, A., Hansen, H.D., Svarer, C., Lehel, S., Leth-Petersen, S., Kristensen, J.L., Gillings, N., Knudsen, G.M., 2018. The importance of small polar radiometabolites in molecular neuroimaging: A PET study with [¹¹C]Cimbi-36 labeled in two positions. *J. Cereb. Blood Flow Metab. Off. J. Int. Soc. Cereb. Blood Flow Metab.* 38, 659–668. <https://doi.org/10.1177/0271678X17746179>
- Johansen, A., Holm, S., Dall, B., Keller, S., Kristensen, J.L., Knudsen, G.M., Hansen, H.D., 2019. Human biodistribution and radiation dosimetry of the 5-HT_{2A} receptor agonist Cimbi-36 labeled with carbon-11 in two positions. *EJNMMI Res.* 9, 71. <https://doi.org/10.1186/s13550-019-0527-4>
- Johnson, M.W., Garcia-Romeu, A., Griffiths, R.R., 2017. Long-term follow-up of psilocybin-facilitated smoking cessation. *Am. J. Drug Alcohol Abuse* 43, 55–60. <https://doi.org/10.3109/00952990.2016.1170135>
- Johnson, M.W., Griffiths, R.R., Hendricks, P.S., Henningfield, J.E., 2018. The abuse potential of medical psilocybin according to the 8 factors of the Controlled Substances Act. *Neuropharmacology, Psychedelics: New Doors, Altered Perceptions* 142, 143–166. <https://doi.org/10.1016/j.neuropharm.2018.05.012>
- Johnson, M.W., Richards, W.A., Griffiths, R.R., 2008. Human hallucinogen research: Guidelines for safety. *J. Psychopharmacol. (Oxf.)* 22, 603–620. <https://doi.org/10.1177/0269881108093587>
- Jørgensen, L.M., Weikop, P., Villadsen, J., Visnapuu, T., Ettrup, A., Hansen, H.D., Baandrup, A.O., Andersen, F.L., Bjarkam, C.R., Thomsen, C., Jespersen, B., Knudsen, G.M., 2017. Cerebral 5-HT release correlates with [¹¹C]Cimbi36 PET measures of 5-HT_{2A} receptor occupancy in the pig brain. *J. Cereb. Blood Flow Metab. Off. J. Int. Soc. Cereb. Blood Flow Metab.* 37, 425–434. <https://doi.org/10.1177/0271678X16629483>
- Kim, S., Chen, J., Cheng, T., Gindulyte, A., He, J., He, S., Li, Q., Shoemaker, B.A., Thiessen, P.A., Yu, B., Zaslavsky, L., Zhang, J., Bolton, E.E., 2021. PubChem in 2021: new data content and improved web interfaces. *Nucleic Acids Res.* 49, D1388–D1395. <https://doi.org/10.1093/nar/gkaa971>
- Krebs, T.S., Johansen, P.-Ø., 2012. Lysergic acid diethylamide (LSD) for alcoholism: meta-analysis of

- randomized controlled trials. *J. Psychopharmacol. Oxf. Engl.* 26, 994–1002.
<https://doi.org/10.1177/0269881112439253>
- Kringelbach, M.L., Cruzat, J., Cabral, J., Knudsen, G.M., Carhart-Harris, R., Whybrow, P.C., Logothetis, N.K., Deco, G., 2020. Dynamic coupling of whole-brain neuronal and neurotransmitter systems. *Proc. Natl. Acad. Sci. U. S. A.* 117, 9566–9576. <https://doi.org/10.1073/pnas.1921475117>
- Kung, Y.-C., Li, C.-W., Hsiao, F.-C., Tsai, P.-J., Chen, S., Li, M.-K., Lee, H.-C., Chang, C.-Y., Wu, C.W., Lin, C.-P., 2022. Cross-Scale Dynamicity of Entropy and Connectivity in the Sleeping Brain. *Brain Connect.* 12, 835–845. <https://doi.org/10.1089/brain.2021.0174>
- Lammertsma, A.A., Bench, C.J., Hume, S.P., Osman, S., Gunn, K., Brooks, D.J., Frackowiak, R.S., 1996. Comparison of methods for analysis of clinical [¹¹C]raclopride studies. *J. Cereb. Blood Flow Metab. Off. J. Int. Soc. Cereb. Blood Flow Metab.* 16, 42–52.
<https://doi.org/10.1097/00004647-199601000-00005>
- Lammertsma, A.A., Hume, S.P., 1996. Simplified Reference Tissue Model for PET Receptor Studies. *NeuroImage* 4, 153–158. <https://doi.org/10.1006/nimg.1996.0066>
- Larsen, K., Lindberg, U., Ozenne, B., McCulloch, D.E., Armand, S., Madsen, M.K., Johansen, A., Stenbæk, D.S., Knudsen, G.M., Fisher, P.M., 2025. Acute psilocybin and ketanserin effects on cerebral blood flow: 5-HT_{2A}R neuromodulation in healthy humans. *J. Cereb. Blood Flow Metab.* 0271678X251323364. <https://doi.org/10.1177/0271678X251323364>
- Laurell, G.L., Plavén-Sigray, P., Svarer, C., Ogden, R.T., Knudsen, G.M., Schain, M., 2022. Designing drug occupancy studies with PET neuroimaging: Sample size, occupancy ranges and analytical methods. *NeuroImage* 263, 119620. <https://doi.org/10.1016/j.neuroimage.2022.119620>
- Lebedev, A.V., Kaelen, M., Lövdén, M., Nilsson, J., Feilding, A., Nutt, D.J., Carhart-Harris, R.L., 2016. LSD-induced entropic brain activity predicts subsequent personality change. *Hum. Brain Mapp.* 37, 3203–3213. <https://doi.org/10.1002/hbm.23234>
- Lebedev, A.V., Lövdén, M., Rosenthal, G., Feilding, A., Nutt, D.J., Carhart-Harris, R.L., 2015. Finding the self by losing the self: Neural correlates of ego-dissolution under psilocybin. *Hum. Brain Mapp.* 36, 3137–3153. <https://doi.org/10.1002/hbm.22833>
- Lee, O.E., Braun, T.M., Lee, O.E., Braun, T.M., 2012. Permutation Tests for Random Effects in Linear Mixed Models Published by : International Biometric Society Stable URL :
<https://www.jstor.org/stable/23270450> REFERENCES Linked references are available on JSTOR for this article : reference # references _ t 68, 486–493.
- Lempel, A., Ziv, J., 1976. On the Complexity of Finite Sequences. *IEEE Trans. Inf. Theory* 22, 75–81.
<https://doi.org/10.1109/TIT.1976.1055501>
- Letheby, C., 2021. *Philosophy of psychedelics*. Oxford University Press, Oxford.
- Liechti, M.E., 2017. Modern Clinical Research on LSD. *Neuropsychopharmacology* 42, 2114–2127.
<https://doi.org/10.1038/npp.2017.86>
- Liechti, M.E., Holze, F., 2022. Dosing Psychedelics and MDMA, in: Barrett, F.S., Preller, K.H. (Eds.), *Disruptive Psychopharmacology*. Springer International Publishing, Cham, pp. 3–21.
https://doi.org/10.1007/7854_2021_270
- Liechti, M.E., Saur, M.R., Gamma, A., Hell, D., Vollenweider, F.X., 2000. Psychological and physiological effects of MDMA ('Ecstasy') after pretreatment with the 5-HT₂ antagonist ketanserin in healthy humans. *Neuropsychopharmacology* 23, 396–404. [https://doi.org/10.1016/S0893-133X\(00\)00126-3](https://doi.org/10.1016/S0893-133X(00)00126-3)
- Lindquist, M.A., Xu, Y., Nebel, M.B., Caffo, B.S., 2014. Evaluating Dynamic Bivariate Correlations in Resting-state fMRI: A comparison study and a new approach. *NeuroImage* 101, 531–546.
<https://doi.org/10.1016/j.neuroimage.2014.06.052>
- Liu, T.T., 2013. Neurovascular factors in resting-state functional MRI. *NeuroImage* 80, 339–348.
<https://doi.org/10.1016/j.neuroimage.2013.04.071>
- LSD Experiments, 1995.
- Luethi, D., Hoener, M.C., Krähenbühl, S., Liechti, M.E., Duthaler, U., 2019. Cytochrome P450 enzymes contribute to the metabolism of LSD to nor-LSD and 2-oxo-3-hydroxy-LSD: Implications for clinical

- LSD use. *Biochem. Pharmacol.* 164, 129–138. <https://doi.org/10.1016/j.bcp.2019.04.013>
- Luppi, A.I., Carhart-Harris, R.L., Roseman, L., Pappas, I., Menon, D.K., Stamatakis, E.A., 2021. LSD alters dynamic integration and segregation in the human brain. *NeuroImage* 227, 117653. <https://doi.org/10.1016/j.neuroimage.2020.117653>
- Madsen, M.K., Fisher, P.M., Burmester, D., Dyssegaard, A., Stenbæk, D.S., Kristiansen, S., Johansen, S.S., Lehel, S., Linnet, K., Svarer, C., Erritzoe, D., Ozenne, B., Knudsen, G.M., 2019. Psychedelic effects of psilocybin correlate with serotonin 2A receptor occupancy and plasma psilocin levels. *Neuropsychopharmacology* 44, 1328–1334. <https://doi.org/10.1038/s41386-019-0324-9>
- Madsen, M.K., Fisher, P.M.D., Stenbæk, D.S., Kristiansen, S., Burmester, D., Lehel, S., Páleníček, T., Kuchař, M., Svarer, C., Ozenne, B., Knudsen, G.M., 2020. A single psilocybin dose is associated with long-term increased mindfulness, preceded by a proportional change in neocortical 5-HT_{2A} receptor binding. *Eur. Neuropsychopharmacol.* 33, 71–80. <https://doi.org/10.1016/j.euroneuro.2020.02.001>
- Madsen, M.K., Petersen, A.S., Stenbæk, D.S., Sørensen, I.M., Schiønning, H., Fjeld, T., Nykjaer, C.H., Marie, S., Larsen, U., Grzywacz, M., Mathiesen, T., Klausen, I.L., Overgaard-Hansen, O., Brendstrup-Brix, K., Linnet, K., Johansen, S.S., Fisher, P.M., Jensen, R.H., Knudsen, G.M., 2022. Psilocybin-induced reduction in chronic cluster headache attack frequency correlates with changes in hypothalamic functional connectivity. *medRxiv* 2022.07.10.22277414. <https://doi.org/10.1101/2022.07.10.22277414>
- Madsen, M.K., Stenbæk, D.S., Arvidsson, A., Armand, S., Marstrand-Joergensen, M.R., Johansen, S.S., Linnet, K., Ozenne, B., Knudsen, G.M., Fisher, P.M., 2021. Psilocybin-induced changes in brain network integrity and segregation correlate with plasma psilocin level and psychedelic experience. *Eur. Neuropsychopharmacol.* 50, 121–132. <https://doi.org/10.1016/j.euroneuro.2021.06.001>
- Mallaroni, P., Singleton, P., Mason, N.L., Satterthwaite, T.D., Ramaekers, J.G., 2024. The forgotten psychedelic: Spatiotemporal mapping of brain organisation following the administration of 2C-B and psilocybin. <https://doi.org/10.1101/2024.10.22.619393>
- Manevski, N., Kurkela, M., Höglund, C., Mauriala, T., Court, M.H., Yli-Kauhaluoma, J., Finel, M., 2010. Glucuronidation of psilocin and 4-hydroxyindole by the human UDP-glucuronosyltransferases. *Drug Metab. Dispos. Biol. Fate Chem.* 38, 386–395. <https://doi.org/10.1124/dmd.109.031138>
- Marona-Lewicka, D., Nichols, D.E., 1995. Complex stimulus properties of LSD: a drug discrimination study with alpha 2-adrenoceptor agonists and antagonists. *Psychopharmacology (Berl.)* 120, 384–391. <https://doi.org/10.1007/BF02245809>
- McCulloch, D.E.-W., Knudsen, G.M., Barrett, F.S., Doss, M.K., Carhart-Harris, R.L., Rosas, F.E., Deco, G., Kringelbach, M.L., Preller, K.H., Ramaekers, J.G., Mason, N.L., Müller, F., Fisher, P.M., 2022. Psychedelic resting-state neuroimaging: A review and perspective on balancing replication and novel analyses. *Neurosci. Biobehav. Rev.* 138, 104689. <https://doi.org/10.1016/j.neubiorev.2022.104689>
- McCulloch, D.E.-W., Liechti, M.E., Kuypers, K.P.C., Nutt, D., Lundberg, J., Stenbæk, D.S., Goodwin, G.M., Gründer, G., Butlen-Ducuing, F., Haberkamp, M., Thirstrup, S., Knudsen, G.M., 2024. Knowledge gaps in psychedelic medicalisation: Clinical studies and regulatory aspects. *Neurosci. Appl.* 3, 103938. <https://doi.org/10.1016/j.nsa.2024.103938>
- McGlothlin, W.H., Arnold, D.O., 1971. LSD Revisited: A Ten-Year Follow-up of Medical LSD Use. *Arch. Gen. Psychiatry* 24, 35–49. <https://doi.org/10.1001/archpsyc.1971.01750070037005>
- McRobbie, D.W., Moore, E.A., Graves, M.J., Prince, M.R., 2006. *MRI from Picture to Proton*, 2nd ed. Cambridge University Press, Cambridge. <https://doi.org/10.1017/CBO9780511545405>
- Miller, K.L., Alfaro-Almagro, F., Bangerter, N.K., Thomas, D.L., Yacoub, E., Xu, J., Bartsch, A.J., Jbabdi, S., Sotiropoulos, S.N., Andersson, J.L.R., Griffanti, L., Douaud, G., Okell, T.W., Weale, P., Dragonu, I., Garratt, S., Hudson, S., Collins, R., Jenkinson, M., Matthews, P.M., Smith, S.M., 2016. Multimodal population brain imaging in the UK Biobank prospective epidemiological study. *Nat. Neurosci.* 19, 1523–1536. <https://doi.org/10.1038/nn.4393>
- Moreno, F.A., Wiegand, C.B., Taitano, E.K., Delgado, P.L., 2006. Safety, tolerability, and efficacy of

- psilocybin in 9 patients with obsessive-compulsive disorder. *J. Clin. Psychiatry* 67, 1735–1740. <https://doi.org/10.4088/JCP.v67n1110>
- Mueller, L., Santos de Jesus, J., Schmid, Y., Müller, F., Becker, A., Klaiber, A., Straumann, I., Luethi, D., Haijen, E.C.H.M., Hurks, P.P.M., Kuypers, K.P.C., Liechti, M.E., 2025. Safety and Efficacy of Repeated Low-Dose LSD for ADHD Treatment in Adults. *JAMA Psychiatry* e250044. <https://doi.org/10.1001/jamapsychiatry.2025.0044>
- Müller, F., Dolder, P.C., Schmidt, A., Liechti, M.E., Borgwardt, S., 2018. Altered network hub connectivity after acute LSD administration. *NeuroImage Clin.* 18, 694–701. <https://doi.org/10.1016/j.nicl.2018.03.005>
- Müller, F., Zaczek, H., Becker, A.M., Ley, L., Borgwardt, S., Jesus, J.S. de, Loh, N., Kohut, J., Auernig, M., Boehlke, C., Liechti, M.E., 2025. Efficacy and safety of low- versus high-dose-LSD-assisted therapy in patients with major depression: A randomized trial. *Med 0*. <https://doi.org/10.1016/j.medj.2025.100725>
- Murray, C.H., Frohlich, J., Haggarty, C.J., Tare, I., Lee, R., de Wit, H., 2024. Neural complexity is increased after low doses of LSD, but not moderate to high doses of oral THC or methamphetamine. *Neuropsychopharmacology* 1–9. <https://doi.org/10.1038/s41386-024-01809-2>
- Muthukumaraswamy, S.D., Forsyth, A., Lumley, T., 2021. Blinding and expectancy confounds in psychedelic randomized controlled trials. *Expert Rev. Clin. Pharmacol.* 1–20. <https://doi.org/10.1080/17512433.2021.1933434>
- Nash, J.F., Roth, B.L., Brodtkin, J.D., Nichols, D.E., Gudelsky, G.A., 1994. Effect of the R(-) and S(+) isomers of MDA and MDMA on phosphatidyl inositol turnover in cultured cells expressing 5-HT_{2A} or 5-HT_{2C} receptors. *Neurosci. Lett.* 177, 111–115. [https://doi.org/10.1016/0304-3940\(94\)90057-4](https://doi.org/10.1016/0304-3940(94)90057-4)
- Nichols, D.E., Frescas, S., Marona-Lewicka, D., Kurrasch-Orbaugh, D.M., 2002. Lysergamides of isomeric 2,4-dimethylazetidines map the binding orientation of the diethylamide moiety in the potent hallucinogenic agent N,N-diethyllysergamide (LSD). *J. Med. Chem.* 45, 4344–4349. <https://doi.org/10.1021/jm020153s>
- Nichols, D.E., Grob, C.S., 2018. Is LSD toxic? *Forensic Sci. Int.* 284, 141–145. <https://doi.org/10.1016/j.forsciint.2018.01.006>
- Nielson, E.M., May, D.G., Forcehimes, A.A., Bogenschutz, M.P., 2018. The Psychedelic Debriefing in Alcohol Dependence Treatment: Illustrating Key Change Phenomena through Qualitative Content Analysis of Clinical Sessions. *Front. Pharmacol.* 9, 132. <https://doi.org/10.3389/fphar.2018.00132>
- Niendam, T.A., Laird, A.R., Ray, K.L., Dean, Y.M., Glahn, D.C., Carter, C.S., 2012. Meta-analytic evidence for a superordinate cognitive control network subserving diverse executive functions. *Cogn. Affect. Behav. Neurosci.* 12, 241–268. <https://doi.org/10.3758/s13415-011-0083-5>
- Noble, S., Scheinost, D., Constable, R.T., 2019. A decade of test-retest reliability of functional connectivity: A systematic review and meta-analysis. *NeuroImage* 203, 116157. <https://doi.org/10.1016/j.neuroimage.2019.116157>
- Noorani, T., Garcia-Romeu, A., Swift, T.C., Griffiths, R.R., Johnson, M.W., 2018. Psychedelic therapy for smoking cessation: Qualitative analysis of participant accounts. *J. Psychopharmacol. Oxf. Engl.* 32, 756–769. <https://doi.org/10.1177/0269881118780612>
- Nørgaard, M., Ganz, M., Svarer, C., Frokjaer, V.G., Greve, D.N., Strother, S.C., Knudsen, G.M., 2020. Different preprocessing strategies lead to different conclusions: A [11C]DASB-PET reproducibility study. *J. Cereb. Blood Flow Metab. Off. J. Int. Soc. Cereb. Blood Flow Metab.* 40, 1902–1911. <https://doi.org/10.1177/0271678X19880450>
- Nour, M.M., Evans, L., Nutt, D., Carhart-Harris, R.L., 2016. Ego-dissolution and psychedelics: Validation of the ego-dissolution inventory (EDI). *Front. Hum. Neurosci.* 10, 1–13. <https://doi.org/10.3389/fnhum.2016.00269>
- Nutt, D.J., Hunt, P., Schlag, A.K., Fitzgerald, P., 2024. The Australia story: Current status and future challenges for the clinical applications of psychedelics. *Br. J. Pharmacol.* <https://doi.org/10.1111/bph.17398>

- Nutt, D.J., King, L.A., Nichols, D.E., 2013. Effects of Schedule I drug laws on neuroscience research and treatment innovation. *Nat. Rev. Neurosci.* 14, 577–585. <https://doi.org/10.1038/nrn3530>
- Nutt, D.J., King, L.A., Phillips, L.D., 2010. Drug harms in the UK: a multicriteria decision analysis. *The Lancet* 376, 1558–1565. [https://doi.org/10.1016/S0140-6736\(10\)61462-6](https://doi.org/10.1016/S0140-6736(10)61462-6)
- Oehen, P., Gasser, P., 2022. Using a MDMA- and LSD-Group Therapy Model in Clinical Practice in Switzerland and Highlighting the Treatment of Trauma-Related Disorders. *Front. Psychiatry* 13, 863552. <https://doi.org/10.3389/fpsyt.2022.863552>
- Olson, D.E., 2021. The Subjective Effects of Psychedelics May Not Be Necessary for Their Enduring Therapeutic Effects. *ACS Pharmacol. Transl. Sci.* 4, 563–567. <https://doi.org/10.1021/acspsci.0c00192>
- Ozenne, B., Fisher, P.M., Budtz-Jørgensen, E., 2020. Small sample corrections for Wald tests in latent variable models. *J. R. Stat. Soc. Ser. C Appl. Stat.* 69, 841–861. <https://doi.org/10.1111/rssc.12414>
- Pallavicini, C., Cavanna, F., Zamberlan, F., de la Fuente, L.A., Ilksoy, Y., Perl, Y.S., Arias, M., Romero, C., Carhart-Harris, R., Timmermann, C., Tagliazucchi, E., 2021. Neural and subjective effects of inhaled N,N-dimethyltryptamine in natural settings. *J. Psychopharmacol. (Oxf.)* 35, 406–420. <https://doi.org/10.1177/0269881120981384>
- Pasquini, L., Palhano-Fontes, F., Araujo, D.B., 2020. Subacute effects of the psychedelic ayahuasca on the salience and default mode networks. *J. Psychopharmacol. (Oxf.)*. <https://doi.org/10.1177/0269881120909409>
- Peck, S.K., Shao, S., Gruen, T., Yang, K., Babakanian, A., Trim, J., Finn, D.M., Kaye, W.H., 2023. Psilocybin therapy for females with anorexia nervosa: a phase 1, open-label feasibility study. *Nat. Med.* 29, 1947–1953. <https://doi.org/10.1038/s41591-023-02455-9>
- Penny, W., Friston, K., Ashburner, J., Kiebel, S., Nichols, T., 2007. Statistical Parametric Mapping: The Analysis of Functional Brain Images, Statistical Parametric Mapping: The Analysis of Functional Brain Images. <https://doi.org/10.1016/B978-0-12-372560-8.X5000-1>
- Preller, K.H., Burt, J.B., Ji, J.L., Schleifer, C.H., Adkinson, B.D., Stämpfli, P., Seifritz, E., Repovš, G., Krystal, J.H., Murray, J.D., Vollenweider, F.X., Anticevic, A., 2018. Changes in global and thalamic brain connectivity in LSD-induced altered states of consciousness are attributable to the 5-HT_{2A} receptor. *eLife* 7, 1–31. <https://doi.org/10.7554/eLife.35082>
- Preller, K.H., Duerler, P., Burt, J.B., Ji, J.L., Adkinson, B., Stämpfli, P., Seifritz, E., Repovš, G., Krystal, J.H., Murray, J.D., Anticevic, A., Vollenweider, F.X., 2020. Psilocybin Induces Time-Dependent Changes in Global Functional Connectivity. *Biol. Psychiatry*. <https://doi.org/10.1016/j.biopsych.2019.12.027>
- Preller, K.H., Herdener, M., Pokorny, T., Planzer, A., Kraehenmann, R., Stämpfli, P., Liechti, M.E., Seifritz, E., Vollenweider, F.X., 2017. The Fabric of Meaning and Subjective Effects in LSD-Induced States Depend on Serotonin 2A Receptor Activation. *Curr. Biol.* 27, 451–457. <https://doi.org/10.1016/j.cub.2016.12.030>
- Preller, K.H., Vollenweider, F.X., 2018. Phenomenology, structure, and dynamic of psychedelic states, in: *Current Topics in Behavioral Neurosciences*. https://doi.org/10.1007/7854_2016_459
- Project MKUltra, The CIA's Program of Research in Behavioral Modification, 1977.
- Raichle, M.E., 2015. The restless brain: How intrinsic activity organizes brain function. *Philos. Trans. R. Soc. B Biol. Sci.* <https://doi.org/10.1098/rstb.2014.0172>
- Raichle, M.E., 2011. The Restless Brain. *Brain Connect.* 1, 3–12. <https://doi.org/10.1089/brain.2011.0019>
- Raichle, M.E., MacLeod, A.M., Snyder, A.Z., Powers, W.J., Gusnard, D.A., Shulman, G.L., 2001. A default mode of brain function. *Proc. Natl. Acad. Sci. U. S. A.* 98, 676–682. <https://doi.org/10.1073/pnas.98.2.676>
- Raison, C.L., Sanacora, G., Woolley, J., Heinzerling, K., Dunlop, B.W., Brown, R.T., Kakar, R., Hassman, M., Trivedi, R.P., Robison, R., Gukasyan, N., Nayak, S.M., Hu, X., O'Donnell, K.C., Kelmendi, B., Sloschower, J., Penn, A.D., Bradley, E., Kelly, D.F., Mletzko, T., Nicholas, C.R., Hutson, P.R., Tarpley, G., Utzinger, M., Lenocho, K., Warchol, K., Gapasin, T., Davis, M.C., Nelson-Douthitt, C., Wilson, S., Brown, C., Linton, W., Ross, S., Griffiths, R.R., 2023. Single-Dose Psilocybin Treatment

- for Major Depressive Disorder: A Randomized Clinical Trial. *JAMA* 330, 843–853. <https://doi.org/10.1001/jama.2023.14530>
- Reckweg, J.T., van Leeuwen, C.J., Henquet, C., van Amelsvoort, T., Theunissen, E.L., Mason, N.L., Paci, R., Terwey, T.H., Ramaekers, J.G., 2023. A phase 1/2 trial to assess safety and efficacy of a vaporized 5-methoxy-N,N-dimethyltryptamine formulation (GH001) in patients with treatment-resistant depression. *Front. Psychiatry* 14.
- Richman, J.S., Moorman, J.R., 2000. Physiological time-series analysis using approximate entropy and sample entropy maturity in premature infants Physiological time-series analysis using approximate entropy and sample entropy. *Am. J. Physiol. Heart Circ. Physiol.* 278, H2039–H2049.
- Rickli, A., Luethi, D., Reinisch, J., Buchy, D., Hoener, M.C., Liechti, M.E., 2015. Receptor interaction profiles of novel N-2-methoxybenzyl (NBOMe) derivatives of 2,5-dimethoxy-substituted phenethylamines (2C drugs). *Neuropharmacology* 99, 546–553. <https://doi.org/10.1016/j.neuropharm.2015.08.034>
- Rickli, A., Moning, O.D., Hoener, M.C., Liechti, M.E., 2016. Receptor interaction profiles of novel psychoactive tryptamines compared with classic hallucinogens. *Eur. Neuropsychopharmacol.* 26, 1327–1337. <https://doi.org/10.1016/j.euroneuro.2016.05.001>
- Rieser, N.M., Gubser, L.P., Moujaes, F., Duerler, P., Lewis, C.R., Michels, L., Vollenweider, F.X., Preller, K.H., 2023. Psilocybin-induced changes in cerebral blood flow are associated with acute and baseline inter-individual differences. *Sci. Rep.* 13, 17475. <https://doi.org/10.1038/s41598-023-44153-z>
- Rolls, E.T., Huang, C.-C., Lin, C.-P., Feng, J., Joliot, M., 2020. Automated anatomical labelling atlas 3. *NeuroImage* 206, 116189. <https://doi.org/10.1016/j.neuroimage.2019.116189>
- Roseman, L., Nutt, D.J., Carhart-Harris, R.L., 2018. Quality of Acute Psychedelic Experience Predicts Therapeutic Efficacy of Psilocybin for Treatment-Resistant Depression. *Front. Pharmacol.* 8. <https://doi.org/10.3389/fphar.2017.00974>
- Rosenblat, J.D., Leon-Carlyle, M., Ali, S., Husain, M.I., McIntyre, R.S., 2023. Antidepressant Effects of Psilocybin in the Absence of Psychedelic Effects. *Am. J. Psychiatry* 180, 395–396. <https://doi.org/10.1176/appi.ajp.20220835>
- Ross, S., Bossis, A., Guss, J., Agin-Liebes, G., Malone, T., Cohen, B., Mennenga, S.E., Belser, A., Kalliontzi, K., Babb, J., Su, Z., Corby, P., Schmidt, B.L., 2016. Rapid and sustained symptom reduction following psilocybin treatment for anxiety and depression in patients with life-threatening cancer: A randomized controlled trial. *J. Psychopharmacol. (Oxf.)* 30, 1165–1180. <https://doi.org/10.1177/0269881116675512>
- Rubinov, M., Sporns, O., 2010. Complex network measures of brain connectivity: Uses and interpretations. *NeuroImage* 52, 1059–1069. <https://doi.org/10.1016/j.neuroimage.2009.10.003>
- Sacks, O., 2012. Hallucinations, Hallucinations. Alfred A. Knopf, New York, NY, US.
- Salkind, N., 2012. Holm's Sequential Bonferroni Procedure, in: *Encyclopedia of Research Design*. <https://doi.org/10.4135/9781412961288.n178>
- Sanders, J.W., Zijlmans, J., 2021. Moving Past Mysticism in Psychedelic Science. *ACS Pharmacol. Transl. Sci.* 4, 1253–1255. <https://doi.org/10.1021/acspsci.1c00097>
- Schaefer, A., Kong, R., Gordon, E.M., Laumann, T.O., Zuo, X.-N., Holmes, A.J., Eickhoff, S.B., Yeo, B.T.T., 2018. Local-Global Parcellation of the Human Cerebral Cortex from Intrinsic Functional Connectivity MRI. *Cereb. Cortex*. <https://doi.org/10.1093/cercor/bhx179>
- Schartner, M.M., Carhart-Harris, R.L., Barrett, A.B., Seth, A.K., Muthukumaraswamy, S.D., 2017. Increased spontaneous MEG signal diversity for psychoactive doses of ketamine, LSD and psilocybin. *Sci. Rep.* 7, 46421. <https://doi.org/10.1038/srep46421>
- Schindler, E.A.D., Sewell, R.A., Gottschalk, C.H., Luddy, C., Flynn, L.T., Zhu, Y., Lindsey, H., Pittman, B.P., Cozzi, N.V., D'Souza, D.C., 2022. Exploratory investigation of a patient-informed low-dose psilocybin pulse regimen in the suppression of cluster headache: Results from a randomized, double-blind, placebo-controlled trial. *Headache* 62, 1383–1394. <https://doi.org/10.1111/head.14420>

- Schlag, A.K., Aday, J., Salam, I., Neill, J.C., Nutt, D.J., 2022. Adverse effects of psychedelics: From anecdotes and misinformation to systematic science. *J. Psychopharmacol. Oxf. Engl.* 36, 258–272. <https://doi.org/10.1177/02698811211069100>
- Schmid, Y., Liechti, M.E., 2018. Long-lasting subjective effects of LSD in normal subjects. *Psychopharmacology (Berl.)* 235, 535–545. <https://doi.org/10.1007/s00213-017-4733-3>
- Schneier, F.R., Feusner, J., Wheaton, M.G., Gomez, G.J., Cornejo, G., Naraindas, A.M., Hellerstein, D.J., 2023. Pilot Study of Single-Dose Psilocybin for Serotonin Reuptake Inhibitor-Resistant Body Dysmorphic Disorder. *J. Psychiatr. Res.* 161, 364–370. <https://doi.org/10.1016/j.jpsychires.2023.03.031>
- Shalit, N., Rehm, J., Lev-Ran, S., 2019. Epidemiology of hallucinogen use in the U.S. results from the National epidemiologic survey on alcohol and related conditions III. *Addict. Behav.* 89, 35–43. <https://doi.org/10.1016/j.addbeh.2018.09.020>
- Shannon, C.E., 1948. A mathematical theory of communication. *Bell Syst. Tech. J.* 27, 379–423. <https://doi.org/10.1002/j.1538-7305.1948.tb01338.x>
- Shen, X., Tokoglu, F., Papademetris, X., Constable, R.T., 2013. Groupwise whole-brain parcellation from resting-state fMRI data for network node identification. *NeuroImage*. <https://doi.org/10.1016/j.neuroimage.2013.05.081>
- Shulgin, Alexander, Shulgin, Ann, 1997. *TiHKAL: The Continuation*. Transform Press, Berkeley, California.
- Shulgin, Alexander, Shulgin, Ann, 1991. *PiHKAL: A Chemical Love Story*. Transform Press, Berkeley, California.
- Siegel, J.S., Subramanian, S., Perry, D., Kay, B.P., Gordon, E.M., Laumann, T.O., Reneau, T.R., Metcalf, N.V., Chacko, R.V., Gratton, C., Horan, C., Krimmel, S.R., Shimony, J.S., Schweiger, J.A., Wong, D.F., Bender, D.A., Scheidter, K.M., Whiting, F.I., Padawer-Curry, J.A., Shinohara, R.T., Chen, Y., Moser, J., Yacoub, E., Nelson, S.M., Vizioli, L., Fair, D.A., Lenze, E.J., Carhart-Harris, R., Raison, C.L., Raichle, M.E., Snyder, A.Z., Nicol, G.E., Dosenbach, N.U.F., 2024. Psilocybin desynchronizes the human brain. *Nature* 632, 131–138. <https://doi.org/10.1038/s41586-024-07624-5>
- Singleton, S.P., Luppi, A.I., Carhart-Harris, R.L., Cruzat, J., Roseman, L., Nutt, D.J., Deco, G., Kringelbach, M.L., Stamatakis, E.A., Kuceyeski, A., 2022. Receptor-informed network control theory links LSD and psilocybin to a flattening of the brain’s control energy landscape. *Nat. Commun.* 13, 5812. <https://doi.org/10.1038/s41467-022-33578-1>
- Sloshower, J., Skosnik, P.D., Safi-Aghdam, H., Pathania, S., Syed, S., Pittman, B., D’Souza, D.C., 2023. Psilocybin-assisted therapy for major depressive disorder: An exploratory placebo-controlled, fixed-order trial. *J. Psychopharmacol. Oxf. Engl.* 37, 698–706. <https://doi.org/10.1177/02698811231154852>
- Smigielski, L., Scheidegger, M., Kometer, M., Vollenweider, F.X., 2019. Psilocybin-assisted mindfulness training modulates self-consciousness and brain default mode network connectivity with lasting effects. *NeuroImage* 196, 207–215. <https://doi.org/10.1016/j.neuroimage.2019.04.009>
- Smith, S.M., Fox, P.T., Miller, K.L., Glahn, D.C., Fox, P.M., Mackay, C.E., Filippini, N., Watkins, K.E., Toro, R., Laird, A.R., Beckmann, C.F., 2009. Correspondence of the brain’s functional architecture during activation and rest. *Proc. Natl. Acad. Sci. U. S. A.* <https://doi.org/10.1073/pnas.0905267106>
- Søndergaard, A., Madsen, M.K., Ozenne, B., Armand, S., Knudsen, G.M., Fisher, P.M., Stenbæk, D.S., 2022. Lasting increases in trait mindfulness after psilocybin correlate positively with the mystical-type experience in healthy individuals. *Front. Psychol.* 13, 948729. <https://doi.org/10.3389/fpsyg.2022.948729>
- Spies, M., Nasser, A., Ozenne, B., Jensen, P.S., Knudsen, G.M., Fisher, P.M., 2020. Common HTR2A variants and 5-HTTLPR are not associated with human in vivo serotonin 2A receptor levels. *Hum. Brain Mapp.* 41, 4518–4528. <https://doi.org/10.1002/hbm.25138>
- Sporns, O., 2018. Graph theory methods: applications in brain networks. *Dialogues Clin. Neurosci.* 20, 111. <https://doi.org/10.31887/DCNS.2018.20.2/OSPORN>
- Straumann, I., Avedisian, I., Klaiber, A., Varghese, N., Eckert, A., Rudin, D., Luethi, D., Liechti, M.E., 2024.

- Acute effects of R-MDMA, S-MDMA, and racemic MDMA in a randomized double-blind cross-over trial in healthy participants. *Neuropsychopharmacol. Off. Publ. Am. Coll. Neuropsychopharmacol.* 50, 362–371. <https://doi.org/10.1038/s41386-024-01972-6>
- Straumann, I., Ley, L., Holze, F., Becker, A.M., Klaiber, A., Wey, K., Duthaler, U., Varghese, N., Eckert, A., Liechti, M.E., 2023. Acute effects of MDMA and LSD co-administration in a double-blind placebo-controlled study in healthy participants. *Neuropsychopharmacol. Off. Publ. Am. Coll. Neuropsychopharmacol.* 48, 1840–1848. <https://doi.org/10.1038/s41386-023-01609-0>
- Studerus, E., Gamma, A., Vollenweider, F.X., 2010. Psychometric evaluation of the altered states of consciousness rating scale (OAV). *PLoS ONE* 5. <https://doi.org/10.1371/journal.pone.0012412>
- Suzuki, J., Dekker, M.A., Valenti, E.S., Arbelo Cruz, F.A., Correa, A.M., Poklis, J.L., Poklis, A., 2015. Toxicities associated with NBOMe ingestion, a novel class of potent hallucinogens: A review of the literature. *Psychosomatics* 56, 129–139. <https://doi.org/10.1016/j.psym.2014.11.002>
- Svarer, C., Madsen, K., Hasselbalch, S.G., Pinborg, L.H., Haugbøl, S., Frøkjær, V.G., Holm, S., Paulson, O.B., Knudsen, G.M., 2005. MR-based automatic delineation of volumes of interest in human brain PET images using probability maps. *NeuroImage*. <https://doi.org/10.1016/j.neuroimage.2004.10.017>
- Swift, T.C., Belser, A.B., Agin-Liebes, G., Devenot, N., Terrana, S., Friedman, H.L., Guss, J., Bossis, A.P., Ross, S., 2017. Cancer at the Dinner Table: Experiences of Psilocybin-Assisted Psychotherapy for the Treatment of Cancer-Related Distress. *J. Humanist. Psychol.* 57, 488–519. <https://doi.org/10.1177/0022167817715966>
- Tagliazucchi, E., Carhart-Harris, R., Leech, R., Nutt, D., Chialvo, D.R., 2014. Enhanced repertoire of brain dynamical states during the psychedelic experience. *Hum. Brain Mapp.* 35, 5442–5456. <https://doi.org/10.1002/hbm.22562>
- Tagliazucchi, E., Roseman, L., Kaelen, M., Orban, C., Muthukumaraswamy, S.D., Murphy, K., Laufs, H., Leech, R., McGonigle, J., Crossley, N., Bullmore, E., Williams, T., Bolstridge, M., Feilding, A., Nutt, D.J., Carhart-Harris, R., 2016. Increased Global Functional Connectivity Correlates with LSD-Induced Ego Dissolution. *Curr. Biol.* 26, 1043–1050. <https://doi.org/10.1016/j.cub.2016.02.010>
- Taylor, P.A., Aggarwal, H., Bandettini, P.A., Barilari, M., Bright, M.G., Caballero-Gaudes, C., Calhoun, V.D., Chakravarty, M., Devenyi, G.A., Evans, J.W., Garza-Villarreal, E.A., Rasgado-Toledo, J., Gau, R., Glen, D.R., Goebel, R., Gonzalez-Castillo, J., Gulban, O.F., Halchenko, Y., Handwerker, D.A., Hanayik, T., Lauren, P.D., Leopold, D.A., Lerch, J.P., Mathys, C., McCarthy, P., McLeod, A., Mejia, A., Moia, S., Nichols, T.E., Pernet, C., Pessoa, L., Pfleiderer, B., Rajendra, J.K., Reyes, L.D., Reynolds, R.C., Roopchansingh, V., Rorden, C., Russ, B.E., Sundermann, B., Thirion, B., Torrisi, S., Chen, G., 2025. Go Figure: Transparency in neuroscience images preserves context and clarifies interpretation. *ArXiv arXiv:2504.07824v1*.
- Ter-Pogossian, M.M., Phelps, M.E., Hoffman, E.J., Mullani, N.A., 1975. A positron-emission transaxial tomograph for nuclear imaging (PETT). *Radiology* 114, 89–98. <https://doi.org/10.1148/114.1.89>
- Thomann, J., Kolaczynska, K.E., Stoeckmann, O.V., Rudin, D., Vizeli, P., Hoener, M.C., Pryce, C.R., Vollenweider, F.X., Liechti, M.E., Duthaler, U., 2024. In vitro and in vivo metabolism of psilocybin's active metabolite psilocin. *Front. Pharmacol.* 15. <https://doi.org/10.3389/fphar.2024.1391689>
- Tian, Y., Margulies, D.S., Breakspear, M., Zalesky, A., 2020. Topographic organization of the human subcortex unveiled with functional connectivity gradients. *Nat. Neurosci.* <https://doi.org/10.1038/s41593-020-00711-6>
- Timmermann, C., Roseman, L., Haridas, S., Rosas, F.E., Luan, L., Kettner, H., Martell, J., Erritzoe, D., Tagliazucchi, E., Pallavicini, C., Girn, M., Alamia, A., Leech, R., Nutt, D.J., Carhart-Harris, R.L., 2023. Human brain effects of DMT assessed via EEG-fMRI. *Proc. Natl. Acad. Sci.* 120, e2218949120. <https://doi.org/10.1073/pnas.2218949120>
- Timmermann, C., Roseman, L., Scharfner, M., Milliere, R., Williams, L.T.J., Erritzoe, D., Muthukumaraswamy, S., Ashton, M., Bendrioua, A., Kaur, O., Turton, S., Nour, M.M., Day, C.M., Leech, R., Nutt, D.J., Carhart-Harris, R.L., 2019. Neural correlates of the DMT experience assessed with multivariate EEG. *Sci. Rep.* 9, 16324. <https://doi.org/10.1038/s41598-019-51974-4>

- Truth and Reconciliation Commission of South Africa, 1998. Special Investigation into Project Coast: South Africa's Chemical and Biological Warfare Programme (Commission Report), Truth and Reconciliation Commission of South Africa Report. Cape Town.
- Tzourio-Mazoyer, N., Landeau, B., Papathanassiou, D., Crivello, F., Etard, O., Delcroix, N., Mazoyer, B., Joliot, M., 2002. Automated anatomical labeling of activations in SPM using a macroscopic anatomical parcellation of the MNI MRI single-subject brain. *NeuroImage*.
<https://doi.org/10.1006/nimg.2001.0978>
- van Amsterdam, J., Nutt, D., Phillips, L., van den Brink, W., 2015. European rating of drug harms. *J. Psychopharmacol. (Oxf.)* 29, 655–660. <https://doi.org/10.1177/0269881115581980>
- Varley, T.F., Carhart-Harris, R., Roseman, L., Menon, D.K., Stamatakis, E.A., 2020. Serotonergic psychedelics LSD & psilocybin increase the fractal dimension of cortical brain activity in spatial and temporal domains. *NeuroImage* 220, 117049. <https://doi.org/10.1016/j.neuroimage.2020.117049>
- Viol, A., Palhano-Fontes, F., Onias, H., de Araujo, D.B., Hövel, P., Viswanathan, G.M., 2019. Characterizing Complex Networks Using Entropy-Degree Diagrams: Unveiling Changes in Functional Brain Connectivity Induced by Ayahuasca. *Entropy* 2019 Vol 21 Page 128 21, 128.
<https://doi.org/10.3390/E21020128>
- Viol, A., Palhano-Fontes, F., Onias, H., De Araujo, D.B., Viswanathan, G.M., 2017. Shannon entropy of brain functional complex networks under the influence of the psychedelic Ayahuasca. *Sci. Rep.* 7, 1–13. <https://doi.org/10.1038/s41598-017-06854-0>
- Vizeli, P., Straumann, I., Holze, F., Schmid, Y., Dolder, P.C., Liechti, M.E., 2021. Genetic influence of CYP2D6 on pharmacokinetics and acute subjective effects of LSD in a pooled analysis. *Sci. Rep.* 11, 10851. <https://doi.org/10.1038/s41598-021-90343-y>
- Vizeli, P., Studerus, E., Holze, F., Schmid, Y., Dolder, P.C., Ley, L., Straumann, I., Becker, A.M., Müller, F., Arikci, D., Liechti, M.E., 2024. Pharmacological and non-pharmacological predictors of the LSD experience in healthy participants. *Transl. Psychiatry* 14, 1–8.
<https://doi.org/10.1038/s41398-024-03074-9>
- Vollenweider, F.X., Leenders, K.L., Scharfetter, C., Maguire, P., Stadelmann, O., Angst, J., 1997. Positron emission tomography and fluorodeoxyglucose studies of metabolic hyperfrontality and psychopathology in the psilocybin model of psychosis. *Neuropsychopharmacology* 16, 357–372.
[https://doi.org/10.1016/S0893-133X\(96\)00246-1](https://doi.org/10.1016/S0893-133X(96)00246-1)
- Vollenweider, F.X., Vontobel, P., Hell, D., Leenders, K.L., 1999. 5-HT modulation of dopamine release in basal ganglia in psilocybin-induced psychosis in Man - A PET study with [¹¹C]raclopride. *Neuropsychopharmacology* 20, 424–433. [https://doi.org/10.1016/S0893-133X\(98\)00108-0](https://doi.org/10.1016/S0893-133X(98)00108-0)
- von Rotz, R., Schindowski, E.M., Jungwirth, J., Schuldt, A., Rieser, N.M., Zahoranszky, K., Seifritz, E., Nowak, A., Nowak, P., Jäncke, L., Preller, K.H., Vollenweider, F.X., 2023. Single-dose psilocybin-assisted therapy in major depressive disorder: A placebo-controlled, double-blind, randomised clinical trial. *EClinicalMedicine* 56, 101809.
<https://doi.org/10.1016/j.eclinm.2022.101809>
- Wallach, J., Cao, A.B., Calkins, M.M., Heim, A.J., Lanham, J.K., Bonniwell, E.M., Hennessey, J.J., Bock, H.A., Anderson, E.I., Sherwood, A.M., Morris, H., de Klein, R., Klein, A.K., Cuccurazzu, B., Gamrat, J., Fannana, T., Zauhar, R., Halberstadt, A.L., McCorvy, J.D., 2023. Identification of 5-HT_{2A} receptor signaling pathways associated with psychedelic potential. *Nat. Commun.* 14, 8221.
<https://doi.org/10.1038/s41467-023-44016-1>
- Wang, Z., Li, Y., Childress, A.R., Detre, J.A., 2014. Brain Entropy Mapping Using fMRI. *PLOS ONE* 9, e89948. <https://doi.org/10.1371/journal.pone.0089948>
- Warburton, D.M., Wesnes, K., Edwards, J., Larrad, D., 1985. Scopolamine and the sensory conditioning of hallucinations. *Neuropsychobiology* 14, 198–202. <https://doi.org/10.1159/000118227>
- Westfall, P.H., Troendle, J.F., 2008. Multiple Testing with Minimal Assumptions. *Biom. J. Biom. Z.* 50, 745–755. <https://doi.org/10.1002/bimj.200710456>
- Whitfield-Gabrieli, S., Nieto-Castanon, A., 2012. Conn: A Functional Connectivity Toolbox for Correlated

- and Anticorrelated Brain Networks. *Brain Connect.* <https://doi.org/10.1089/brain.2012.0073>
- World Medical Association, 2025. World Medical Association Declaration of Helsinki: Ethical Principles for Medical Research Involving Human Participants. *JAMA* 333, 71–74. <https://doi.org/10.1001/jama.2024.21972>
- Yang, A.C., Hong, C.-J., Liou, Y.-J., Huang, K.-L., Huang, C.-C., Liu, M.-E., Lo, M.-T., Huang, N.E., Peng, C.-K., Lin, C.-P., Tsai, S.-J., 2015. Decreased resting-state brain activity complexity in schizophrenia characterized by both increased regularity and randomness. *Hum. Brain Mapp.* 36, 2174–2186. <https://doi.org/10.1002/hbm.22763>
- Yang, K.-C., Stepanov, V., Martinsson, S., Ettrup, A., Takano, A., Knudsen, G.M., Halldin, C., Farde, L., Finnema, S.J., 2017. Fenfluramine Reduces [¹¹C]Cimbi-36 Binding to the 5-HT_{2A} Receptor in the Nonhuman Primate Brain. *Int. J. Neuropsychopharmacol.* 20, 683–691. <https://doi.org/10.1093/ijnp/pyx051>
- Yeo, B.T., Krienen, F.M., Sepulcre, J., Sabuncu, M.R., Lashkari, D., Hollinshead, M., Roffman, J.L., Smoller, J.W., Zöllei, L., Polimeni, J.R., Fisch, B., Liu, H., Buckner, R.L., 2011. The organization of the human cerebral cortex estimated by intrinsic functional connectivity. *J. Neurophysiol.* <https://doi.org/10.1152/jn.00338.2011>
- Zentner, M., Grandjean, D., Scherer, K.R., 2008. Emotions evoked by the sound of music: characterization, classification, and measurement. *Emot. Wash. DC* 8, 494–521. <https://doi.org/10.1037/1528-3542.8.4.494>
- Zhou, K., de Wied, D., Carhart-Harris, R.L., Kettner, H., 2025. Prediction of hallucinogen persisting perception disorder and thought disturbance symptoms following psychedelic use. *PNAS Nexus* 4, pgae560. <https://doi.org/10.1093/pnasnexus/pgae560>
- Ziv, J., Lempel, A., 1978. Compression of individual sequences via variable-rate coding. *IEEE Trans. Inf. Theory* 24, 530–536. <https://doi.org/10.1109/TIT.1978.1055934>

Appendix

1. McCulloch, D.E.-W., Madsen, M.K., Stenbæk, D.S., Kristiansen, S., Ozenne, B., Jensen, P.S., Knudsen, G.M., Fisher, P.M., 2021. **Lasting effects of a single psilocybin dose on resting-state functional connectivity in healthy individuals.** *J. Psychopharmacol. (Oxf.)*
2. McCulloch, D.E.-W., Grzywacz, M.Z., Madsen, M.K., Jensen, P.S., Ozenne, B., Armand, S., Knudsen, G.M., Fisher, P.M., Stenbæk, D.S., 2022. **Psilocybin-Induced Mystical-Type Experiences are Related to Persisting Positive Effects: A Quantitative and Qualitative Report.** *Frontiers in Pharmacology. 13*, 1–17.

Supplementary Table for Paper 2 are available at

<https://www.frontiersin.org/journals/pharmacology/articles/10.3389/fphar.2022.841648/full>

3. McCulloch, D.E.-W., Olsen, A.S., Ozenne, B., Stenbæk, D.S., Armand, S., Madsen, M.K., Knudsen, G.M., Fisher, P.M., 2023. **Navigating the chaos of psychedelic neuroimaging: A multi-metric evaluation of acute psilocybin effects on brain entropy.** (*Manuscript submitted to Neuroimage December 2024*)

Supplementary Tables for Paper 3 are available at

<https://www.medrxiv.org/content/10.1101/2023.07.03.23292164v2.supplementary-material>

4. McCulloch, D.E.-W., Larsen, K., Johansen, A., Jensen, K.H.R., Nykjær, C.H., Holze, F., Falck, N., Neufeld, V., Steenstrup, E., Skov-Andersen, P., Spangsgård, A., Geisler, M., Randrup, P.P., Jensen, P.S., Shulganov, V., Johansen, S.S., Nielsen, M.K.K., Andersen, T.L., Stenbæk, D.S., Svarer, C., Fisher, P.M., Knudsen, G.M., 2025. **Molecular, haemodynamic, and functional effects of LSD in the human brain.** (*Manuscript submitted to Nature Neuroscience June 2025*)

Supplementary Tables for Paper 4 are available at

<https://www.medrxiv.org/content/10.1101/2025.06.17.25329677v1.supplementary-material>

DECLARATION OF CO-AUTHORSHIP

The declaration is for PhD students and must be completed for each conjointly authored article.

Please note that if a manuscript or published paper has eleven or less authors, all authors must sign a declaration of co-authorship. If it has twelve or more authors, only the PhD student, the corresponding author(s), the senior author, and the principal supervisor need to sign the declaration of co-authorship.

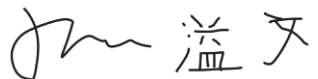
1. Declaration by	
Name of PhD student	Drummond McCulloch
E-mail	Drummond.mcculloch@nru.dk
Name of principal supervisor	Patrick Fisher
Title of the PhD thesis	Pharmacokinetic and pharmacodynamic evaluation of classical psychedelic substances in the human brain

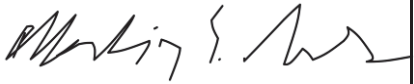
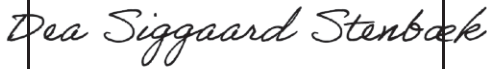
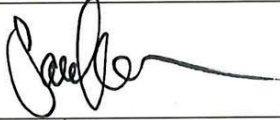




2. The declaration applies to the following article	
Title of article	Lasting effects of a single psilocybin dose on resting-state functional connectivity in healthy individuals
Article status	
Published <input checked="" type="checkbox"/>	Accepted for publication <input type="checkbox"/>
Date: Jan 2022	Date:
Manuscript submitted <input type="checkbox"/>	Manuscript not submitted <input type="checkbox"/>
Date:	
If the article is published or accepted for publication, please state the name of journal, year, volume, page and DOI (if you have the information).	J Psychopharmacol 2022 Jan;36(1):74-84. doi: 10.1177/02698811211026454. Epub 2021 Jun 30.

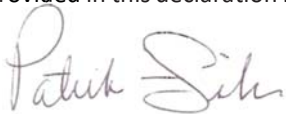
3. The PhD student's contribution to the article (please use the scale A-F as benchmark)	
<u>Benchmark scale of the PhD-student's contribution to the article</u>	
A. Has essentially done all the work (> 90 %) B. Has done most of the work (60-90 %) C. Has contributed considerably (30-60 %) D. Has contributed (10-30 %) E. No or little contribution (<10 %) F. Not relevant	A, B, C, D, E, F
1. Formulation/identification of the scientific problem	D
2. Development of the key methods	D

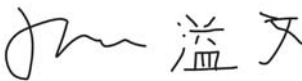
3. The PhD student's contribution to the article (please use the scale A-F as benchmark) <u>Benchmark scale of the PhD-student's contribution to the article</u> A. Has essentially done all the work (> 90 %) B. Has done most of the work (60-90 %) C. Has contributed considerably (30-60 %) D. Has contributed (10-30 %) E. No or little contribution (<10 %) F. Not relevant		A, B, C, D, E, F
3. Planning of the experiments and methodology design and development	E	
4. Conducting the experimental work/clinical studies/data collection/obtaining access to data	D	
5. Conducting the analysis of data	A	
6. Interpretation of the results	A	
7. Writing of the first draft of the manuscript	A	
8. Finalisation of the manuscript and submission	A	
Provide a short description of the PhD student's specific contribution to the article. ⁱ Formulated the research question, processed the data, performed analyses, made figures, wrote the manuscript.		

4. Material from another thesis / dissertation ⁱⁱ	
Does the article contain work which has also formed part of another thesis, e.g. master's thesis, PhD thesis or doctoral dissertation (the PhD student's or another person's)?	Yes: <input type="checkbox"/> No: <input checked="" type="checkbox"/>
If yes, please state name of the author and title of thesis / dissertation.	
If the article is part of another author's academic degree, please describe the PhD student's and the author's contributions to the article so that the individual contributions are clearly distinguishable from one another.	

5. Signatures of the authors incl. the PhD student				
	Date	Name	Title	Signature
1.	23/6/2025	Drummond McCulloch	Mr.	

5. Signatures of the authors incl. the PhD student				
2.	17/06/2025	Martin Korsbak Madsen	Dr.	
3.	24/06/2025	Dea Siggard Stenbæk	Prof.	
4.	24/06/2025	Sara Kristiansen		
5.	24/06/2025	Brice Ozenne	Prof.	
6.	17/06/2025	Peter Steen Jensen	Mr.	
7.	17/06/2025	Gitte Moos Knudsen	Prof.	
8.	17/06/2025	Patrick Fisher	Prof.	
9.				
10.				
11.				

6. Signature of the principal supervisor I solemnly declare that the information provided in this declaration is accurate to the best of my knowledge. Date: 27-06-2025 Principal supervisor: Patrick Fisher 
--

7. Signature of the PhD student I solemnly declare that the information provided in this declaration is accurate to the best of my knowledge. Date: 17-06-2025 PhD student: Drummond McCulloch 


Please learn more about responsible conduct of research on the [Faculty of Health and Medical Sciences' website](#).

ⁱ This can be supplemented with an additional letter if needed.

ⁱⁱ Please see Ministerial Order on the PhD Programme at the Universities and Certain Higher Artistic Educational Institutions (PhD Order) § 12 (4):

"Any articles included in the thesis may be written in cooperation with others, provided that each of the co -authors submits a written declaration stating the PhD student's or the author's contribution to the work."

Lasting effects of a single psilocybin dose on resting-state functional connectivity in healthy individuals

Drummond E-Wen McCulloch¹ , Martin Korsbak Madsen^{1,2},
Dea Siggaard Stenbæk^{1,3} , Sara Kristiansen¹, Brice Ozenne^{1,4},
Peter Steen Jensen¹, Gitte Moos Knudsen^{1,2}
and Patrick MacDonald Fisher¹ 

Psychopharm

Journal of Psychopharmacology
2022, Vol. 36(1) 74–84
© The Author(s) 2021



Article reuse guidelines:
sagepub.com/journals-permissions
DOI: 10.1177/02698811211026454
journals.sagepub.com/home/jop



Abstract

Background: Psilocybin is a psychedelic drug that has shown lasting positive effects on clinical symptoms and self-reported well-being following a single dose. There has been little research into the long-term effects of psilocybin on brain connectivity in humans.

Aim: Evaluate changes in resting-state functional connectivity (RSFC) at 1 week and 3 months after one psilocybin dose in 10 healthy psychedelic-naïve volunteers and explore associations between change in RSFC and related measures.

Methods: Participants received 0.2–0.3 mg/kg psilocybin in a controlled setting. Participants completed resting-state functional magnetic resonance imaging (fMRI) scans at baseline, 1-week and 3-month post-administration and [11C]Cimbi-36 PET scans at baseline and 1 week. We examined changes in within-network, between-network and region-to-region RSFC. We explored associations between changes in RSFC and psilocybin-induced phenomenology as well as changes in psychological measures and neocortex serotonin 2A receptor binding.

Results: Psilocybin was well tolerated and produced positive changes in well-being. At 1 week only, executive control network (ECN) RSFC was significantly decreased (Cohen's $d = -1.73$, $p_{FWE} = 0.010$). We observed no other significant changes in RSFC at 1 week or 3 months, nor changes in region-to-region RSFC. Exploratory analyses indicated that decreased ECN RSFC at 1 week predicted increased mindfulness at 3 months ($r = -0.65$).

Conclusions: These findings in a small cohort indicate that psilocybin affects ECN function within the psychedelic 'afterglow' period. Our findings implicate ECN modulation as mediating psilocybin-induced, long-lasting increases in mindfulness. Although our findings implicate a neural pathway mediating lasting psilocybin effects, it is notable that changes in neuroimaging measures at 3 months, when personality changes are observed, remain to be identified.

Keywords

Functional magnetic resonance imaging, resting-state connectivity, psilocybin, psychedelic, executive control network

Introduction

Psilocybin is a prodrug of the psychedelic psilocin (4-hydroxy-N,N-dimethyltryptamine) (Nichols, 2016). Effects include profound alterations in consciousness that last approximately 6 h and are characterised by perceptual alterations and synaesthesia, experiences of non-duality and transcendence and profound changes in affect (Preller and Vollenweider, 2018). Therapeutic effects of psilocybin have been reported following between one and three moderate-to-high doses (0.025–0.42 mg/kg) in brain-related disorders including major depressive disorder (MDD) (Davis et al., 2020), treatment-resistant depression (Carhart-Harris et al., 2018), obsessive-compulsive disorder (Moreno et al., 2006), terminal cancer-associated anxiety (Griffiths et al., 2016), demoralisation (Anderson et al., 2020), as well as smoking (Johnson et al., 2017) and alcohol addiction (Garcia-Romeu et al., 2019). Psilocybin is currently in phase 2b for the treatment of treatment-resistant depression (COMPASS Pathways Ltd., London, UK) and in phase 2a for major depressive disorder (Usona Institute, Madison, WI, USA).

Persistent changes in personality and mood have also been observed in healthy volunteers following a single medium-to-high

dose of psilocybin. These include, for example, increases in personality traits openness and extraversion, decreases in neuroticism and increases in mindful awareness (Erritzoe et al., 2018; MacLean et al., 2011; Madsen et al., 2020). These therapeutic and personality effects appear to persist for at least months, and in some cases have been reported to last more than a year (Gasser et al., 2014; Johnson et al., 2017; MacLean et al., 2011).

¹Neurobiology Research Unit and NeuroPharm, Rigshospitalet, Copenhagen, Denmark

²Institute of Clinical Medicine, University of Copenhagen, Copenhagen, Denmark

³Department of Psychology, University of Copenhagen, Copenhagen, Denmark

⁴Section of Biostatistics, Department of Public Health, University of Copenhagen, Copenhagen, Denmark

Corresponding author:

Patrick MacDonald Fisher, Neurobiology Research Unit, Rigshospitalet Building 8057, 8 Inge Lehmanns Vej, Copenhagen 2100, Denmark.
Email: patrick@nru.dk

The medicalisation of psychedelic drugs is expanding rapidly despite a limited understanding of the neurobiology underpinning therapeutic effects. Psychological theories of psychedelic therapy, such as reduced negative affect (Barrett et al., 2020), increased mindfulness (Madsen et al., 2020; Murphy-Beiner and Soar, 2020; Smigielski et al., 2019), increased cognitive flexibility (Murphy-Beiner and Soar, 2020) and reduced experiential avoidance (Zeifman et al., 2020) have been proposed, as well as increased acceptance and processing of traumatic autobiographical memories (Sloshower et al., 2020), but these have no current grounding in neurobiology. Thus, in order to maximise psilocybin's safety and efficacy as a potential therapeutic, it is important to investigate mechanisms by which psilocybin exerts its effects.

Functional magnetic resonance imaging (fMRI) resting-state functional connectivity (RSFC) measures correlations between blood-oxygen-level-dependent (BOLD) signals in participants instructed to simply let their mind wander (Lee et al., 2013). Despite not being focused on any task, the brain remains organised into networks (Raichle, 2015), the character of which correlates with personality traits (Cai et al., 2020; Hsu et al., 2018) and aligns with known functional and structural topology (Straathof et al., 2019). During the psychedelic experience, psilocybin produces a reduction in the synchronised BOLD activity of the major hubs of the default mode network (DMN) (Carhart-Harris et al., 2012; Mason et al., 2020), increases between-network RSFC (Roseman et al., 2014) and increases global RSFC across the sensory cortex while decreasing the global connectivity in associative regions (Preller et al., 2020). Similarly, lysergic acid diethylamide (LSD) increases RSFC between high-level association cortices, which correlates with subjective reports of ego-dissolution (Tagliazucchi et al., 2016). Although understanding the neurological basis of the acute psychedelic experience is widely informative, the long-term psychological effects of psychedelics may be distinct (Carhart-Harris et al., 2016).

Five studies to date have reported effects on human brain function after the psychoactive effects of a classical psychedelic have subsided: two studies with ayahuasca and three with psilocybin (Barrett et al., 2020; Carhart-Harris et al., 2017; Pasquini et al., 2020; Sampedro et al., 2017; Smigielski et al., 2019). Post-drug brain imaging was performed within 24 h after the psychedelic session in all but one study (Barrett et al., 2020), during which time 'afterglow' effects and potential residual drug availability confounds relating effects to lasting changes (Madsen et al., 2019; Majić et al., 2015). By 'afterglow', we allude to the experience of 'elevated and energetic mood with a relative freedom from concerns of the past and from guilt and anxiety' up to 2 weeks after the experience, as described as early as during the 1960s and the 'first-wave' of psychedelic research (Grob et al., 1996; Pahnke, 1969). More recently, transient elevations in mood have been reported (Majić et al., 2015; Murphy-Beiner and Soar, 2020). Barrett et al. (2020) reported an increase in the number of significant RSFC across the brain in 12 healthy individuals from baseline to 1-week and 1-month post-psilocybin, hypothesising that psilocybin may increase emotional and brain plasticity. None of these previous studies evaluated correlations between change in RSFC and change in personality or other psychological traits. Furthermore, none of these studies have explored neuromolecular mechanisms mediating these effects. The psychoactive effects of psilocybin stem from agonism at the serotonin 2A receptor (5-HT_{2A}) (Vollenweider et al., 1998). Positron emission tomography (PET)

with the radiotracer [¹¹C]Cimbi-36 enables the quantification of brain 5-HT_{2A} levels in humans in vivo, which has been previously associated with aspects of the psychedelic experience (Ettrup et al., 2014, 2016; Finnema et al., 2014; Madsen et al., 2020; Stenbæk et al., 2020). Combining [¹¹C]Cimbi-36 PET with RSFC would provide insight into the neuromolecular mechanisms associated with psychedelic effects on brain connectivity.

In the current study, we evaluated the effect of a single psilocybin dose on RSFC in 10 healthy psychedelic-naïve individuals at 1 week and 3 months after administration, evaluating changes in within- and between-network RSFC. Further, we sought to replicate a previous finding of changes in region-to-region RSFC (Barrett et al., 2020). Lastly, in an exploratory analysis, we assessed correlations between network RSFC change and variables associated with increased well-being. These included personality measures, well-being and mindfulness, which we recently showed were altered 3 months after psilocybin, as well as correlated with change in the neocortex 5-HT_{2A} binding (Madsen et al., 2020). Additionally, the baseline neocortex 5-HT_{2A} binding was related to the temporal character of the psychedelic experience (Stenbæk et al., 2020). Finally, we examined whether the self-reported experience was correlated with long-term changes in brain connectivity.

Materials and methods

Participants

Detailed information about participants and protocol are described in a previous study (Madsen et al., 2020) and one more study, which included these and other participants (Stenbæk et al., 2020). The study was approved by the Danish Medicines Agency (EudraCT ID: 2016-004000-61, amendments: 2017014166, 2017082837, 2018023295) and by the ethics committee for the capital region of Copenhagen (journal ID: H-16028698, with amendments). The study was preregistered at ClinicalTrials.gov (identifier: NCT03289949). Six male and four female participants took part in this study (mean \pm SD age = 28.3 \pm 3.4 years).

Participants were recruited from a list of individuals who expressed interest in participating in a psilocybin brain scanning study. After obtaining the informed consent, participants underwent screening for somatic illness, including a medical examination, an electrocardiogram (ECG), blood screening for somatic disease, and screening for psychiatric disorders using Mini International Neuropsychiatric Interview, Danish translation version 6.0.0 (Sheehan et al., 1998). Exclusion criteria were: (1) present or previous primary psychiatric disease (DSM axis 1 or WHO ICD-10 diagnostic classifications) or in first-degree relatives; (2) present or previous neurological condition/disease, significant somatic condition/disease; (3) intake of drugs suspected to influence test results; (4) non-fluent Danish language skills; (5) vision or hearing impairment; (6) previous or present learning disability; (7) pregnancy; (8) breastfeeding; (9) magnetic resonance imaging (MRI) contraindications; (10) alcohol or drug abuse; (11) allergy to test drugs; (12) significant exposure to radiation within the past year (e.g. medical imaging investigations); (13) intake of QT-prolonging medication or ECG results indicative of heart disease, (14) blood donation less than 3 months before project participation; (15) bodyweight less than 50 kg; and (16) low plasma ferritin levels (<12 µg/L).

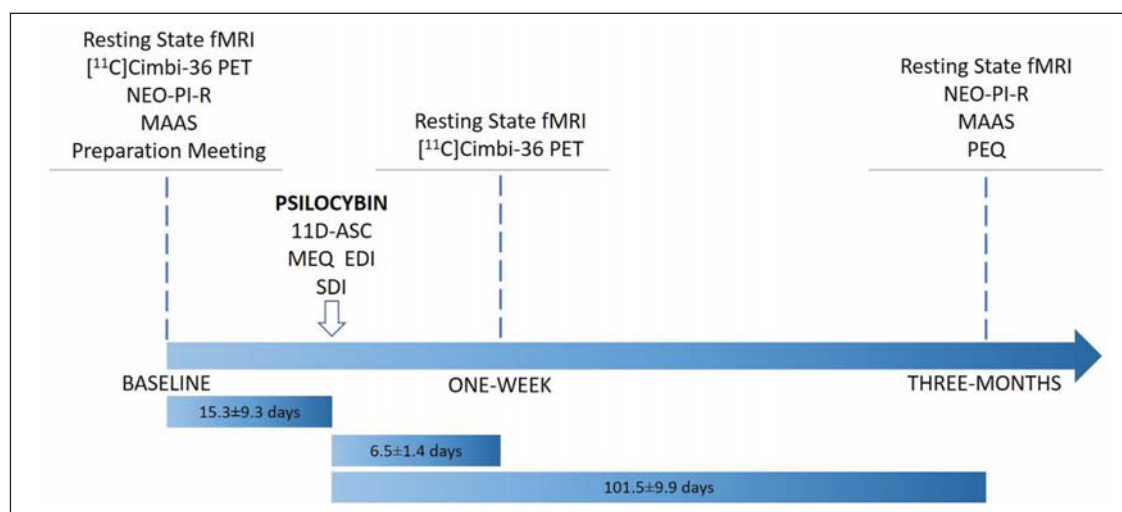


Figure 1. Flowchart describing study design. Note that not all data collected at a single time point was collected on a single day. Time lengths (mean \pm SD) describe time between MRI scan sessions and psilocybin session.

EDI: ego-dissolution inventory; MAAS: mindful attention awareness scale; MEQ: mystical experience questionnaire; MRI: magnetic resonance imaging; NEO-PI-R: revised NEO personality inventory; PEQ: persisting effects questionnaire; SDI: subjective drug intensity.

Experimental procedures

Figure 1 provides an overview of the study design. Prior to inclusion, participants were informed about the study, including safety precautions and potential effects and side effects of psilocybin. Before the psilocybin session, all participants met at least one of the two staff members present on the psilocybin intervention day. A urine test was used to screen for common drugs of abuse (Rapid Response, BTNX Inc., Markham, ON, Canada) on baseline imaging days. At baseline, participants filled out questionnaires including the NEO Personality Inventory-Revised (NEO PI-R) (Costa and McCrae, 2008; Skovdahl-Hansen et al., 2004) and the mindfulness attention and awareness scale (MAAS) (Brown and Ryan, 2003; Jensen et al., 2016) and completed an magnetic resonance imaging (MRI) scan session.

On a separate day, open-label psilocybin sessions were conducted including two supporting psychologists familiar with effects of psilocybin, safety precautions and interpersonal support methods (Johnson et al., 2008). Psilocybin was administered in the morning; a number of 3 mg capsules were taken with a glass of water to approximate dose (dose: 0.2 mg/kg ($n=4$) and 0.3 mg/kg ($n=6$)), considered 'medium' and 'high' doses, respectively (Hasler et al., 2004). Participants listened to a standardised music playlist, adapted from one kindly provided by Prof. Roland Griffiths, Johns Hopkins Medicine. Music was played using a stereo system. Subjective drug intensity (SDI) was measured every 20 min using a 0–10 Likert scale (question: 'How intense is your experience right now?' 0='Not at all', 10='Very much'). Measurements were obtained from the time of drug administration to the end of the session. Participants responded orally and the supporting psychologists noted their responses. At the end of psilocybin session days, participants completed questionnaires aimed to quantify aspects of the psychedelic experience, including the 11-dimensional altered states of consciousness (11D-ASC) questionnaire (Studerus et al., 2010), the revised mystical experience questionnaire (MEQ30) (Barrett et al., 2015), and the ego-dissolution inventory (EDI) (Nour et al., 2016) (median

[range]: 6.4 [5.9–7.4] h after psilocybin intake). One week and 3 months after psilocybin administration, participants returned for MRI scan sessions identical to the baseline scan session. At 3 months, participants filled out questionnaires including the NEO PI-R, MAAS and persisting effects questionnaire (PEQ) (Griffiths et al., 2006, 2011), which measures psychological changes (both positive and negative) that are subjectively perceived to be due to the psilocybin experience. Number of days between psilocybin sessions and follow-up questionnaires: mean (SD) [range] = 97.8 (11.9) [79–120 days]].

Positron emission tomography

The PET data used in this analysis are the same as those reported previously (Madsen et al., 2020; Stenbæk et al., 2020). For a more in-depth description of the PET methods, please refer Madsen et al. (2020). [¹¹C]Cimbi-36 is an agonist radioligand selective for serotonin (5-HT) 2A (5-HT_{2A}R) and 2C receptors (Ettrup et al., 2014). Participants completed 120-min scans on a high-resolution research tomograph (HRRT) PET-scanner (CTI/Siemens, Knoxville, TN, USA) at baseline and 1 week following psilocybin administration. Regional time-activity curves were extracted using Pvelab (Svarer et al., 2005) from a neocortex and cerebellum region for estimation of non-displaceable binding potential (BPND) using the simplified reference tissue model (Ettrup et al., 2016; Innis et al., 2007). Neocortex [¹¹C]Cimbi-36 binding predominantly reflects 5-HT_{2A}R binding (Finnema et al., 2014). The neocortex and cerebellum regions of interest (ROIs) were defined a priori in Pvelab (Svarer et al., 2005). The neocortex ROI comprises occipital, orbitofrontal and parietal cortex as well as pre/post central, middle/inferior frontal, middle/inferior temporal, superior frontal and superior temporal gyri. A composite neocortex ROI was used because the signal is very highly correlated between these regions (Spies et al., 2020). Subcortical [¹¹C]Cimbi-36 binding was not considered because the signal is low and noisy. The cerebellum ROI encompasses only the grey matter of the cerebellum.

Magnetic resonance imaging scan parameters

Participants completed three identical MRI scan sessions: baseline, 1-week, and 3-month post-psilocybin. The MRI data were acquired on a 3T Prisma scanner (Siemens, Erlangen, Germany) using a 64-channel head/neck coil. A high-resolution 3D T1-weighted structural image was acquired: inversion time=900ms, echo time=2.58ms, repetition time=1900ms, flip angle=9°, in-plane matrix=256 × 256, in-plane resolution=0.9 × 0.9mm, 224 slices, and a slice thickness of 0.9mm, no gap. Ten minutes of resting-state BOLD fMRI data was acquired: repetition time=2000ms, echo time=30ms, flip angle=90°, 32 axial slices with a slice thickness of 3mm, 0.75mm gap, in-plane resolution: 3.6 × 3.6mm, iPAT acceleration factor=2. A gradient-echo field map of the same spatial dimensions was acquired to resolve spatial distortions due to inhomogeneities in the magnetic field (repetition time=400ms, echo times=4.92 and 7.38ms). Prior to the resting-state scan sessions, participants were instructed to close their eyes, let their mind wander freely and to not to fall asleep. Resting-state scan sessions were acquired after structural image acquisition (~15–20min after scanning onset) and prior to task-related fMRI measures not described here.

Resting-state fMRI pre-processing

Resting-state fMRI data were pre-processed using SPM12 (Penny et al., 2007). This process included slice-timing correction, realignment and unwarping, co-registration of the high-resolution T1 structural image to the fMRI data, segmentation of the high-resolution T1 structural image, applying warping parameters estimated for the high-resolution T1 into MNI space to fMRI data and smoothing with an 8-mm full width at half maximum (FWHM) Gaussian filter. Additional denoising of time-series data was performed using CONN (version 17.c) (Whitfield-Gabrieli and Nieto-Castanon, 2012). Time series were filtered using a bandpass filter from 0.008 to 0.09Hz. Additionally, we performed an estimation of physiological noise sources using anatomical component correction (aCompCor): regressing out the time series (and first derivative) of the first five principal components from a decomposition of the time series from white-matter and cerebrospinal fluid voxels, separately. Additionally, we regressed the time series for the six motion parameters (and first derivatives) (Behzadi et al., 2007; Whitfield-Gabrieli and Nieto-Castanon, 2012). Individual outlier volumes were identified and censored using the Artifact Detection Tools (ART) (global variance threshold=4 and composite motion threshold=2) (<http://web.mit.edu/swg/software.htm>). Mean denoised time series were extracted from ROIs for further analysis. We calculated the between-region correlation across the entire time series. The Pearson's rho correlation estimates were transformed using Fisher's *r*-to-*z* transform (i.e. $r\text{-to-}z = 0.5 \times (\ln((1+r)/(1-r)))$), where *r* is the Pearson's rho and *ln* represent taking the natural logarithm). These *r*-to-*z* values were included in the statistical analyses related to the connectivity strength.

Brain atlases

Regions of interest and networks were defined using an a priori defined atlas (Raichle, 2011). This atlas defines 36 regions belonging to seven canonical resting-state networks: network (DMN),

dorsal attention network (DAN), executive control network (ECN), salience network (SN), sensorimotor network (SMN), visual network (VN) and auditory network (AN). Montreal Neurological Institute (MNI) coordinates for each network can be found in Raichle (2011) and in Supplemental Table S1. Within-network connectivity was defined as the mean connectivity between each unique pair of ROIs comprising a given network. Henceforth ECN integration and disintegration refer to increased and decreased mean within-network connectivity, respectively. Between-network connectivity was defined as the mean connectivity between all ROIs from two networks, where each pair of ROIs contained a region from each network. To draw comparisons with a similar previous study, we also evaluated a 268-region atlas (https://www.nitrc.org/frs/?group_id=51) described previously (Barrett et al., 2020; Shen et al., 2013).

Statistical analysis

All statistical analyses were calculated in R (v4.0.2) (R Studio Team, 2020). Plots were constructed using the *ggplot2* package (Wickham, 2016).

Paired *t*-tests were performed to investigate if there were any significant differences in ART censored volumes between time points (1 week vs. 3 months). Effects of time (1 week vs. baseline or 3 months vs. baseline) were compared separately using paired *t*-tests to determine the effect of time on within- and between-network connectivity and related estimates. The *p*-values across the 28 within- and between-network comparisons at each time point were adjusted using the Bonferroni–Holm method, which controls the family-wise type-I error rate (Holm, 1979). Unadjusted *p*-values are denoted p_{unc} , whereas adjusted *p*-values are denoted p_{FWE} . Where an effect of psilocybin on connectivity exceeded our statistical significance threshold ($p_{\text{FWE}} < 0.05$), exploratory post hoc analyses were performed. We report the Cohen's *d* value for each post hoc effect evaluated. Due to limited statistical power stemming from a small sample, we do not draw inference on statistical significance for post hoc analyses, but instead report standardised effect sizes and 95% confidence intervals.

Correlations. The post hoc Pearson's product-moment correlations were performed between change in ECN connectivity and change in MAAS, change in neocortex 5-HT_{2A}R (i.e. [¹¹C] Cimbi-36 BP_{ND}) (Madsen et al., 2020) as well as measures of the acute psychedelic experience (SDI, EDI, MEQ and 11-D-ASC) and change in personality (NEO-PIR). Change in ECN RSFC was also compared with the PEQ using a linear latent variable model capturing shared covariance in individual behavioural change measures using the *lava* package (v. 1.6.8 in R (Holst and Budtz-Jørgensen, 2013)).

Barrett replication analysis. We attempted to replicate a previously described analysis framework applied to the Shen268 atlas (Barrett et al., 2020). As described, we applied a one-sample *t*-test to all ROI-to-ROI connectivity estimates and retained only those edges with a statistically significant non-zero mean connectivity after the Bonferroni correction for 35,778 edges tested at each time point (i.e. $p_{\text{unc}} < 1.4 \times 10^{-6}$). Paired *t*-tests evaluating change from baseline at 1 week or 3 months were performed for each edge surviving correction. Suprathreshold edges were

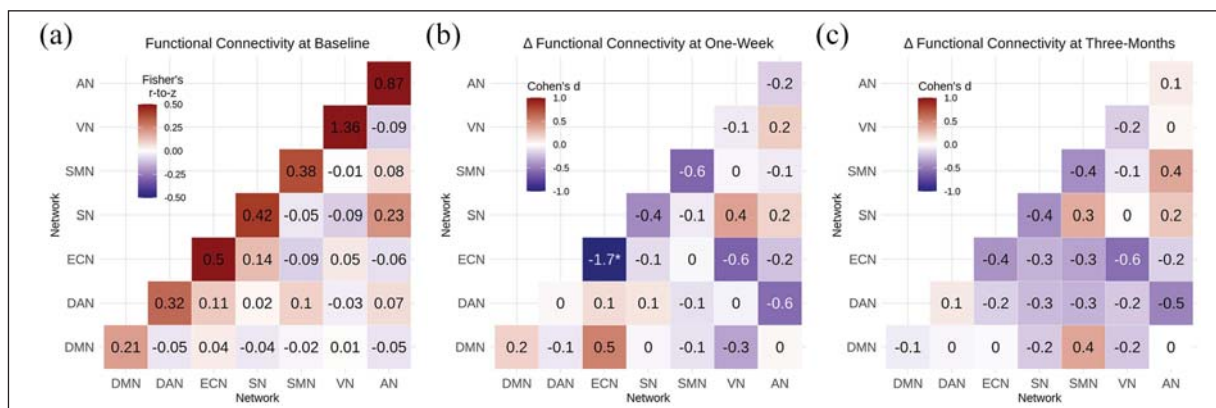


Figure 2. Psilocybin effects on within- and between-network resting-state connectivity: (a) mean within- and between-network functional connectivity, cell values and colour scale represent mean r -to- z values across participants, (b) change in connectivity from baseline to 1-week rescan, (c) change in connectivity from baseline to 3 month rescan. Cell values and colour scale in (b) and (c) represent effect size (Cohen's d). * denotes change that is statistically significant after adjustment across 28 tests (i.e. $p_{FWE} < 0.05$).

identified as either increases or decreases in connectivity following psilocybin.

In our view, the type-I error for the test of interest (i.e. effect of psilocybin) is inflated by the initial 'edge filtering' step considering each time point separately and further inflated by not adjusting for the family of tests of interest (695 reported in Barrett et al., 2020). Accordingly, we report paired t -tests evaluating changes from baseline to 1 week or 3 months, adjusting p -values using the Bonferroni–Holm method for the set of edges tested.

The R Notebook containing code used in the production of this manuscript is available at <https://github.com/Pneumaethylamine/LastingPsilocybinRSFC>

Results

Population

Acute psychedelic effects were well tolerated in all participants, and no serious adverse events occurred. Based on self-report SDI scores throughout the sessions, the psychedelic experiences were characterised by three distinct phases, the onset, peak plateau and descent (Stenbæk et al., 2020). As previously reported, participants in this study self-reported changes in personality, including increased trait openness and mindfulness (Madsen et al., 2020). Self-reported increases in positive attributes from the PEQ (including spirituality) were $25.9\% \pm 21.5\%$ (mean \pm SD), whereas increased negative attributes reported were $1.4\% \pm 1.7\%$. Time between baseline and psilocybin intervention was 15.3 ± 9.3 days, intervention and 1 week rescan was 6.5 ± 1.4 days and intervention and 3 month rescan was 101.5 ± 9.9 days (mean \pm SD).

Lasting psilocybin effects on network connectivity

Within- and between-network RSFC structure was as expected, for example, high within-network connectivity and relatively lower between-network connectivity (Figure 2(a)). Mean composite motion and censored volumes were low (3.5 ± 4.0 volumes; mean \pm SD) and not statistically significantly different between scan times ($p_{unc} > 0.05$).

ECN within-network connectivity was statistically significantly decreased at 1 week ($p_{unc} = 0.00039$, $p_{FWE} = 0.010$, Cohen's $d = -1.73$; Figures 2(b) and 3). Nine of 10 participants showed numerically reduced ECN RSFC at 1 week. Examination of individual ECN edges showed that nine of 10 edges had decreased connectivity across the 10 participants. At 3 months, ECN RSFC remained numerically decreased as compared to baseline, but this effect was not statistically significant ($p_{unc} = 0.23$, $p_{FWE} = 1$, Cohen's $d = -0.4$). No other within- or between-network connectivity estimates were statistically significantly altered at 1 week or 3 months (Supplemental Table S2). Additional network connectivity effects with a $|Cohen's d| > 0.5$ include at 1 week, SMN–SMN, ECN–VN and DAN–AN connectivity decreased (Cohen's $d = -0.6$), whereas DMN–ECN connectivity increased (Cohen's $d = 0.5$). At 3 months, ECN–VN and DAN–AN connectivity remained decreased (Cohen's $d = -0.6$ and -0.5 , respectively). A Cohen's d magnitude > 0.5 represents a 'medium' effect size (Ferguson, 2009).

Replication of previous study

Later, we attempted to replicate previously reported findings from a similar study (Barrett et al., 2020). Of the 35,778 edges defined by the Shen268 atlas, 405 showed evidence for significant connectivity based on the strategy described by Barrett and colleagues, who reported 695 suprathreshold edges. RSFC was altered in 25 edges at 1 week (19 increased and six decreased) and 18 edges at 3 months (12 increased and six decreased) at a statistical threshold of $p_{unc} < 0.05$. Two of these edges were altered in the same direction at both time points (one increased and one decreased). Although we observed fewer total edges showing evidence for significant connectivity, we observed a similar proportion of edges showing a time effect (i.e. 25/405 and 18/405 are approximately similar to 48/695 and 29/695, respectively). None of the 25 nor 18 edges remained statistically significant after controlling the type-I error for the 405 tests using the Bonferroni–Holm method.

Exploratory associations with ECN functional connectivity

Lastly, we explored the association between change in ECN RSFC at 1 week and self-report measures of the psychedelic

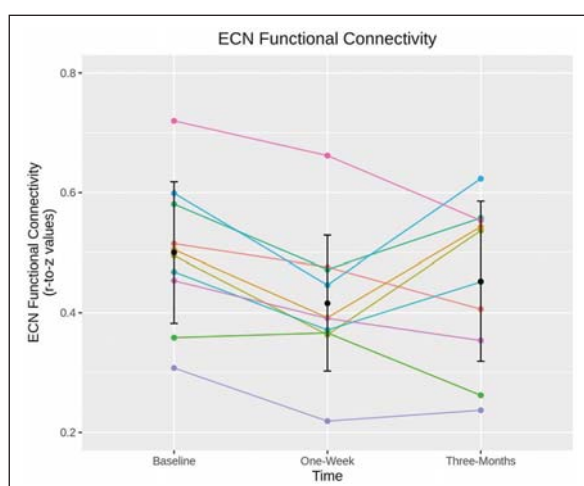


Figure 3. Executive control network (ECN) connectivity by participant. Spaghetti plot showing individual changes in mean ECN connectivity scores (y-axis) and time point (x-axis). Error bars represent mean \pm standard deviation. Colours represent individual participants. ECN connectivity is significantly decreased at 1 week but not at 3 months.

experience acquired immediately after the experience, change in neocortex 5-HT_{2A}R (at 1 week), change in personality (at 3 months) and self-reported persisting effects of the psychedelic experience (3 months). A summary of correlations can be found in Supplemental Table S3.

The most promising associations were observed between changes in ECN functional connectivity at 1 week and 3 months with self-reported change in MAAS at 3 months (r [95% CI] = -0.65 [-0.91 , -0.04]) and (r [95% CI] = 0.71 [0.15 , 0.93]) respectively, that is, the greater the decrease in ECN connectivity at 1 week, the greater the increase in MAAS score at 3 months (Figure 4). A smaller ECN connectivity change from baseline to 3 months was associated with a greater increase in MAAS score.

Neocortex 5-HT_{2A}R. Change in neocortex 5-HT_{2A}R binding measured with [¹¹C]Cimbi-36 BP_{ND} at 1 week was not correlated with change in ECN connectivity at 1 week (r [95% CI] = 0.52 [-0.15 , 0.87]). However, change in neocortex 5-HT_{2A}R at 1 week correlated more strongly with the ECN RSFC change at 3 months (r [95% CI] = -0.67 [-0.91 , -0.06]). In other words, greater disintegration of the ECN correlated with more neocortex 5-HT_{2A}R.

Persisting effects questionnaire. The positive subscales of the PEQ loaded strongly onto a single latent construct, indicating high shared correlation ($p < 10^{-6}$). Change in ECN RSFC at 1 week was negatively associated with the underlying latent variable (-19.9 [-41.7 , 1.93], units: change in Life Positivity PEQ per 0.1-unit change in ECN RSFC; Figure 5). Individual estimates are reported in Figure 5.

Discussion

Our results show that psilocybin, when administered to healthy volunteers in a controlled environment, statistically significantly

decreases ECN RSFC at 1 week, but not at 3 months. We observed correlations between ECN RSFC changes and changes in MAAS, neocortex 5-HT_{2A}R and positive aspects of the PEQ, implicating alterations in ECN connectivity as a potential mechanism underlying the clinical and behavioural effects of psilocybin. No other network connectivity estimates were statistically significantly affected at 1 week or 3 months. Our study is small, but nevertheless implicates a candidate brain system underlying lasting psilocybin effects that can be examined in future studies in healthy and patient populations.

Executive control network connectivity

A single psilocybin administration decreased ECN RSFC; nine out of 10 participants showed decreased ECN RSFC and nine out of 10 ECN edges showed decreased RSFC across all participants. This distributed effect is consistent with this representing a network-wide effect not driven by a specific participant or edge. Executive functions include, for example, cognitive flexibility, goal setting, attentional control and information processing (Niendam et al., 2012). This is consistent with qualitative reports in addiction patients who report persistent changes in attentional control and goal setting following psilocybin intervention (Nielson et al., 2018; Noorani et al., 2018). Though little research has been performed on ECN RSFC and its association with trait changes in executive functions, one study reported lower FC within the ECN in long-term tai-chi practitioners relative to controls. These practitioners also showed increased trait mindfulness and performed better on emotion regulation tasks (Liu et al., 2018), aligning with our finding that decreased ECN connectivity predicted increased trait mindfulness. Change in ECN connectivity was not associated with any measures of the acute experience (Supplemental Table S3), suggesting it might not simply be mediated by brain psilocin concentration (Madsen et al., 2019).

Psilocybin has been shown in small open-label trials to be efficacious in the treatment of depression (Cohen's $d = -2.1$ and -2.5 at 5-week post-administration) (Carhart-Harris et al., 2018; Davis et al., 2020), a disorder, which is partly characterised by deficits in executive functions (Snyder, 2013). Our finding that psilocybin decreased ECN RSFC is consistent with a recent study reporting that unmedicated, first-time MDD patients demonstrated hyper-connectivity between the left dorsolateral prefrontal cortex (PFC) and frontal and parietal regions, nodes which commonly constitute cognitive control networks (Shen et al., 2015). However, another study reported that MDD is characterised by reduced frontoparietal control system connectivity (Kaiser et al., 2015). Although it is intriguing that in healthy individuals we observe an effect of psilocybin on a resting-state network that displays pathological connectivity in depressed patients, future studies are necessary to more clearly establish this network's relation to treatment-induced changes in measures of personality and well-being. Additionally, it remains to be established whether psilocybin-induced changes in connectivity would produce the well-being states described by such connectivity signatures in healthy, untreated individuals.

The observed effect on ECN RSFC may also align with psilocybin's potential effects on obsessive-compulsive disorder (OCD) (Moreno et al., 2006) and addiction (Bogenschutz et al., 2015; Johnson et al., 2017), disorders broadly characterised by aberrant control of behaviour. The OCD patients display greater

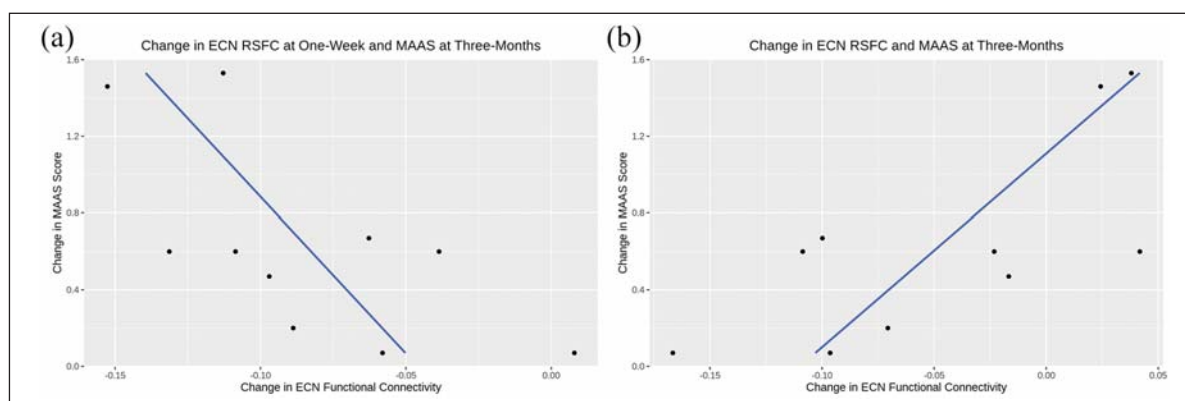


Figure 4. Correlations between executive control network (ECN) connectivity and mindful attention awareness scale (MAAS). Scatter plots with linear regressions between MAAS score (y -axis) and (a) change in ECN connectivity at 1 week, and (b) change in ECN connectivity at 3 months. Blue lines represent lines of best fit and black dots denote observed data.

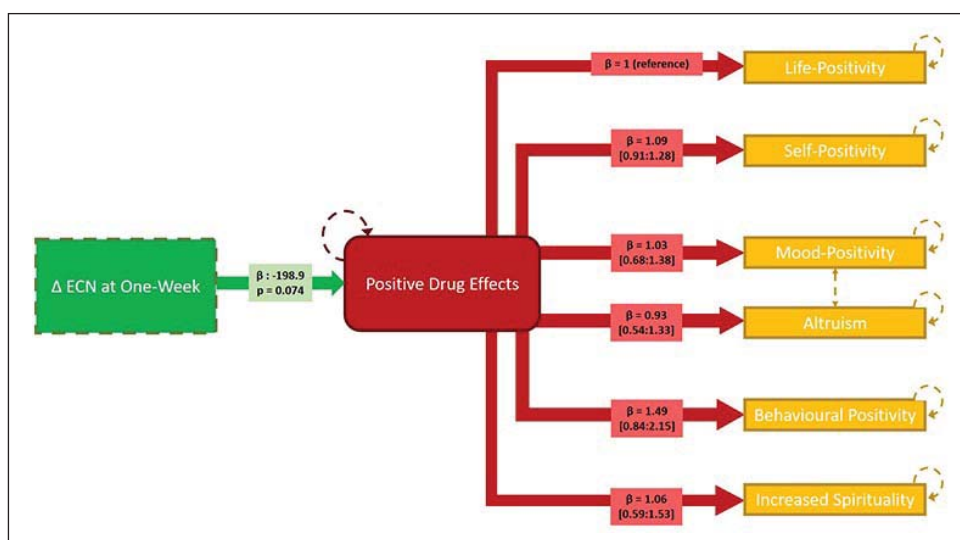


Figure 5. Linear latent variable model linking change in executive control network (ECN) connectivity at 1 week and persisting effects questionnaire (PEQ) responses at 3 months. The green box denotes observed change in ECN connectivity at 1 week. The red box denotes the latent variable ('positive drug change'). The yellow boxes denote observed PEQ scores. Hatched orange lines between 'mood-positivity' and 'altruism' indicate additional shared covariance. Hatched lines denote model components estimated with error. The loading parameter, β , reflecting the correlation of the score with the latent variable for each model path is noted in respective boxes (95% confidence intervals indicated for estimates between latent variable and PEQ subscale scores). Significance of the estimated effect of the ECN change on the latent variable is also noted.

connectivity in ECN regions, including dorsolateral PFC (Chen et al., 2016), suggesting that reducing ECN connectivity could be therapeutically beneficial. Although individuals with addiction disorder show neuropsychological impairment in brain regions associated with cognitive control (Goldstein et al., 2004), RSFC investigations of control networks in addiction have so far utilised alternative network definitions, and thus are not directly comparable to these findings (Sutherland et al., 2012).

As we only see a significant change in ECN connectivity at 1 week and not at 3 months, this change may underlie the 'after-glow' effect. Despite the lack of long-term effects, the association between the 1 week effect and long-term measures of well-being suggests a role for this period in mediating long-term effects on well-being, the neural correlates of which were not detected in

this study. Detailed quantitative characterisation of the 'after-glow' phenomenon could enable optimisation around this potentially clinically important phase of psychedelic psychotherapy by, for example, informing best practice surrounding post-session integration.

Additional effects on connectivity

Besides ECN RSFC at 1 week, all other standardised effect sizes for psilocybin induced change in RSFC (within- and between-network) were small to medium (i.e. $|Cohen's d| < 0.5$). This suggests that future studies evaluating similar effects of psilocybin on RSFC would require sample sizes >60 to be adequately statistically powered (i.e. $(1-\beta) > 0.8$). Thus, our findings argue

against large-scale changes in network connectivity structure insofar as we have quantified them here. This is notable considering participants report substantive changes in personality and well-being lasting for at least 1 year (Erritzoe et al., 2018; MacLean et al., 2011; Madsen et al., 2020) that are likely not entirely explained by ECN changes.

Our results suggest a small effect of psilocybin on DMN RSFC (Cohen's $d=0.19$). This is noteworthy because DMN disintegration has been reported when scanning participants during the psychedelic experience (Carhart-Harris et al., 2012; Preller et al., 2020) and may be implicated in the therapeutic effects of psilocybin as DMN connectivity is elevated in a range of conditions and is reduced following administration of psilocybin to experienced meditators (Smigielski et al., 2019; Whitfield-Gabrieli and Ford, 2012). Although we do not see a persistent effect on DMN connectivity, acute disruption of the DMN may still be therapeutically relevant (Carhart-Harris and Friston, 2019; Mason et al., 2020). Intake of both Salvinorin-A, a 5-HT_{2A}R-independent hallucinogen, and 3,4-methylenedioxymethamphetamine (MDMA), which has a subjective effect profile distinct from serotonergic psychedelics (Doss et al., 2020; Müller et al., 2020; Roseman et al., 2014), leads to a reduction in DMN connectivity. Reduced DMN connectivity is not associated with ego-dissolution in response to psilocybin (Lebedev et al., 2015). This muted effect on DMN RSFC after the psychedelic session is consistent with a study that scanned MDD individuals 1 day after the psychedelic experience (Carhart-Harris et al., 2017) and healthy volunteers 1 week and 1 month after psilocybin (Barrett et al., 2020). Thus, convergent evidence indicates that persistent alterations in DMN RSFC are unlikely to be a critical mechanism underlying lasting psilocybin effects.

Associations with executive control network change

Through exploratory analyses, we observed three notable associations with change in ECN RSFC. Firstly, a greater decrease in ECN RSFC at 1 week and a lesser decrease in ECN RSFC at 3 months both correlated with increased mindfulness score at 3 months. This could reflect that ECN disintegration followed by reintegration produces lasting increases in mindful awareness, a trait that is associated with reduced stress and better mood (Brown and Ryan, 2003). Secondly, building on our previous finding that change in 5-HT_{2A}R correlated negatively with change in mindfulness (Madsen et al., 2020), we observed that a greater decrease in ECN RSFC 1 week and a lesser decrease in ECN RSFC at 3 months was associated with decreased 5-HT_{2A}R at 1 week. Although speculative, our findings suggest that individual change in neocortex 5-HT_{2A}R following psilocybin administration may effect a change in mindfulness that is mediated by changes in ECN connectivity. Thirdly, decrease in ECN at 1 week was positively associated with a latent construct of positive persisting effects, reflecting positive items from the PEQ, at 3 months. This effect was particularly pronounced regarding 'behavioural positivity', aligning with qualitative reports from patients in clinical trials (Nielson et al., 2018; Noorani et al., 2018). Although exploratory, these observations provide a framework for linking brain and behavioural changes effected by psilocybin administration in future studies in healthy and clinical cohorts. Although we see changes in personality-trait

openness, neuroticism and conscientiousness in this sample (Madsen et al., 2020), these changes were not correlated with change in ECN RSFC (Supplemental Table S3).

Barrett replication

Replication is critical for identifying reliable brain markers of psilocybin effects. Here, we sought to replicate recently reported findings from a study very similar to ours (Barrett et al., 2020). We replicated the scale of region-to-region RSFC estimates that were affected by psilocybin. However, none of these effects remained statistically significant when controlling for multiple comparisons. Ours and the previous study have small sample sizes, which exacerbate the statistical power limitations of an exploratory region-to-region RSFC analysis strategy. Without substantively larger samples, this analysis framework would likely benefit from a hypothesis-driven evaluation of specific region pairs. Notably, the Shen268 atlas does not describe an ECN, and thus these results cannot be compared with our ECN finding using the Raichle atlas. This heterogeneity highlights a case for co-ordination of spatial parcellation within this corner of neuroimaging.

Limitations

As noted previously, our sample size of 10 individuals limits statistical power. Nevertheless, the data reported here provide a firmer foundation for future studies in clinical and healthy cohorts with larger samples. Although psilocybin seems to have positive behavioural and mood effects in healthy individuals, it is not clear how closely our observed effects on brain connectivity would generalise to clinical cohorts. Additional studies in patient groups are needed to delineate the neurobiological basis of therapeutic effects of serotonergic psychedelics including psilocybin. There is variation across resting-state atlases in how cognitive control networks are defined, limiting our ability to draw firm conclusions with previous related studies (Raichle, 2015; Schaefer et al., 2018; Shen et al., 2020). Alternative analytic strategies (e.g. dynamic functional connectivity and entropy analyses) or task-based fMRI may reveal more pronounced effects on brain function and connectivity than those reported here. Future studies integrating fMRI with PET markers may offer deeper insights into the neurobiological mechanisms mediating psilocybin effects on behaviour (Fisher and Hariri, 2012). Although the observed effect on ECN may be related to individual differences in pharmacodynamics (i.e. drug availability and metabolism), we did not measure individual plasma psilocin levels (Madsen et al., 2019).

Conclusion

In conclusion, we report effects of a single psilocybin administration on RSFC networks at 1 week and 3 months in a cohort of 10 individuals. Although a small sample, we identified a statistically significant reduction in ECN RSFC at 1 week but not at 3 months (although numerically decreased). Exploratory correlations with change in ECN at 1 week suggest that it may be associated with change in neocortex 5-HT_{2A}R at 1 week as well as change in mindfulness and persistent positive psychological effects at

3 months. Nevertheless, future studies are necessary to more thoroughly map psilocybin effects on to changes in brain function and connectivity that may mediate its lasting clinical and behavioural effects.

Acknowledgements

Psilocybin was kindly supplied by National Institute of Mental Health, Klecany, Czech Republic and Forensic Laboratory of Biologically Active Compounds, Department of Chemistry of Natural Compounds, University of Chemistry and Technology Prague, Prague, Czech Republic.

Declaration of conflicting interests

The author(s) declared the following potential conflicts of interest with respect to the research, authorship, and/or publication of this article: DEM's salary was supported by an unrestricted grant from COMPASS Pathways Ltd., which had no involvement in this manuscript or related data collection. GMK has received honoraria as consultant for Sanos and for Sage Therapeutics. All other authors declare that there are no conflicts of interest.

Funding

The author(s) disclosed receipt of the following financial support for the research, authorship, and/or publication of this article: This study was supported by Innovation Fund Denmark (grant number: 4108-00004B), Independent Research Fund Denmark (grant number: 6110-00518B), and Ester M. og Konrad Kristian Sigurdssons Dyreværnsfond (grant number: 850-22-55166-17-LNG). MKM was supported by the Rigshospitalet Research Council (grant number: R130-A5324). BO was supported by the Lundbeck Foundation (grant number: R231-2016-3236) and Marie-Curie-NEUROMODEL (grant number: 746850). DEM was supported by an unrestricted grant from COMPASS Pathways Ltd.

ORCID iDs

Drummond E-Wen McCulloch  <https://orcid.org/0000-0001-6360-5224>

Dea Siggaard Stenbæk  <https://orcid.org/0000-0002-5439-4637>

Patrick MacDonald Fisher  <https://orcid.org/0000-0002-8115-0611>

Supplemental material

Supplemental material for this article is available online.

References

- Anderson BT, Danforth A, Daroff R, et al. (2020) Psilocybin-assisted group therapy for demoralized older long-term AIDS survivor men: An open-label safety and feasibility pilot study. *EClinicalMedicine* 27: 100538. DOI: 10.1016/j.eclim.2020.100538.
- Barrett FS, Doss MK, Sepeda ND, et al. (2020) Emotions and brain function are altered up to one month after a single high dose of psilocybin. *Sci Rep* 10: 2214. DOI: 10.1038/s41598-020-59282-y.
- Barrett FS, Johnson MW and Griffiths RR (2015) Validation of the revised Mystical Experience Questionnaire in experimental sessions with psilocybin. *J Psychopharmacol* 29: 1182–1190. DOI: 10.1177/0269881115609019.
- Behzadi Y, Restom K, Liau J, et al. (2007) A component based noise correction method (CompCor) for BOLD and perfusion based fMRI. *NeuroImage* 37: 90–101. DOI: 10.1016/j.neuroimage.2007.04.042.
- Bogenschutz MP, Forcehimes AA, Pommy JA, et al. (2015) Psilocybin-assisted treatment for alcohol dependence: A proof-of-concept study. *J Psychopharmacol* 29: 289–299. DOI: 10.1177/0269881115456144.
- Brown KW and Ryan RM (2003) The benefits of being present: Mindfulness and its role in psychological well-being. *J Pers Soc Psychol* 84: 822–848. DOI: 10.1037/0022-3514.84.4.822.
- Cai H, Zhu J and Yu Y (2020) Robust prediction of individual personality from brain functional connectome. *Soc Cogn Affect Neurosci* 15: 359–369. DOI: 10.1093/scan/nsaa044.
- Carhart-Harris RL and Friston KJ (2019) REBUS and the anarchic brain: Toward a unified model of the brain action of psychedelics. *Pharmacol Rev* 71: 316–344. DOI: 10.1124/pr.118.017160.
- Carhart-Harris RL, Bolstridge M, Day CMJ, et al. (2018) Psilocybin with psychological support for treatment-resistant depression: Six-month follow-up. *Psychopharmacology* 235: 399–408.
- Carhart-Harris RL, Erritzoe D, Williams T, et al. (2012) Neural correlates of the psychedelic state as determined by fMRI studies with psilocybin. *Proc Natl Acad Sci U S A* 109: 2138–2143. DOI: 10.1073/pnas.1119598109.
- Carhart-Harris RL, Kaelen M, Bolstridge M, et al. (2016) The paradoxical psychological effects of lysergic acid diethylamide (LSD). *Psychol Med* 46: 1379–1390. DOI: 10.1017/S0033291715002901.
- Carhart-Harris RL, Roseman L, Bolstridge M, et al. (2017) Psilocybin for treatment-resistant depression: FMRI-measured brain mechanisms. *Sci Rep* 7: 13187. DOI: 10.1038/s41598-017-13282-7.
- Chen Y, Meng X, Hu Q, et al. (2016) Altered resting-state functional organization within the central executive network in obsessive-compulsive disorder. *Psychiatry Clin Neurosci* 70: 448–456. DOI: 10.1111/pcn.12419.
- Costa PT and McCrae RR (2008) The revised NEO personality inventory (NEO-PI-R). In: Boyle GJ, Matthews G and Saklofske DH (eds) *The SAGE Handbook of Personality Theory and Assessment: Volume 2 - Personality Measurement and Testing*. London: SAGE, pp.179–198. DOI: 10.4135/9781849200479.n9.
- Davis AK, Barrett FS, May DG, et al. (2020) Effects of psilocybin-assisted therapy on major depressive disorder: A randomized clinical trial. *JAMA Psychiatry* 78: 481–489. DOI: 10.1001/jamapsychiatry.2020.3285.
- Doss MK, May DG, Johnson MW, et al. (2020) The acute effects of the atypical dissociative hallucinogen salvinorin A on functional connectivity in the human brain. *Sci Rep* 10: 16392. DOI: 10.1038/s41598-020-73216-8.
- Erritzoe D, Roseman L, Nour MM, et al. (2018) Effects of psilocybin therapy on personality structure. *Acta Psychiatr Scand* 138: 368–378. DOI: 10.1111/acps.12904.
- Ettrup A, da Cunha-Bang S, McMahon B, et al. (2014) Serotonin 2A receptor agonist binding in the human brain with [11 C]Cimbi-36. *J Cereb Blood Flow Metab* 34: 1188–1196. doi: 10.1038/jcbfm.2014.68.
- Ettrup A, Svarer C, McMahon B, et al. (2016) Serotonin 2A receptor agonist binding in the human brain with [11C]Cimbi-36: Test-retest reproducibility and head-to-head comparison with the antagonist [18F]altanserin. *NeuroImage* 130: 167–174. DOI: 10.1016/j.neuroimage.2016.02.001.
- Ferguson CJ (2009) An effect size primer: A guide for clinicians and researchers. *Prof Psychol Res Pr* 40: 532–538. DOI: 10.1037/a0015808.
- Finnema SJ, Stepanov V, Ettrup A, et al. (2014) Characterization of [11C]Cimbi-36 as an agonist PET radioligand for the 5-HT_{2A} and 5-HT_{2C} receptors in the nonhuman primate brain. *NeuroImage* 84: 342–353. DOI: 10.1016/j.neuroimage.2013.08.035.
- Fisher PM and Hariri AR (2012) Linking variability in brain chemistry and circuit function through multimodal human neuroimaging. *Genes Brain Behav* 11: 633–642. DOI: 10.1111/j.1601-183X.2012.00786.x.
- Garcia-Romeu A, Davis AK, Erowid F, et al. (2019) Cessation and reduction in alcohol consumption and misuse after psychedelic use. *J Psychopharmacol* 33: 1088–1101. DOI: 10.1177/0269881119845793.
- Gasser P, Holstein D, Michel Y, et al. (2014) Safety and efficacy of lysergic acid diethylamide-assisted psychotherapy for anxiety associated

- with life-threatening diseases. *J Nerv Ment Dis* 202: 513–520. DOI: 10.1097/NMD.0000000000000113.
- Goldstein RZ, Leskovan AC, Hoff AL, et al. (2004) Severity of neuropsychological impairment in cocaine and alcohol addiction: Association with metabolism in the prefrontal cortex. *Neuropsychologia* 42: 1447–1458. DOI: 10.1016/j.neuropsychologia.2004.04.002.
- Griffiths RR, Johnson MW, Carducci MA, et al. (2016) Psilocybin produces substantial and sustained decreases in depression and anxiety in patients with life-threatening cancer: A randomized double-blind trial. *J Psychopharmacol* 30: 1181–1197. DOI: 10.1177/0269881116675513.
- Griffiths RR, Johnson MW, Richards WA, et al. (2011) Psilocybin occasioned mystical-type experiences: Immediate and persisting dose-related effects. *Psychopharmacology* 218: 649–665. DOI: 10.1007/s00213-011-2358-5.
- Griffiths RR, Richards WA, McCann U, et al. (2006) Psilocybin can occasion mystical-type experiences having substantial and sustained personal meaning and spiritual significance. *Psychopharmacology* 187: 268–283. DOI: 10.1007/s00213-006-0457-5.
- Grob CS, McKenna DJ, Callaway JC, et al. (1996) Human psychopharmacology of hoasca, a plant hallucinogen used in ritual context in Brazil. *J Nerv Ment Dis* 184: 86–94. DOI: 10.1097/00005053-199602000-00004.
- Hasler F, Grimberg U, Benz MA, et al. (2004) Acute psychological and physiological affects of psilocybin in healthy humans: A double-blind, placebo-controlled dose-effect study. *Psychopharmacology* 172: 145–156. DOI: 10.1007/s00213-003-1640-6.
- Holm S (1979) A simple sequentially rejective multiple test procedure. *Scand J Stat* 6: 65–70.
- Holst KK and Budtz-Jørgensen E (2013) Linear latent variable models: The lava-package. *Comput Stat* 28: 1385–1452. DOI: 10.1007/s00180-012-0344-y.
- Hsu WT, Rosenberg MD, Scheinost D, et al. (2018) Resting-state functional connectivity predicts neuroticism and extraversion in novel individuals. *Soc Cogn Affect Neurosci* 13: 224–232. DOI: 10.1093/scan/nsy002.
- Innis RB, Cunningham VJ, Delforge J, et al. (2007) Consensus nomenclature for in vivo imaging of reversibly binding radioligands. *J Cereb Blood Flow Metab* 27: 1533–1539. DOI: 10.1038/sj.jcbfm.9600493.
- Jensen CG, Niclasen J, Vangkilde SA, et al. (2016) Research on translations of tests: General inattentiveness is a long-term reliable trait independently predictive of psychological health: Danish validation studies of the mindful attention awareness scale. *Psychol Assess* 28: e70–e87. DOI: 10.1037/pas0000196.
- Johnson MW, Garcia-Romeu A and Griffiths RR (2017) Long-term follow-up of psilocybin-facilitated smoking cessation. *Am J Drug Alcohol Abuse* 43: 55–60. DOI: 10.3109/00952990.2016.1170135.
- Johnson MW, Richards WA and Griffiths RR (2008) Human hallucinogen research: Guidelines for safety. *J Psychopharmacol* 22: 603–620. DOI: 10.1177/0269881108093587.
- Kaiser RH, Andrews-Hanna JR, Wager TD, et al. (2015) Large-scale network dysfunction in major depressive disorder: A meta-analysis of resting-state functional connectivity. *JAMA Psychiatry* 72: 603–611. DOI: 10.1001/jamapsychiatry.2015.0071.
- Lebedev AV, Lövdén M, Rosenthal G, et al. (2015) Finding the self by losing the self: Neural correlates of ego-dissolution under psilocybin. *Hum Brain Mapp* 36: 137–153. DOI: 10.1002/hbm.22833.
- Lee MH, Smyser CD and Shimony JS (2013) Resting-state fMRI: A review of methods and clinical applications. *Am J Neuroradiol* 34: 1866–1872. DOI: 10.3174/ajnr.A3263.
- Liu Z, Wu Y, Li L, et al. (2018) Functional connectivity within the executive control network mediates the effects of long-term Tai Chi exercise on elders' emotion regulation. *Front Aging Neurosci* 10: 315. doi: 10.3389/fnagi.2018.00315.
- MacLean KA, Johnson MW and Griffiths RR (2011) Mystical experiences occasioned by the hallucinogen psilocybin lead to increases in the personality domain of openness. *J Psychopharmacol* 25: 1453–1461. DOI: 10.1177/0269881111420188.
- Madsen MK, Fisher PM, Burmester D, et al. (2019) Psychedelic effects of psilocybin correlate with serotonin 2A receptor occupancy and plasma psilocin levels. *Neuropsychopharmacology* 44: 1328–1334. DOI: 10.1038/s41386-019-0324-9.
- Madsen MK, Fisher PM, Stenbæk DS, et al. (2020) A single psilocybin dose is associated with long-term increased mindfulness, preceded by a proportional change in neocortical 5-HT_{2A} receptor binding. *Eur Neuropsychopharmacol* 33: 71–80. DOI: 10.1016/j.euroneuro.2020.02.001.
- Majić T, Schmidt TT and Gallinat J (2015) Peak experiences and the afterglow phenomenon: When and how do therapeutic effects of hallucinogens depend on psychedelic experiences? *J Psychopharmacol* 29: 241–253. DOI: 10.1177/0269881114568040.
- Mason NL, Kuypers KPC, Müller F, et al. (2020) Me, myself, bye: Regional alterations in glutamate and the experience of ego dissolution with psilocybin. *Neuropsychopharmacology* 45: 2003–2011. DOI: 10.1038/s41386-020-0718-8.
- Moreno FA, Wiegand CB, Keolani Taitano E, et al. (2006) Safety, tolerability, and efficacy of psilocybin in 9 patients with obsessive-compulsive disorder. *J Clin Psychiatry* 67: 1735–1740. DOI: 10.4088/JCP.v67n1110.
- Müller F, Holze F, Dolder P, et al. (2020) MDMA-induced changes in within-network connectivity contradict the specificity of these alterations for the effects of serotonergic hallucinogens. *Neuropsychopharmacology* 46: 545–553. DOI: 10.1038/s41386-020-00906-2.
- Murphy-Beiner A and Soar K (2020) Ayahuasca's "afterglow": Improved mindfulness and cognitive flexibility in ayahuasca drinkers. *Psychopharmacology* 237: 1161–1169. DOI: 10.1007/s00213-019-05445-3.
- Nichols DE (2016) Psychedelics. *Pharmacol Rev* 68: 264–355. DOI: 10.1124/pr.115.011478.
- Nielson EM, May DG, Forcehimes AA, et al. (2018) The psychedelic debriefing in alcohol dependence treatment: Illustrating key change phenomena through qualitative content analysis of clinical sessions. *Front Pharmacol* 9: 132. DOI: 10.3389/fphar.2018.00132.
- Niendam TA, Laird AR, Ray KL, et al. (2012) Meta-analytic evidence for a superordinate cognitive control network subserving diverse executive functions. *Cogn Affect Behav Neurosci* 12: 241–268. doi: 10.3758/s13415-011-0083-5.
- Noorani T, Garcia-Romeu A, Swift TC, et al. (2018) Psychedelic therapy for smoking cessation: Qualitative analysis of participant accounts. *J Psychopharmacol* 32: 756–769. DOI: 10.1177/0269881118780612.
- Nour MM, Evans L, Nutt D, et al. (2016) Ego-dissolution and psychedelics: Validation of the ego-dissolution inventory (EDI). *Front Hum Neurosci* 10: 269. DOI: 10.3389/fnhum.2016.00269.
- Pahnke WN (1969) The psychedelic mystical experience in the human encounter with death. *Harv Theol Rev* 62: 1–21. DOI: 10.1017/S0017816000027577.
- Pasquini L, Palhano-Fontes F and Araujo DB (2020) Subacute effects of the psychedelic ayahuasca on the salience and default mode networks. *J Psychopharmacol* 34: 623–635. DOI: 10.1177/0269881120909409.
- Penny W, Friston K, Ashburner J, et al. (2007) *Statistical Parametric Mapping: The Analysis of Functional Brain Images, Statistical Parametric Mapping: The Analysis of Functional Brain Images*. Academic Press. DOI: 10.1016/B978-0-12-372560-8.X5000-1.
- Preller KH and Vollenweider FX (2018) Phenomenology, structure, and dynamic of psychedelic states. *Curr Top Behav Neurosci* 36: 221–256. DOI: 10.1007/7854_2016_459.
- Preller KH, Duerler P, Burt JB, et al. (2020) Psilocybin induces time-dependent changes in global functional connectivity. *Biol Psychiatry* 88: 197–207. DOI: 10.1016/j.biopsych.2019.12.027.
- R Studio Team (2020) R Studio. Available at: <http://www.rstudio.com/>
- Raichle ME (2011) The restless brain. *Brain Connect* 1: 3–12. doi: 10.1089/brain.2011.0019.

- Raichle ME (2015) The restless brain: How intrinsic activity organizes brain function. *Philos Trans R Soc Lond B Biol Sci* 370: 20140172. DOI: 10.1098/rstb.2014.0172.
- Roseman L, Leech R, Feilding A, et al. (2014) The effects of psilocybin and MDMA on between-network resting state functional connectivity in healthy volunteers. *Front Hum Neurosci* 8: 204. DOI: 10.3389/fnhum.2014.00204.
- Sampedro F, de la Fuente Revenga M, Valle M, et al. (2017) Assessing the psychedelic “after-glow” in ayahuasca users: Post-acute neuro-metabolic and functional connectivity changes are associated with enhanced mindfulness capacities. *Int J Neuropsychopharmacol* 20: 698–711. DOI: 10.1093/ijnp/pyx036.
- Schaefer A, Kong R, Gordon EM, et al. (2018) Local-global parcellation of the human cerebral cortex from intrinsic functional connectivity MRI. *Cereb Cortex* 28: 3095–3114. DOI: 10.1093/cercor/bhx179.
- Sheehan DV, Lecrubier Y, Sheehan KH, et al. (1998) The Mini-International Neuropsychiatric Interview (M.I.N.I.): The development and validation of a structured diagnostic psychiatric interview for DSM-IV and ICD-10. *J Clin Psychiatry* 59: 22–33.
- Shen K, Welton T, Lyon M, et al. (2020) Structural core of the executive control network: A high angular resolution diffusion MRI study. *Hum Brain Mapp* 41: 1226–1236. DOI: 10.1002/hbm.24870.
- Shen T, Li C, Wang B, et al. (2015) Increased cognition connectivity network in major depression disorder: A fMRI study. *Psychiatry Investig* 12: 227–234. DOI: 10.4306/pi.2015.12.2.227.
- Shen X, Tokoglu F, Papademetris X, et al. (2013) Groupwise whole-brain parcellation from resting-state fMRI data for network node identification. *NeuroImage* 82: 403–415. DOI: 10.1016/j.neuroimage.2013.05.081.
- Skovdahl-Hansen H, Mortensen EL and Scioetz H (2004) Dokumentation for den danske udgave af NEO PI-R og NEO PI-R Kort Version. Copenhagen, Denmark: *Dansk Psykologisk Forlag*.
- Sloshower J, Guss J, Krause R, et al. (2020) Psilocybin-assisted therapy of major depressive disorder using acceptance and commitment therapy as a therapeutic frame. *J Contextual Behav Sci* 15: 12–19. DOI: 10.1016/j.jcbs.2019.11.002.
- Smigielski L, Scheidegger M, Kometer M, et al. (2019) Psilocybin-assisted mindfulness training modulates self-consciousness and brain default mode network connectivity with lasting effects. *NeuroImage* 196: 207–215. DOI: 10.1016/j.neuroimage.2019.04.009.
- Snyder HR (2013) Major depressive disorder is associated with broad impairments on neuropsychological measures of executive function: A meta-analysis and review. *Psychol Bull* 139: 81–132. DOI: 10.1037/a0028727.
- Spies M, Nasser A, Ozenne B, et al. (2020) Common HTR2A variants and 5-HTTLPR are not associated with human in vivo serotonin 2A receptor levels. *Hum Brain Mapp* 41: 4518–4528. DOI: 10.1002/hbm.25138.
- Stenbæk DS, Madsen MK, Ozenne B, et al. (2021) Brain serotonin 2A receptor binding predicts subjective temporal and mystical effects of psilocybin in healthy humans. *J Psychopharmacol* 35: 459–468. DOI: 10.1177/0269881120959609.
- Straathof M, Rt Sinke M, Dijkhuizen RM, et al. (2019) A systematic review on the quantitative relationship between structural and functional network connectivity strength in mammalian brains. *J Cereb Blood Flow Metab* 39: 189–209. DOI: 10.1177/0271678X18809547.
- Studerus E, Gamma A and Vollenweider FX (2010) Psychometric evaluation of the altered states of consciousness rating scale (OAV). *PLoS One* 5: e12412. DOI: 10.1371/journal.pone.0012412.
- Sutherland MT, McHugh MJ, Pariyadath V, et al. (2012) Resting state functional connectivity in addiction: Lessons learned and a road ahead. *NeuroImage* 62: 2281–2295. DOI: 10.1016/j.neuroimage.2012.01.117.
- Svarer C, Madsen K, Hasselbalch SG, et al. (2005) MR-based automatic delineation of volumes of interest in human brain PET images using probability maps. *NeuroImage* 24: 969–979. DOI: 10.1016/j.neuroimage.2004.10.017.
- Tagliazucchi E, Roseman L, Kaelen M, et al. (2016) Increased global functional connectivity correlates with LSD-induced ego dissolution. *Curr Biol* 26: 1043–1050. DOI: 10.1016/j.cub.2016.02.010.
- Vollenweider FX, Vollenweider-Scherpenhuyzen MF, Bähler A, et al. (1998) Psilocybin induces schizophrenia-like psychosis in humans via a serotonin-2 agonist action. *NeuroReport* 9: 3897–3902. DOI: 10.1097/00001756-199812010-00024.
- Whitfield-Gabrieli S and Ford JM (2012) Default mode network activity and connectivity in psychopathology. *Annu Rev Clin Psychol* 8: 49–76. DOI: 10.1146/annurev-clinpsy-032511-143049.
- Whitfield-Gabrieli S and Nieto-Castanon A (2012) Conn: A functional connectivity toolbox for correlated and anticorrelated brain networks. *Brain Connect* 2: 125–141. DOI: 10.1089/brain.2012.0073.
- Wickham H (2016) *ggplot2: Elegant Graphics for Data Analysis*. New York: Springer-Verlag. Available at: <https://ggplot2.tidyverse.org/>
- Zeifman RJ, Wagner AC, Watts R, et al. (2020) Post-psychedelic reductions in experiential avoidance are associated with decreases in depression severity and suicidal ideation. *Front Psychiatry* 11: 782. DOI: 10.3389/fpsy.2020.00782.

Figure S1

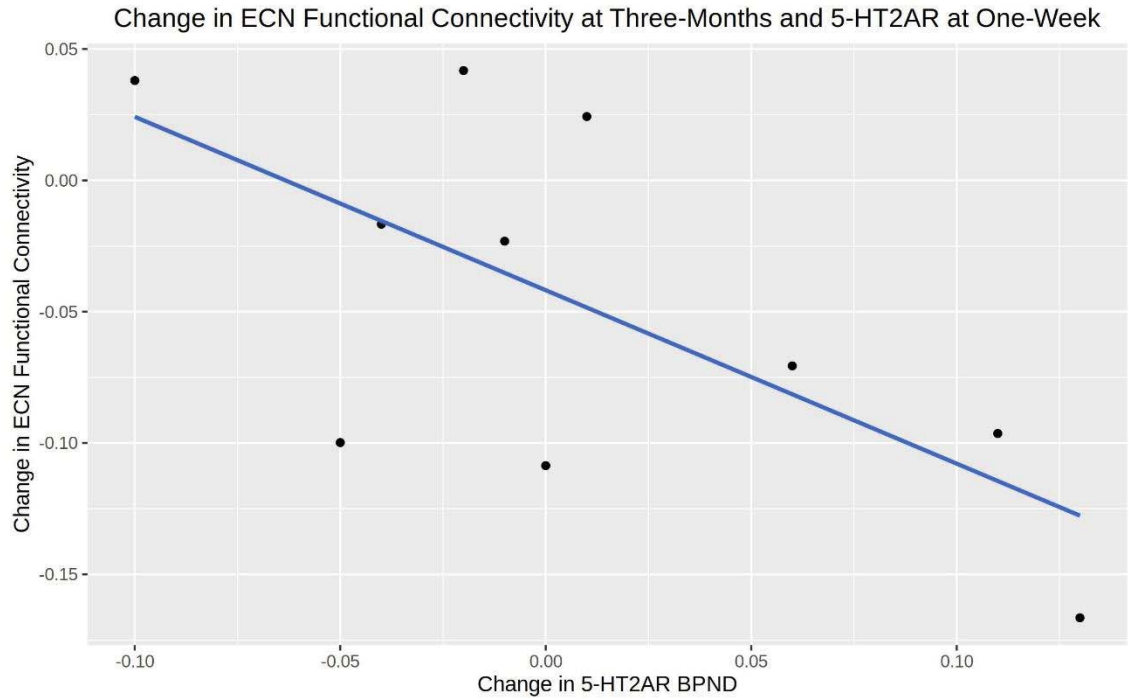


Figure S1. Correlation between the change in neocortex [^{11}C]Cimbi-36 BPND and change in ECN connectivity. Scatter plot showing the change in [^{11}C]Cimbi-36 BP_{ND} at one-week (x-axis) and change in ECN connectivity at three-months (y-axis). The blue line represents the line of best fit and black dots denote observed data.

Network	Region	MNI Coordinates
Executive Control	Dorsal Medial Prefrontal Cortex	0, 24, 46
Executive Control	Left Anterior Prefrontal Cortex	-44, 45, 0
Executive Control	Right Anterior Prefrontal Cortex	44, 45, 0
Executive Control	Left Superior Parietal Cortex	-50, -51, 45
Executive Control	Right Superior Parietal Cortex	50, 51, 45
Default Mode	Posterior Cingulate/Precuneus	0, -52, 27
Default Mode	Medial Prefrontal Cortex	-1, 54, 27
Default Mode	Left Lateral Parietal Cortex	-46, -66, 30
Default Mode	Right Lateral Parietal Cortex	49, -63, 33
Default Mode	Left Inferior Temporal Cortex	-61, -24, -9
Default Mode	Right Inferior Temporal Cortex	58, -24, -9
Default Mode	Medial Dorsal Thalamus	0, -12, 9
Default Mode	Right Posterior Cerebellum	-25, -81, -33
Default Mode	Left Posterior Cerebellum	25, -81, -33
Dorsal Attention	Left Frontal Eye Field	-29, -9, 54
Dorsal Attention	Right Frontal Eye Field	29, -9, 54
Dorsal Attention	Left Posterior IPS	-26, -66, 48
Dorsal Attention	Right Posterior IPS	26, -66, 48
Dorsal Attention	Left Anterior IPS	-44, -39, 45
Dorsal Attention	Right Anterior IPS	41, -39, 45
Dorsal Attention	Left MT	-50, -66, -6
Dorsal Attention	Right MT	53, -63, -6
Salience	Dorsal Anterior Cingulate Cortex	0, 21, 36
Salience	Left Anterior Prefrontal Cortex	-35, 45, 30
Salience	Right Anterior Prefrontal Cortex	32, 45, 30
Salience	Left Insula	-41, 3, 6
Salience	Right Insula	41, 3, 6
Salience	Left Lateral Parietal Cortex	-62, -45, 30
Salience	Right Lateral Parietal Cortex	62, -45, 30
Sensorimotor	Left Motor Cortex	-39, -26, 51
Sensorimotor	Right Motor Cortex	38, -26, 48
Sensorimotor	Supplementary Motor Area	0, -21, 48
Visual	Left V1	-7, 83, 2
Visual	Right V1	7, 83, 2
Auditory	Left A1	-62, -30, 12
Auditory	Right A1	59, -27, 15

Table S1. Regions and associated brain networks as described in (Raichle, 2011).
ROIs described by 10 mm radius spheres centred on given MNI coordinates.



DECLARATION OF CO-AUTHORSHIP

The declaration is for PhD students and must be completed for each conjointly authored article.

Please note that if a manuscript or published paper has eleven or less authors, all authors must sign a declaration of co-authorship. If it has twelve or more authors, only the PhD student, the corresponding author(s), the senior author, and the principal supervisor need to sign the declaration of co-authorship.

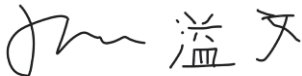
1. Declaration by	
Name of PhD student	Drummond McCulloch
E-mail	Drummond.mcculloch@nru.dk
Name of principal supervisor	Patrick Fisher
Title of the PhD thesis	Pharmacokinetic and pharmacodynamic evaluation of classical psychedelic substances in the human brain

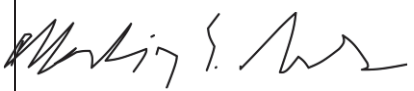





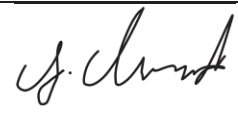

2. The declaration applies to the following article	
Title of article	Psilocybin-Induced Mystical-Type Experiences are Related to Persisting Positive Effects: A Quantitative and Qualitative Report
Article status	
Published <input checked="" type="checkbox"/>	Accepted for publication <input type="checkbox"/>
Date: March 2022	Date:
Manuscript submitted <input type="checkbox"/>	Manuscript not submitted <input type="checkbox"/>
Date:	
If the article is published or accepted for publication, please state the name of journal, year, volume, page and DOI (if you have the information).	Front. Pharmacol., 09 March 2022 Sec. Neuropharmacology Volume 13 - 2022 https://doi.org/10.3389/fphar.2022.841648

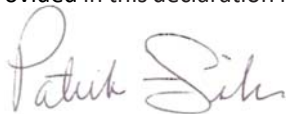
3. The PhD student's contribution to the article (please use the scale A-F as benchmark)	
<u>Benchmark scale of the PhD-student's contribution to the article</u>	A, B, C, D, E, F
A. Has essentially done all the work (> 90 %) B. Has done most of the work (60-90 %) C. Has contributed considerably (30-60 %) D. Has contributed (10-30 %) E. No or little contribution (<10 %) F. Not relevant	
1. Formulation/identification of the scientific problem	C
2. Development of the key methods	D

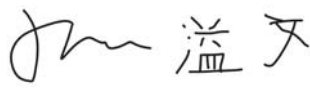
3. The PhD student's contribution to the article (please use the scale A-F as benchmark) <u>Benchmark scale of the PhD-student's contribution to the article</u> A. Has essentially done all the work (> 90 %) B. Has done most of the work (60-90 %) C. Has contributed considerably (30-60 %) D. Has contributed (10-30 %) E. No or little contribution (<10 %) F. Not relevant		A, B, C, D, E, F
3. Planning of the experiments and methodology design and development		E
4. Conducting the experimental work/clinical studies/data collection/obtaining access to data		C
5. Conducting the analysis of data		B
6. Interpretation of the results		B
7. Writing of the first draft of the manuscript		B
8. Finalisation of the manuscript and submission		C
Provide a short description of the PhD student's specific contribution to the article. ⁱ Formulated the research question, processed the data, performed analyses, made figures, wrote the manuscript.		

4. Material from another thesis / dissertation ⁱⁱ	
Does the article contain work which has also formed part of another thesis, e.g. master's thesis, PhD thesis or doctoral dissertation (the PhD student's or another person's)?	Yes: <input type="checkbox"/> No: <input checked="" type="checkbox"/>
If yes, please state name of the author and title of thesis / dissertation.	
If the article is part of another author's academic degree, please describe the PhD student's and the author's contributions to the article so that the individual contributions are clearly distinguishable from one another.	

5. Signatures of the authors incl. the PhD student				
	Date	Name	Title	Signature
1.	17/06/2025	Drummond McCulloch	Mr.	

5. Signatures of the authors incl. the PhD student				
2.	17/06/2025	Martin Korsbak Madsen	Dr.	
3.	25/06/2025	Dea Siggaard Stenbæk	Prof.	
4.	23/06/2025	Brice Ozenne	Prof.	
5.	17/06/2025	Peter Steen Jensen	Mr.	
6.	17/06/2025	Gitte Moos Knudsen	Prof.	
7.	17/06/2025	Patrick Fisher	Prof.	
8.	27/06/2025	Sophia Armand	Prof.	
9.	24/06/2025	Maria Zofia Grzywacz	Ms.	
10.				
11.				

6. Signature of the principal supervisor I solemnly declare that the information provided in this declaration is accurate to the best of my knowledge. Date: 27-06-2025 Principal supervisor: Patrick Fisher 
--

7. Signature of the PhD student I solemnly declare that the information provided in this declaration is accurate to the best of my knowledge. Date: 17-06-2025 PhD student: Drummond McCulloch 

Please learn more about responsible conduct of research on the [Faculty of Health and Medical Sciences' website](#).

ⁱ This can be supplemented with an additional letter if needed.

ⁱⁱ Please see Ministerial Order on the PhD Programme at the Universities and Certain Higher Artistic Educational Institutions (PhD Order) § 12 (4):

"Any articles included in the thesis may be written in cooperation with others, provided that each of the co -authors submits a written declaration stating the PhD student's or the author's contribution to the work."



Psilocybin-Induced Mystical-Type Experiences are Related to Persisting Positive Effects: A Quantitative and Qualitative Report

Drummond E-Wen McCulloch¹, Maria Zofia Grzywacz¹, Martin Korsbak Madsen¹, Peter Steen Jensen¹, Brice Ozenne^{1,2}, Sophia Armand¹, Gitte Moos Knudsen^{1,3}, Patrick MacDonald Fisher¹ and Dea Siggaard Stenbæk^{1,4*}

¹Neurobiology Research Unit and NeuroPharm, Copenhagen University Hospital Rigshospitalet, Copenhagen, Denmark, ²Department of Public Health, Section of Biostatistics, University of Copenhagen, Copenhagen, Denmark, ³Institute of Clinical Medicine, University of Copenhagen, Copenhagen, Denmark, ⁴Department of Psychology, University of Copenhagen, Copenhagen, Denmark

OPEN ACCESS

Edited by:

Matthew McMurray,
Miami University, United States

Reviewed by:

Enzo Tagliazucchi,
Goethe University Frankfurt, Germany
Matthias E. Liechti,
University Hospital of Basel,
Switzerland

*Correspondence:

Dea Siggaard Stenbæk
dea@nru.dk

Specialty section:

This article was submitted to
Neuropharmacology,
a section of the journal
Frontiers in Pharmacology

Received: 22 December 2021

Accepted: 08 February 2022

Published: 09 March 2022

Citation:

McCulloch DE, Grzywacz MZ, Madsen MK, Jensen PS, Ozenne B, Armand S, Knudsen GM, Fisher PM and Stenbæk DS (2022) Psilocybin-Induced Mystical-Type Experiences are Related to Persisting Positive Effects: A Quantitative and Qualitative Report.
Front. Pharmacol. 13:841648.
doi: 10.3389/fphar.2022.841648

Psychedelic drugs such as psilocybin have shown substantial promise for the treatment of several psychiatric conditions including mood and addictive disorders. They also have the remarkable property of producing persisting positive psychological changes in healthy volunteers for at least several months. In this study (NCT03289949), 35 medium-high doses of psilocybin were administered to 28 healthy volunteers (12 females). By the end of the dosing day, participants reported the intensity of their acute experience using the 30-item Mystical Experience Questionnaire (MEQ) and an open-form qualitative report from home. Persisting psychological effects attributed to the psilocybin experience were measured using the Persisting Effects Questionnaire (PEQ) 3-months after administration. Using a linear latent-variable model we show that the MEQ total score is positively associated with the later emergence of positive PEQ effects ($p = 3 \times 10^{-5}$). Moreover, the MEQ subscales “Positive Mood” ($p_{\text{corr}} = 4.1 \times 10^{-4}$) and “Mysticality” ($p_{\text{corr}} = 2.0 \times 10^{-4}$) are associated with positive PEQ whereas the subscales “Transcendence of Time and Space” ($p_{\text{corr}} = 0.38$) and “Ineffability” ($p_{\text{corr}} = 0.45$) are not. Using natural language pre-processing, we provide the first qualitative descriptions of the “Complete Mystical Experience” induced by orally administered psilocybin in healthy volunteers, revealing themes such as a sense of connection with the Universe, familial love, and the experience of profound beauty. Combining qualitative and quantitative methods, this paper expands understanding of the acute psilocybin induced experience in healthy volunteers and suggests an importance of the type of experience in predicting lasting positive effects.

Keywords: psychedelic, psilocybin, qualitative, psychology, natural language processing, mystical, phenomenology, persisting effects

INTRODUCTION

Psilocybin is a prodrug to the 5-HT_{2A} agonist psilocin (4-hydroxy-N,N-dimethyltryptamine) (Passie et al., 2002), which is the drug responsible for the psychoactive effects of “magic mushrooms”. Preliminary evidence from the last 15 years suggest that psilocybin has a rapid and potent positive treatment effect in affective and addictive disorders (Moreno et al., 2006; Grob et al., 2011; Bogenschutz et al., 2015; Griffiths et al., 2016; Ross et al., 2016; Johnson et al., 2017; Carhart-Harris et al., 2018; Garcia-Romeu et al., 2019; Anderson et al., 2020; Davis et al., 2020; Carhart-Harris et al., 2021). In healthy individuals and patients, psilocybin has been associated with long-lasting positive psychological effects and self-reported positive changes in mood, behaviour (Griffiths et al., 2011; Barrett et al., 2020) and personality (e.g., increased openness; (MacLean et al., 2011; Erritzoe et al., 2018; Schmid and Liechti, 2018; Madsen et al., 2020; Kettner et al., 2021), while no association with persisting effects on cognition has been observed (Rucker et al., 2021).

The subjective effects of psychedelics vary between individuals (Stenbæk et al., 2020) and are substantially affected by dose, CYP2D6 phenotype (Vizeli et al., 2021) and non-pharmacological factors like emotional “set”, i.e., a person’s current psychological state, and environmental “setting”, i.e., the immediate surroundings (Hyde, 1960; Hartogsohn, 2017; Strickland et al., 2021). The acute effects of medium-high oral doses (i.e., >0.2 mg/kg) of psilocybin last approximately four to six hours (Passie et al., 2002; Hasler et al., 2004; Preller et al., 2018; Madsen et al., 2019; Stenbæk et al., 2020; Madsen et al., 2021) though psilocybin may produce a misjudged perception of time on behalf of the recipient of the drug (Wackermann et al., 2008). Subjective psychedelic effects are characterised by changes in bodily experience, cognition, and alterations in the visual field (Preller and Vollenweider, 2018; Hirschfeld and Schmidt, 2021), and by pseudohallucinations but not “true hallucinations” (sensory phenomena indistinguishable from reality) (Sanati, 2012). The typical experience induced by a medium-high dose of psilocybin has a plateau of maximum subjective intensity which, for some participants, can occasion transient, profound alterations in consciousness described as a sense of unity with all things accompanied by dissolution of ego or personhood, blissful mood and ecstasy, and aberrant sense of time and space (Preller and Vollenweider, 2018; Stenbæk et al., 2020). Despite extensive quantitative characterisation, no papers so far have reported a qualitative description of the subjective experience of orally administered psilocybin in healthy volunteers, though the effects of 2 mg of intravenous psilocybin in an MR scanning environment (Turton et al., 2014) and of 75 µg of oral LSD (Sanz et al., 2021) have been described previously.

At maximum intensity psychedelic experiences can share many similar features with traditional “mystical-type” or “peak” experiences which have a potential for psychological transformation (Maslow, 1959; Griffiths et al., 2006; Griffiths et al., 2011; Lyvers and Meester, 2012). A subset of these, known as “Complete Mystical Experiences” (CME) are hypothesised to

be instrumental in the lasting positive effects of psychedelics (Yaden and Griffiths, 2021). The magnitude of psilocybin-induced mystical-type experience has shown positive correlations with improvements in subjective life quality, meaning in life, and mood in patients suffering from anxiety and depression associated with life threatening cancer (Griffiths et al., 2016; Ross et al., 2016), cigarette addiction (Garcia-Romeu et al., 2015) and major depressive disorder (Roseman et al., 2018; Davis et al., 2020). In healthy volunteers, the degree of mystical experience has been positively associated with increases in personality-domain openness up to 14-months after psilocybin (Griffiths et al., 2008; MacLean et al., 2011; Griffiths et al., 2018) and self-rated persisting positive effects 12-months after psilocybin (Schmid and Liechti, 2018). Despite replicated research investigating the acute effects of psychedelics, comparatively little is known about the relation between the character of the acute psychedelic experience (i.e., the way the experience feels, not simply the intensity) and the persisting changes in mood, behaviour, and personality.

Qualitative research so far has provided insight into themes that patients report as important in the lasting effects of psychedelic therapy including increased aesthetic appreciation and experiences of interconnectedness (Noorani et al., 2018), movement from disconnection to connection with senses, self, others and the world, and from emotional avoidance or numbness to emotional acceptance (Watts et al., 2017). In terminally ill patients, themes observed to be associated with clinical improvement include reconciliation with death and reconnection with life (Swift et al., 2017). Patients’ qualitative reports also describe meaningful aspects of the acute experience including altered perception of relationships and the appearance of meaningful visual phenomena (Belser et al., 2017) as well as acutely felt motivation and commitment to behavioural change (Nielson et al., 2018). However, qualitative analyses are particularly susceptible to investigator bias, as quote selection can be driven by the investigator’s proposed narrative (Galdas, 2017). We aimed to control for this for by first pre-analysing data using an unbiased natural language processing (NLP) script to steer qualitative analyses.

In this study, we contribute to the ongoing research concerning the relation between the acute subjective effects of psilocybin and their lasting effects. We do so by examining whether the self-reported intensity of the mystical-type experience is associated with persisting effects reported 3 months later in healthy volunteers. Further, we examined whether NLP of qualitative reports can be used to differentiate participants who have a CME compared to those who do not. We also expand the literature describing the subjective mystical-type experience induced by psilocybin by providing curated quotes from the qualitative reports guided by NLP results.

We hypothesise that there will be a positive association between intensity of the mystical-type experience and persisting positive effects attributed to the psilocybin experience at 3-month follow-up. In addition, we provide

NLP of qualitative reports to describe the experiences of participants who have a CME compared to those who do not.

METHODS

Participants

Recruitment

We recruited 28 healthy participants (12 females) ≥ 18 years of age from a list of individuals that expressed interest in participating in a psilocybin neuroscience study. Individuals participated in at least one of three sub-projects (sub-project 1 ($n = 4$), sub-project 2 ($n = 10$) and sub-project 3 ($n = 21$)) for a total of 35 psilocybin administrations (i.e., seven participants took part in two sub-projects). The sample included in this study only included those who had completed the Qualitative Experience Report as described below, and received at least 12 mg of psilocybin.

All participants underwent screening for somatic illness, including a medical examination, an ECG, blood screening for somatic disease, and screening for psychiatric disorders using the Mini International Neuropsychiatric Interview, Danish translation version 6.0.0 (Sheehan et al., 1998). Exclusion criteria for all sub-projects were: (Passie et al., 2002) present or previous primary psychiatric disease (DSM axis 1 or WHO ICD-10 diagnostic classifications) or in first-degree relatives; (Carhart-Harris et al., 2018) present or previous neurological condition/disease, significant somatic condition/disease; (Carhart-Harris et al., 2021) intake of drugs suspected to influence test results; (Davis et al., 2020) non-fluent Danish language skills; (Moreno et al., 2006) vision or hearing impairment; (Bogenschutz et al., 2015) previous or present learning disability; (Garcia-Romeu et al., 2019) pregnancy; (Johnson et al., 2017) breastfeeding; (Griffiths et al., 2016) magnetic resonance imaging (MRI) contraindications; (Grob et al., 2011) alcohol or drug abuse; (Ross et al., 2016) allergy to test drugs; (Anderson et al., 2020) significant exposure to radiation within the past year (e.g., medical imaging investigations); (Barrett et al., 2020) intake of QT-prolonging medication or electrocardiogram (ECG) results indicative of heart disease (Griffiths et al., 2011), blood donation less than 3 months before project participation; (MacLean et al., 2011) bodyweight less than 50 kg; (Erritzoe et al., 2018) low plasma ferritin levels ($<12 \mu\text{g/L}$).

Ethics

Written informed consent was obtained from all individuals before inclusion. The study was conducted in accordance with the Declaration of Helsinki. The study was approved by the ethics committee for the Capital Region of Copenhagen (journal identifier: H-16028698, amendments: 56,023, 56,967, 57,974, 59,673, 60,437, 62,255, and Danish Medicines Agency (EudraCT identifier: 2016-004000-61, amendments: 2017014166, 2017082837, and 2018023295). The study was also preregistered at ClinicalTrials.gov (identifier: NCT03289949).

Psilocybin Intervention

Prior to the intervention day, all participants attended a preparatory consultation with the study psychologists who would assist them on the intervention day. In all three sub-projects, psilocybin was administered orally in 3 mg capsules with a glass of water. Dose was adjusted for bodyweight: mean (SD) [range] = 0.26 (0.04) [0.19–0.31] mg/kg, absolute dose: mean (SD) [range] = 19.4 (3.7) [12–30] mg. Interpersonal support was provided throughout the interventions in all three sub-projects by the same leading psychologist (DSS) assisted by psychologist trainees. Likewise, the same medical doctor was involved in all three sub-projects (MKM). A light lunch and beverages (i.e., water + juice) were offered to the participants on all intervention days. Among the 35 sessions, four were conducted in the context of up to two positron emission tomography (PET) scans on the intervention day in sub-project 1 (Madsen et al., 2019), 10 sessions were conducted in a comfortable hotel-room-like setting in sub-project 2 (Madsen et al., 2020; Stenbæk et al., 2020), and 21 were conducted in the context of MRI scans on the intervention day in sub-project 3 (Madsen et al., 2021). All participants returned 1 day after the intervention day for a post-session consultation with the assisting psychologists.

Data Collection and Outcome Measures

Baseline Psychometrics

The outcome measures used in this study consisted of qualitative and questionnaire data collected on the day of psilocybin intervention and at 3-month follow-up. At baseline, we also collected descriptive information about depressive symptoms, perceived stress and sleep quality with the Major Depression Inventory (MDI) (Bech et al., 2001), Cohen's Perceived Stress Scale (PSS) (Cohen et al., 1983) and Pittsburgh Sleep Quality Index (PSQI) (Buysse et al., 1989), respectively.

Mystical Experience Questionnaire

At the end of the psilocybin intervention (~6 to 8 hours after ingestion of psilocybin), participants completed the self-report revised 30-item Mystical Experience Questionnaire (MEQ) (Barrett et al., 2015). The MEQ is a validated questionnaire comprising 30 items that capture the essential elements of a mystical-type experience relating to a single, discrete event (e.g., one psilocybin administration). The MEQ was derived from the MEQ43 which in turn was developed from the States of Consciousness Questionnaire based on classical descriptive work on mystical experiences and the psychology of religion (Stace, 1960; Pahnke, 1969; Richards, 1975). Items in the MEQ are rated using a 6-point Likert scale from 0 (none, not at all) to 5 (extreme, more than any other time in my life and more than a rating of 4). It has four sub-scales: Mysticality, Positive Mood, Transcendence of Time and Space and Ineffability (e.g., MEQ items: "Experience of unity with ultimate reality", "Experience of ecstasy", "Loss of your usual sense of time" and "Sense that the experience cannot be described adequately in words", respectively). The threshold for a CME is a score of $>60\%$ on all sub-scales (Barrett et al., 2015). This threshold was used to divide data into CME and non-CME. MEQ total score was calculated as the mean of all items.

Mandala Drawing

Following completion of the MEQ, participants were asked to draw a mandala of their experience using coloured pencils. Mandala is the Sanskrit word for “circle”, and it is typically interpreted as symbolising a transcendent function in the psyche (Bailer and Leeming, 2020). Practically, participants were given a paper with a circle represented on it and asked to draw their psilocybin experience within the circle using coloured pencils.

Qualitative Experience Report

In the evening on the day of psilocybin intervention, participants completed a qualitative report describing their experience in free writing using a secured online survey system (<https://www.limesurvey.org/>). There were no constraints and no minimum or maximum length to the experience report, only that it had to be completed before the participants went to sleep.

Persisting Effects Questionnaire

Approximately 3 months following the psilocybin sessions, participants completed the Persisting Effects Questionnaire (PEQ) (Griffiths et al., 2006). The PEQ is used to measure long-lasting positive and negative effects attributed directly to the psychedelic experience. The PEQ is a non-validated self-report questionnaire that has been used, among others, by Griffiths et al. (2006), Griffiths et al. (2008), Griffiths et al. (2011), Griffiths et al. (2016) to assess persisting effects of psychedelics as well as long-term positive effects attributable to “naturally occurring” mystical-type experiences (Griffiths et al., 2019). The PEQ comprises 145 questions that describe how the participants perceive changes in their life that they feel are “due to the experiences during your last session [of psilocybin] and your contemplation of those experiences”. Items are rated using a 6-point Likert scale from 0 (none, not at all) to 5 (extreme, more than any other time in my life and more than a rating of 4). It has 12 subscale-themes, namely a positive and a negative change in: Attitudes About Life, Attitudes About Self, Mood Changes, Social Effects, Behavioural Changes, and Spirituality (e.g., Attitudes about life: “You have more joy in your life” and “You have less joy in your life”, Social Effects: “You express more love toward others” and “You express more hatred toward others”). Subscale scores were converted to percentage of maximum score as performed in previous analyses (Griffiths et al., 2011; Griffiths et al., 2016). For the statistical analyses within study, we used the positive subscales only since very few persisting negative effects were rated. See Figure 2.

Plasma Psilocin Levels

In sub-project 3 plasma samples were drawn before and approximately 40, 80, 110, 160, 190, and 340 min post-psilocybin administration, and plasma psilocin levels (PPL) were evaluated as described in (Madsen et al., 2019). Peak values were chosen as the MEQ specifies “at any time during that session you experienced the following phenomena”.

Statistical Analyses

Descriptive Analyses

Differences at baseline between those who experienced a CME and did not experience a CME (non-CME) on the MDI, PSS, PSQI, age differences, bodyweight, dose administered, and naivety to psychedelic experiences were compared using a random intercept model to take into account that some participants participated twice. Sex differences in MEQ subscale and total score were also estimated using a similar model. Associations between the highest PPL value, i.e., representing peak effects of the drug, for each participant and MEQ total score or PPE_{LV} were evaluated using univariate linear models. There were no repeated observations in this subgroup.

Association Between MEQ and PEQ

The association between the MEQ and the PEQ, was investigated with linear latent variable models (LVMs) using the “lava” package for R (Holst and Budtz-Jørgensen, 2013). LVMs can be seen as an extension of linear mixed models for the analysis of multiple repeated measurements. While linear models parameterised with a random slope assume a constant correlation between measurements, LVMs relax this assumption allowing certain measurements to be more correlated than others (i.e., measurements from certain subscales can be more intercorrelated than others). LVMs were evaluated using the “modelsearch” function from the lava package and typically structured as shown in Figure 1 with some variation in covariance as described in section *Latent-Variable Model Construction*. A latent variable representing the six subscales of the PEQ was constructed and termed Positive Persisting Effects (PPE_{LV}). The association between the MEQ total and PPE_{LV} was evaluated within this model. Post hoc analyses of the associations between MEQ subscale scores and PPE_{LV} were also evaluated, each in a separate model. In order to calculate the potential direct and indirect mediation effects of the co-variables “Age”, “Sex”, “Dose”, “Project 2” and “Project 3”, both direct regressions of these onto PPE_{LV} and indirect effects of these via MEQ total or subscales were calculated in each model. “Sex-Female” and “Project 1” are reported as the intercept in the analysis of these co-variables. We report loadings (i.e., parameter for the association subscale-latent variable, denoted by “ β ” in Figure 1) and confidence intervals of each PEQ subscale onto PPE_{LV} with “life-positivity” arbitrarily chosen as a reference. To control for the small sample size and repeated measures, robust standard error was used (Ozenne et al., 2020). The MEQ total model was evaluated first as a primary hypothesis and the p -value for the relation between the MEQ total score and PPE_{LV} is reported. Subsequent tests investigating the subscales report the p -value for the same interaction in the model, corrected using the Bonferroni method for a family of four tests (Dunn, 1961).

Language Analyses

Lemmatisation

All evaluations were performed on the untranslated Danish text. Instances of words and quotes presented in this paper were independently translated by two bilingual individuals and recombined by a native English speaker and a third bilingual person.

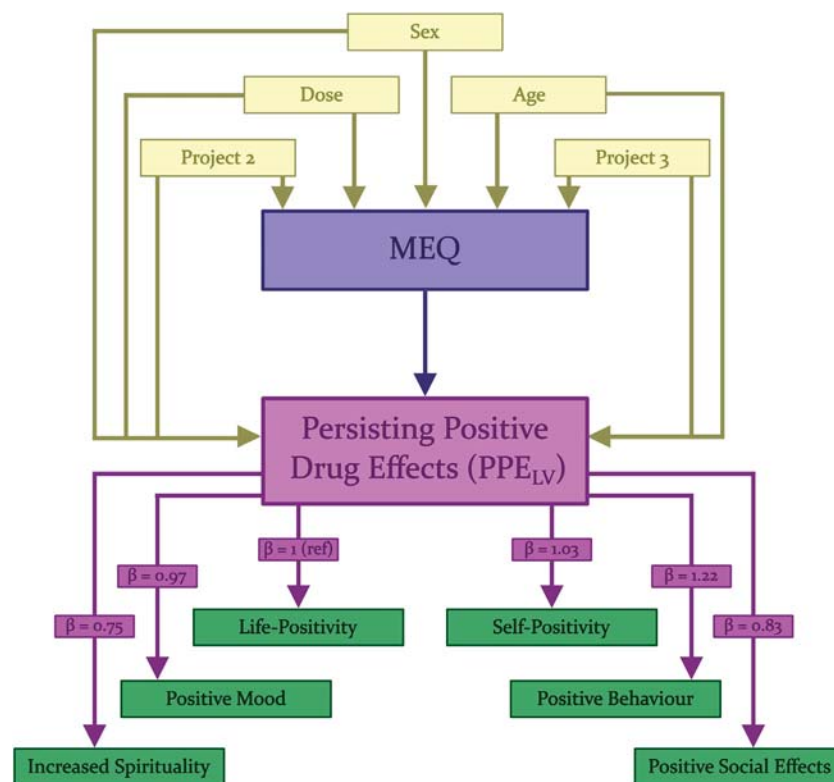


FIGURE 1 | Latent Variable Model. Schematic diagram describing the structure of the LVM used in the analysis of the relation between MEQ and the latent variable PPE_{LV} . “MEQ” (blue) represents either the MEQ total score or one of the four different subscales of the MEQ. Each was analysed using a different model; therefore, regression outputs are not reported in this figure and are instead reported in **Table 2**. Loadings of the individual positive subscales of the PEQ are stable between models and are thus reported on the lines between PPE_{LV} and the subscales. Loadings of co-variables are reported in **Supplementary Table S3**.

In order to pre-process the qualitative data for this analysis, words were lemmatised using the python package “lemmy” v 2.1.0 (<https://github.com/sorenind/lemmy>). Lemmatisation is the process of converting a word back to its root (i.e., “running” “ran” and “runs” would each be lemmatised to “run”). Danish words are not easily lemmatised as any given word may represent different cases for several different roots. For example, “slappe” (relax) could be lemmatised to “slappe” (relax), “slap” (loose), or “slippe” (drop). In order to control for this, the first lemma for each word was selected and others discarded. Upon random manual checking, this was accurate in all instances.

Tf-idf Analyses

In this paper we attempt to control for investigator-narrative bias by utilising term-frequency inverse document frequency (tf-idf) to identify distinguishing themes in the text prior to qualitative analysis (Ramos, 2003). The corpus of all reports was split into two documents containing reports from either CME or non-CME. Tf-idf is a statistic that reflects the importance of a term to a specific subset of documents within a wider corpus. Term frequency is the number of times the word appears in each document divided by the total number of words in that document. Inverse document

frequency is the log of the total number of documents divided by the number of documents containing the word, and tf-idf is the product of these. Reports were pre-processed by lemmatisation as described above, but stop-words (e.g., “the”, “if”, “and” etc.) were not removed as the tf-idf process accounts for these. Tf-idf scores were computed for each term within CME and non-CME documents. Analyses were performed using the R package “tidytext” (Silge and Robinson, 2016).

$$\text{tf-idf} = \frac{\text{incidence of } x \text{ in document}}{\text{total length of document}} \times \log_{10} \left(\frac{\text{total number of documents}}{\text{number of documents containing } x} \right)$$

Post-hoc Qualitative Analyses

To further investigate the terms with the highest tf-idf scores, we manually searched through all reports and extracted quotes that included each of the five highest tf-idf terms. We first checked that each term was not driven by a single report that used the word repeatedly. We then selected quotes that reflected the most representative thematic usages of these terms.

TABLE 1 | Descriptive statistics of the participants split by Complete Mystical Experience (CME).

Measure	All	CME	Non-CME	p value
Participants (no.)	28	16*	12*	NA
Psilocybin sessions (no.)	35	21	14	NA
Project 1 (PET) (no.)	4	1	3	0.31
Project 2 (no.)	10	7	3	0.21
Project 3 (MRI) (no.)	21	13	8	0.28
Female (%)	15 (43%)	8 (38%)	7 (50%)	0.50
Mean age (SD) (years)	31.7 (7.0)	30.8 (4.9)	33.1 (9.4)	0.45
Mean weight (SD) (kg)	72.4 (12.2)	75.5 (11.9)	72.7 (12.7)	0.44
Psychedelic Naïve (no. (%))	23 (66%)	14 (67%)	9 (64%)	0.89
Mean dose (SD) (mg)	19.4 (3.7)	19.3 (3.5)	19.5 (4.2)	0.80
Mean dose (SD) (mg/kg)	0.26 (0.04)	0.26 (0.04)	0.27 (0.04)	0.34
Mean baseline MDI	4.2 (2.4)	4.1 (2.6)	4.3 (2.2)	0.94
Mean baseline PSS	6.8 (3.8)	6.7 (3.6)	7.1 (4.1)	0.70
Mean baseline PSQI	3.7 (1.7)	3.3 (1.5)	4.3 (1.9)	0.18

All descriptive statistics are mean (Standard Deviation) unless otherwise stated. These describe the baseline characteristics including Major Depressive Inventory (MDI), Perceived Stress Scale (PSS), and Pittsburgh Sleep Quality Index (PSQI), aspects of the acute experience including dose of psilocybin administered (per os) and subproject. p-values for projects were calculated using a chi-squared test. All other p-values were calculated using a linear mixed-effects model controlling for participant ID as a random variable. PET, Positron Emission Tomography; MRI, Magnetic Resonance Imaging. *All individuals observed twice had either a CME or non-CME both times.

Mandala Assignment

To further illustrate our qualitative findings, available mandala drawings were located that aligned with the qualitative reports presented. Those interpreted as aligning with the themes of the associated qualitative report were selected, and the five participants were contacted to ensure that perception of depicted themes was accurate. These are presented in the results alongside their respective quotes.

Code Availability

R and python scripts used in analyses are available at <https://github.com/Pneumaethylamine/MysticalPEQ>.

Statistical Inference

Throughout the paper statistical significance was considered at an alpha of $p < 0.05$ following Bonferroni correction for multiple comparisons where appropriate (Haynes, 2013). We report corrected and uncorrected p -values, estimates and 95% confidence intervals.

RESULTS

Descriptive Analyses

In total 35 reports from 28 individual participants were recorded as seven participants took part in two projects. Of the 35 reports, the mean age (SD) was 31.7 (7.0) [range = 24.3 to 58.8] years, and 15 were from female subjects. One participant had missing PEQ data at 3-month follow-up. Therefore, this dataset was not included in the analyses involving the PEQ. Individual doses, sex, MEQ total and subscale scores are reported in **Supplementary Table S1**.

Descriptive statistics of participants, psilocybin sessions, project, sex, age, weight, naivety to psychedelics, dose, and baseline psychometrics for all participants combined and split by CME and non-CME are shown in **Table 1**, indicating no significant differences in these metrics between groups. PEQ subscale scores split by CME are presented in **Figure 2**. MEQ total and subscale scores are reported in **Supplementary Table S2**. A linear mixed effects model comparing MEQ total score and subscales between males and females, accounting for participant as a random variable and treating “Female” as the intercept showed no significant sex difference in any score ($p_{\text{corr}} > 0.31$). A description of the direct and indirect mediation effects of sex and other co-variables on PPE_{LV} can be found in **Supplementary Table S3**. No relation was observed between peak PPL and MEQ total score ($p = 0.88$, uncorrected) or PPE_{LV} ($p = 0.35$, uncorrected). See **Supplementary Figure S2**.

Association Between MEQ and PEQ Latent-Variable Model Construction

All six positive subscales of the PEQ loaded well onto the latent variable PPE_{LV} (Estimate range = 0.75:1.22, $p < 1.1 \times 10^{-10}$ for all subscales). All subscale loadings for each model are reported in **Supplementary Table S4**. No additional covariances were modelled in the main analysis evaluating MEQ total. The models for subscales Ineffability, Transcendence of Time and Space, and Mysticality contained covariance between the PEQ subscales “Positive Attitudes about Life” and “Positive Attitudes about Self” whereas the model investigating the Positive Mood subscale contains a covariance between the MEQ subscale Positive Mood and the PEQ subscale “Increased Spirituality”.

Association Between PEQ and MEQ

The LVM investigating the association between MEQ total score and PPE_{LV} showed a statistically significant positive association ($\beta = 14.8$, 95%CI = 8.66:20.96, $p = 3 \times 10^{-5}$). The subsequent LVMs investigating effects of the MEQ subscales on PPE_{LV} showed significant positive association with Positive Mood ($\beta = 14.5$, 95%CI = 7.90:21.11, $p_{\text{corr}} = 4.1 \times 10^{-4}$), as did the LVM evaluating Mysticality ($\beta = 10.8$, 95%CI = 6.14:15.51, $p_{\text{corr}} = 2.0 \times 10^{-4}$). However, no significant associations were observed for Transcendence of Time and Space ($\beta = 9.4$, 95% CI = -1.72:20.56, $p_{\text{corr}} = 0.38$) or Ineffability ($\beta = 11.2$, 95% CI = -2.75:25.14, $p_{\text{corr}} = 0.45$). See **Table 2** for a full summary of the LVM results and **Figure 3** for a graphical representation. LVM model summaries are reported in **Supplementary Table S4**. Direct and indirect mediation effects of covariates are reported in **Supplementary Table S3**. No indirect effects of any covariate via MEQ were significant (all $p > 0.1$, uncorrected). Scatter plots of MEQ total and subscales by PPE_{LV} are reported in **Supplementary Figure S1**.

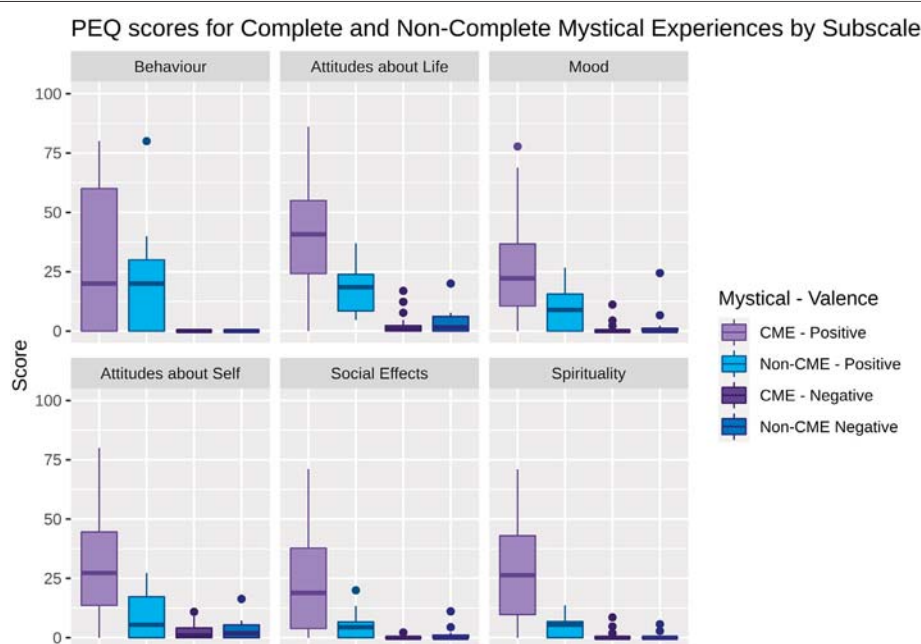


FIGURE 2 | Boxplots showing Persisting Effect Questionnaire (PEQ) scores relating to either Complete Mystical Experiences (CME) (Purple) or non-CME (Blue). Each plot represents the positive (lighter colours, left) and negative (darker colours, right) aspects of each PEQ subscale. The middle line in each box represents the median. Lower and upper hinges represent first and third quartiles. Datapoints more than 1.5 interquartile range beyond the hinges are plotted as outliers.

TABLE 2 | Results from the Latent Variable Model analyses for Mystical Experience Questionnaire (MEQ) total score and subsequent subscale analyses.

Variable	β	95% CI	p-value	p-value (corrected)
MEQ total	14.8	8.66:20.96	3.0×10^{-5}	3.0×10^{-5}
Positive Mood	14.5	7.90:21.11	1.0×10^{-4}	4.1×10^{-4}
Mysticality	10.8	6.14:15.51	5.1×10^{-5}	2.0×10^{-4}
Transcendence of Time and Space	9.4	-1.72:20.56	0.094	0.377
Ineffability	11.2	-2.75:25.14	0.111	0.446

β and 95% CI indicate effect size and 95% confidence interval in units of the latent variable PPE_{LV} which represents persisting positive effects attributable to the drug experience as a % of maximum possible score.

Language Differences in Mystical and Non-Mystical Experiences

Natural Language Processing

Of the 35 reports analysed, 21 met the criteria for a CME i.e., scoring at least 60% on all subscales of the MEQ. The words with the highest tf-idf score from CME Qualitative Experience Reports indicating the greatest distinction from the overall corpus, were “Universe”, “dad”, “MR” (Magnetic Resonance), “beautiful”, “simultaneous”, “infinite”, “purple”, “in relation to”, “ray”, “happy”, and “brother” (See **Figure 4**). The highest tf-idf scores from non-CME reports were “gloomy”, “cycle”, “evil”, “cold” and “need”. To expand on these findings, these words were identified in text and a selection of quotes are presented below. Notably, as there are only two documents within the corpus (CME and non-CME), any word which appears in both documents has a tf-idf score of zero. Thus, tf-idf scores distinguish words that only appear in one document set (CME or non-CME).

Qualitative Reports of the Complete Mystical Experience

By manually searching through the document body, we confirmed that high tf-idf scores were not driven by single individuals utilising the identified word multiple times. The word with the highest tf-idf score from the CME reports was “Universe”. Viewed in context, these references to the Universe appear to relate to feelings of unity and connectedness, analogous to MEQ item 14 “Freedom from the limitations of your personal self and feeling a unity or bond with what was felt to be greater than your personal self”, as well as a wonderment around the complexity of conscious experience.

The trip was mostly concerned with the love pertaining to the different relations in my life, but also the love that exists between human beings in general, to the planet and to the universe.

Report 3, female, CME, MEQ total 3.9

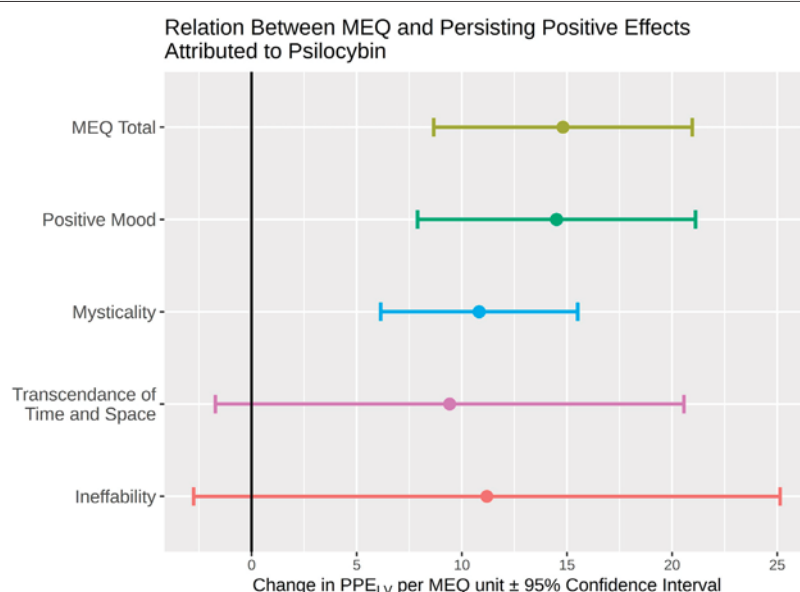


FIGURE 3 | Results of the latent variable model describing the estimate of effect of the MEQ total and subscale scores measured on the day of psilocybin on PPE_{LV} measured 3 months after psilocybin. The y-axis represents each individual subscale while the x-axis provides an estimate of the difference in PPE_{LV} associated with a one-unit increase in the indicated MEQ subscale.

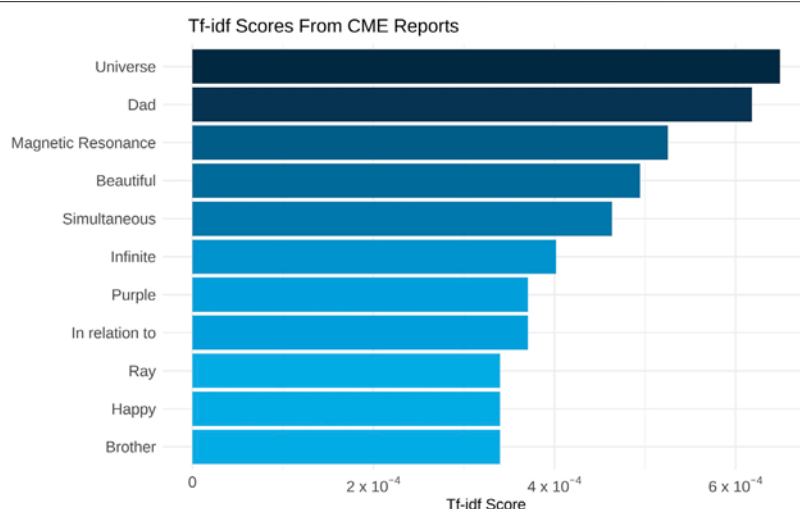


FIGURE 4 | Bar chart displaying the term-frequency inverse document frequency (tf-idf) values for the words that only appear in "Complete Mystical Experience" (CME) reports. Analyses were performed on Danish words and are only translated into English for display in this figure.

The light of love brings clarity to everything. I get a deep feeling of purity and feel that everything is beautiful, and that love is what makes up the world and the universe and connects everything like a network of roots.

Report 22, female, CME, MEQ total 3.9

Several times during the trip, I found myself laughing in sheer admiration of the impressive and wondrous universe of human consciousness.

Report 10, male, CME, MEQ total 4.7

When I close my eyes, I am in a fantastic world. Suspended in the whole universe. Stretched across the cosmos. When I open my eyes, I am being prepared for the MR-scanner. [...] I can hear the sounds of the scanner which influence my universe, white and silver lines unfold, make sudden angles and travel onwards abruptly.

Report 31, male, CME, MEQ total 4.2

One report juxtaposes the profound noetic quality of the experience with the tasks that participants were asked to perform in the scanner environment. This aligns with item 9 of the MEQ, i.e., “Certainty of encounter with ultimate reality (in the sense of being able to “know” and “see” what is really real at some point during your experience).”

I have the answer to the riddle of the universe, but I’m forced to look into a TV-screen.

Report 31, male, CME, MEQ total 4.2

The word that next-best distinguished the CME was “dad”. The reports describe feelings of gratitude, love and respect for the participants’ fathers. There are no items of the MEQ that reflect this theme directly. Notably, references to the participants mothers appeared in both CME and non-CME reports and thus had a tf-idf score of zero.

I had the feeling that I was experiencing the world through myself as a little girl holding her dad’s hand. My dad and I were observing what was happening around us. I think we saw something that resembled beautiful nature and charming castles.

Report 6, female, CME, MEQ total 3.9, see Figure 5

My mum and dad are opposites, red and white, cold and warm, but they are like a perfect yin-yang melting together, like my drawing shows, and their dynamic dance of east and west creates a space in the middle where it is purple—I am purple—I am both of them.

Report 14, female, CME, MEQ total 4.5

In two cases, the participants describe a desire to share this experience with their fathers specifically.

The tears run down my cheeks as I feel an enormous sense of closeness and connectedness. I feel an enormous sense of love towards my dad, his way of being and his patience. I want my dad to experience the feeling of ultimate love as I do, and for him to have the same experience. I wish to share my love with him.

Report 12, male, CME, MEQ total 4.9

The word with the third highest tf-idf score was “MR” referring to the MRI scanner. In several cases, participants found the intense noises of the scanner influenced their experience, in some cases inducing synaesthesia-like experiences. More broadly, this represents the profound impact of the environment on the experience.

The sounds from the MR scanner each cast a specific hue, with high-frequency tones giving a yellowish tinge and low-frequency tones having a purple tinge.

Report 22, female, CME, MEQ total 3.9

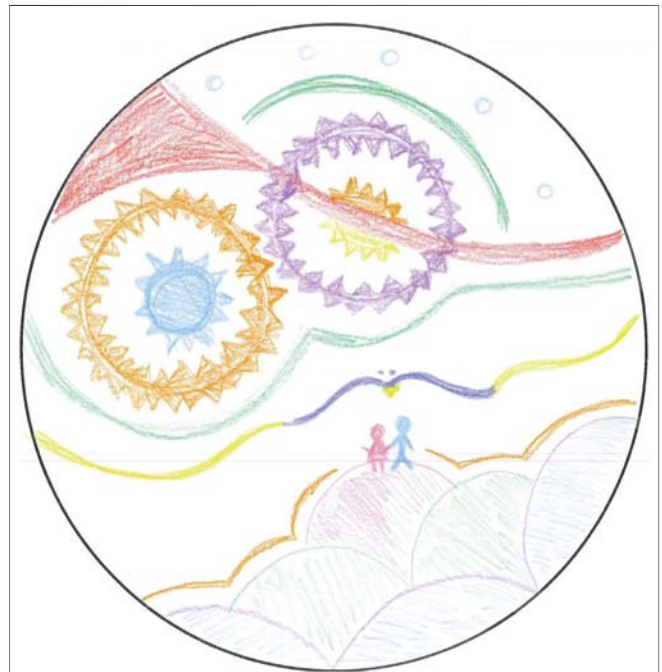


FIGURE 5 | I had the feeling that I was experiencing the world through myself as a little girl holding her dad’s hand. My dad and I were observing what was happening around us. I think we saw something that resembled beautiful nature and charming castles. Report 6, female, CME, MEQ total 3.9

The MR environment was the setting for 21 out of the 35 experiences collected (sub-project 3). Some felt that it played a positive role in the experience, as described in item 6 of the MEQ “Experience of oneness or unity with objects and/or persons perceived in your surroundings.”

I felt a sense of no longer being connected to my own body. The MRI scanner and I stepped into a different reality together. With colours, and shapes, and figures.

Report 32, female, CME, MEQ total 4.7, see Figure 6

The word with the fourth highest score was “beautiful”. This particular excerpt below combines the themes of universality, family and beauty that appear repeatedly in the CME reports. This report also aligns with item 8 in the MEQ “Feelings of tenderness and gentleness”.

The feeling of joy and love was the energy in the universe, completely intense and multiplied by 100. It was like taking those two emotions and concentrating them, to have them in their purest form without any worries or other troubles that can come with everyday reality. Everything else ceased to matter while those two emotions were so pure—they made everything incredibly beautiful. When I was soaring through the soundwaves with this energy, I could see all the people

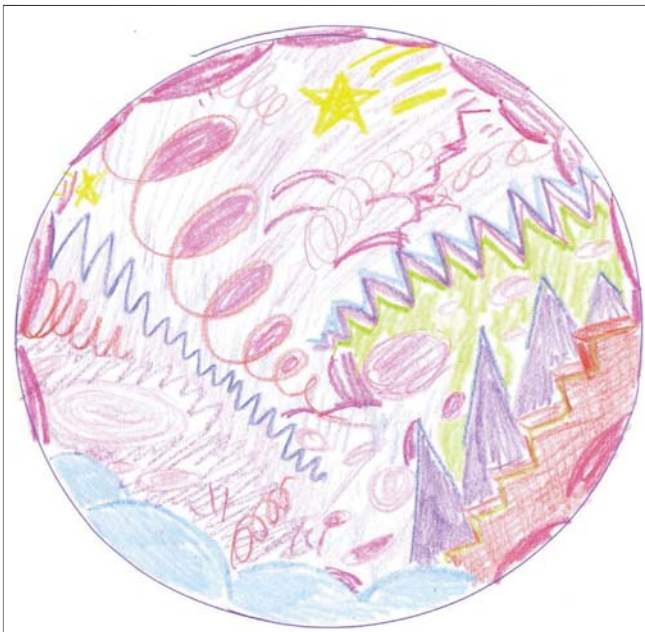


FIGURE 6 | I felt a sense of no longer being connected to my own body. The MRI scanner and I stepped into a different reality together. With colours, and shapes, and figures. Report 32, female, CME, MEQ total 4.7.

close to me in my life appear. My partner, my sister and her boyfriend and their new-born son, my mother, my amazing friends. I felt immensely privileged to be part of this universe / community, to be able to feel those feelings in such a pure form, to have such deep emotions in my body—and I was overwhelmed with gratitude for this world. That everything simply is. And with that I was overtaken by a desire to protect it all, to show the world how beautiful it is and to take care of it.

Report 3, female, CME, MEQ total 3.9, see **Figure 7**

Several reports refer to the beauty of the closed eye visual effects and the participants interactions with them. Perceptual effects are not measured by the MEQ.

Beautiful, beautiful geometrical shapes—and I spin around, do backflips—for a moment I just enjoy doing summersaults. My body diffuses into rays of sand/light and disappear, but as soon as they're completely gone and I think to myself "oh, all gone, oh well", they re-manifest themselves into a new meaningful picture.

Report 14, female, CME, MEQ total 4.5

My inner vision became the universe, filled with colourful waterfalls, glistening like stars, not bound by gravity. They floated in the air and folded around each other. Totally quiet. The streams were infinite and beautiful.

Report 15, female, CME, MEQ total 3.5, see **Figure 8**

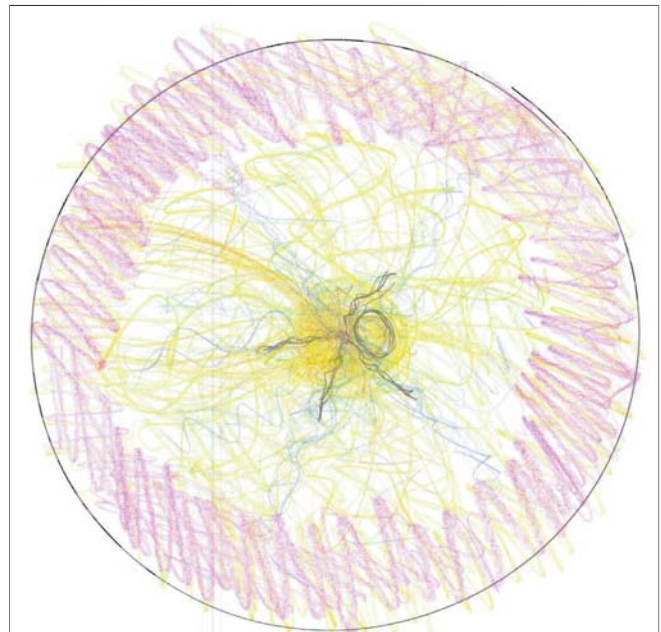


FIGURE 7 | The feeling of joy and love was the energy in the universe, completely intense and multiplied by 100. It was like taking those two emotions and concentrating them, to have them in their purest form without any worries or other troubles that can come with everyday reality. Everything else ceased to matter while those two emotions were so pure—they made everything incredibly beautiful. When I was soaring through the soundwaves with this energy, I could see all the people close to me in my life appear. My partner, my sister and her boyfriend and their new-born son, my mother, my amazing friends. I felt immensely privileged to be part of this universe/community, to be able to feel those feelings in such a pure form, to have such deep emotions in my body—and I was overwhelmed with gratitude for this world. That everything simply is. And with that I was overtaken by a desire to protect it all, to show the world how beautiful it is and to take care of it. Report 3, female, CME, MEQ total 3.9.

Some of the reports of beauty refer to participants experiences of reflecting on the nature of their consciousness and emotions.

It gave me insights into consciousness as an abstract type of cake: Normally, unaffected, you see it as a beautiful object with all of its whipped cream and frosting, but throughout the experience it was as if you entered the different layers; all of them had their own contents to offer; and one only had to choose.

Report 13, male, CME, MEQ total 3.6

I think it is absurd that we try to examine this phenomenon. That we are scanning my brain to figure out what's happening. I know that we can't understand it, that we can't put an equation on it and figure it out. I feel it is human arrogance, trying to tame all the beauty. I think, "Scan me then! We won't get any closer to the truth!"

Report 31, male, CME, MEQ total 4.2



FIGURE 8 | My inner vision became the universe, filled with colourful waterfalls, glistening like stars, not bound by gravity. They floated in the air and folded around each other. Totally quiet. The streams were infinite and beautiful. Report 15, female, CME, MEQ total 3.5.

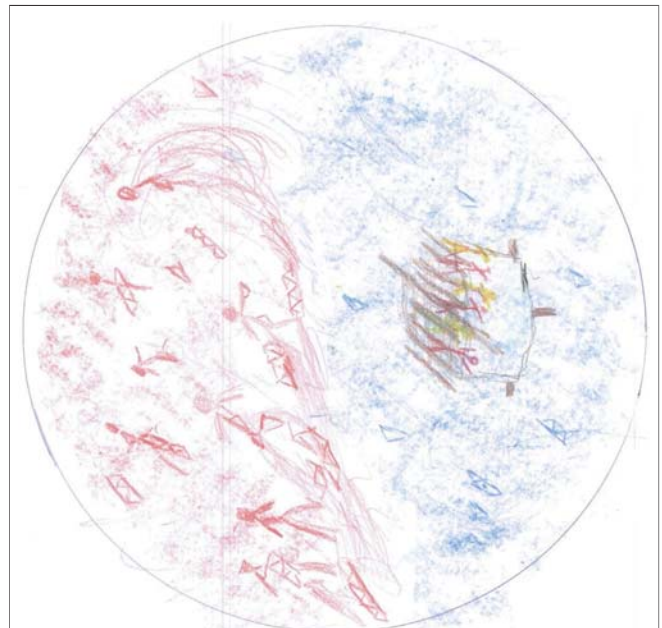


FIGURE 9 | With high spirits and a child-like excitement, I started to think about how the Norwegian adventurer Thor Heyerdahl crossed the Pacific Ocean on a raft to prove that life was big and beautiful. I see long realistic passages that made me laugh and feel a great inner joy. Report 19, male, CME, MEQ total 3.8.

Finally, many participants who had CMEs describe the beauty of the world and Universe around them, both natural and interpersonal. This is reflected in MEQ item 27 “sense of awe or awesomeness”

With high spirits and a child-like excitement, I started to think about how the Norwegian adventurer Thor Heyerdahl crossed the Pacific Ocean on a raft to prove that life was big and beautiful. I see long realistic passages that made me laugh and feel a great inner joy.

Report 19, male, CME, MEQ total 3.8, see **Figure 9**

The fifth highest tf-idf word was “simultaneous”. These quotes largely refer to a duality of experience (e.g., perceived disconnection of body and mind) wherein participants report feeling several, sometimes conflicting, emotions at the same time or reflect on their experience as it is ongoing. No specific items in the MEQ match these themes.

In my thoughts, mentally, physically, and bodily. I desire the togetherness of being a pair, but simultaneously I feel a togetherness with the whole world and all people.

Report 12, male, CME, MEQ total 4.9

The next sequence was a mixture of thinking about different relationships and at the same time being present on a different level of consciousness, which transcended my body and my mind.

Report 16, male, CME, MEQ total 4.6

I open my eyes and cry with happiness. I am completely one with the past, the future and the present—stretched, but at the same time not in my body.

Report 31, male, CME, MEQ total 4.2

Qualitative Reports of the Non-Complete Mystical Experience

Upon inspection, many of the words that had high tf-idf values from non-CME reports were driven primarily by one or two reports that used the words repeatedly. Thus, we did not feel that they provided a sound reflection of the themes within the non-CME. The only exception was the word “gloomy” which was used six times in non-CME reports, never in CME reports, and was reported by several individuals. In context this referred largely to interpretation of music.

The physical insecurities I have about myself and the gloomy music made me feel uneasy

Report 7, female, non-CME, MEQ total 2.8

DISCUSSION

Summary

This study investigated how persistent positive effects of psilocybin attributed to the psychedelic experience are

associated with the self-reported “mystical” nature of the experience in healthy volunteers. Analyses showed that the intensity and character of mystical-type experiences were associated with these, a relation which could be considered predictive as MEQ was collected approximately 3 months before PEQ. We provide qualitative lexical and pictorial descriptions of the psilocybin-induced Complete Mystical Experience (CME) describing themes such as connection to the Universe, familial love, beauty, and highlighting the importance of setting. Beyond replicating the relation between MEQ and PEQ in healthy volunteers, this paper shows that the character of mystical-type experience may be important for lasting positive effects in healthy volunteers and provides a qualitative description of the psilocybin experience in healthy volunteers that can be used to inform practice and future research around the administration of psilocybin in this population.

Relation Between MEQ and PEQ

Previous research suggests that the mystical-type experience is qualitatively linked to patient outcomes (Belser et al., 2017; Swift et al., 2017; Nielson et al., 2018; Noorani et al., 2018) as well as being quantitatively linked to positive persisting effects in healthy volunteers (Griffiths et al., 2006; Griffiths et al., 2008; Griffiths et al., 2011; Griffiths et al., 2018; Schmid and Liechti, 2018) and patients (Garcia-Romeu et al., 2015; Griffiths et al., 2016; Ross et al., 2016; Davis et al., 2020). In this study we provide quantitative estimates of these effects in a population of carefully screened healthy Danish individuals. We also show that the degree to which these experiences were described as positively emotionally valenced, i.e., MEQ item 17 “Experience of ecstasy” or as feelings of connectedness, i.e., MEQ item 28 “Experience of unity with ultimate reality” were robustly associated with lasting positive effects. However, the degree to which the experiences were described as beyond typical comprehension of space and time, i.e., MEQ item 7 “Loss of your usual sense of space” or difficult to describe, i.e., MEQ item 10 “Feeling that you could not do justice to your experience by describing it in words” were not significantly associated with persisting positive effects. Importantly, the effect sizes for each subscale were similar, but the variance of the latter two subscales was too broad to conclude a significant association between these subscale scores and positive persisting effects. Although other papers have shown a relation between MEQ total score and persisting positive effects of psilocybin (Griffiths et al., 2011; Schmid and Liechti, 2018), this is the first paper to show a subscale-specific effect. Our results indicate that the subjective nature of the psychedelic experience is indeed linked to lasting positive outcomes, though it is argued that such links may be mere epiphenomena (Hibicke et al., 2020; Olson, 2021). Due to the lack of adequate controls and mechanistic antagonists, our study design is not suited to test whether the persisting positive effects of psilocybin are caused by the subjective or non-subjective effects of psilocybin. We did not observe a relation between peak plasma psilocin levels and MEQ score or persisting positive effects in the 20-participant subgroup for whom such data was available.

Given the above findings we may consider how to optimise the conditions that permit mystical-type experiences to unfold safely and allow patients to surrender to the experience (Aday et al., 2021), since this has been consistently associated with persisting positive outcomes. These may be modulated by parameters such as dose (Holze et al., 2021), choice of psychedelic compound, as preliminary literature suggests differential phenomenology between compounds (Richards, 1975; Shulgin and Shulgin, 1991; Shulgin and Shulgin, 1997; Metzner, 2015; Papaseit et al., 2018), or “set” and “setting” (Hartogsohn, 2017; Hartogsohn, 2021; Kettner et al., 2021; Perkins et al., 2021; Strickland et al., 2021). Notably, despite previous research showing that the scanning environment was strongly associated with negative reactions (Studerus et al., 2012), our mediation analysis showed no overall mediation effect of sub-project on persisting effects. A weak direct negative effect of sub-project 2 (comfortable environment) and sub-project 3 (MR scanner) was observed on lasting effects, compared to sub-project 1 (PET scanner). However, these associations do not survive multiple comparisons correction. Curiously, the term “MR” only appeared in CME reports and not in non-CME reports.

Qualitative Findings

In this paper, we provide the first extensive qualitative descriptions of the subjective experience of healthy volunteers given medium-high doses of oral psilocybin in a modern research environment. The tf-idf analyses revealed themes in open-ended reports that aligned with items of the MEQ such as 1) connection with the Universe: “Experience of the fusion of your personal self into a larger whole.” (MEQ item 26), 2) A sense of infinity: “Feeling that you experienced eternity of infinity” (MEQ item 5) and 3) Wonderment/beauty: “Sense of reverence” (MEQ item 21) and “Sense of awe or awesomeness” (MEQ item 27) (Barrett et al., 2015). Despite playing prominent roles in the CME open-ended reports, certain themes emerged that are not described in the MEQ such as familial love, gratitude, and the simultaneous presence of contradictory feelings. The themes of family (Breeksema et al., 2020) and gratitude are also described in other qualitative reports (Watts et al., 2017; Noorani et al., 2018), and while not “mystical” in nature these may reliably co-emerge with the CME. None of the themes identified in the CME reports have connotations of the “challenging” or “dysphoric” experiences that have been reported in the qualitative literature of patient experiences (Belser et al., 2017; Swift et al., 2017; Nielson et al., 2018). Although this may be in part driven by the Positive Mood criteria of the CME, it still highlights the distinction between experiences in healthy volunteers and patients that deserves further investigation. We were not able to distinguish themes that surround non-mystical experiences, likely due to greater descriptive variability among these states relative to CME.

Ineffability

One notable finding from the descriptive analyses was that even those who had non-CME had an average MEQ subscale Ineffability score of 3.9 out of 5, and every participant

surpassed the threshold of 3 for CME relating to Ineffability. Some experts consider ineffability to be an essential component of an authentic CME (Papanicolaou, 2021), yet the idea that psychedelic phenomena are particularly ineffable is at odds with the idea that all phenomena are inherently ineffable, thus there is nothing special about psychedelia phenomena (Nagel, 1974). If we consider other phenomena to be “effable”, then describing psychedelic phenomena as ineffable can be considered scientifically pessimistic, and contribute to the culture of “psychedelic exceptionalism” (Johnson, 2021; Sanders and Zijlmans, 2021). What is it about a psychedelic experience, i.e., “Being in a realm with no space boundaries” (MEQ item 19) that is judged to be more ineffable than the inability to describe the colour blue, without resorting to comparison? It has been argued that “effability” is the product of shared experience and the subsequent production of language (Millikan, 2005), which is why “blueness” is easy to convey, at least to those who have experienced it (Jackson, 1982; Jackson, 1986). Therefore, the ineffability of these CME may reflect the novel nature of the experience to individuals without indicating any epistemic truth about the experience. If many people underwent high dose psychedelic experiences, then we might expect a new language to emerge that facilitates the description of such experiences between individuals. An example of this is the term “ego-dissolution” which is now widely used across psychedelic science (Lebedev et al., 2015; Nour et al., 2016; Preller and Vollenweider, 2018; Mason et al., 2020).

Scientific Inquiry Into the “Mystical-Type Experience”

The focus of this paper is the investigation of the mystical-type experience, an area of inquiry with which some researchers have taken issue (Sanders and Zijlmans, 2021). Critics highlight the pervasive culture of mysticism in psychedelic science (including the MEQ itself) which may bias participants towards interpreting their experiences through a supernatural, unscientific, or spiritual lens where they may not have done so otherwise. It has been argued that the epistemic status of metaphysical conclusions drawn from psychedelic experiences are relevant to whether we should endorse psychedelics as a means to lasting positive psychological changes (Flanagan and Graham, 2017). Following psychedelic experiences, individuals may draw comfort from beliefs that are not veridical, which may be considered troublesome. This stance is known as the “Comforting Delusion Objection” and is discussed and objected to in detail by Letheby (Letheby, 2021). Nevertheless, psychedelic drugs reliably induce the sorts of experiences wherein individuals feel that statements such as “Certainty of encounter with ultimate reality” (MEQ item 9) and “Sense of being at a spiritual height” (MEQ item 15) accurately describe a component of their experience (Griffiths et al., 2006; MacLean et al., 2012; Barrett et al., 2015). As participants feel justified in describing their experiences with such language, the framework of “mystical-type experiences” is a useful one for describing a cluster of co-occurring experiences, independent of ontological judgement of their content, especially given the apparent predictive utility of such experiences.

Limitations

In the latent variable model analyses, we attempted to control the type-1 error at its nominal level using a method described by Ozenne, Fisher, and Budtz-Jørgensen (Ozenne et al., 2020). Additionally, we accounted for individuals who took part in two projects using robust standard error (section 6 of Ozenne, Fisher and Budtz-Jørgensen). Despite these corrections, it is still noteworthy that the type-1 error may be inflated by the sample size and we urge independent replication with larger samples, especially given these scales are widely used in psychedelic research.

This study had a low sample size of 28 participants and 35 observations, was not blinded, and did not account for expectancy effects which have been theorised to mediate some of the persisting positive effects of psychedelics (Muthukumaraswamy et al., 2021). Rigorous future work should aim to replicate these findings with such controls and evaluate the role of expectancy in the intensity and character of mystical-type experiences induced by psilocybin. By performing a mediation analysis, it may be possible to delineate the degree to which expectancy is either related to persisting positive effects and whether independent of or via MEQ. The PEQ specifically asks participants to evaluate changes that are *due to* the experience, thus further work could aim to investigate the subjectively experienced causal link between the content of the experience and persisting positive effects. Additionally, we do not collect data on whether participants recreationally consume psilocybin between administration within the study and 3-month follow up, which has the potential to bias evaluation of persisting effects.

The PEQ scores that we report are similar in value to those reported by a group based in Basel, Switzerland for a comparable dose of LSD (Schmid and Liechti, 2018). Curiously, these scores are equal to the PEQ scores reported for the placebo group from studies at Johns Hopkins in the United States, and far lower than the PEQ scores reported following similar doses of psilocybin (Griffiths et al., 2011). This suggests that there may be a relevant difference between studies, such as recruitment basis, age, preparation, setting, and integration practices, or cultural differences that should be taken into account when considering the generalisability of these findings. Notably, the PEQ has not been robustly compared to other measures of persisting psychological change, or undergone factor analyses. Our sample is drawn from three separate settings, namely PET scanning, a comfortable environment, and MRI scanning. This adds heterogeneity to our sample, though our mediation analysis did not show a significant effect of setting on PEQ either directly or via MEQ. Nevertheless, analyses comparing the mystical-type experience to persisting positive effects could be repeated with a more homogenous setting.

Due to the lack of generalisability of the terms within the corpus of non-CME reports, we did not feel that these were sufficient to provide a qualitative characterisation of non-CME. The only exception was “gloomy” that referred in several cases to the music, a sentiment that has been identified in previous qualitative psychedelic research (Watts et al., 2017).

Qualitative analyses are often limited by biased selection of quotes that fit the narrative of the paper (Galdas, 2017). We attempted to control for this by utilising a natural language processing procedure, tf-idf, to delineate themes without a priori criteria. However, quotes selected after this filtering step are not entirely unbiased, as not all quotes are reported. Additionally, although tf-idf analyses account for total corpus length, they are susceptible to bias from a single report containing a specific word repeatedly. We attempted to control for this bias by manually searching to ensure each word described was used in multiple reports. Tf-idf analyses are limited in cases where there are only two document bodies as a single incidence of the term in both bodies results in a tf-idf value of zero. Therefore, the high tf-idf scores reported above represent the most frequently used terms that only appear in the CME reports, though this may also be considered a strength of these findings. Further collection of these open-form reports on the night of the session will allow for more nuanced natural language processing of the data, as there were several analyses that we were unable to perform due to a small sample (e.g., thematic analyses, n-gram analyses, splitting into smaller subgroups). These may provide a deeper understanding of the phenomenology of the psychedelic experience.

Conclusion

In this paper we show a relation between the intensity of the psilocybin-induced mystical-type experience and lasting positive psychological effects and extend previous work by showing that the MEQ subscales Mysticality and Positive Mood were more closely associated with lasting positive effects than Transcendence of Time and Space or Ineffability. This suggests that the phenomenology of the psychedelic experience is relevant to lasting positive effects. Additionally, we provide the first extensive qualitative descriptions of orally administered psilocybin in healthy volunteers revealing themes including universal connectedness, experience of beauty, and familial love that may be used to inform future research utilising psilocybin in healthy volunteers.

DATA AVAILABILITY STATEMENT

Data may be made available on request to the CIMBI database. Requests to access the datasets should be directed to <https://www.cimbi.dk/>.

ETHICS STATEMENT

The studies involving human participants were reviewed and approved by the Ethics committee for the Capital Region of Copenhagen Danish Medicines Agency. The patients/

participants provided their written informed consent to participate in this study.

AUTHOR CONTRIBUTIONS

DM collected data, performed analyses and wrote the manuscript, MG assisted with writing the manuscript, MM and SA collected data and provided feedback on the manuscript, BO provided statistical consultation, PJ managed data and provided feedback on the manuscript, PF assisted with analyses and provided feedback on the manuscript, GK critically evaluated the manuscript and supervised data collection, DS conceptualised the study, collected data and supervised writing of the manuscript.

FUNDING

Data collected in the present paper was supported by Innovation Fund Denmark (grant number 4108-00004B), Independent Research Fund Denmark (grant number 6110-00518B and 9058-00017A), and Ester M. og Konrad Kristian Sigurdssons Dyreværnsfond (grant number 850-22-55166-17-LNG). MKM was supported through a stipend from Rigshospitalet's Research Council (grant number R130-A5324). BO was supported by the Lundbeck Foundation (grant number R231-2016-3236) and Marie-Curie-NEUROMODEL (Grant number 746850), DEM's salary was supported by an unrestricted grant from COMPASS Pathways Ltd.

ACKNOWLEDGMENTS

Psilocybin was kindly supplied by National Institute of Mental Health, Klecany Czech Republic and Forensic Laboratory of Biologically Active Compounds, Department of Chemistry of Natural Compounds, University of Chemistry and Technology Prague, Prague, Czech Republic. Thank you to Anna Søndergaard and Harald Arnaud Gangneron Schiønning for providing beautiful translations of quotes from Danish to English.

SUPPLEMENTARY MATERIAL

The Supplementary Material for this article can be found online at: <https://www.frontiersin.org/articles/10.3389/fphar.2022.841648/full#supplementary-material>

REFERENCES

- Aday, J. S., Davis, A. K., Mitzkovitz, C. M., Bloesch, E. K., and Davoli, C. C. (2021). Predicting Reactions to Psychedelic Drugs: A Systematic Review of States and Traits Related to Acute Drug Effects. *ACS Pharmacol. Transl. Sci.* 4 (2), 424–435. doi:10.1021/acspsci.1c00014

- Anderson, B. T., Danforth, A., Daroff, P. R., Stauffer, C., Ekman, E., Agin-Liebes, G., et al. (2020). Psilocybin-assisted Group Therapy for Demoralized Older Long-Term AIDS Survivor Men: An Open-Label

- Safety and Feasibility Pilot Study. *EClinicalMedicine* 27, 100538. doi:10.1016/j.eclinm.2020.100538
- Bailer, L. W. (2020). in *Encyclopedia of Psychology and Religion [Internet]*. Editor D. A. Leeming. 3rd ed. (Cham: Springer International Publishing), 1394–1406. Available from: <http://link.springer.com/10.1007/978-3-030-24348-7>.
- Barrett, F. S., Doss, M. K., Sepeda, N. D., Pekar, J. J., and Griffiths, R. R. (2020). Emotions and Brain Function Are Altered up to One Month after a Single High Dose of Psilocybin. *Sci. Rep.* 10 (1), 2214–14. doi:10.1038/s41598-020-59282-y
- Barrett, F. S., Johnson, M. W., and Griffiths, R. R. (2015). Validation of the Revised Mystical Experience Questionnaire in Experimental Sessions with Psilocybin. *J. Psychopharmacol.* 29 (11), 1182–1190. doi:10.1177/0269881115609019
- Bech, P., Rasmussen, N. A., Olsen, L. R., Noerholm, V., and Abildgaard, W. (2001). The Sensitivity and Specificity of the Major Depression Inventory, Using the Present State Examination as the index of Diagnostic Validity. *J. Affect Disord.* 66 (2–3), 159–164. doi:10.1016/s0165-0327(00)00309-8
- Belser, A. B., Agin-Liebes, G., Swift, T. C., Terrana, S., Devenot, N., Friedman, H. L., et al. (2017). Patient Experiences of Psilocybin-Assisted Psychotherapy: An Interpretative Phenomenological Analysis. *J. Humanistic Psychol.* 57 (4), 354–388. doi:10.1177/0022167817706884
- Bogenschutz, M. P., Forchimes, A. A., Pommy, J. A., Wilcox, C. E., Barbosa, P. C., and Strassman, R. J. (2015). Psilocybin-assisted Treatment for Alcohol Dependence: A Proof-Of-Concept Study. *J. Psychopharmacol.* 29 (3), 289–299. doi:10.1177/0269881114565144
- Breeksema, J. J., Niemeijer, A. R., Krediet, E., Vermetten, E., and Schoevers, R. A. (2020). Psychedelic Treatments for Psychiatric Disorders: A Systematic Review and Thematic Synthesis of Patient Experiences in Qualitative Studies. *CNS Drugs* 34, 925–946. doi:10.1007/s40263-020-00748-y
- Busyes, D. J., Reynolds, C. F., Monk, T. H., Berman, S. R., and Kupfer, D. J. (1989). The Pittsburgh Sleep Quality index: A New Instrument for Psychiatric Practice and Research. *Psychiatry Res.* 28 (2), 193–213. doi:10.1016/0165-1781(89)90047-4
- Carhart-Harris, R., Giribaldi, B., Watts, R., Baker-Jones, M., Murphy-Beiner, A., Murphy, R., et al. (2021). Trial of Psilocybin versus Escitalopram for Depression. *N. Engl. J. Med.* 384 (15), 1402–1411. doi:10.1056/NEJMoa2032994
- Carhart-Harris, R. L., Bolstridge, M., Day, C. M. J., Rucker, J., Watts, R., Erritzoe, D. E., et al. (2018). Psilocybin with Psychological Support for Treatment-Resistant Depression: Six-Month Follow-Up. *Psychopharmacology (Berl)* 235, 399–408. doi:10.1007/s00213-017-4771-x
- Cohen, S., Kamarck, T., and Mermelstein, R. (1983). A Global Measure of Perceived Stress. *J. Health Soc. Behav.* 24 (4), 385–396. doi:10.2307/2136404
- Davis, A. K., Barrett, F. S., May, D. G., Cosimano, M. P., Sepeda, N. D., Johnson, M. W., et al. (2020). Effects of Psilocybin-Assisted Therapy on Major Depressive Disorder: A Randomized Clinical Trial. *JAMA Psychiatry* 78 (5), 481–489. doi:10.1001/jamapsychiatry.2020.3285
- Dunn, O. J. (1961). Multiple Comparisons Among Means. *J. Am. Stat. Assoc.* 56 (293), 52–64. doi:10.1080/01621459.1961.10482090
- Erritzoe, D., Roseman, L., Nour, M. M., MacLean, K., Kaelen, M., Nutt, D. J., et al. (2018). Effects of Psilocybin Therapy on Personality Structure. *Acta Psychiatr. Scand.* 138 (5), 368–378. doi:10.1111/acps.12904
- Flanagan, O., and Graham, G. (2017). *Truth and Sanity: Positive Illusions, Spiritual Delusions, and Metaphysical Hallucinations*. Cambridge, MA: MIT Press.
- Galdas, P. (2017). Revisiting Bias in Qualitative Research. *Int. J. Qual. Methods* 16 (1), 160940691774899. doi:10.1177/1609406917748992
- Garcia-Romeu, A., Davis, A. K., Erowid, F., Erowid, E., Griffiths, R. R., and Johnson, M. W. (2019). Cessation and Reduction in Alcohol Consumption and Misuse after Psychedelic Use. *J. Psychopharmacol.* 33 (9), 1088–1101. doi:10.1177/0269881119845793
- Garcia-Romeu, A., Griffiths, R., and Johnson, M. (2015). Psilocybin-Occasioned Mystical Experiences in the Treatment of Tobacco Addiction. *Curr. Drug Abuse Rev.* 7 (3), 157–164. doi:10.2174/1874473708666150107121331
- Griffiths, R., Richards, W., Johnson, M., McCann, U., and Jesse, R. (2008). Mystical-type Experiences Occasioned by Psilocybin Mediate the Attribution of Personal Meaning and Spiritual Significance 14 Months Later. *J. Psychopharmacol.* 22 (6), 621–632. doi:10.1177/0269881108094300
- Griffiths, R. R., Johnson, M. W., Carducci, M. A., Umbricht, A., Richards, W. A., Richards, B. D., et al. (2016). Psilocybin Produces Substantial and Sustained Decreases in Depression and Anxiety in Patients with Life-Threatening Cancer: A Randomized Double-Blind Trial. *J. Psychopharmacol.* 30 (12), 1181–1197. doi:10.1177/0269881116675513
- Griffiths, R. R., Johnson, M. W., Richards, W. A., Richards, B. D., Jesse, R., MacLean, K. A., et al. (2018). Psilocybin-occasioned Mystical-type Experience in Combination with Meditation and Other Spiritual Practices Produces Enduring Positive Changes in Psychological Functioning and in Trait Measures of Prosocial Attitudes and Behaviors. *J. Psychopharmacol.* 32 (1), 49–69. doi:10.1177/0269881117731279
- Griffiths, R. R., Johnson, M. W., Richards, W. A., Richards, B. D., McCann, U., and Jesse, R. (2011). Psilocybin Occasioned Mystical-type Experiences: Immediate and Persisting Dose-Related Effects. *Psychopharmacology (Berl)* 218 (4), 649–665. doi:10.1007/s00213-011-2358-5
- Griffiths, R. R., Richards, W. A., McCann, U., and Jesse, R. (2006). Psilocybin Can Occasion Mystical-type Experiences Having Substantial and Sustained Personal Meaning and Spiritual Significance. *Psychopharmacology (Berl)* 187 (3), 268–292. doi:10.1007/s00213-006-0457-5
- Griffiths, R. R., Hurwitz, E. S., Davis, A. K., Johnson, M. W., and Jesse, R. (2019). Survey of Subjective "God Encounter Experiences": Comparisons Among Naturally Occurring Experiences and Those Occasioned by the Classic Psychedelics Psilocybin, LSD, Ayahuasca, or DMT. *PLoS ONE* 14 (4), e0214377. doi:10.1371/journal.pone.0214377
- Grob, C. S., Danforth, A. L., Chopra, G. S., Hagerty, M., McKay, C. R., Halberstadt, A. L., et al. (2011). Pilot Study of Psilocybin Treatment for Anxiety in Patients with Advanced-Stage Cancer. *Arch. Gen. Psychiatry* 68 (1), 71–78. doi:10.1001/archgenpsychiatry.2010.116
- Hartogsohn, I. (2017). Constructing Drug Effects: A History of Set and Setting. *Drug Sci. Pol. L.* 3, 205032451668332. doi:10.1177/2050324516683325
- Hartogsohn, I. (2021). Set and Setting in the Santo Daime. *Front. Pharmacol.* 12, 651037. doi:10.3389/fphar.2021.651037
- Hasler, F., Grimberg, U., Benz, M. A., Huber, T., and Vollenweider, F. X. (2004). Acute Psychological and Physiological Effects of Psilocybin in Healthy Humans: a Double-Blind, Placebo-Controlled Dose-Effect Study. *Psychopharmacology (Berl)* 172 (2), 145–156. doi:10.1007/s00213-003-1640-6
- Haynes, W. (2013). "Bonferroni Correction," in *Encyclopedia of Systems Biology* (New York, NY: Springer New York), 154. doi:10.1007/978-1-4419-9863-7_1213
- Hibicke, M., Landry, A. N., Kramer, H. M., Talman, Z. K., and Nichols, C. D. (2020). Psychedelics, but Not Ketamine, Produce Persistent Antidepressant-like Effects in a Rodent Experimental System for the Study of Depression. *ACS Chem. Neurosci.* 11 (6), 864–871. doi:10.1021/acscchemneuro.9b00493
- Hirschfeld, T., and Schmidt, T. T. (2021). Dose-response Relationships of Psilocybin-Induced Subjective Experiences in Humans. *J. Psychopharmacol.* 35 (4), 384–397. doi:10.1177/0269881121992676
- Holst, K. K., and Budtz-Jørgensen, E. (2013). Linear Latent Variable Models: the Lava-Package. *Comput. Stat.* 28 (4), 1385–1452. doi:10.1007/s00180-012-0344-y
- Holze, F., Vizeli, P., Ley, L., Müller, F., Dolder, P., Stocker, M., et al. (2021). Acute Dose-dependent Effects of Lysergic Acid Diethylamide in a Double-Blind Placebo-Controlled Study in Healthy Subjects. *Neuropsychopharmacology* 46, 537–544. doi:10.1038/s41386-020-00883-6
- Hyde, R. W. (1960). "Psychological and Social Determinants of Drug Action," in *The Dynamics of Psychiatric Drug Therapy*, 1st Edn. Editors G. J. Sarwer-Foner (Springfield, IL: C.C. Thomas), 297–315.
- Jackson, F. (1982). Epiphenomenal Qualia. *Philos. Q.* 32 (127), 127. doi:10.2307/2960077
- Jackson, F. (1986). What Mary Didn't Know. *J. Philos.* 83 (5), 291. doi:10.2307/2026143
- Johnson, M. W. (2021). Consciousness, Religion, and Gurus: Pitfalls of Psychedelic Medicine. *ACS Pharmacol. Transl. Sci.* 4 (2), 578–581. doi:10.1021/acpsptsci.0c00198
- Johnson, M. W., Garcia-Romeu, A., and Griffiths, R. R. (2017). Long-term Follow-Up of Psilocybin-Facilitated Smoking Cessation. *Am. J. Drug Alcohol. Abuse* 43 (1), 55–60. doi:10.3109/00952990.2016.1170135
- Kettner, H., Rosas, F. E., Timmermann, C., Kärtner, L., Carhart-Harris, R. L., and Roseman, L. (2021). Psychedelic Communitas: Intersubjective Experience during Psychedelic Group Sessions Predicts Enduring Changes in Psychological Wellbeing and Social Connectedness. *Front. Pharmacol.* 12, 623985. doi:10.3389/fphar.2021.623985

- Lebedev, A. V., Lövdén, M., Rosenthal, G., Feilding, A., Nutt, D. J., and Carhart-Harris, R. L. (2015). Finding the Self by Losing the Self: Neural Correlates of Ego-Dissolution under Psilocybin. *Hum. Brain Mapp.* 36 (8), 3137–3153. doi:10.1002/hbm.22833
- Letheby, C. (2021). *Philosophy of Psychedelics [Internet]*. 1st ed. Oxford: Oxford University Press, 27–33. Available from: <https://global.oup.com/academic/product/philosophy-of-psychedelics-9780198843122?cc=dk&lang=en&#>
- Lyvers, M., and Meester, M. (2012). Illicit Use of LSD or Psilocybin, but Not MDMA or Nonpsychedelic Drugs, Is Associated with Mystical Experiences in a Dose-dependent Manner. *J. Psychoactive Drugs* 44 (5), 410–417. doi:10.1080/02791072.2012.736842
- MacLean, K. A., Johnson, M. W., and Griffiths, R. R. (2011). Mystical Experiences Occasioned by the Hallucinogen Psilocybin lead to Increases in the Personality Domain of Openness. *J. Psychopharmacol.* 25 (11), 1453–1461. doi:10.1177/0269881111420188
- MacLean, K. A., Leoatsakos, J. M., Johnson, M. W., and Griffiths, R. R. (2012). Factor Analysis of the Mystical Experience Questionnaire: A Study of Experiences Occasioned by the Hallucinogen Psilocybin. *J. Sci. Study Relig* 51 (4), 721–737. doi:10.1111/j.1468-5906.2012.01685.x
- Madsen, M. K., Fisher, P. M., Burmester, D., Dyssegaard, A., Stenbæk, D. S., Kristiansen, S., et al. (2019). Psychedelic Effects of Psilocybin Correlate with Serotonin 2A Receptor Occupancy and Plasma Psilocin Levels. *Neuropsychopharmacology* 44 (7), 1328–1334. doi:10.1038/s41386-019-0324-9
- Madsen, M. K., Fisher, P. M., Stenbæk, D. S., Kristiansen, S., Burmester, D., Lehel, S., et al. (2020). A Single Psilocybin Dose Is Associated with Long-Term Increased Mindfulness, Preceded by a Proportional Change in Neocortical 5-HT_{2A} Receptor Binding. *Eur. Neuropsychopharmacol.* 33, 71–80. doi:10.1016/j.euroneuro.2020.02.001
- Madsen, M. K., Stenbæk, D. S., Arvidsson, A., Armand, S., Marstrand-Joergensen, M. R., Johansen, S. S., et al. (2021). Psilocybin-induced Changes in Brain Network Integrity and Segregation Correlate with Plasma Psilocin Level and Psychedelic Experience. *Eur. Neuropsychopharmacol.* 50, 121–132. doi:10.1016/j.euroneuro.2021.06.001
- Maslow, A. H. (1959). Cognition of Being in the Peak Experiences. *J. Genet. Psychol.* 94 (1), 43–66. doi:10.1080/00221325.1959.10532434
- Mason, N. L., Kuypers, K. P. C., Müller, F., Reckweg, J., Tse, D. H. Y., Toennes, S. W., et al. (2020). Me, Myself, Bye: Regional Alterations in Glutamate and the Experience of Ego Dissolution with Psilocybin. *Neuropsychopharmacology* 45, 2003–2011. doi:10.1038/s41386-020-0718-8
- Metzner, R. (2015). *Allies for Awakening, Guidelines for Productive and Safe Experiences with Entheogens*. 1st ed. Berkeley, CA: Regent Press.
- Millikan, R. G. (2005). *Language: A Biological Model [Internet]*. Oxford, United Kingdom: Oxford University Press. Available from: <https://oxford.universitypressscholarship.com/view/10.1093/0199284768.001.0001/acprof-9780199284764>
- Moreno, F. A., Wiegand, C. B., Taitano, E. K., and Delgado, P. L. (2006). Safety, Tolerability, and Efficacy of Psilocybin in 9 Patients with Obsessive-Compulsive Disorder. *J. Clin. Psychiatry* 67 (11), 1735–1740. doi:10.4088/jcp.v67n1110
- Muthukumaraswamy, S. D., Forsyth, A., and Lumley, T. (2021). Blinding and Expectancy Confounds in Psychedelic Randomized Controlled Trials. *Expert Rev. Clin. Pharmacol.* 14 (9), 1133–1152. doi:10.1080/17512433.2021.1933434
- Nagel, T. (1974). What Is it like to Be a Bat. *Philos. Rev.* 83 (4), 435. doi:10.2307/2183914
- Nielson, E. M., May, D. G., Forchimes, A. A., and Bogenschütz, M. P. (2018). The Psychedelic Debriefing in Alcohol Dependence Treatment: Illustrating Key Change Phenomena through Qualitative Content Analysis of Clinical Sessions. *Front. Pharmacol.* 9, 132. doi:10.3389/fphar.2018.00132
- Noorani, T., Garcia-Romeu, A., Swift, T. C., Griffiths, R. R., and Johnson, M. W. (2018). Psychedelic Therapy for Smoking Cessation: Qualitative Analysis of Participant Accounts. *J. Psychopharmacol.* 32 (7), 756–769. doi:10.1177/0269881118780612
- Nour, M. M., Evans, L., Nutt, D., and Carhart-Harris, R. L. (2016). Ego-dissolution and Psychedelics: Validation of the Ego-Dissolution Inventory (EDI). *Front. Hum. Neurosci.* 10 (June), 269. doi:10.3389/fnhum.2016.00269
- Olson, D. E. (2021). The Subjective Effects of Psychedelics May Not Be Necessary for Their Enduring Therapeutic Effects. *ACS Pharmacol. Transl Sci.* 4 (2), 563–567. doi:10.1021/acspstsci.0c00192
- Ozenne, B., Fisher, P. M., and Budtz-Jørgensen, E. (2020). Small Sample Corrections for Wald Tests in Latent Variable Models. *J. R. Stat. Soc. C* 69 (4), 841–861. doi:10.1111/rssc.12414
- Pahnke, W. N. (1969). The Psychedelic Mystical Experience in the Human Encounter with Death. *H. Theolo. Rev.* 62 (1), 1–21. doi:10.1017/s0017816000027577
- Papanicolaou, A. C. (2021). *A Scientific Assessment of the Validity of Mystical Experiences: Understanding Altered Psychological and Neurophysiological States*. New York, NY: Routledge.
- Papaseit, E., Farré, M., Pérez-Mañá, C., Torrens, M., Ventura, M., Pujadas, M., et al. (2018). Acute Pharmacological Effects of 2C-B in Humans: An Observational Study. *Front. Pharmacol.* 9, 206. doi:10.3389/fphar.2018.00206
- Passie, T., Seifert, J., Schneider, U., and Emrich, H. M. (2002). The Pharmacology of Psilocybin. *Addict. Biol.* 7 (4), 357–364. doi:10.1080/1355621021000005937
- Perkins, D., Schubert, V., Simonová, H., Tófoli, L. F., Bousso, J. C., Horák, M., et al. (2021). Influence of Context and Setting on the Mental Health and Wellbeing Outcomes of Ayahuasca Drinkers: Results of a Large International Survey. *Front. Pharmacol.* 12, 623979. doi:10.3389/fphar.2021.623979
- Preller, K. H., Burt, J. B., Ji, J. L., Schleifer, C. H., Adkinson, B. D., Stämpfli, P., et al. (2018). Changes in Global and Thalamic Brain Connectivity in LSD-Induced Altered States of Consciousness Are Attributable to the 5-HT_{2A} Receptor. *Elife* 7, 1–31. doi:10.7554/eLife.35082
- Preller, K. H., and Vollenweider, F. X. (2018). Phenomenology, Structure, and Dynamic of Psychedelic States. *Curr. Top. Behav. Neurosciences* 36, 221–256. doi:10.1007/7854_2016_459
- Ramos, J. (2003). “Using Tf-Idf to Determine Word Relevance in Document Queries,” in *Proceedings of the First Instructional Conference on Machine Learning* (Citeseer), 29–48.
- Richards, W. A. (1975). *Counseling, Peak Experiences and the Human Encounter with Death: An Empirical Study of the Efficacy of DPT-Assisted Counseling in Enhancing the Quality of Life of Persons with Terminal Cancer and Their Closest Family Members*. Ph. D. Thesis. Washington, DC: The Catholic University of America.
- Roseman, L., Nutt, D. J., and Carhart-Harris, R. L. (2018). Quality of Acute Psychedelic Experience Predicts Therapeutic Efficacy of Psilocybin for Treatment-Resistant Depression. *Front. Pharmacol.* 8, 974. doi:10.3389/fphar.2017.00974
- Ross, S., Bossis, A., Guss, J., Agin-Liebes, G., Malone, T., Cohen, B., et al. (2016). Rapid and Sustained Symptom Reduction Following Psilocybin Treatment for Anxiety and Depression in Patients with Life-Threatening Cancer: A Randomized Controlled Trial. *J. Psychopharmacol.* 30 (12), 1165–1180. doi:10.1177/0269881116675512
- Rucker, J., Young, A., Bird, C., Harrison, J., Marwood, L., Mistry, S., et al. (2021). The Effects of COMP360 (Psilocybin Formulation) on Cognitive Function: Results from a Randomized, Placebo-Controlled Trial in Healthy Participants. *J. Psychopharmacol.* 36 (1), 114–125. doi:10.1177/02698811211064720
- Sanati, A. (2012). Pseudohallucinations: A Critical Review. *Dialogues Phil. Mental NeuroSci.* 5 (2), 42–47.
- Sanders, J. W., and Zijlmans, J. (2021). Moving Past Mysticism in Psychedelic Science. *ACS Pharmacol. Transl Sci.* 4 (3), 1253–1255. doi:10.1021/acspstsci.1c00097
- Sanz, C., Pallavicini, C., Carrillo, F., Zamberlan, F., Sigman, M., Mota, N., et al. (2021). The Entropic Tongue: Disorganization of Natural Language under LSD. *Conscious. Cogn.* 87, 103070. doi:10.1016/j.concog.2020.103070
- Schmid, Y., and Liechti, M. E. (2018). Long-lasting Subjective Effects of LSD in normal Subjects. *Psychopharmacology (Berl)* 235 (2), 535–545. doi:10.1007/s00213-017-4733-3
- Sheehan, D. V., Lecrubier, Y., Sheehan, K. H., Amorim, P., Janavs, J., Weiller, E., et al. (1998). The Mini-International Neuropsychiatric Interview (M.I.N.I.): The Development and Validation of a Structured Diagnostic Psychiatric Interview for DSM-IV and ICD-10. *J. Clin. Psychiatry* 59 (Suppl. 20), 22–33.
- Shulgin, A., and Shulgin, A. (1991). *Phenethylamines I Have Known and Loved: A Chemical Love Story*. 1st ed. Berkeley, CA: Transform Press.
- Shulgin, A., and Shulgin, A. (1997). *Tryptamines I Have Known and Loved: The Continuation*. 1st ed. Berkeley, CA: Transform Press.
- Silge, J., and Robinson, D. (2016). Tidytext: Text Mining and Analysis Using Tidy Data Principles in R. *J. Open Source Softw.* 1 (3), 37. doi:10.21105/joss.00037
- Stace, W. T. (1960). *Mysticism and Philosophy*. Philadelphia: St. Martin's Press.

- Stenbæk, D. S., Madsen, M. K., Ozenne, B., Kristiansen, S., Burmester, D., Erritzoe, D., et al. (2020). Brain Serotonin 2A Receptor Binding Predicts Subjective Temporal and Mystical Effects of Psilocybin in Healthy Humans. *J. Psychopharmacol.* 35 (4), 459–468. doi:10.1177/0269881120959609
- Strickland, J. C., Garcia-Romeu, A., and Johnson, M. W. (2021). Set and Setting: A Randomized Study of Different Musical Genres in Supporting Psychedelic Therapy. *ACS Pharmacol. Transl Sci.* 4 (2), 472–478. doi:10.1021/acspsci.0c00187
- Studerus, E., Gamma, A., Komater, M., and Vollenweider, F. X. (2012). Prediction of Psilocybin Response in Healthy Volunteers. *PLoS One* 7 (2), e30800. doi:10.1371/journal.pone.0030800
- Swift, T. C., Belser, A. B., Agin-Liebes, G., Devenot, N., Terrana, S., Friedman, H. L., et al. (2017). Cancer at the Dinner Table: Experiences of Psilocybin-Assisted Psychotherapy for the Treatment of Cancer-Related Distress. *J. Humanistic Psychol.* 57 (5), 488–519. doi:10.1177/0022167817715966
- Turton, S., Nutt, D. J., and Carhart-Harris, R. L. (2014). A Qualitative Report on the Subjective Experience of Intravenous Psilocybin Administered in an fMRI Environment. *Curr. Drug Abuse Rev.* 7 (2), 117–127. doi:10.2174/1874473708666150107120930
- Vizeli, P., Straumann, I., Holze, F., Schmid, Y., Dolder, P. C., and Liechti, M. E. (2021). Genetic Influence of CYP2D6 on Pharmacokinetics and Acute Subjective Effects of LSD in a Pooled Analysis. *Sci. Rep.* 11 (1), 10851. doi:10.1038/s41598-021-90343-y
- Wackermann, J., Wittmann, M., Hasler, F., and Vollenweider, F. X. (2008). Effects of Varied Doses of Psilocybin on Time Interval Reproduction in Human Subjects. *Neurosci. Lett.* 435 (1), 51–55. doi:10.1016/j.neulet.2008.02.006
- Watts, R., Day, C., Krzanowski, J., Nutt, D., and Carhart-Harris, R. (2017). Patients' Accounts of Increased "Connectedness" and "Acceptance" after Psilocybin for Treatment-Resistant Depression. *J. Humanistic Psychol.* 57 (5), 520–564. doi:10.1177/0022167817709585
- Yaden, D. B., and Griffiths, R. R. (2021). The Subjective Effects of Psychedelics Are Necessary for Their Enduring Therapeutic Effects. *ACS Pharmacol. Transl Sci.* 4 (2), 568–572. doi:10.1021/acspsci.0c00194

Conflict of Interest: DEM's salary was supported by an unrestricted grant from COMPASS Pathways Ltd., which had no involvement in this manuscript or related data collection. MM has received an honorarium as a speaker for Lundbeck Pharma. GK has received honoraria as a consultant for Sanos and Sage Therapeutics.

Publisher's Note: All claims expressed in this article are solely those of the authors and do not necessarily represent those of their affiliated organizations, or those of the publisher, the editors and the reviewers. Any product that may be evaluated in this article, or claim that may be made by its manufacturer, is not guaranteed or endorsed by the publisher.

Copyright © 2022 McCulloch, Grzywacz, Madsen, Jensen, Ozenne, Armand, Knudsen, Fisher and Stenbæk. This is an open-access article distributed under the terms of the Creative Commons Attribution License (CC BY). The use, distribution or reproduction in other forums is permitted, provided the original author(s) and the copyright owner(s) are credited and that the original publication in this journal is cited, in accordance with accepted academic practice. No use, distribution or reproduction is permitted which does not comply with these terms.

Psilocybin-Induced Mystical-Type Experiences are Related to Persisting Positive Effects: A Quantitative and Qualitative Report **Supplementary Material**

1 Supplementary Data

1.1 Supplementary Tables

Report	Gender	Dose (mg)	Dose (mg/kg)	Mystical Experience Questionnaire Subscale (out of 5)				Persisting Effects Questionnaire Subscale (out of 100)					
				Mystical	Positive Mood	Transcendence of Time and Space	Ineffability	Attitudes About Life (Positive)	Attitudes About Self (Positive)	Mood Changes (Positive)	Altruistic/Positive Social Effects	Behaviour Changes (Positive)	Increased Spirituality
1	Male	15	0.20	2.9	2.5	1.8	3.7	23	5	11	9	20	5
2	Male	18	0.20	1.3	2.2	2.0	4.0	22	18	20	20	40	11
3	Female	12	0.20	3.8	3.3	4.5	4.0	23	5	11	0	0	4
4	Male	18	0.20	4.7	4.8	4.5	5.0	71	69	78	64	80	70
5	Male	21	0.19	4.1	3.7	4.7	5.0	14	0	9	0	0	0
6	Female	12	0.19	3.7	3.3	4.5	5.0	42	33	33	38	60	15
7	Female	18	0.27	2.8	3.8	1.8	3.0	37	27	11	4	80	7
8	Male	18	0.25	4.3	4.0	2.7	4.3	28	18	13	0	0	9
9	Female	24	0.29	0.9	2.2	4.5	4.3	5	2	0	2	0	0
10	Male	21	0.28	4.8	4.8	4.3	5.0	46	29	31	24	40	57
11	Male	30	0.31	3.0	2.8	3.7	3.7	54	53	69	58	80	7
12	Male	24	0.30	4.9	4.7	5.0	5.0	37	22	22	18	20	30
13	Male	21	0.27	3.1	3.2	4.7	5.0	54	44	22	11	60	24
14	Female	24	0.27	4.5	4.8	4.5	4.0	77	67	60	42	80	71
15	Female	15	0.19	3.3	3.7	4.0	3.0	0	0	0	0	0	0
16	Male	18	0.23	4.5	4.3	5.0	5.0	54	27	24	20	40	56
17	Female	15	0.24	2.0	2.8	2.3	4.0	34	22	27	4	40	14
18	Male	21	0.28	5.0	5.0	5.0	5.0	86	80	69	49	80	42
19	Male	21	0.28	3.7	4.5	3.5	3.3	40	27	18	7	0	37
20	Male	21	0.28	3.7	4.0	4.3	5.0	42	16	13	4	0	9
21	Female	18	0.29	2.0	2.7	4.2	4.7	25	11	9	13	20	5
22	Female	18	0.30	3.9	3.5	4.5	3.7	9	0	2	0	0	1
23	Male	21	0.27	0.7	1.0	3.8	4.0	14	0	7	0	0	0
24	Female	18	0.30	2.4	3.2	3.5	4.0	18	16	27	0	20	6
25	Male	21	0.27	3.5	3.7	3.0	4.0	58	55	47	71	60	29
26	Female	18	0.28	3.2	3.7	4.8	4.0	29	22	22	27	20	14
27	Female	18	0.28	4.6	5.0	5.0	5.0						
28	Male	21	0.27	3.2	3.2	5.0	5.0	25	15	0	2	0	24
29	Female	18	0.31	1.7	2.5	4.2	3.7	5	0	0	4	0	0
30	Female	15	0.26	1.4	3.5	2.7	3.0	8	0	0	0	0	5
31	Male	24	0.30	4.1	4.0	4.3	4.7	31	35	16	38	20	30
32	Female	15	0.26	4.6	4.8	4.8	5.0	66	47	60	38	60	46
33	Male	21	0.27	3.7	3.5	3.7	4.0	17	11	9	7	20	10
34	Male	24	0.27	1.7	2.8	3.3	4.7	9	0	0	0	0	0
35	Male	21	0.30	2.7	3.7	3.7	3.3	60	33	40	16	40	20

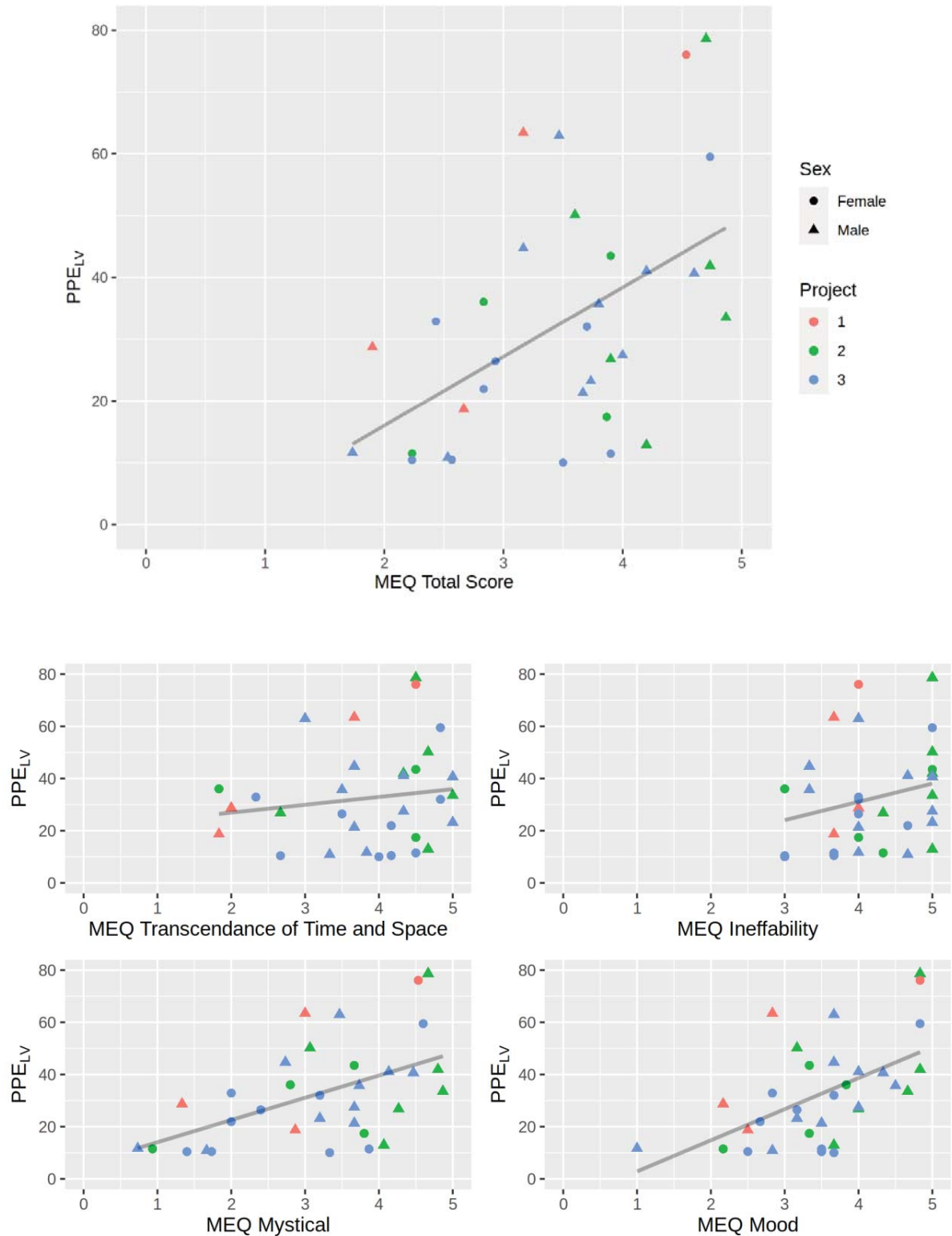
Supplementary Table 1 Individual MEQ and PEQ subscale scores

Subscale Mean (SD)	All	CME	Non-CME
MEQ total	3.6 (0.9)	4.2 (0.5)	2.7 (0.6)
Mysticality	3.3 (1.2)	4.0 (0.6)	2.1 (0.9)
Positive Mood	3.6 (0.9)	4.1 (0.7)	2.8 (0.8)
Transcendence of Time and Space	3.9 (1.0)	4.5 (0.5)	3.2 (0.9)
Ineffability	4.3 (0.7)	4.5 (0.7)	3.9 (0.5)

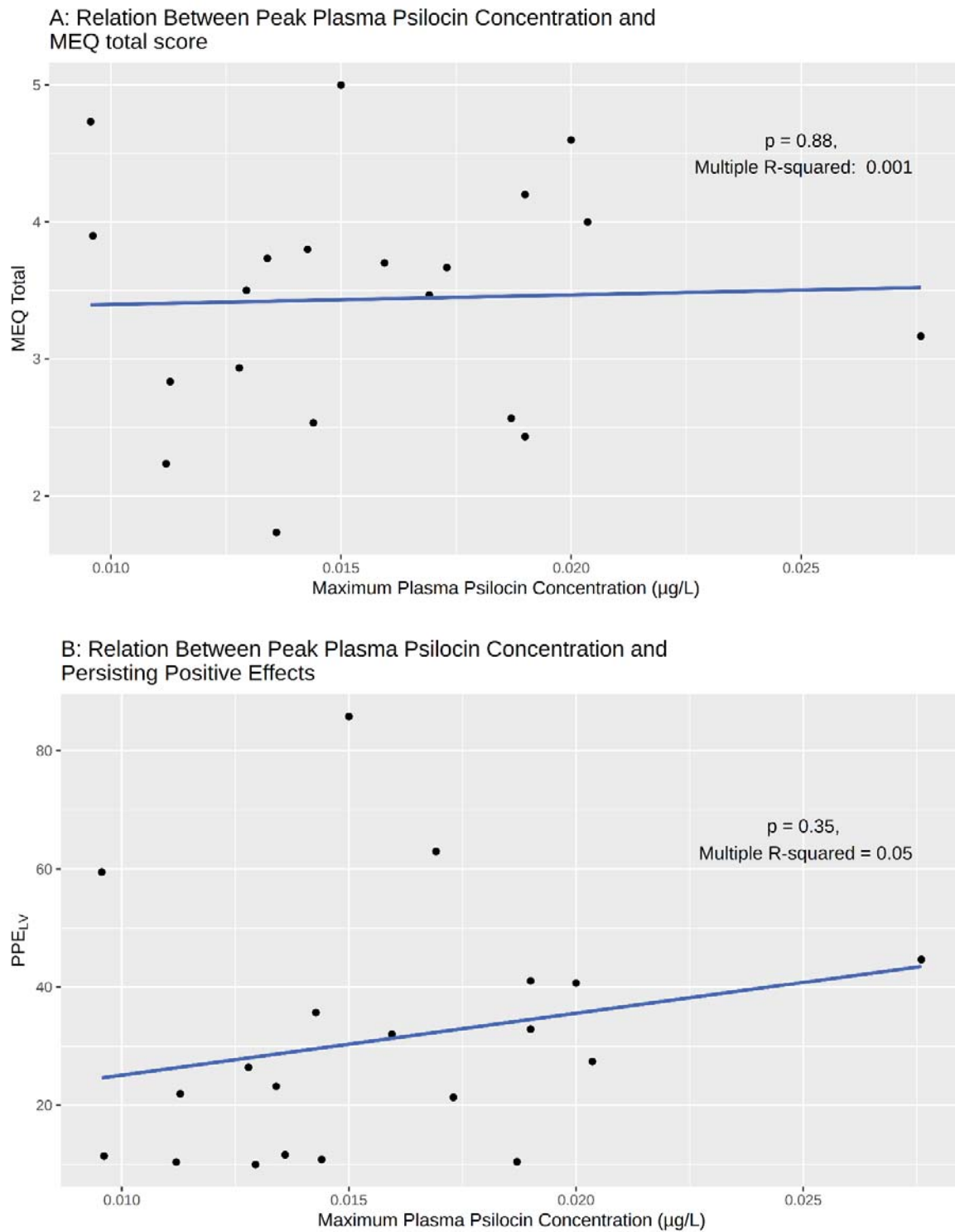
Supplementary Table 2 MEQ total and subscale scores as split by CME and non-CME

Supplementary Table 3 (LVM mediation analysis results) and **Supplementary Table 4** (Complete descriptions of LVMs) are provided as standalone excel files

1.2 Supplementary Figures



Supplementary Figure 1 Scatter plots showing MEQ total score or subscale scores and PPE_{LV} and a univariate linear model. Colour denotes subproject involvement and shape denotes the sex of the participant. No formal statistics were evaluated as these plots are only for visualisation purposes.



Supplementary Figure 2 Scatter plots showing (A) MEQ total score or (B) PPE_{LV} and Maximum plasma psilocin concentrations for the 20 participants from project 3 with complete data. Neither association is statistically significant.



DECLARATION OF CO-AUTHORSHIP

The declaration is for PhD students and must be completed for each conjointly authored article.

Please note that if a manuscript or published paper has eleven or less authors, all authors must sign a declaration of co-authorship. If it has twelve or more authors, only the PhD student, the corresponding author(s), the senior author, and the principal supervisor need to sign the declaration of co-authorship.

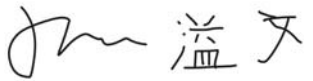
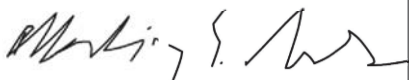
1. Declaration by	
Name of PhD student	Drummond McCulloch
E-mail	Drummond.mcculloch@nru.dk
Name of principal supervisor	Patrick Fisher
Title of the PhD thesis	Pharmacokinetic and pharmacodynamic evaluation of classical psychedelic substances in the human brain

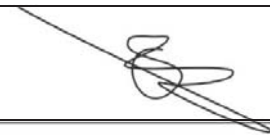
2. The declaration applies to the following article	
Title of article	Navigating the chaos of psychedelic fMRI brain-entropy via multi-metric evaluations of acute psilocybin effects
Article status	
Published <input type="checkbox"/>	Accepted for publication <input type="checkbox"/>
Date: March 2022	Date:
Manuscript submitted <input checked="" type="checkbox"/>	Manuscript not submitted <input type="checkbox"/>
Date: 19-12-2024	
If the article is published or accepted for publication, please state the name of journal, year, volume, page and DOI (if you have the information).	

3. The PhD student's contribution to the article (please use the scale A-F as benchmark)	
Benchmark scale of the PhD-student's contribution to the article	
A. Has essentially done all the work (> 90 %) B. Has done most of the work (60-90 %) C. Has contributed considerably (30-60 %) D. Has contributed (10-30 %) E. No or little contribution (<10 %) F. Not relevant	A, B, C, D, E, F
1. Formulation/identification of the scientific problem	C
2. Development of the key methods	C
3. Planning of the experiments and methodology design and development	E
4. Conducting the experimental work/clinical studies/data collection/obtaining access to data	D

3. The PhD student's contribution to the article (please use the scale A-F as benchmark) <u>Benchmark scale of the PhD-student's contribution to the article</u> A. Has essentially done all the work (> 90 %) B. Has done most of the work (60-90 %) C. Has contributed considerably (30-60 %) D. Has contributed (10-30 %) E. No or little contribution (<10 %) F. Not relevant		A, B, C, D, E, F
5. Conducting the analysis of data		
6. Interpretation of the results		
7. Writing of the first draft of the manuscript		
8. Finalisation of the manuscript and submission		
Provide a short description of the PhD student's specific contribution to the article. ⁱ Formulated the research question, processed the data, performed analyses, made figures, wrote the manuscript with co-first author.		

4. Material from another thesis / dissertation ⁱⁱ	
Does the article contain work which has also formed part of another thesis, e.g. master's thesis, PhD thesis or doctoral dissertation (the PhD student's or another person's)?	Yes: <input type="checkbox"/> No: <input checked="" type="checkbox"/>
If yes, please state name of the author and title of thesis / dissertation.	
If the article is part of another author's academic degree, please describe the PhD student's and the author's contributions to the article so that the individual contributions are clearly distinguishable from one another.	

5. Signatures of the authors incl. the PhD student				
	Date	Name	Title	Signature
1.		Drummond McCulloch	Mr.	
2.	June 17 2025	Martin Korsbak Madsen	Dr.	

5. Signatures of the authors incl. the PhD student				
3.		Dea Siggard Stenbæk	Prof.	<i>Dea Siggard Stenbæk</i>
4.		Anders Stevnhoved Olsen	Dr.	<i>Anders S. Olsen</i>
5.		Brice Ozenne	Prof.	
6.		Gitte Moos Knudsen	Prof.	<i>GMK</i>
7.		Patrick Fisher	Prof.	<i>Patrick Fisher</i>
8.		Sophia Armand	Prof.	<i>S. Armand</i>
9.				
10.				
11.				

6. Signature of the principal supervisor I solemnly declare that the information provided in this declaration is accurate to the best of my knowledge. Date: Principal supervisor: Patrick Fisher

7. Signature of the PhD student I solemnly declare that the information provided in this declaration is accurate to the best of my knowledge. Date: 17-06-2025 PhD student: Drummond McCulloch

Please learn more about responsible conduct of research on the [Faculty of Health and Medical Sciences' website](#).

ⁱ This can be supplemented with an additional letter if needed.

ⁱⁱ Please see Ministerial Order on the PhD Programme at the Universities and Certain Higher Artistic Educational Institutions (PhD Order) § 12 (4):

“Any articles included in the thesis may be written in cooperation with others, provided that each of the co-authors submits a written declaration stating the PhD student's or the author's contribution to the work.”

Navigating the chaos of psychedelic fMRI brain-entropy via multi-metric evaluations of acute psilocybin effects

Drummond E-Wen McCulloch^{1,2,†}, Anders Stevnhoved Olsen^{1,3,†}, Brice Ozenne^{1,4}, Dea Siggaard Stenbæk^{1,5}, Sophia Armand^{1,5}, Martin Korsbak Madsen^{1,6}, Gitte Moos Knudsen^{1,7}, Patrick MacDonald Fisher^{1,8}

¹Neurobiology Research Unit, Copenhagen University Hospital, Rigshospitalet, Copenhagen, Denmark

²Faculty of Health and Medical Sciences, University of Copenhagen, Denmark

³Department of Applied Mathematics and Computer Science, Technical University of Denmark, Kgs. Lyngby, Denmark

⁴Section of Biostatistics, Department of Public Health, University of Copenhagen, Copenhagen, Denmark

⁵Department of Psychology, University of Copenhagen, Denmark

⁶Department of Psychiatry Svendborg, Svendborg, Denmark

⁷Department of Clinical Medicine, University of Copenhagen, Copenhagen, Denmark

⁸Department of Drug Design and Pharmacology, University of Copenhagen, Copenhagen, Denmark

[†]These authors contributed equally to this work

Abstract

A prominent theory of psychedelics is that they increase brain entropy. Twelve studies have evaluated psychedelic effects on fMRI brain entropy quantifications, no findings have been replicated. Here we evaluated these metrics in an independent 28-participant healthy cohort with 121 pre- and post-psilocybin fMRI scans. We assessed relations between brain entropy and plasma psilocin, brain serotonin 2A receptor occupancy, and a subjective drug intensity rating using linear mixed-effects models. We observed significant positive associations for Shannon entropy of path-length, instantaneous correlation distributions, and divergent associations of sample entropy at varying time-scales. We did not observe significant effects for 8 of 13 entropy metrics. Brain entropy quantifications showed limited inter-measure correlations. Our observations support a nuanced acute psychedelic effect on brain entropy, underscoring the need for replication and that these metrics do not reflect a singular construct. Our findings highlight candidate brain entropy metrics that may mediate clinical effects of psychedelics.

Introduction

Psychedelic drugs induce profound altered states of consciousness including affective, sensory and cognitive effects mediated by activation of downstream pathways initiated by agonism at the brain serotonin 2A receptor¹⁻⁴. In combination with psychological support, clinical studies up to phase 2b indicate promising clinical efficacy of psychedelics in the treatment of affective and behavioural neuropsychiatric disorders that may be associated with their acute effects^{5-10,10-12}. Similarly, psychedelics induce acute and lasting effects on behaviour and personality in healthy participants¹³⁻¹⁵. In parallel to evaluating clinical treatment effects, human brain functional magnetic resonance imaging (fMRI) has begun to shed light on neural pathways affected by psychedelics¹⁶.

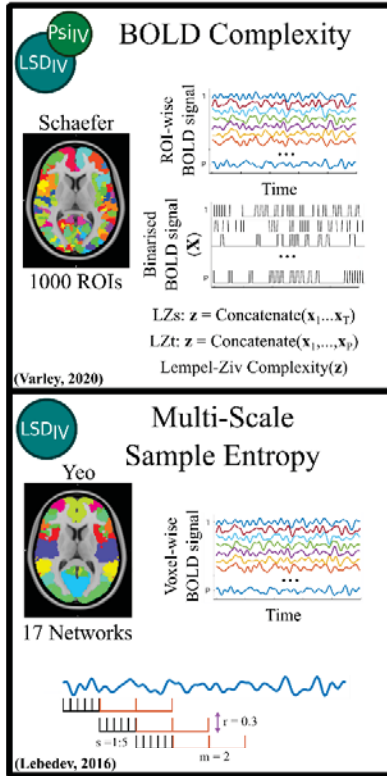
Several prominent theories of critically relevant psychedelic effects on brain function have been advanced¹⁷. A prominent theory is the “Entropic Brain Hypothesis” (EBH), which posits that the 'richness' of the phenomenology of the acute psychedelic state reflects brain-wide increases in entropy of functional brain signals^{18,19}. The concept of "entropy" serves as a quantification of the degree of information or complexity contained in a system; it is typically expressed in bits, without physical dimensions. Entropy has been conceptualised as a metric of information content and is largely defined in terms of a probability distribution; the metric is commonly referred to by the eponymous name “Shannon entropy” $H(X) = - \sum_{x \in X} p(x) \cdot \log_2 p(x)$ where $H(X)$ refers to the Shannon entropy of probability mass function X containing bins (x) with height (p)²⁰. Other entropy metrics have been defined, e.g., Lempel-Ziv complexity and sample entropy²¹⁻²⁴, and adapted to characterise information contained in various objects, e.g., complex networks or graph structures²⁵.

To date, 12 studies have evaluated either acute or lasting psychedelic effects on the information-entropy of brain-activity or connectivity using blood oxygen level dependent (BOLD) fMRI data (Figure 1), one of which evaluates two metrics, thus 13 entropy metrics have been previously evaluated in this field. Four papers analysed data from a study evaluating 2mg intravenous psilocybin administration in up to 15 healthy participants^{19,26-28}. Two papers reported effects from a study evaluating 75µg intravenous LSD administration in 15 healthy participants^{29,30}. Two papers evaluated data from both datasets^{31,32}. Three papers reported effects from a study evaluating oral ayahuasca administration, containing 96-160mg DMT and 25.2-42mg harmine (a monoamine oxidase inhibitor that facilitated the oral bioavailability of DMT) in 9 healthy participants³³⁻³⁵. Finally, one paper reported effects from a study evaluating lasting effects of 25mg/70kg bodyweight orally administered psilocybin in 11 healthy participants³⁶. Notably, and highlighted in a recent review¹⁶, each of these reports quantified a distinctly different metric of brain entropy. Here we group these metrics into three categories: 1) “static connectivity”, 2) “dynamic connectivity”, i.e., the time-varying relation between two or more time-series, 3) “dynamic activity”, i.e., the entropy of regional time-series (Figure 1). Nine of these metrics are based on the Shannon entropy of distributions, three are Lempel-Ziv complexity metrics of a time-series and one is the sample entropy of a time-series. Taken together, although there is a clear interest in evaluating psychedelic effects on brain entropy, prominent limitations include that none of these measures have been evaluated in an independent cohort, the set of effects have been evaluated in only a few datasets, some with atypical modes of drug administration, and the inter-correlation between these metrics has not been considered. Previous studies compared pre-drug or placebo and a single post-drug scan. For the most part, these previous studies report increased brain entropy with only a few exceptions, e.g., two studies report non-significant psilocybin

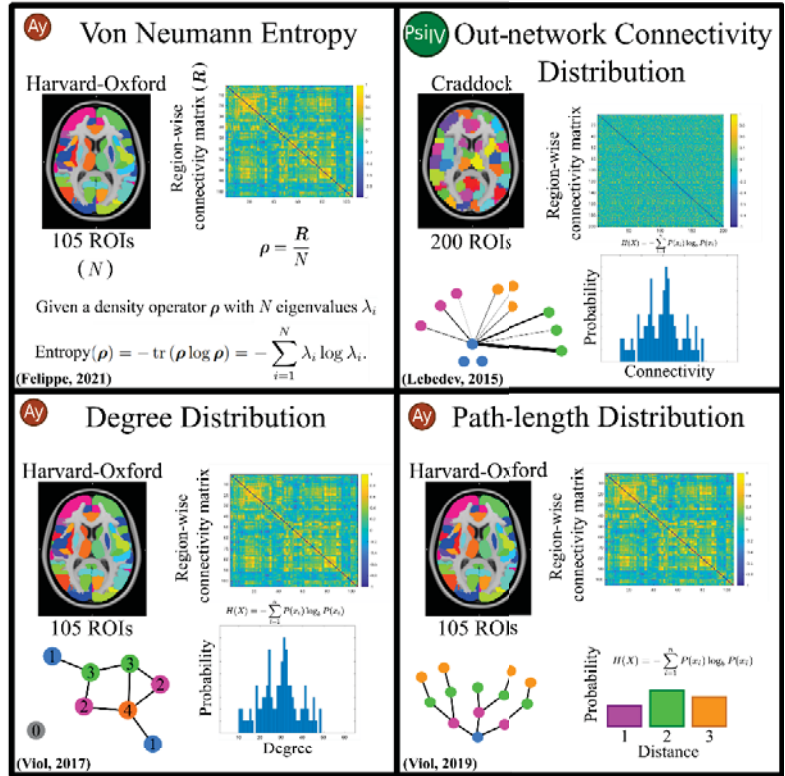
effects and one study reports no lasting changes (Figure 1, Table 1). See Supplementary Table S1 for more details about the previous studies. Previous fMRI studies have reported reduced brain entropy in other states of "reduced consciousness", including NREM sleep ³⁷, minimal-consciousness ³⁸, and anaesthesia ³⁹, whereas other studies have shown increased brain entropy following caffeine ⁴⁰ and Salvinorin A intake ⁴¹.

In the current study, we sought to evaluate the acute effects of 0.2-0.3mg/kg psilocybin administration on these 13 brain entropy metrics in an independent dataset of 28 healthy individuals. Based on the entropic brain hypothesis, we hypothesised that brain entropy metrics would be increased following psilocybin administration. Participants completed a 5 or 10-min resting-state fMRI scan a single time before, and multiple times following psilocybin administration (121 total scan sessions). All scans for each participant were performed on one of two scanners. Each scan was accompanied by a self-report measure of subjective drug intensity (SDI) and a blood sample to quantify plasma psilocin level (PPL), from which brain serotonin 2A (5-HT_{2A}) receptor occupancy (Occ_{2A}), was estimated based on its relation to PPL established in a previous study from our lab ². We evaluated the relations between each entropy metric and SDI, PPL and Occ_{2A} using linear mixed-effect model with a subject-specific random intercept and correction for age, sex, scanner, and motion (see Methods Supplementary Material for more details). We report uncorrected permutation p-values (p_{perm}) for each metric producing a single whole-brain value. For entropy metrics producing regional values, we report family-wise error rate corrected permutation p-values (p_{FWER}) with correction across all regions within each metric using maxT correction ⁴². We report as significant those metrics which were significantly (i.e., $p < 0.05$) associated with SDI, PPL and Occ_{2A}, collectively referred to as "PsiFx". Standardised effect sizes are reported (Pearson's rho). This evaluation was repeated across two parcellation strategies and seven pre-processing pipelines to explore the robustness of effects to pre-processing decisions. Finally, we explored the inter-correlation between brain entropy metrics to characterise their associations.

Dynamic Activity



Static Connectivity



Dynamic Connectivity

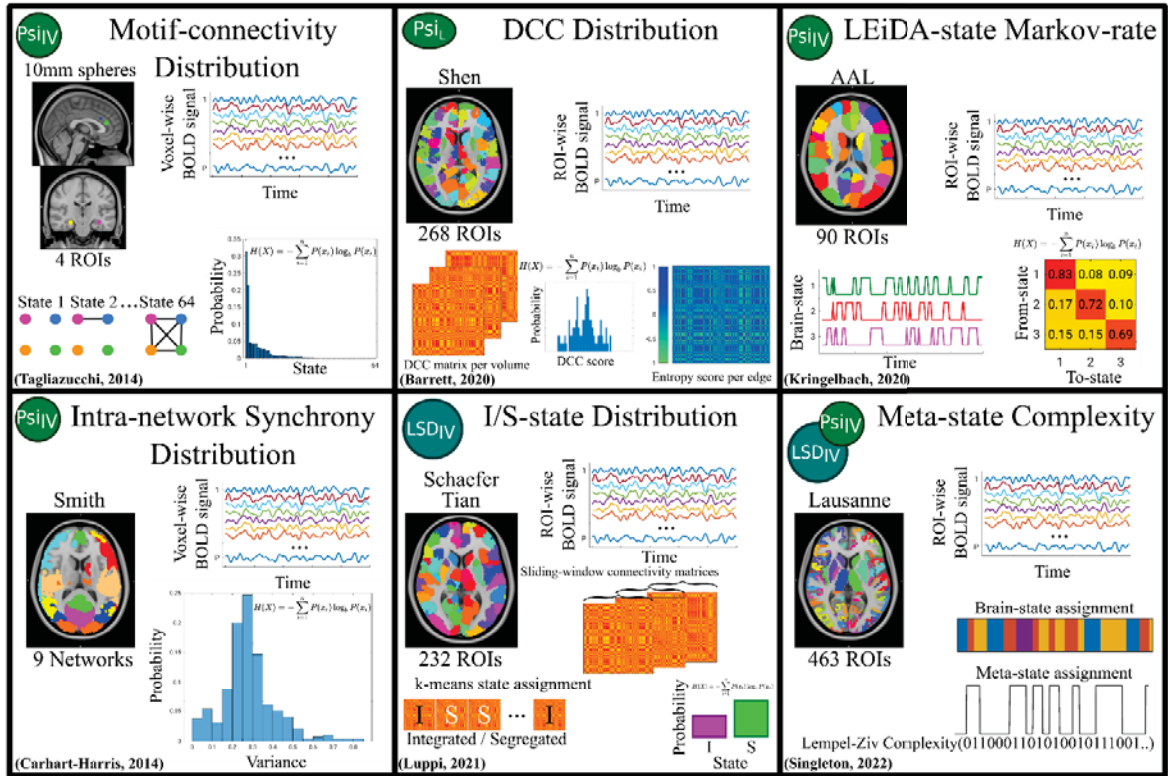


Figure 1: Overview of previous psychedelic fMRI entropy quantifications. Methods are grouped according to the type of brain entropy metric. Symbols in the top left of each box represent the dataset that the original publication analysed. LSD_{IV} (blue) refers to data collected in relation to a 75 µg intravenous LSD administration ($n \leq 15$), Psi_{IV} (green) refers to data collected in relation to a 2 mg intravenous psilocybin administration ($n \leq 15$), Ay (orange) refers to data collected in relation to an oral ayahuasca administration ($n = 9$), and Psi_L (green oval) refers to data collected one-week before, one-week after, and one-month after a 25 mg/70 kg oral psilocybin administration ($n = 11$). Brain images show an axial slice illustrating the parcellation/atlas used. Images in the top right describe the input into the entropy function as one of "region-wise connectivity matrix", "ROI-wise BOLD signal" and "voxel-wise BOLD signal". Illustrations in the lower part of each box graphically represent simplified analysis steps for each method. The original publication for each metric is denoted in the bottom left corner of each box. See Supplementary Table 1 for more details.

Results

Participants showed substantial SDI and PPL following drug administration as anticipated (Supplementary Figure S1). See Figure 1, Supplementary Table S1 and Table 1 for a summary of entropy metrics, previous findings, and our findings respectively.

Entropy of Static Connectivity

Out-network Connectivity Distribution

Shannon entropy of regional out-network connectivity was not significantly associated with psilocybin effects (PsiFx) in any of the 181 non-cerebellar brain regions after controlling for multiple comparisons ($p_{\text{FWER}} > 0.07$ for all regions for at least one of PsiFx, Supplementary Table S2).

Degree Distribution

The entropy of degree distribution at a correlation coefficient threshold corresponding to a mean degree of 27 was not associated with any of PsiFx ($p_{\text{perm}} > 0.18$, Figure 2A). We also did not observe significant effects for thresholds producing a mean degree between 1 and 48 (Supplementary Table S3).

Path-length Distribution

The entropy of path-length distribution was significantly positively associated with PsiFx at the a priori described threshold producing mean degree 27 ($p_{\text{perm}} < 0.04$, Figure 2B). The associations were weak to moderate (Pearson's $\rho = 0.39, 0.27$, and 0.23 for PPL, Occ_{2A} and SDI, respectively). Significant weak to moderate positive associations with PsiFx were also observed across thresholds producing mean degrees from 22 to 38 (Supplementary Table S3).

Von Neumann Entropy

The Von Neumann entropy of correlation matrices was not significantly associated with PsiFx ($p_{\text{perm}} > 0.35$, Figure 2C and Supplementary Table S3).

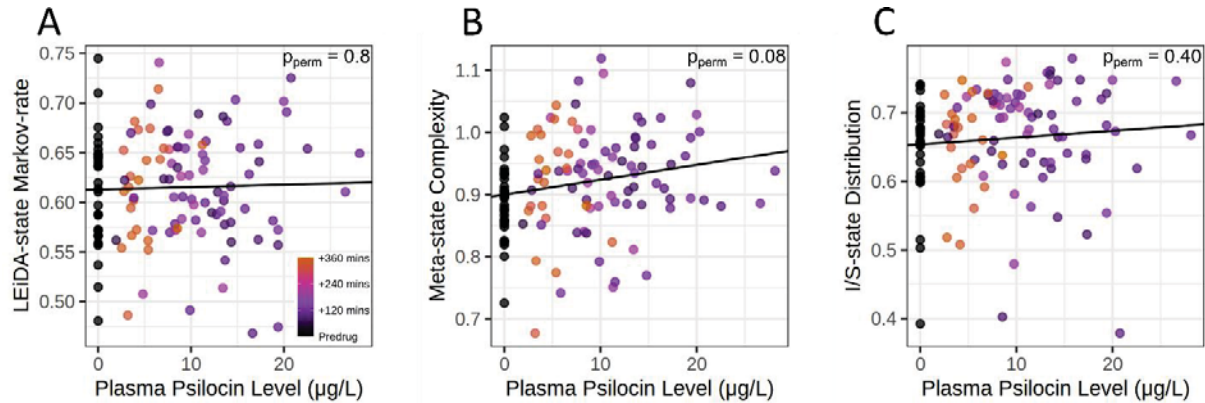


Figure 2: Scatter plots describing the relation between static connectivity entropy and PPL. Y-axis values are partial residuals i.e., entropy values adjusted for age, sex, MR scanner and motion. Degree distribution and path-length distribution statistics are computed using a correlation coefficient threshold corresponding to a mean-degree of 27.

Entropy of Dynamic Connectivity

Intra-network Synchrony Distribution

Intra-network synchrony distribution was not significantly associated with PsiFx in any of nine networks (All $p_{\text{FWER}} > 0.98$, Supplementary Table S2, Supplementary Figure S2).

Motif-connectivity Distribution

The four-ROI motif-connectivity state distribution was not significantly associated with PsiFx at any window length from 15 to 150s except a single weak association at window-length 100s ($p_{\text{perm}} < 0.05$, Pearson's rho 0.30, 0.25, and 0.24 for PPL, Occ_{2A}, and SDI, respectively) surrounded by non-significant findings (Supplementary Figure S3 and Supplementary Table S3).

LEiDA-state Markov-rate

LEiDA-state Markov-rate was not significantly associated with PsiFx ($p_{\text{perm}} > 0.7$ for all PsiFx, Figure 3A, Supplementary Table S3).

Meta-state Complexity

Meta-state entropy was positively associated with Occ_{2A} ($p_{perm} = 0.03$) and SDI ($p_{perm} = 0.003$), but not PPL ($p_{perm} = 0.076$, Figure 3B). Associations were weak (Pearson's $\rho = 0.22$, 0.33 , and 0.20 for Occ_{2A} , SDI, and PPL, respectively; Supplementary Table S3).

Integration/Segregation-state Distribution

Integration sub-state entropy was not significantly associated with PsiFx ($p_{perm} > 0.06$ for all PsiFx, Figure 3C, Supplementary Table S3).

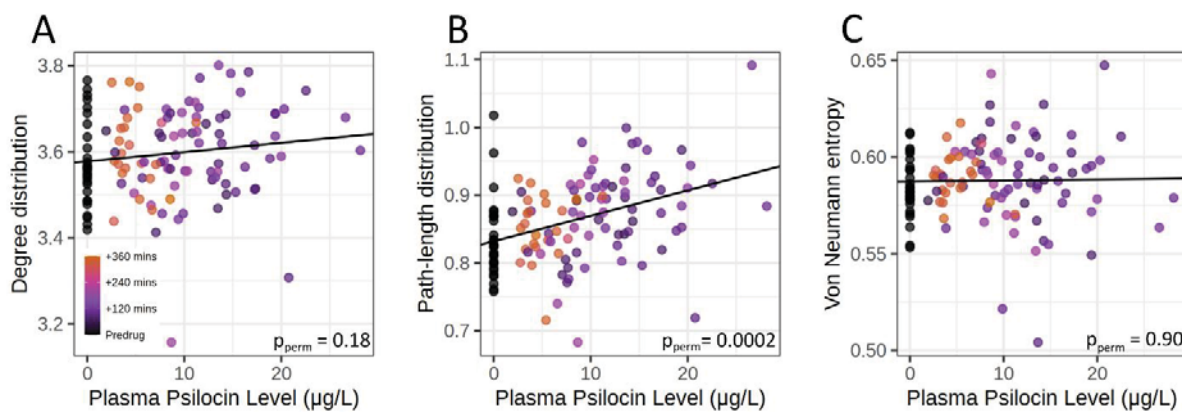


Figure 3: Scatter plots and linear models describing the relation between whole-brain dynamic connectivity entropy measures and plasma psilocin levels. Y-axis values are partial residuals i.e., entropy values adjusted for age, sex, MR scanner and motion. Panel B (Meta-state complexity) shows a non-significant association with PPL but this entropy metric does show a significant linear relation with Occ_{2A} and SDI.

Dynamic Conditional Correlation Distribution

Dynamic conditional correlation entropy was significantly positively associated with PsiFx in 35 of 36 network-network connections (18/36 $p_{FWER} < 0.0001$, i.e., observed data superseded all permutations, 29/36 $p_{FWER} < 0.001$, 35/36 $p_{FWER} < 0.05$; Figure 4A; Supplementary Table S2). Associations were moderate to strong (Pearson's ρ range: 0.35 to 0.78 , Supplementary Table S2). The one association with at least one non-significant relation was for edges within the motor cortex.

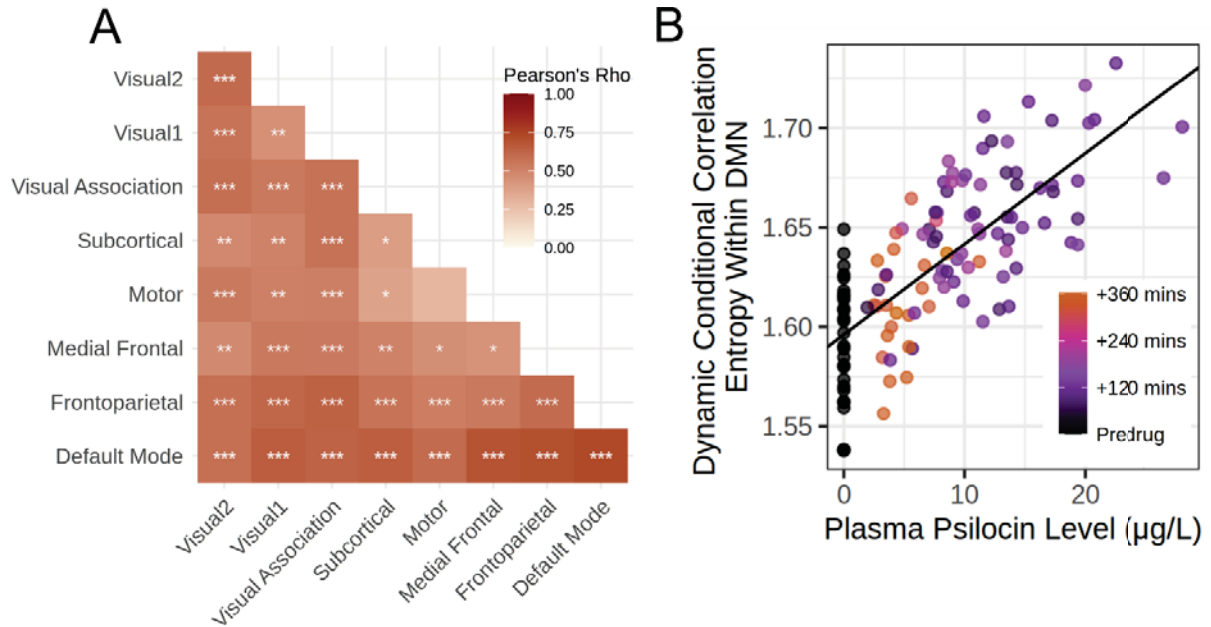


Figure 4: **A:** Heatmap of the Pearson's correlation and p-values for the association between Dynamic Conditional Correlation entropy and plasma psilocin level for each within and between network entropy estimate. *** represents $p_{FWER} < 0.0001$, ** $p_{FWER} < 0.001$, and * $p_{FWER} < 0.05$ for associations with PPL. **B:** A scatter plot of the network edge with the strongest association between DCC entropy and PPL (Pearson's Rho = 0.74). Y-axis values are partial residuals i.e., entropy values adjusted for age, sex, MR scanner and motion.

Entropy of Dynamic Activity

Multi-Scale Sample Entropy

At scale 1, (i.e., no time-series compression), sample entropy was significantly positively associated with PsiFx ($p_{FWER} < 0.05$) in 7 of 17 networks (i.e., Central Visual, Dorsal Attention A, Control A, B and C, Default-Mode A and C). At scales 2, 3, and 4, no associations were significantly associated with PsiFx ($p_{FWER} > 0.05$). At scale 5, sample entropy was significantly negatively associated with PsiFx in 14 of 17 networks; Control A and C and Default-Mode A ($p_{FWER} < 0.001$), Somatomotor A, Dorsal Attention A and B, Salience-Ventral-Attention B, Limbic B, Control B, Temporal-Parietal, Default-Mode B and C ($p_{FWER} < 0.05$, Figure 5, Supplementary Table S2). Scale 1 associations were weak to moderate (Pearson's rho range: 0.26 to 0.47), as were Scale 5 associations (Pearson's rho range: -0.27 to -0.49).

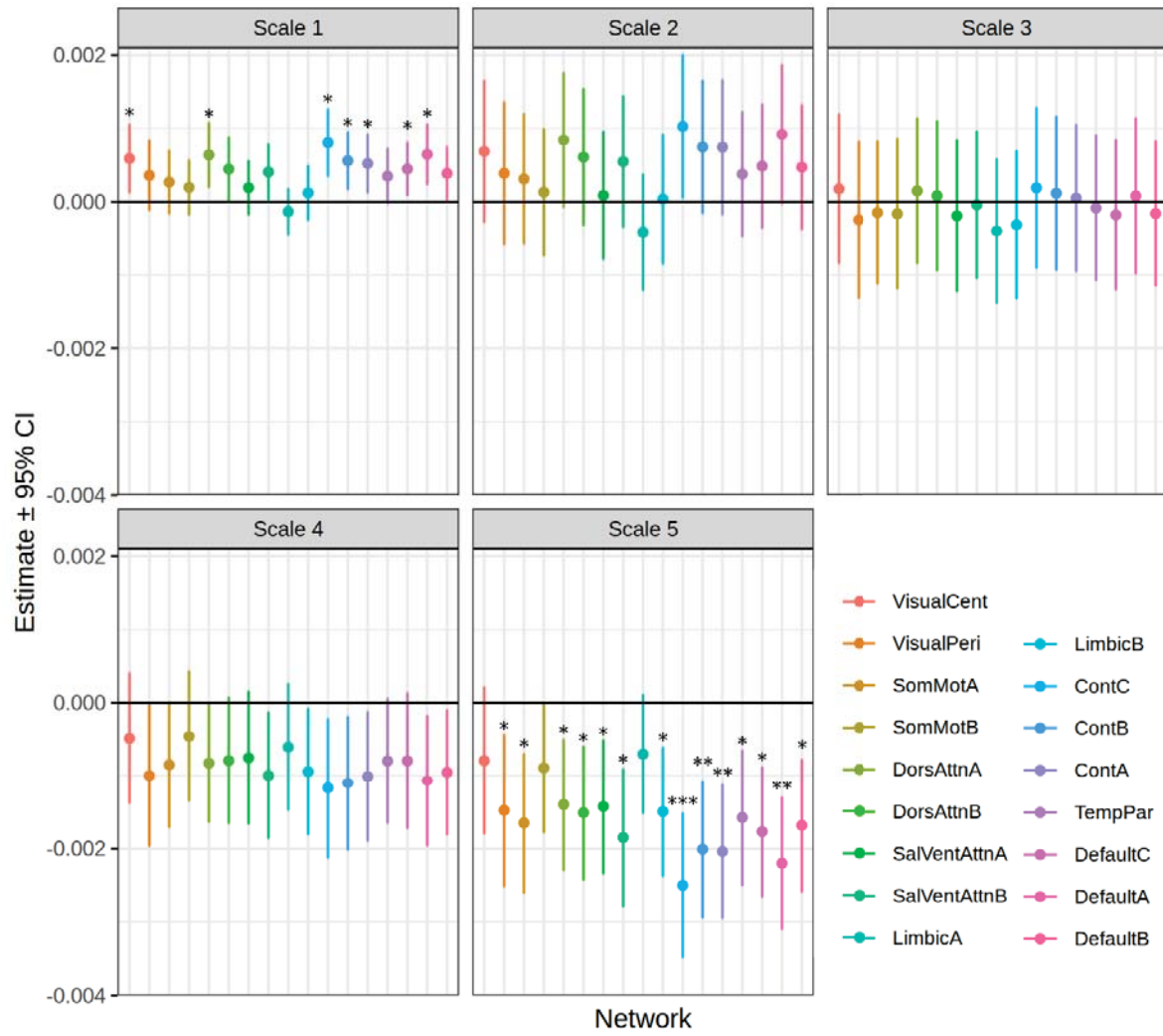


Figure 5: Forest plots representing the estimate of the association between sample entropy and PPL in each network of the Yeo-17 network parcellation and at each of scales 1 to 5. Colours represent networks and error bars represent the 95% confidence interval. *** $p_{FWER} < 0.0001$, ** $p_{FWER} < 0.001$ and * $p_{FWER} < 0.05$ for associations with PPL.

Spatial and Temporal Dynamic BOLD Complexity

Temporal BOLD complexity (LZct) was not associated with PPL ($p_{\text{perm}} = 0.14$, Figure 6B) but was associated with Occ_{2A} ($p_{\text{perm}} = 0.03$) and SDI ($p_{\text{perm}} = 0.009$). Associations were weak (Pearson's $\rho = 0.23$, 0.30 and 0.17 for Occ_{2A}, SDI, and PPL respectively). Spatial BOLD complexity (LZcs) was not significantly associated with PsiFx ($p_{\text{perm}} > 0.6$, Figure 6A, Supplementary Table S3).

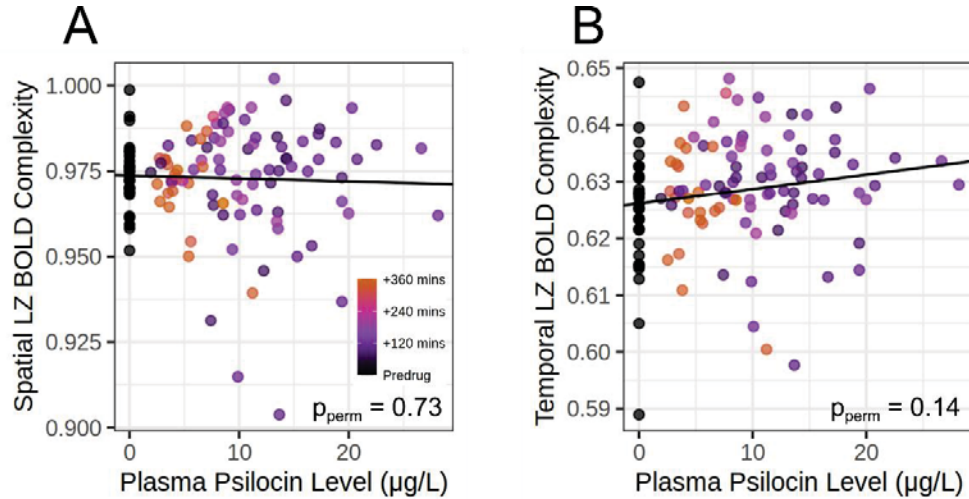


Figure 6: Scatter plots and linear models describing the relation between spatial (A) and temporal (B) Lempel-Ziv entropy of dynamic BOLD activity and PPL. Y-axis values are partial residuals i.e., entropy values adjusted for age, sex, MR scanner and motion. Temporal BOLD complexity (LZct) was significantly, but weakly associated with both Occ_{2A} and SDI despite not being significantly associated with PPL.

Effect of Parcellation

To evaluate PsiFx on brain entropy metrics using a common parcellation, all analyses were re-run using an atlas combining the Schaefer-100 (7 Yeo networks) and Tian-16 subcortical atlases^{43,44}. Path-length distribution showed a weak positive association with all PsiFx at mean degrees 31 to 38. Meta-state complexity was weakly positively associated with Occ, but not PPL nor SDI. LEiDA-state Markov-rate was weakly negatively associated with all PsiFx and DCC distribution was weak-to-strongly associated with all PsiFx across most network edges. Sample Entropy was weak-to-moderately associated with PsiFx at scale 1 but no significant associations were observed at longer scales, though the trend of increased entropy at short scales and decreased entropy at long-scales was maintained. All other metrics were not significantly associated with PsiFx. See Table 1 for a summary and Supplementary Table S5 for detailed results.

Effect of Pre-processing Pipeline

To explore moderating effects of pre-processing pipelines on PsiFx associations with brain entropy metrics, we considered six variations on the above Schaefer-100, Yeo-7, Tian-16 pipeline: 1) including global-signal regression, 2) removal of the low-pass filter (0.09 Hz), 3) applying a narrow bandpass filter (0.03-0.07 Hz), 4) regressing 24 motion parameters, 5) omitting scrubbing, and 6) a stricter scrubbing threshold ($z > 3$ SDs, motion > 0.5 mm). Some brain entropy metrics were relatively robust to pre-processing pipeline, i.e., showing significant associations with PsiFx across most pipelines: sample entropy (scale 1), dynamic conditional correlation entropy, meta-state complexity and path-length distribution. Some metrics were consistently not associated with PsiFx across pipelines: motif-connectivity distribution, I/S state distribution, LEiDA-state distribution and Intra-network synchrony. Some metrics were significantly associated with PsiFx for some pipelines and not others: temporal BOLD complexity (i.e., only significant with no-scrubbing and strict scrubbing) and Von Neuman Entropy (i.e., only significant with GSR and significant associated with SDI and Occ_{2A} when the low-pass filter was removed). Two pre-processing pipelines modulating signal-filtering had substantial effects on results. First, removing the low-pass filter flipped the sign to negative for the association between PsiFx and dynamic conditional correlation entropy and sample entropy (scale 1). Second, a narrow-band filter (0.03-0.07 Hz) made non-significant all PsiFx associations with dynamic and dynamic-connectivity metrics. See Supplementary Table S8 for a summary and Supplementary Table S9 for a full detailing of pre-processing effects.

Moderating Effect of Scanner

To evaluate scanner effects on observed associations, we fit linear mixed models estimating the moderating effect of scanner. Of the three entropy metrics that had a significant association with PsiFx, we observed a significant moderating effect of scanner on the relation between PPL and entropy for path-length distribution over the range of thresholds at which we observe significant associations with PsiFx. The nature of this interaction was that for scanner A the effect was closer to zero than for scanner B. We also show a significant moderating effect of scanner for Sample Entropy scale 5 across many ROIs that are significantly associated with PsiFx. However, the observed effect is the same direction for scanner A and B, only numerically stronger for scanner A. We do not observe a significant moderating effect of scanner for DCC entropy, further supporting the robustness of this metric. For entropy metrics that were not associated with PsiFx in the main model, we observed moderating effects of scanner for I/S-state distribution, some window-lengths of motif-connectivity distribution, some ROIs of out-network connectivity, degree distribution, and some sample entropy scale 4 ROIs. See Supplementary Table S6 for full results.

Correlation Between Whole-brain Entropy Quantifications

We estimated the correlation between whole-brain entropy metrics to explore their association with one another across all included scans. Some pairs of metrics were both positively correlated and negatively correlated and some pairs were effectively not correlated with one another (Figure 7). After correction for multiple comparisons, five entropy quantification pairs were positively related (LZcs & LZct, LZcs & Von-Neumann, Path-distribution & Degree-distribution, LEiDA state & Von-Neumann, Motif Connectivity Distribution-window100 & Von-Neumann) and four were negatively related (Path-distribution & LEiDA state, Path-distribution & Von-Neumann, Degree-distribution & LEiDA state, Degree-distribution & Von-

Neumann). LZcs was significantly negatively associated with motion. See Supplementary Table S4 for pairwise correlation coefficients and p-values.

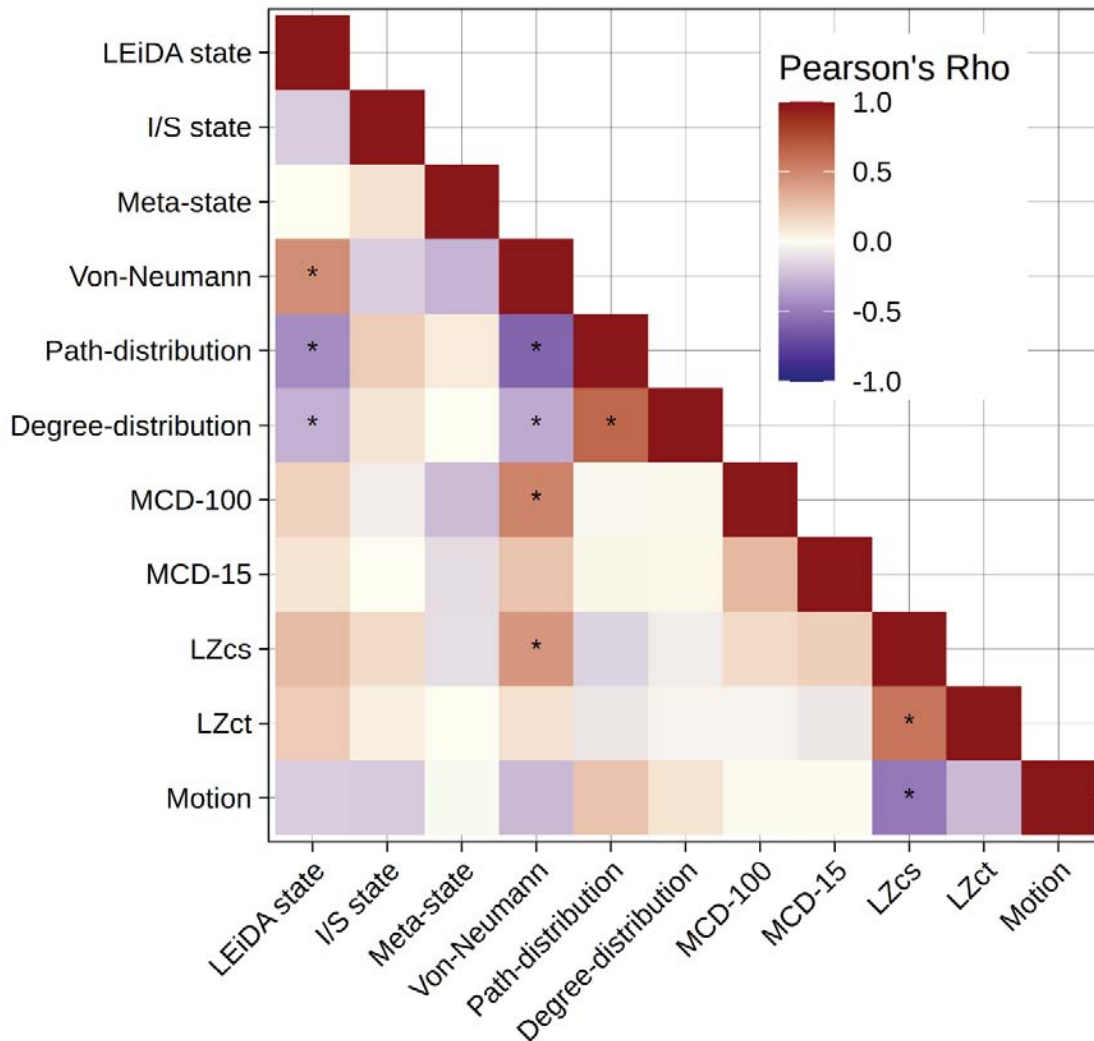


Figure 7: Heatmap showing the correlations between whole-brain entropy metrics and motion. Colours represent the Pearson's correlation coefficient. * represents $p_{\text{corr}} < 0.05$. I/S state, Integration/Segregation state distribution; MCD, Motif connectivity distribution (with either 100 or 15 second windows); LZcs, Spatial Lempel-Ziv complexity. LZct, Temporal Lempel-Ziv complexity.

Entropy	Original dataset	Original findings	Our findings (original atlases)	Our findings (common atlas)
Static Connectivity				
Out-network connectivity	IV Psi	Region-specific effects	Not associated with PsIFx	Not associated with PsIFx
Degree distribution	Oral Aya	Increased	Not associated with PsIFx	Not associated with PsIFx
Path-length distribution	Oral Aya	Increased	Weak-moderate association with PsIFx†	Weak-moderate association with PsIFx‡
Von Neumann Entropy	Oral Aya	Numerically increased	Not associated with PsIFx	Not associated with PsIFx
Dynamic Connectivity				
Intra-network synchrony	IV Psi	Increased (some networks)	Not associated with PsIFx	Not associated with PsIFx
Motif-connectivity distribution	IV Psi	Increased	Not associated with PsIFx	Not atlas dependent
Meta-state complexity	IV Psi & IV LSD	No change	Weak association with SDI and Occ but not PPL	Weak association with Occ but not SDI or PPL
I/S state distribution	IV LSD	No change	Not associated with PsIFx	Not associated with PsIFx
LEIDA state Markov Rate	IV LSD	Not reported	Not associated with PsIFx	Weak negative association with all PsIFx
Edge-wise DCC distribution	Oral Psi*	No persisting change	Moderate-strong association with all PsIFx all networks except within motor cortex	Weak-strong association with all PsIFx in most networks
Dynamic Activity				
Multi-scale sample entropy	IV LSD	Increased at scales 1 2 and 3. Decreased at scale 5	Weak-moderate association with all PsIFx in several networks. Positive at scale 1, negative at scale 5	Weak-moderate association with all PsIFx in several networks. Positive at scale 1
BOLD complexity (spatial)	IV Psi & IV LSD	Increased (LSD) No change (psilocybin)	Not associated with PsIFx	Not associated with PsIFx
BOLD complexity (temporal)	IV Psi & IV LSD	Not reported	Weak association with SDI and Occ but not PPL	Not associated with PsIFx

*Investigates persisting effects at 1 week and 1 month post-psilocybin administration

† at thresholds producing a mean degree of 22-38

‡ at thresholds producing a mean degree of 31-38

Table 1: Summary of entropy quantification methods, previous findings, and findings reported within this manuscript. For the “Original findings” and “Our findings” columns, grey cells describe no association of effect, light grey refers to no reporting of acute effects on brain entropy, yellow describes marginal effects, and green statistically significant effects. For a more in-depth evaluation of our findings please see supplementary tables 1 and 2.

Discussion

Overview

Recent studies have reported acute psychedelic effects on functional brain entropy, but to date none of these metrics have been evaluated in an independent sample. In this study we evaluated 13 previously reported entropy metrics in a novel sample of 28 healthy participants scanned with BOLD fMRI before and several times after psilocybin with concomitant measurements of subjective drug intensity and plasma psilocin level. We observed statistically significant psilocybin effects that echoed previous reports for only two brain entropy metrics: path-length distribution, wherein we replicate increased entropy at previously reported thresholds; and sample entropy, wherein we replicate a previously observed increase in entropy at short scales and decrease at long scales. We observed a strong positive relation between psilocybin effects and brain entropy measured by Dynamic Conditional Correlation analyses that has not been previously reported. Two Lempel-Ziv complexity metrics showed some evidence for associations with psilocybin effects. For 8 of 13 brain entropy metrics previously reported, we did not observe a significant association with psilocybin measures and we see limited correlation between entropy metrics. These mixed findings underscore the importance of corroborating outcomes in independent datasets. Although we observe some evidence supporting the entropic brain hypothesis, these variable findings underscore the broadness of this theory and the need to more clearly establish which brain entropy metrics of functional brain imaging signals are acutely affected by psychedelics.

Path-length Distribution

We report a significant positive association between the Shannon entropy of the distribution of path lengths across the whole brain as previously reported by Viol and colleagues³⁴ and all three psilocybin metrics evaluated: PPL, Occ_{2A} , and SDI. We observed statistically significant associations at a range of correlation coefficient thresholds that produce graphs with a mean degree from 22 to 38, Viol and colleagues reported significant differences between conditions at thresholds producing mean degrees from 24 to 35. Characteristic path length is a description of the number of edges that must be traversed to get from any one brain region to another, a putative measure of capacity for information flow. Our results suggest that one of the effects of psilocybin on the brain can be described as a broadening of the histogram of path lengths across region-to-region connections in the brain. Notably, this does not imply that the average path length is shorter or longer, only that there is a wider distribution of these across the whole brain i.e., it is more equally likely that the path-length between any two nodes is 1, 2 or 3 instead of being more likely to be one of these. Our convergent results are encouraging considering that the previously reported dataset used a different drug (ayahuasca, which contains MAOIs as well as the psychedelic N,N-dimethyltryptamine) and different imaging parameters, suggesting robustness of the metric. This association with PsiFx was relatively robust to pre-processing strategies, though did appear sensitive to scanning parameters between the two explored in this study. Thus, path-length entropy may be a useful candidate biomarker of neural psychedelic effects, though associations were weak-moderate and interpretation is not straightforward. We are not aware of other studies evaluating the entropy of path-length distribution so comparison to other drugs or psychiatric conditions are not yet possible and should be evaluated in future studies.

Dynamic Conditional Correlation Distribution

We observed a statistically significant positive relation between psilocybin effects and Dynamic Conditional Correlation (DCC) Distribution for all within or between network relations except within the motor network. DCC distribution is a measure of the width of the distribution of instantaneous connectivity values for any region-region edge across each scan. The previous study found no change in DCC distribution at one-week and one-month post administration³⁶ and importantly did not evaluate acute effects during psilocybin. We observed moderate to strong correlations with psilocybin effects (i.e., Pearson's rho with PPL > 0.7 for three edges, all including DMN (DMN-DMN, DMN-Frontoparietal, DMN-Medial Frontal), and Pearson's rho > 0.5 for 28/36 network edges). The strength of these associations is remarkable, perhaps as large as any previously reported fMRI effect of psychedelic action, suggesting that DCC distribution may be a strong candidate neural correlate of acute psychedelic effects and among the strongest correlations observed in pharmaco-fMRI. Our results suggest that psilocybin increases the variability of connectivity between regions across time across almost all region-region pairs, which are summarised into networks. Furthermore, this association was robust to most pre-processing strategies and was similar across the two scanning parameters applied in this study. As above, we are not aware of other pharmaco-fMRI studies evaluating DCC distribution. Notwithstanding, the sheer magnitude of the observed associations suggests DCC distribution may be a sensitive marker for acute psychedelic effects on the brain and so we encourage independent replication.

Multi-scale Sample Entropy

We observed a significant positive relation between psilocybin effects and scale-1 sample entropy (i.e., temporal resolution = 2-seconds) in seven out of 17 brain networks. Conversely, we observed a significant negative relation between scale 5 sample entropy (temporal resolution = 10-seconds) in 14 out of 17 networks. This association at short-scale was somewhat robust to pre-processing pipelines and at all scales consistent across scanning parameters. Multi-scale sample entropy measures the irregularity of a signal over its entire length. Increased sample entropy in most networks at scale-1 and decreased sample entropy at scale-5 align in both cases with the original observation²⁹. Unfortunately, we were unable to align the previously reported network labels with available versions of the atlas; thus, it is hard to resolve the spatial overlap between studies. fMRI-measured multi-scale sample entropy has been shown to be increased in the default-mode, visual, motor and lateral-prefrontal networks following caffeine⁴⁰ and decreased at scale 1 during sleep³⁷, although certain parameters used in their calculations were different to those employed here. As such, it is possible that the effects that we, and Lebedev and colleagues, observed may reflect differences in wakefulness and may thus be non-specific to psychedelic effects. Positive symptoms of schizophrenia have been positively associated with sample entropy at scales 1 and 2, and negatively associated in certain brain regions at scales 3, 4, and 5⁴⁵. This is consistent with our observations and is also phenomenologically consistent, as the high-dose psychedelic state has some overlap with some positive symptoms of schizophrenia e.g., verisimilitude, alterations in visual perception (though psychedelics do not normally produce 'true' hallucinations, i.e., sensory appearances indistinguishable from reality, as are present in schizophrenia), and sense of self. We are aware of the problematic history of psychedelic 'psychotomimetic' research and urge caution in overinterpretation of this apparent convergence⁴⁶. Our convergent results with Lebedev and colleagues are intriguing considering that the original paper reported effects following intravenous LSD administration whereas we administered psilocybin orally. Taken

together, divergent effects on sample entropy at short and long temporal resolutions may be a candidate biomarker for psychedelic effects, if they cannot be explained by, e.g., wakefulness state.

Lempel-Ziv Complexity

Intriguingly, Lempel-Ziv complexity of two measures (meta-state complexity and temporal BOLD complexity (LZct)) were significantly positively associated with Occ_{2A} and SDI, but not PPL. LZct was significantly moderately associated with all PsiFx in the no-scrubbing and strict-scrubbing pre-processing pipelines, and meta-state complexity was significantly weak-moderately associated with at least one PsiFx in all but one pre-processing pipeline. The original study of meta-state complexity does not report a statistical analysis of intravenous LSD nor intravenous psilocybin effects, but the data are publicly available and do not support a significant effect of either drug³¹. The original study of BOLD complexity reports an increase in spatial BOLD complexity following LSD, but not psilocybin and does not report any findings pertaining to temporal BOLD complexity. We speculate that the less significant relations with PPL reflect that PPL is non-linearly related to brain 5-HT_{2A} receptor occupancy, which is ultimately responsible for the neural effects of psychedelics². Therefore, PPL may be a less precise metric of acute psychedelic effects on brain function. One MEG and four EEG studies have reported increased LZc following psychedelic administration⁴⁷⁻⁵¹, providing convergence for its utility as a marker of psychedelic effects, however one reports increases in LZct in the absence of subjective drug effects, indicating a potential epiphenomenon. Across previous studies analysing regional timeseries, there is inconsistency in the quantification of LZc in the temporal (LZct) and spatial (LZcs) domain. Our borderline statistically significant associations were observed for LZct only. It is our perspective that LZct is more sensible and should be used in future studies as it preserves region-specific temporal information, whereas LZcs is sensitive to arbitrary region order.

Null Findings

We did not observe a significant association between 8 of the 13 brain entropy metrics considered here (Table 1). Of these seven metrics, the original studies reported either increased entropy following psychedelic drug administration^{19,27,28,35}, no effect³⁰, or did not formally evaluate the effect of psychedelic drug administration^{26,33} (Table 1, Supplementary Table S1). Our observed entropy estimates for hippocampal-ACC motif entropy are markedly different from those previously reported²⁸. We are concerned that the originally reported values are not mathematically possible, see the Supplementary Text and Supplementary Figure S3 for a detailed consideration. Although our null findings with respect to these metrics does not establish that they have no relation to acute psychedelic drug effects, they imply a smaller relation that limits their utility as biomarkers of acute psychedelic effects. The discrepancy between our observations and those reported previously underscores the need to replicate or corroborate findings in independent cohorts to validate initial reports.

Our inability to replicate previous findings may be due to greater statistical power and different statistical models i.e., linear regression with PsiFx. Incongruence may also be attributed to differences in data collection. All previous studies reporting acute effects on brain entropy administered either 2mg of intravenous psilocybin, 75µg of intravenous LSD or 96-160mg of oral DMT with harmine, yet we administer 0.2-0.3mg/kg oral psilocybin, though the acute effect appear similar, we cannot rule out differences due to drug or route of administration. However, if entropic brain effects are not consistent

across drugs this would indicate that these metrics are not useful neural correlates of the psychedelic experience. We encourage all future fMRI studies evaluating psychedelic effects on brain function to measure subjective drug intensity at time of scanning and to collect plasma samples for quantification of plasma drug levels as described in the psychedelic fMRI consensus paper ¹⁶.

Inter-correlation Between Entropy Metrics

Despite the large set of brain entropy metrics that have been reported previously, no studies have considered whether these measures are inter-correlated. We observed positive associations between path-length and degree distribution, which are based on the same graph-theory representation of connectivity, and between LZcs and LZct which are conceptually very much related. Notably, we observed four pairs of brain entropy metrics that were significantly negatively correlated. This highlights the importance of specificity in describing “brain entropy”. Many of these metrics represent distinctly different constructs, their individual meaning and collective representation of psychedelic effects is muddled by superficially considering them all metrics of “brain entropy”. Future studies should be cognisant of this variable relation in considering whether findings are consistent or convergent across studies.

Alternative Neuroimaging Techniques

Although we focus here on fMRI quantifications of entropy, it is worth noting that psychedelic effects on brain entropy, specifically LZc, have been applied to five original MEG and EEG datasets, over eight papers ^{47–54}. The entropy measures applied in these studies leverage the high temporal sampling rate that is not clearly applicable to temporally slower fMRI and were not evaluated here. Further, the methods capture different aspects of physiological response to psychedelics. Future work evaluating psychedelic effects on brain entropy using multimodal neuroimaging and evaluating relations between alternative quantifications of brain-entropy will contribute meaningfully to the field.

Limitations

Our study is not without its limitations. Brain imaging data were acquired on two different MRI scanners with different sequences (e.g., different TRs) requiring temporal downsampling of some data to match the other. However, each participant was scanned on only one scanner, enabling us to map within-subject changes onto psilocybin effects independent of scanner differences. Our study did not include a placebo condition, but we did acquire a pre-drug scan with which we estimated brain entropy metrics in the absence of psilocybin effects. Due to the large within-subject variability in fMRI outcomes in participants scanned several days apart, pre-drug vs post-drug scans performed on the same day may be superior to placebo scans performed weeks apart for evaluating drug effects because it limits this within-subject variance component ⁵⁵. PPL and SDI were associated with increased motion in the scanner, see Supplementary Figure S4; although we included an estimate of motion as a covariate in our models, employed scrubbing, motion correction and denoising strategies, and show that motion was not positively associated with any whole-brain entropy metrics, we cannot rule out that motion confounds our reported effects. It has been reported in many groups that head motion is increased following psychedelic drug administration so this is not a limitation unique to our data ⁴⁸. Most fMRI scans were 10 minutes long, though some were only five. This may not be long enough to derive stable estimates of brain entropy metrics, e.g., previous studies have

recommended >13 minutes for single-echo fMRI ⁵⁶. Future studies, e.g., using openly available data with longer scan durations, could inform recommended scan durations to establish stable brain entropy estimates or other methods that improve signal quality, e.g., multi-echo fMRI ⁵⁷. Approximately half of the scans analysed herein utilised a multi-band acceleration protocol that may negatively affect signal-to-noise ⁵⁸, though these effects may be less pronounced for task-free imaging as performed here ⁵⁹. We corrected for estimated physiological noise using aCompCor but did not statistically model physiological effects such as changes in respiration, heart rate, or vasoconstriction which are affected by psilocybin and may have confounded our findings ^{60,61}. Our statistical models assume a close temporal relation between brain entropy and PsiFx (measured adjacent to scans), thus, if changes in brain entropy occur after PsiFx, they would not be well captured.

Pre-processing

A prevailing challenge in fMRI research is how best to handle the enormous flexibility in data pre-processing ⁶². Here we explored this space by evaluating brain entropy metrics across a set of pre-processing strategies. Most of our results were robust to using the original and common atlases, indicating robustness to parcellation choice. We also considered six different denoising strategies. The associations with PsiFx of some metrics (DCC distribution, Sample Entropy (scale 1), Meta-state complexity and Path-length distribution) were robust to most pre-processing strategies, whereas some were sensitive to pre-processing strategy, e.g., temporal BOLD complexity (LZct). For those metrics which remained significantly associated with PsiFx across pipelines, the strength of some associations varied across pipelines. Notably, the removing the low-pass filter and applying a relatively narrow bandpass filter both substantively affected the statistical relations between PsiFx and brain entropy metrics. This is consistent with previous reports that pre-processing decisions can influence observed effects on fMRI outcome measures⁶², which underscores the need for future studies in large, normative datasets probing brain entropy metric characteristics in the context of this pre-processing multiverse. This is all the more relevant to advance their predictive or prognostic utility in clinical cohorts.

We provide a public MATLAB-toolbox, the Copenhagen Brain Entropy toolbox (CopBET <https://github.com/anders-s-olsen/CopBET>), containing functions to evaluate each of the entropy metrics evaluated here, allowing future studies to determine how these entropy metrics are affected by the multitude of possible fMRI pre-processing pipelines. For the purposes of this manuscript, we show that our pre-processing pipeline was very similar to all previously applied in this space (See Supplementary Table S7) and thus believe that our results are directly comparable with previously reported findings. We have shown that one of our findings was more strongly supported using a multi-band sequence (path-length distribution) and another when not using multi-band (Long-scale Sample Entropy). Further work may therefore also wish to apply CopBET to data collected using a range of scanning sequences to evaluate the effect of scanning parameters such as multi-band acceleration or multi-echo recording. However, given the enormous number of possible parameter choices and the unsupervised nature of the problem, interpretation of results from such an analysis remains a challenge ⁶².

Conclusion

In conclusion, we observed acute effects of psilocybin on 3 of 13 previously reported brain entropy metrics. We report novel evidence for a strong association effect on DCC distribution entropy, implicating it as a potential biomarker of acute psychedelic effects. We also present convergent evidence for weak associations with increases in path-length distribution entropy. In addition, two Lempel Ziv complexity measures showed marginal associations with psilocybin measures. We did not observe significant associations for 8 of 13 metrics evaluated, suggesting nuanced support for the popular theory that psychedelics acutely increase brain entropy. Our observations implicate potential brain biomarkers of acute psychedelic effects and emphasise the need for both transparency in reporting brain entropy metrics and corroborating previously reported findings in independent datasets.

Methods

Twenty-eight healthy volunteers participated in the study (10 female, mean age \pm SD : 33 ± 8) and were recruited from a database of individuals interested in participating in a study involving psychedelics. A detailed description of the study design can be found in the Supplementary Text and has been reported previously⁶⁴. The study protocol was approved by the ethics committee of the capital region of Copenhagen (H-16026898) and the Danish Medicines Agency (EudraCT no.: 2016-004000-61). The study was registered at clinicaltrials.gov (NCT03289949). Data presented here were collected between 2018 and 2021. A subset of the functional brain imaging data presented here has been included in different studies reported previously^{64,65}. Details of recruitment, procedures during the psilocybin session, ethical approvals, MRI acquisition and quality control, are described in the Supplementary Text. Analyses were pre-registered on the 3rd of August 2022 (<https://aspredicted.org/bw8y7.pdf>). Some analyses that met our inclusion criteria (i.e., fMRI studies investigating entropy changes pertaining to psychedelics) were identified after pre-registration and were added. No statistical methods were used to pre-determine sample sizes but our sample sizes are larger than all previous publications (see Figure 1).

Data Collection

After obtaining written informed consent and screening for neurological, somatic and psychiatric illness, participants completed a single-blind, cross-over study design wherein participants received a single 0.2-0.3 mg/kg dose of psilocybin (mean \pm SD dose: 19.7 ± 3.6 mg, administered in units of 3 mg capsules) or 20 mg of ketanserin. Data from ketanserin scans are outside the scope of the current evaluation and not presented here. After drug administration, participants completed MRI scan sessions including resting-state fMRI (see Supplementary Text for details) approximately 40, 80, 130, and 300 minutes after administration. Following each scan, participants were asked, "On a scale from 0 to 10 how intense is your experience right now" to measure SDI and a venous blood-draw used to quantify PPL (see Supplementary Text for details). After each resting-state fMRI scan, participants were asked if they had fallen asleep (no participants reported doing so). Occ_{2A} , i.e., occupancy of psilocybin at the 5-HT_{2A} receptor is closely related to PPL and SDI². Here we applied the previously reported parameter estimates relating PPL to occupancy based on the Hill-Langmuir equation: $Occ_{2A} = \frac{Occ_{max} \times C_p}{EC_{50} + C_p}$ where Occ_{max} refers to the maximum measurable occupancy, C_p refers to the measured concentration of the ligand in plasma (i.e., PPL), and EC_{50} refers to

the concentration in plasma at which occupancy is equal to 50% of Occ_{max} (fixed parameters used to compute Occ_{2A} : $\text{EC}_{50} = 1.95 \mu\text{g/L}$ and $\text{Occ}_{\text{max}} = 76.6\%$).

Pre-processing

Pre-processing and denoising was uniform across all entropy metrics despite differences in the pipelines of the original publications. Our pipeline included slice-timing correction (where applicable), unwarping, realignment, co-registration of structural scans to functional data, segmentation, normalisation, and smoothing. Two MR-scanners were used to acquire the data, and some functional data were temporally downsampled so that the sampling frequency was consistent across scan sessions. Denoising in CONN⁶⁶ included linear detrending, aCompCor⁶⁷, 12-motion (three translations, three rotations and their first derivatives) and artefact-flagged volume regression ($z > 4$ SDs or motion > 2 mm using ART), band-pass filtering (0.008-0.09 Hz) and parcellation. Cerebellar ROIs were removed from included atlases as they were not consistently within the field of view. See Supplementary Text for more details.

Entropy of Static Connectivity

Four studies evaluated the entropy of static connectivity given by the matrix of Pearson correlation coefficients, \mathbf{R} , computed from N -regional time-series data^{27,33–35}, N being the number of ROIs in the atlas used by the study.

Out-network Connectivity Distribution

Following a graph-theory framework, ROIs from the 200-region Craddock-atlas⁶⁸ were partitioned into “networks” using the Louvain modularity algorithm applied to the average connectivity matrix across scan sessions⁶⁹. The “Out-network Connectivity”, referred to as “diversity coefficient” in the original publication and “Brain Connectivity Toolbox”^{27,70}, of an ROI was calculated for each scan session as the Shannon entropy of the distribution of connectivity estimates between a given ROI and the set of ROIs assigned to a different network.

Degree Distribution

Degree refers to the number of non-zero elements in any given row of a thresholded matrix. ROI-specific degrees are computed based on \mathbf{R} , the Pearson correlation matrix between ROIs, with $N=105$ using the Harvard-Oxford-105 atlas⁷¹. Both this analysis and Path-length distribution use the absolute correlation values. The thresholding for this analysis occurred in two steps. In the first step, any correlation for which the corresponding p-value was above 0.05 was set to 0. In the second step the goal is to reach a pre-specified mean degree across rows. In order to achieve this, a threshold below which all absolute values are set to 0 is gradually increased until the mean number of non-zero elements is at the desired level. Here we applied a scan-specific threshold that produced a mean degree of 27 because this was the threshold that produced the largest effect in the original publication³⁵. This means that each scan may have a different absolute threshold value, but identical mean degree. The final entropy quantification is simply the Shannon entropy of the distribution of degrees across ROIs. We also calculated entropy for mean degrees of 1 up to the point at which for any given scan session an increase in absolute threshold did not produce an increase in mean degree, i.e., 48. This also applies to the path-length entropy described below.

Path-length Distribution

Again using absolute correlation values, the matrix was thresholded using only the mean-degree criteria and not the p-value threshold. The matrix was then binarised, setting all non-zero elements to 1. The "shortest path length" was then computed as the fewest edges one must traverse to go from one node to another. The Shannon entropy of the distribution of path lengths from each node to all other nodes was then calculated³⁴. Path-length distribution was evaluated for correlation coefficient thresholds up to a mean degree of 53.

Von Neumann Entropy

Entropy of the Pearson correlation matrix, \mathbf{R} , derived for the Harvard-Oxford-105 atlas, was calculated through the von Neumann entropy: $S(\mathbf{p}) = -\sum_{i=1}^N \lambda_i \log \lambda_i$, where λ are the eigenvalues of the scaled correlation matrix $\mathbf{p}=\mathbf{R}/N$. The von Neumann entropy may also be defined as $S(\mathbf{p}) = -\text{tr}(\mathbf{p} \log \mathbf{p})$, where \log represents the matrix logarithm³³.

Entropy of Dynamic Connectivity

Intra-network Synchrony Distribution

Nine brain networks were defined according to a previous study⁷²: auditory, dorsal attention, default mode, left and right frontoparietal, motor, salience, visual 1 and visual 2. For a given network, for a given time point, the variance across voxels within the network was evaluated. The Shannon entropy was then calculated on the histogram of the variance estimates over time¹⁹.

Motif-connectivity Distribution

Dynamic functional brain connectivity was evaluated in four regions (10mm diameter spheres) located at bilateral hippocampi, MNI coordinates: right: (26, -21, -16), left: (-34, -22, -16), and anterior cingulate cortices, right: (4, 35, 18), left: (-2, 23, 28) using a non-overlapping sliding window approach with varying window lengths (15-150s). In each window, the partial correlation coefficient and corresponding p-value was calculated for every region pair, controlling for the remaining regions and the motion framewise displacement time-series. These time-series were standardised before windowing. The 4 x 4 partial correlation matrix was binarised for every window, according to a corrected significance threshold $p=0.0083$ (i.e., $0.05/6$, where 6 is the number of region pairs). A probability distribution of the frequency of each of the 64 possible graph structures was established and the Shannon entropy was calculated²⁸.

LEiDA-state Markov-rate

Notably, this entropy metric was not applied to evaluate psychedelic effects in the original paper. Rather, the authors provided a computational framework wherein parameters were learned by optimising this entropy measure. For each scan session, Leading Eigenvector Dynamics Analysis (LEiDA)⁷³ was applied to the time-series of 90 AAL atlas regions⁷⁴. The phase series was computed using the Hilbert transform and, for each time point, a phase coherence matrix was estimated based on the cosine of the difference between pairwise instantaneous phases. The phase coherence matrices were decomposed using the

eigenvalue decomposition and the first eigenvector was retained for every time point. The set of eigenvectors was clustered using K -means with $K = 3$ states. Subsequently, the transition probability matrix was computed for each scan session. The entropy rate of the transition matrix, $P(i, j)$, for each state, i , was calculated as $S_i = -p(i) \sum_{j=1}^K P(i, j) \log P(i, j)$, where, p is the leading eigenvector of P . The final entropy measure is given as $S = \sum_{i=1}^K S_i / \log_2(K)$ ²⁶.

Dynamic Conditional Correlation Distribution

Regional time-series were evaluated for each of the regions described in the Shen 268 region atlas ⁷⁵. Windowless framewise correlation coefficients were calculated for all edges using the Dynamic Conditional Correlation (DCC) toolbox ⁷⁶. Subsequently, the probability distribution over each ROI-to-ROI DCC time-series was established, and the Shannon entropy was calculated. Each ROI was assigned to one of eight networks: default mode, fronto-parietal, medial-frontal, motor, subcortical-cerebellar, visual association, visual 1, and visual 2. Each ROI-to-ROI pair was assigned to its respective network-to-network association (e.g., motor-to-motor, default mode-to-motor) and the mean entropy of each network-to-network association was calculated. Although the original publication applies bin-width correction, they do not report an effect of bin width and we report findings using MATLAB's *histcounts* function, which automatically calculates bin-width ³⁶. Thus, we did not implement bin-width correction.

Meta-state Complexity

Regional time-series were evaluated for each of the regions described in the Lausanne 463 region atlas ⁷⁷. BOLD time-series across all scan sessions were clustered using K -means into $K = 4$ states using the Pearson correlation distance metric. The clustering procedure was repeated 200 times with random initialisations and the best repeat in terms of K -means loss was extracted. The four states were grouped into two meta-states because the clustering procedure typically produces sign-symmetric states. Each volume was assigned to meta-state 0 or 1 and the Lempel-Ziv complexity (LZ76 exhaustive algorithm) of this binary sequence was calculated ³¹.

Integration/Segregation-state Distribution

Regional time-series were evaluated for each region described in the Schaefer 200 region atlas ⁴⁴, augmented with 32 subcortical regions from the Tian atlas ⁴³. A sliding-window correlation analysis was performed using a window defined by convolving a rectangular window of size 44 seconds with a temporal Gaussian kernel (FWHM = 3s). The correlation matrix was established for each window (stride of 1), and the Louvain modularity algorithm ⁶⁹ was applied to estimate the module degree z-score and participation coefficient for each region. The Louvain modularity algorithm was repeated 100 times to ensure an optimal assignment. K -means clustering with $K = 2$ states was applied to a cartographic profile, i.e., a two-dimensional unnormalised histogram of these measures, using the correlation distance and 500 replications. The Shannon entropy was computed on the probability distribution of state occurrences ³⁰.

Entropy of Regional Dynamics

Multi-scale Sample Entropy

Networks were defined using the Yeo 17-network atlas ⁷⁸. Sample entropy is defined as the negative logarithm of the conditional probability that if two vectors with length m (set to 2) are dissimilar below a threshold distance r (set as 0.3), then vector pairs with length $m + 1$ will also have distance below the threshold ²¹. Scales 1-5 were evaluated for each network, meaning that each time-series was split into non-overlapping windows of length (scale) s volumes and the means of each window were concatenated to form a condensed time-series upon which sample entropy was calculated ²⁹.

BOLD Complexity

Regional time-series were evaluated for each of the regions described in the Schaefer 1000 region atlas ⁴⁴. BOLD time-series for each ROI were first Hilbert-transformed. The amplitude of the Hilbert series was then binarised around the mean amplitude for that region, i.e., assigned as “1” if greater than the mean and “0” if less. These binarised time-series were combined into an $T \times N$ matrix, where $N = 1000$ is the number of regions and T is the number of time points. This matrix was collapsed into a single vector to compute 1) the Lempel-Ziv complexity over time (LZct, LZ78 algorithm) wherein regional time-series were concatenated or 2) Lempel-Ziv complexity over space (LZcs) wherein time-adjacent “region series” were concatenated. LZct represents a calculation of the temporal entropy of each ROI, whereas LZcs represents a calculation of the spatial entropy at each timepoint. The original publication ³² reported only LZcs, but LZct is also described in ⁴⁷ whom Varley and colleagues reference as the source of their methods.

Statistical Model

Effects of psilocybin on brain entropy metrics were estimated using a linear mixed effects model with relevant R packages, i.e., *predictmeans* (v1.0.6), *lme4* (v1.1.30), *nlme* (v3.1.157), *lmerTest* (v3.1.3) and *LMMstar* (v0.7.6). We regressed each metric against each of the three measures (PPL, SDI, or Occ_{2A}) separately with a subject-specific random intercept and adjusting for motion, age, sex, and scanner. A test statistic for the association between metric and measure was obtained using the Wald statistic. To ensure adequate control of the family-wise error rate (FWER) across regions within each of the 13 metrics, (e.g., 17 networks for one time scale of multi-scale sample entropy), we calculate p_{FWER} adjusted using the maxT test method ⁴² in a permutation framework similar to ⁷⁹, employing 10000 permutations. As such, if observed data superseded all permutations, the p-value is reported as $p < 0.0001$. “Motion” reflects the framewise displacement computed using the Artifact Detection Toolbox (ART) (see Supplementary Text) and “scanner” controls for MR scanner, of which there were two. We do not adjust p-values across metrics, nor across SDI, PPL and Occ_{2A}; unadjusted p-values are reported for non-regional metrics as p_{perm} . We defined findings as statistically significant if they were associated with all three psilocybin effects, SDI, PPL and Occ_{2A} (collectively summarised “PsiFx”) at $p_{perm} < 0.05$ for non-regional metrics or $p_{FWER} < 0.05$ for regional metrics. Effect sizes are reported as Pearson’s correlation coefficient between the partial residuals of the entropy metrics (adjusted for covariates using the mixed-model described above) and each of PsiFx. The strength of Pearson’s correlation coefficients for significant associations are described as “weak” (≤ 0.3), “moderate” (> 0.3 and ≤ 0.6), or “strong” (> 0.6) as previously defined ⁸⁰.

Moderating Effect of Scanner

Our data were collected on one of two MRI scanners. In order to investigate whether scanner choice had an impact on the estimated relation between PPL and entropy moderating effects of scanner were explored in separate models that included the scanner-x-PPL interaction as an additional covariate.

Correlation Between Metrics

Simple Pearson correlation coefficients were calculated between each whole-brain entropy metric pair as well as with motion. Of the two graph theory metrics requiring thresholding, the threshold producing a mean degree of 27 was used. For the motif-connectivity distribution, 15 and 100 second windows were selected to represent fast and slow dynamics, respectively. P-values were adjusted using Bonferroni correction⁸¹. All scans remaining after pre-processing were used in these analyses.

Effect of Parcellation

To explore parcellation effects on outcomes, all entropy metrics were evaluated using the Schaefer 100 region atlas with 16 subcortical regions from the Tian atlas^{43,44}. For metrics using network definitions, the Yeo 7-network atlas was applied as a common atlas.

Effect of Pre-processing Pipelines

To explore the effect of pre-processing decisions on the associations between PsiFx and brain entropy metrics, analyses were repeated for six additional pre-processing pipelines. Each pre-processing pipeline was run on the data parcellated as described in the section “Effect of parcellation” i.e., 116 ROIs assigned to seven networks. Each pipeline changed one variable from the “reference” pipeline. These were as follows: 1) adding global signal regression, 2) removing the low-pass 0.09 Hz filter (i.e., not removing high-frequency signal), 3) expanding the 12-motion regressors to include squares of the derivatives (i.e., Volterra expansion), 4) not regressing out flagged volumes 5) regressing flagged volumes with a stricter threshold ($z > 3$ or motion $> 0.5\text{mm}$), (6) applying a narrower bandpass filter (0.03-0.07 Hz).

Code and Data Availability

We shared relevant analysis scripts with original authors, hoping to ensure as much as possible that our computations aligned with original reports; we are thankful for the feedback we received. All functions used to derive entropy estimates from pre-processed data have been compiled into the "Copenhagen Brain Entropy Toolbox" (CopBET), a Matlab-based toolbox that can be found here: <https://github.com/anders-s-olsen/CopBET>. The permutation testing code is also available here. Code for other statistical analyses and figures can be made available upon request. The data that support the findings of this study are available from the corresponding author upon request to the CIMBI database⁸².

Acknowledgements

A sincere thank you to Andrea Luppi, Enzo Tagliazucchi, Alexander Lebedev, Manoj Doss, Thomas Varley, and Parker Singleton for their advice and feedback regarding their entropy metrics, including advice from Drs Doss and Varley to not use their entropy metrics, as they no longer believed them to be valid, which we appreciate, but disregarded.

Conflict Statement

DEWM salary is supported by an unrestricted grant from COMPASS Pathways who have no involvement in the preparation or conception of this manuscript or related data collection. MKM has received an honorarium as a speaker for H. Lundbeck. GMK has served as a consultant for Sanos, Gilgamesh, Onsero, Pangea, Abbvie, PureHealthTech, and has received honoraria as speaker for H. Lundbeck and Sage Therapeutics.

Author Contributions

DEWM conceptualised the manuscript idea, collected data, performed analyses, and wrote the manuscript. ASO conceptualised the manuscript idea, performed analyses, prepared the CopBET, and wrote the manuscript. BO supported statistical analyses and related software. DSS facilitated, supervised, and performed data collection. SA performed data collection. MKM conceptualised the original study, and facilitated and performed data collection. GMK obtained core study funding, conceptualised the original study, and provided feedback on the project. PMF conceptualised the original study, facilitated data collection, and supervised data analysis and manuscript writing. All co-authors reviewed the manuscript, provided feedback, and approved the final version.

References

1. Becker, A. M. *et al.* Acute Effects of Psilocybin After Escitalopram or Placebo Pretreatment in a Randomized, Double-Blind, Placebo-Controlled, Crossover Study in Healthy Subjects. *Clin. Pharmacol. Ther.* **111**, 886–895 (2022).
2. Madsen, M. K. *et al.* Psychedelic effects of psilocybin correlate with serotonin 2A receptor occupancy and plasma psilocin levels. *Neuropsychopharmacology* **44**, 1328–1334 (2019).
3. Nichols, D. E. Psychedelics. *Pharmacol. Rev.* (2016) doi:10.1124/pr.115.011478.
4. Wallach, J. *et al.* Identification of 5-HT_{2A} receptor signaling pathways associated with psychedelic potential. *Nat. Commun.* **14**, 8221 (2023).
5. Anderson, B. T. *et al.* Psilocybin-assisted group therapy for demoralized older long-term AIDS survivor men: An open-label safety and feasibility pilot study. *EClinicalMedicine* **27**, 100538 (2020).
6. Bogenschutz, M. P. *et al.* Percentage of Heavy Drinking Days Following Psilocybin-Assisted Psychotherapy vs Placebo in the Treatment of Adult Patients With Alcohol Use Disorder. *JAMA Psychiatry* **79**, 953 (2022).
7. Carhart-Harris, R. *et al.* Trial of Psilocybin versus Escitalopram for Depression. *N. Engl. J. Med.* **384**, 1402–1411 (2021).
8. Carhart-Harris, R. L. *et al.* Psilocybin with psychological support for treatment-resistant depression: six-month follow-up. *Psychopharmacology (Berl.)* **235**, 399–408 (2018).
9. Goodwin, G. M. *et al.* Single-Dose Psilocybin for a Treatment-Resistant Episode of Major Depression. *N. Engl. J. Med.* **387**, 1637–1648 (2022).
10. Griffiths, R. R. *et al.* Psilocybin produces substantial and sustained decreases in depression and anxiety in patients with life-threatening cancer: A randomized double-blind trial. *J. Psychopharmacol. (Oxf.)* **30**, 1181–1197 (2016).
11. Holze, F., Gasser, P., Müller, F., Dolder, P. C. & Liechti, M. E. Lysergic Acid Diethylamide–Assisted Therapy in Patients With Anxiety With and Without a Life-Threatening Illness: A Randomized,

- Double-Blind, Placebo-Controlled Phase II Study. *Biol. Psychiatry* (2022) doi:10.1016/j.biopsych.2022.08.025.
12. Johnson, M. W., Garcia-Romeu, A. & Griffiths, R. R. Long-term follow-up of psilocybin-facilitated smoking cessation. *Am. J. Drug Alcohol Abuse* **43**, 55–60 (2017).
 13. Griffiths, R. R. *et al.* Psilocybin occasioned mystical-type experiences: Immediate and persisting dose-related effects. *Psychopharmacology (Berl.)* **218**, 649–665 (2011).
 14. McCulloch, D. E.-W. *et al.* Psilocybin-Induced Mystical-Type Experiences are Related to Persisting Positive Effects: A Quantitative and Qualitative Report. *Front. Pharmacol.* **13**, 1–17 (2022).
 15. Schmid, Y. & Liechti, M. E. Long-lasting subjective effects of LSD in normal subjects. *Psychopharmacology (Berl.)* **235**, 535–545 (2018).
 16. McCulloch, D. E.-W. *et al.* Psychedelic resting-state neuroimaging: A review and perspective on balancing replication and novel analyses. *Neurosci. Biobehav. Rev.* **138**, 104689 (2022).
 17. Doss, M. K. *et al.* Models of psychedelic drug action: modulation of cortical-subcortical circuits. *Brain* (2021) doi:10.1093/brain/awab406.
 18. Carhart-Harris, R. L. The entropic brain - revisited. *Neuropharmacology* **142**, 167–178 (2018).
 19. Carhart-Harris, R. L. *et al.* The entropic brain: A theory of conscious states informed by neuroimaging research with psychedelic drugs. *Front. Hum. Neurosci.* **8**, 1–22 (2014).
 20. Shannon, C. E. A mathematical theory of communication. *Bell Syst. Tech. J.* **27**, 379–423 (1948).
 21. Delgado-Bonal, A. & Marshak, A. Approximate Entropy and Sample Entropy: A Comprehensive Tutorial. *Entropy* **21**, 541 (2019).
 22. Lempel, A. & Ziv, J. On the Complexity of Finite Sequences. *IEEE Trans. Inf. Theory* **22**, 75–81 (1976).
 23. Richman, J. S. & Moorman, J. R. Physiological time-series analysis using approximate entropy and sample entropy maturity in premature infants Physiological time-series analysis using approximate entropy and sample entropy. *Am. J. Physiol. Heart Circ. Physiol.* **278**, H2039–H2049 (2000).

24. Ziv, J. & Lempel, A. Compression of individual sequences via variable-rate coding. *IEEE Trans. Inf. Theory* **24**, 530–536 (1978).
25. Rubinov, M. & Sporns, O. Complex network measures of brain connectivity: Uses and interpretations. *NeuroImage* **52**, 1059–1069 (2010).
26. Kringelbach, M. L. *et al.* Dynamic coupling of whole-brain neuronal and neurotransmitter systems. *Proc. Natl. Acad. Sci.* **117**, 9566–9576 (2020).
27. Lebedev, A. V. *et al.* Finding the self by losing the self: Neural correlates of ego-dissolution under psilocybin: Finding the Self by Losing the Self. *Hum. Brain Mapp.* **36**, 3137–3153 (2015).
28. Tagliazucchi, E., Carhart-Harris, R., Leech, R., Nutt, D. & Chialvo, D. R. Enhanced repertoire of brain dynamical states during the psychedelic experience. *Hum. Brain Mapp.* **35**, 5442–5456 (2014).
29. Lebedev, A. V. *et al.* LSD-induced entropic brain activity predicts subsequent personality change: LSD-Induced Entropic Brain Activity. *Hum. Brain Mapp.* **37**, 3203–3213 (2016).
30. Luppi, A. I. *et al.* LSD alters dynamic integration and segregation in the human brain. *NeuroImage* **227**, 117653 (2021).
31. Singleton, S. P. *et al.* Receptor-informed network control theory links LSD and psilocybin to a flattening of the brain’s control energy landscape. *Nat. Commun.* **13**, 5812 (2022).
32. Varley, T. F., Carhart-Harris, R., Roseman, L., Menon, D. K. & Stamatakis, E. A. Serotonergic psychedelics LSD & psilocybin increase the fractal dimension of cortical brain activity in spatial and temporal domains. *NeuroImage* **220**, 117049 (2020).
33. Felipe, H. *et al.* The von Neumann entropy for the Pearson correlation matrix: A test of the entropic brain hypothesis. in (2021).
34. Viol, A. *et al.* Characterizing Complex Networks Using Entropy-Degree Diagrams: Unveiling Changes in Functional Brain Connectivity Induced by Ayahuasca. *Entropy* 2019 Vol 21 Page 128 **21**, 128 (2019).

35. Viol, A., Palhano-Fontes, F., Onias, H., De Araujo, D. B. & Viswanathan, G. M. Shannon entropy of brain functional complex networks under the influence of the psychedelic Ayahuasca. *Sci. Rep.* **7**, 1–13 (2017).
36. Barrett, F. S., Doss, M. K., Sepeda, N. D., Pekar, J. J. & Griffiths, R. R. Emotions and brain function are altered up to one month after a single high dose of psilocybin. *Sci. Rep.* **10**, 2214 (2020).
37. Kung, Y.-C. *et al.* Cross-Scale Dynamicity of Entropy and Connectivity in the Sleeping Brain. *Brain Connect.* **12**, 835–845 (2022).
38. Maki-Marttunen, V., Diez, I., Cortes, J., Chialvo, D. & Villarreal, M. Disruption of transfer entropy and inter-hemispheric brain functional connectivity in patients with disorder of consciousness. *Front. Neuroinformatics* **7**, (2013).
39. Pappas, I., Adapa, R. M., Menon, D. K. & Stamatakis, E. A. Brain network disintegration during sedation is mediated by the complexity of sparsely connected regions. *NeuroImage* **186**, 221–233 (2019).
40. Chang, D. *et al.* Caffeine Caused a Widespread Increase of Resting Brain Entropy. *Sci. Rep.* **8**, 2700 (2018).
41. Doss, M. K. *et al.* The Acute Effects of the Atypical Dissociative Hallucinogen Salvinorin A on Functional Connectivity in the Human Brain. *Sci. Rep.* (2020) doi:10.1038/s41598-020-73216-8.
42. Westfall, P. H. & Troendle, J. F. Multiple Testing with Minimal Assumptions. *Biom. J. Biom. Z.* **50**, 745–755 (2008).
43. Tian, Y., Margulies, D. S., Breakspear, M. & Zalesky, A. Topographic organization of the human subcortex unveiled with functional connectivity gradients. *Nat. Neurosci.* (2020) doi:10.1038/s41593-020-00711-6.
44. Schaefer, A. *et al.* Local-Global Parcellation of the Human Cerebral Cortex from Intrinsic Functional Connectivity MRI. *Cereb. Cortex* (2018) doi:10.1093/cercor/bhx179.
45. Yang, A. C. *et al.* Decreased resting-state brain activity complexity in schizophrenia characterized by both increased regularity and randomness. *Hum. Brain Mapp.* **36**, 2174–2186 (2015).

46. Nichols, D. E. & Walter, H. The History of Psychedelics in Psychiatry. *Pharmacopsychiatry* **54**, 151–166 (2021).
47. Schartner, M. M., Carhart-Harris, R. L., Barrett, A. B., Seth, A. K. & Muthukumaraswamy, S. D. Increased spontaneous MEG signal diversity for psychoactive doses of ketamine, LSD and psilocybin. *Sci. Rep.* **7**, 46421 (2017).
48. Timmermann, C. *et al.* Human brain effects of DMT assessed via EEG-fMRI. *Proc. Natl. Acad. Sci.* **120**, e2218949120 (2023).
49. Timmermann, C. *et al.* Neural correlates of the DMT experience assessed with multivariate EEG. *Sci. Rep.* **9**, 16324 (2019).
50. Pallavicini, C. *et al.* Neural and subjective effects of inhaled N,N-dimethyltryptamine in natural settings. *J. Psychopharmacol. (Oxf.)* **35**, 406–420 (2021).
51. Murray, C. H. *et al.* Neural complexity is increased after low doses of LSD, but not moderate to high doses of oral THC or methamphetamine. *Neuropsychopharmacology* 1–9 (2024) doi:10.1038/s41386-024-01809-2.
52. Singleton, S. P. *et al.* Time-resolved network control analysis links reduced control energy under DMT with the serotonin 2a receptor, signal diversity, and subjective experience. *BioRxiv Prepr. Serv. Biol.* 2023.05.11.540409 (2023) doi:10.1101/2023.05.11.540409.
53. Toker, D. *et al.* Consciousness is supported by near-critical slow cortical electrodynamics. *Proc. Natl. Acad. Sci.* **119**, e2024455119 (2022).
54. Eckernäs, E., Timmermann, C., Carhart-Harris, R., Röshammar, D. & Ashton, M. N,N-dimethyltryptamine affects electroencephalography response in a concentration-dependent manner—A pharmacokinetic/pharmacodynamic analysis. *CPT Pharmacomet. Syst. Pharmacol.* **12**, 474–486 (2023).
55. Noble, S., Scheinost, D. & Constable, R. T. A decade of test-retest reliability of functional connectivity: A systematic review and meta-analysis. *NeuroImage* **203**, 116157 (2019).

56. Birn, R. M. *et al.* The effect of scan length on the reliability of resting-state fMRI connectivity estimates. *NeuroImage* **83**, 550–558 (2013).
57. Kundu, P. *et al.* Multi-echo fMRI: A review of applications in fMRI denoising and analysis of BOLD signals. *NeuroImage* **154**, 59–80 (2017).
58. Risk, B. B. *et al.* Which multiband factor should you choose for your resting-state fMRI study? *NeuroImage* **234**, 117965 (2021).
59. Demetriou, L. *et al.* A comprehensive evaluation of increasing temporal resolution with multiband-accelerated protocols and effects on statistical outcome measures in fMRI. *NeuroImage* **176**, 404–416 (2018).
60. Dyer, D. C. & Gant, D. W. Vasoconstriction Produced by Hallucinogens on Isolated Human and Sheep Umbilical Vasculature. *J. Pharmacol. Exp. Ther.* **184**, 366–375 (1973).
61. Holze, F., Becker, A. M., Kolaczynska, K. E., Duthaler, U. & Liechti, M. E. Pharmacokinetics and Pharmacodynamics of Oral Psilocybin Administration in Healthy Participants. *Clin. Pharmacol. Ther.* **113**, 822–831 (2023).
62. Carp, J. On the Plurality of (Methodological) Worlds: Estimating the Analytic Flexibility of fMRI Experiments. *Front. Neurosci.* **6**, (2012).
63. Van Essen, D. C. *et al.* The WU-Minn Human Connectome Project: An overview. *NeuroImage* (2013) doi:10.1016/j.neuroimage.2013.05.041.
64. Madsen, M. K. *et al.* Psilocybin-induced changes in brain network integrity and segregation correlate with plasma psilocin level and psychedelic experience. *Eur. Neuropsychopharmacol.* **50**, 121–132 (2021).
65. Olsen, A. S. *et al.* Psilocybin modulation of time-varying functional connectivity is associated with plasma psilocin and subjective effects. *NeuroImage* 119716 (2022) doi:10.1016/J.NEUROIMAGE.2022.119716.
66. Whitfield-Gabrieli, S. & Nieto-Castanon, A. Conn: A Functional Connectivity Toolbox for Correlated and Anticorrelated Brain Networks. *Brain Connect.* (2012) doi:10.1089/brain.2012.0073.

67. Behzadi, Y., Restom, K., Liao, J. & Liu, T. T. A component based noise correction method (CompCor) for BOLD and perfusion based fMRI. *NeuroImage* (2007) doi:10.1016/j.neuroimage.2007.04.042.
68. Craddock, R. C., James, G. A., Holtzheimer, P. E., Hu, X. P. & Mayberg, H. S. A whole brain fMRI atlas generated via spatially constrained spectral clustering. *Hum. Brain Mapp.* (2012) doi:10.1002/hbm.21333.
69. Blondel, V. D., Guillaume, J.-L., Lambiotte, R. & Lefebvre, E. Fast unfolding of communities in large networks. *J. Stat. Mech. Theory Exp.* **2008**, P10008 (2008).
70. Bullmore, E. & Sporns, O. Complex brain networks: graph theoretical analysis of structural and functional systems. *Nat. Rev. Neurosci.* **10**, 186–198 (2009).
71. Desikan, R. S. *et al.* An automated labeling system for subdividing the human cerebral cortex on MRI scans into gyral based regions of interest. *NeuroImage* (2006) doi:10.1016/j.neuroimage.2006.01.021.
72. Smith, S. M. *et al.* Correspondence of the brain's functional architecture during activation and rest. *Proc. Natl. Acad. Sci. U. S. A.* (2009) doi:10.1073/pnas.0905267106.
73. Cabral, J. *et al.* Cognitive performance in healthy older adults relates to spontaneous switching between states of functional connectivity during rest. *Sci. Rep.* **7**, 5135 (2017).
74. Tzourio-Mazoyer, N. *et al.* Automated anatomical labeling of activations in SPM using a macroscopic anatomical parcellation of the MNI MRI single-subject brain. *NeuroImage* (2002) doi:10.1006/nimg.2001.0978.
75. Shen, X., Tokoglu, F., Papademetris, X. & Constable, R. T. Groupwise whole-brain parcellation from resting-state fMRI data for network node identification. *NeuroImage* (2013) doi:10.1016/j.neuroimage.2013.05.081.
76. Lindquist, M. A., Xu, Y., Nebel, M. B. & Caffo, B. S. Evaluating Dynamic Bivariate Correlations in Resting-state fMRI: A comparison study and a new approach. *NeuroImage* **101**, 531–546 (2014).
77. Daducci, A. *et al.* The Connectome Mapper: An Open-Source Processing Pipeline to Map Connectomes with MRI. *PLOS ONE* **7**, e48121 (2012).

78. Yeo, B. T. *et al.* The organization of the human cerebral cortex estimated by intrinsic functional connectivity. *J. Neurophysiol.* (2011) doi:10.1152/jn.00338.2011.
79. Lee, O. E. & Braun, T. M. Permutation tests for random effects in linear mixed models. *Biometrics* **68**, 486–493 (2012).
80. Akoglu, H. User's guide to correlation coefficients. *Turk. J. Emerg. Med.* **18**, 91–93 (2018).
81. Haynes, W. Bonferroni Correction. in *Encyclopedia of Systems Biology* 154–154 (Springer New York, New York, NY, 2013). doi:10.1007/978-1-4419-9863-7_1213.
82. Knudsen, G. M. *et al.* The Center for Integrated Molecular Brain Imaging (Cimbi) database. *NeuroImage* **124**, 1213–1219 (2016).

Supplementary Material

Supplementary Text

1. Study Design
2. Plasma Psilocin Level Quantification
3. BOLD scanning parameters
4. BOLD data preprocessing
5. fMRI Quality Control and missing data
6. Partial Residual Plots
7. In-depth Comparison with Tagliazucchi 2015
8. Pre-registration
9. Funding
10. Copenhagen Brain Entropy Toolbox

Supplementary Figures

1. Time courses of subjective drug intensity and plasma psilocin level
2. Intra-network Synchrony Distribution regression plots
3. Tagliazucchi peak vs baseline plot replication
4. Relation between motion and PPL / SDI

Supplementary Tables

1. Previous papers
2. Regional metrics (max T corrected)
3. Whole-brain metrics
4. Correlation between whole-brain entropy metrics
5. Common atlas results
6. Moderating effect of scanner
7. Preprocessing pipeline comparisons
8. Summary of results across all preprocessing pipelines
9. Detailed results across all preprocessing pipelines

Supplementary Text

Study Design

All participants were screened to exclude individuals with significant somatic disease, neurological disorders and/or psychiatric disease using the Mini-International Neuropsychiatric Interview (Danish translation version 6.0.0). Prior to inclusion, participants received written and verbal descriptions of the study protocol, including the expected effects of psilocybin and potential side effects of administration; all participants provided written consent prior to study participation.

Exclusion criteria were 1) present or previous personal or family (first degree relatives) history of psychiatric disease (DSM axis 1 or WHO ICD-10 diagnostic classification) including substance misuse disorder; 2) Present or previous neurological condition/disease, significant somatic disease or any intake of drugs suspected to influence test results; 3) nonfluent Danish language skills; 4) vision or hearing impairment; 5) learning disability; 6) pregnancy; 7) breastfeeding; 8) MRI contraindications; 9) alcohol or drug abuse 10) allergy to test drugs; 11) significant exposure to radiation within the past year (e.g., medical imaging investigations); 12) intake of QT-prolonging medication or electrocardiogram (ECG) results indicative of heart disease, 13) history of significant adverse response to a hallucinogenic drug. 14) use of hallucinogenic drugs less than 6 months prior to inclusion; 15) blood donation less than 3 months before project participation; 16) body weight less than 50 kg; 17) low plasma ferritin levels ($< 12 \mu\text{g/L}$).

The order of psilocybin vs. ketanserin administration was balanced across participants as well as possible, drug sessions were separated by at least three weeks. The data presented here is part of a study approved by the ethics committee for the Capital Region of Copenhagen (journal identifier: H-16028698, amendments: 56023, 56967, 57974, 59673, 60437, 62255) and Danish Medicines Agency (EudraCT identifier: 2016-004000-61, amendments: 2017014166, 2017082837, 2018023295).

Participants were asked to refrain from alcohol the night before intervention days and to eat a light breakfast and refrain from caffeine intake on the morning of intervention. Prior to intervention days, a urine sample was drawn and screened for amphetamines, opioids, benzodiazepines, barbiturates, tetrahydrocannabinol, cocaine, ketamine, phencyclidine, and gamma hydroxybutyrate (Rapid Response, BTNX Inc., Markham, Canada), a blood sample and an electrocardiogram were taken to ensure that individuals were in good overall physiological health (e.g., absent evidence for a prolonged QT interval).

On the day upon which participants received psilocybin, they arrived in the morning, completed state questionnaires and a pre-drug MRI scan session. Following a brief conversation with the psychological support personnel (two people) present for the psilocybin administration day, participants received psilocybin in a room adjacent to the MRI scanner. Participants could lay on a bed or sit in a chair in this room and music was played after psilocybin administration but not during scanning.

Participants were financially compensated for the hours spent taking part in the study.

Components of preparation, support and integration sessions

Preparation:

1. The purpose of the session
2. The participant's motivation for entering the study and expectancy management
3. The participant's personal background
4. Previous experience with psychedelics or altered states of consciousness
5. Information about possible effects of psilocybin
6. Tools for navigating the psychedelic experience, with a particular focus on the MR environment
7. The participant's social support-network and potential contact person
8. Practical road map of the intervention day, including rules for the study
9. Agreements regarding therapeutic touch and physical support

Intervention (before administration):

1. The purpose of the session, including any questions arising since preparation
2. Anchoring - and repetition of tools for navigating the experience
3. Support the participant in letting go of everyday tasks and preoccupations, including hand over of their mobile phone and helping with arrangements of various matters with the participant's family/contact person or social network
4. Repeating the practicalities of the intervention, including rules and agreements made during preparation
5. Administration of psilocybin

Intervention (end of day):

1. Drawing a mandala
2. Information about afterglow effects and making a plan for self-care upon arrival at home
3. Confirmation of time for integration session

Integration:

1. The purpose of the session
2. Integration wheel
3. Eliciting a full narrative about psychedelic experience
4. Witnessing and debriefing of difficult material
5. Relating the psychedelic experience to the participant's life going forward
6. Plan for self-care
7. Thoughts about ending the study and information about the possibility of contacting the psychologists, if needed
8. Any questions that the participant may have

Plasma Psilocin Level Quantification

Plasma psilocin level was measured using ultra performance liquid chromatography and tandem mass spectrometry, reflecting free, unconjugated psilocin and not glucuronidated psilocin ².

7 mL blood samples were drawn from an intravenous access in the antecubital vein and collected in EDTA vials, placed on ice, centrifuged, and plasma was aliquoted and stored at -20 or -80°C. Psilocin was obtained from Lipomed (Arlesheim, Switzerland) and Cerilliant (Round Rock, TX, USA) for calibrator and control batches, respectively, while the deuterated internal standard (IS) psilocin-d10 was from Cerilliant. Acetonitrile, methanol HPLC grade and water were obtained from Fishers Scientific (Loughborough, UK). Ascorbic acid was obtained from VWR (Hassrode, Belgium).

Stock solution (1000 mg/l) of psilocin and IS were prepared in acetonitrile and stored in amber ampoules at -20°C until use. Working standard solutions from 0.5 µg/l to 1000 µg/l were freshly prepared in 50% methanol in water for each analysis, and the IS-solution was 100 µg/l in 50% methanol. For preparation of calibration standards and quality controls blank plasma was preserved with 1% fluoride and stored at -20°C. Two quality controls (QC) were prepared at low (5.0 µg/kg) and high (50 µg/kg) levels and stored at -80°C. These two along with a freshly spiked blank plasma sample at 2.5 µg/kg were analysed in each run.

Protein precipitation was performed on a fully automated Tecan Freedom EVO 200 robotic platform (Tecan group Ltd, Männedorf, Switzerland) that included all pipetting, centrifugation, and evaporation steps. Each plasma sample (100 µg) was transferred to a 96-well 2.0 ml deep-well plate and 20 µl IS-solution was added to each well, followed by precipitation with 700 µl acetonitrile and shaking. The samples were centrifuged at 1000 g for 10 min, and the supernatant was evaporated to dryness under a stream of nitrogen at 35°C. Afterwards, the samples were reconstituted in 100 µl mixture of 12.5% methanol:12.5% acetonitrile:75% 0.05% formic acid in water, shaken and centrifuged again. Finally, the supernatant was transferred to a 96-well plate and 1 µl was injected into the chromatographic system.

Chromatographic separation was performed on a HSS T3 column (100 x 2.1 mm, 1.8µm, Waters, Milford, MA, USA) using an ACQUITY Ultra Performance Liquid Chromatography system (UPLC) from Waters. The mobile phase was composed of solvent A: 1 mM ammonium formate in 0.1% formic acid in water and B: 0.1% formic acid in 1:1 mixture of acetonitrile:methanol. The column was maintained at 45°C with a flow 0.4 ml/min, and a gradient elution was applied from 2% to 100% B within 3.2 min with a total analysis time of 4.5 min. Detection was done by tandem mass spectrometry using an ACQUITY TQS from Waters. Ionisation was achieved by electrospray in positive mode, and the source temperature was set at 150°C and desolvation temperature at 600°C. Two transitions were used for psilocin, m/z 205 → 58 and 205 → 160, with a cone voltage of 20 V and collision energy at 14 and 18 eV, respectively. For the IS the transition was m/z 215 → 164 with cone 20 V and collision energy of 18 eV. Argon was used as collision gas at 0.45 Pa, and desolvation and cone gasflow were fixed at 1000 L/hr and 150 L/hr, respectively. Data were acquired and processed with MassLynx 4.2 software (Waters).

Quantification was performed by an eight-point linear calibration curve (0.1, 0.5, 1.0, 5.0, 25, 50, 100, 200 µg/kg) with weighting 1/x. Limits of detection (LOD) and quantification (LOQ) were 0.1 and 0.5 µg/kg, respectively, while the upper limit of quantification was 200 µg/kg. The overall process efficiency was found to be 63% based on an obtained extraction efficiency of 81% and matrix effect of 25% that the stable isotope labelled IS adjusted for. QC plasma samples were measured in each series with a RSD of 5% and an accuracy of 78% for the low level and less than 5% and an accuracy 89% for the high level. Similar performance was obtained with QCs preserved with 1 mM ascorbic acid demonstrating that stored plasma QCs at -80°C without ascorbic acid were stable for at least 6 months. The freshly spiked plasma QC at 2.5 µg/kg analysed in each series had a RSD of 13% and an accuracy of 88% (n = 11). For the final presentation of results, units of concentration (µg/kg) were converted into µg/L using a conversion factor of 1.02 kg per litre of plasma.

BOLD Scanning Parameters

Due to logistical constraints, MRI scans were acquired on one of two Siemens 3T MAGNETOM Prisma scanners (“Scanner A”, “Scanner B”). The first 15 participants were scanned on Scanner A, the final 13 participants were scanned on Scanner B, all participants completed all scans on a single scanner.

A high-resolution, T1-weighted 3D MPRAGE structural image was acquired (Scanner A: inversion time = 900 ms, TE = 2.58 ms, TR = 1900 ms, flip angle = 9°, in-plane matrix = 256x256, resolution = 0.9x0.9 mm, 224 slices; slice thickness = 0.9 mm, no gap, Scanner B: inversion time = 920 ms, TE = 2.41 ms, TR = 1810 ms, flip angle = 9°, in-plane matrix = 288 × 288, in-plane resolution = 0.8x0.8 mm, number of slices = 224, slice thickness = 0.8 mm).

BOLD fMRI data was obtained using a T2*-weighted gradient echo-planar imaging (EPI) sequence.

Scanner A: 64-channel head coil, TR = 2000 ms, TE = 30 ms, flip angle = 90°, in-plane matrix = 64x64 voxels, in-plane resolution=3.6x3.6 mm, number of slices = 32, slice thickness = 3.0 mm, gap = 0.75 mm, phase-encoding direction = AP, scan time = 10 minutes, volumes = 300.

Scanner B: 32-channel head coil, TR = 800 ms, TE = 37 ms, flip angle = 52°, in-plane matrix = 104x104 voxels, in-plane resolution = 2x2 mm, slices = 72, slice thickness = 2.0 mm, gap = 0, multi-band acceleration factor = 8, scan time = 10 minutes, volumes = 750 (n = 5) or 375 (n = 8, due to an acquisition error).

BOLD Data Preprocessing

BOLD data were preprocessed in SPM12 (<http://www.fil.ion.ucl.ac.uk/spm>) and denoised using the CONN toolbox ³ using MATLAB (The Mathworks, inc., version 2019b 9.7.0). Preprocessing pipelines were identical for both scanners unless specified. We applied slice-timing correction (scanner A only because scanner B used multi-band), data were unwarped and realigned, structural scans were co-registered to functional data. High-resolution structural images were segmented into grey-matter, white-matter and CSF-maps; functional data were normalised to MNI152 space based on parameters estimated during the segmentation procedure and smoothed using a 6mm FWHM gaussian kernel. Denoising included linear

detrending, aCompCor regression of white-matter and CSF time-series (first five components for each and their first derivatives) ⁴ as well as regression of 6-motion parameters and their first derivatives, and scrubbing of volumes flagged using the artifact detection tool (ART, https://www.nitrc.org/projects/artifact_detect, global signal > 4 or motion > 2). Some analyses utilised unsmoothed data to align with previous methods (Intra-network synchrony, Motif-connectivity distribution, Multi-scale Sample Entropy.). A bandpass filter of 0.008 - 0.09 Hz was applied. Regional time-series were averaged in CONN using analysis-specific atlases. Following preprocessing and denoising and to align the temporal frequency between the two scanners, scanner B time-series were temporally downsampled to match the TR of scanner A (i.e., 2s) using the MATLAB command “downsample”.

fMRI Quality Control and Missing Data

All BOLD data were visually inspected to ensure accurate co-registration to MNI space. Connectivity matrices and regional time-series were visually inspected for artefacts or missing data.

Of the 130 resting-state fMRI scan sessions acquired during psilocybin intervention days for the 28 participants (76 Scanner A and 54 Scanner B), Nine scans and no participants were excluded from analyses: two scans from one participant because of excessive head motion through the scan session (>50% of volumes flagged for censoring), one scan from one participant due to technical problems with data acquisition, two scans from one participant due to 1) interrupted scan and 2) technical problems with data acquisition, one scan each from three participants due to interrupted scans. Thus, 121 scan sessions were included in analyses. One scan session did not have an accompanying measure of PPL, another was without a measure of SDI, these individual scans were excluded from these respective analyses.

Partial Residual Plots

To display the relation between PPL and each whole-brain entropy metric, plots were constructed that display PPL values (in $\mu\text{g/L}$) on the x-axis and adjusted residual entropy values on the y-axis. These are adjusted by removing the covariate effects. This was performed by taking the raw entropy score and deducting the beta of each covariate multiplied by the relevant value of that covariate for each scan.

In-depth Comparison with Tagliazucchi 2015

We do not observe a significant relation between psilocybin effects and hippocampal-ACC motif distribution entropy, calculated as described in ⁵. The original publication describes a significant difference comparing both pre-psilocybin vs post-psilocybin and post-psilocybin vs post-placebo at longer (c.75-150 second) windows. Unfortunately, the entropy values presented by Tagliazucchi and colleagues leave significant cause for concern. They use non-overlapping windows, the shortest window-lengths they used were 10-seconds, and their scans were 300-seconds long. Thus, at the shortest window lengths they would observe 30 brain states whereas at the longest window length (150-seconds) only two events would be observed. Thus at the longest window-lengths, there are two possible Shannon entropy values, one (i.e., two different states $-2 \times 0.5 \times \log_2(0.5) = 1$) and zero (i.e., two of the same state $-1 \times 1 \times \log_2(1) = 0$). Thus, it is mathematically impossible to have Shannon entropy values in excess of 1, which are reported in this original publication. Additionally, one would expect the Shannon entropy values at short window-lengths

to be higher than those at long window-lengths, as there are more events in the histogram of motifs (i.e., 5 of state 1, 3 of state 2, 10 of state 3, 6 of state 4, 6 of state 5, Shannon entropy = 2.2 bits) but they report window-lengths approaching zero as window length approaches 10-seconds. Although unlike the high entropy values at long window length, this is mathematically possible, as the same state may reoccur with increasing frequency at shorter window-lengths (i.e., 29 of state 1, 1 of state 2, Shannon entropy = 0.21), but this seems highly unlikely and is contrary to what we observe (Supplementary Figure S3).

Pre-registration

This study was pre-registered on the 3rd of August 2022 and the pre-registration document can be viewed here <https://aspredicted.org/bw8y7.pdf>. Notably, three of 12 papers were identified after pre-registration and therefore not described therein.

Funding

The collection of the data reported here, but not the current analysis work was supported by Innovation Fund Denmark (grant number 4108–00004B), Independent Research Fund Denmark (grant number 6110–00518B), and Ester M. og Konrad Kristian Sigurdssons Dyreværnsfond (grant number 850–22–55,166–17-LNG). MKM was supported during data collection through a stipend from Rigshospitalet’s Research Council (grant number R130-A5324). BO has received funding from the European Union’s Horizon 2020 research and innovation program under the Marie Skłodowska-Curie grant agreement No 746,850. DEWM salary is supported by COMPASS Pathways Ltd. The funders had no role in study design, data collection and analysis, decision to publish or preparation of the manuscript.

Inclusivity and Ethics statement

All aspects of this study were conducted with rigorous adherence to ethical guidelines as evaluated by the Ethics Committee for the Capital Region of Copenhagen and Danish Medicines Agency. Data management was undertaken with utmost care. The secure CIMBI database was employed for all data storage, ensuring participant confidentiality and robust protection of personal data. The conduct of the clinical trial was overseen by the Good Clinical Practice (GCP) unit, ensuring that all procedures adhered to the highest ethical and professional standards.

Copenhagen Brain Entropy Toolbox

The twelve described entropy metrics have been collected in the MATLAB-based “Copenhagen Brain Entropy Toolbox” (CopBET) located here: <https://github.com/anders-s-olsen/CopBET>. The toolbox was developed in MATLAB R2018b and includes external dependencies to the Brain Connectivity Toolbox (BCT) v19.03.03 (<https://sites.google.com/site/bctnet/>), the Complexity Toolbox (LOFT) (<https://loft-lab.org/index-5.html>), and Martin Lindquist’s Dynamic Conditional Correlation toolbox (https://github.com/canlab/Lindquist_Dynamic_Correlation/tree/master/DCC_toolbox). The CopBET has further been tested to ensure functionality using Matlab versions R2019b and R2023a. However, it does not work using versions prior to R2018b. The CopBET contains individual functions for each of the 12 metrics

as well as a script that may be used to test the functions using example data.

An example call to the toolbox could be:

```
>> output_table = CopBET_function(input_table)
```

Here, 'input_table' is a MATLAB-table where each row in the first column contains a regional timeseries, i.e., is a matrix $n \times p$, where n is the number of acquired samples for the scan in question, and p is the number of regions in the atlas used for parcellation. Three of the functions take the path to (denoised) voxel-wise timeseries (4D-nifti file) as inputs instead of regional timeseries. The output, 'output_table' will consist of entropy-values for each scan in 'input_table'. The function name 'CopBET_function' may be replaced with the name of any of the 12 included functions. All atlases described in this paper are also included in the repository in 2mm MNI152 space. Each function outputs either one or several entropy values for each scan, e.g., for each "mean degree" for the degree distribution entropy.

Supplementary Figures

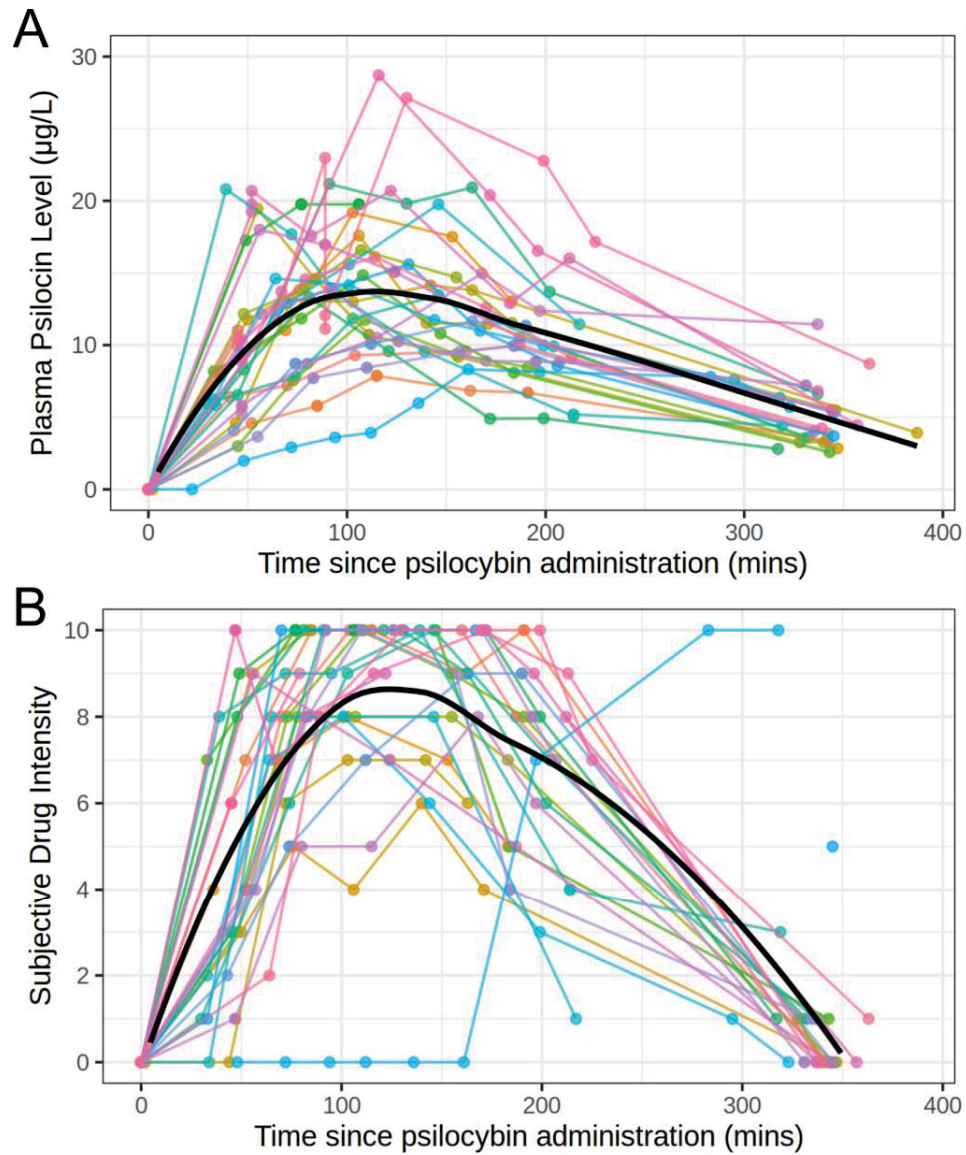


Figure S1: Time-course of (A) plasma psilocin levels and (B) subjective drug intensity per participant. Each colour represents a participant and the black line represents a locally estimated scatter-plot smoothing across the sample. Pre-drug PPL measurements are set at 0 mins. fMRI scans were performed before drug administration and then at approximately +40, +80, +120 and +300 minutes.

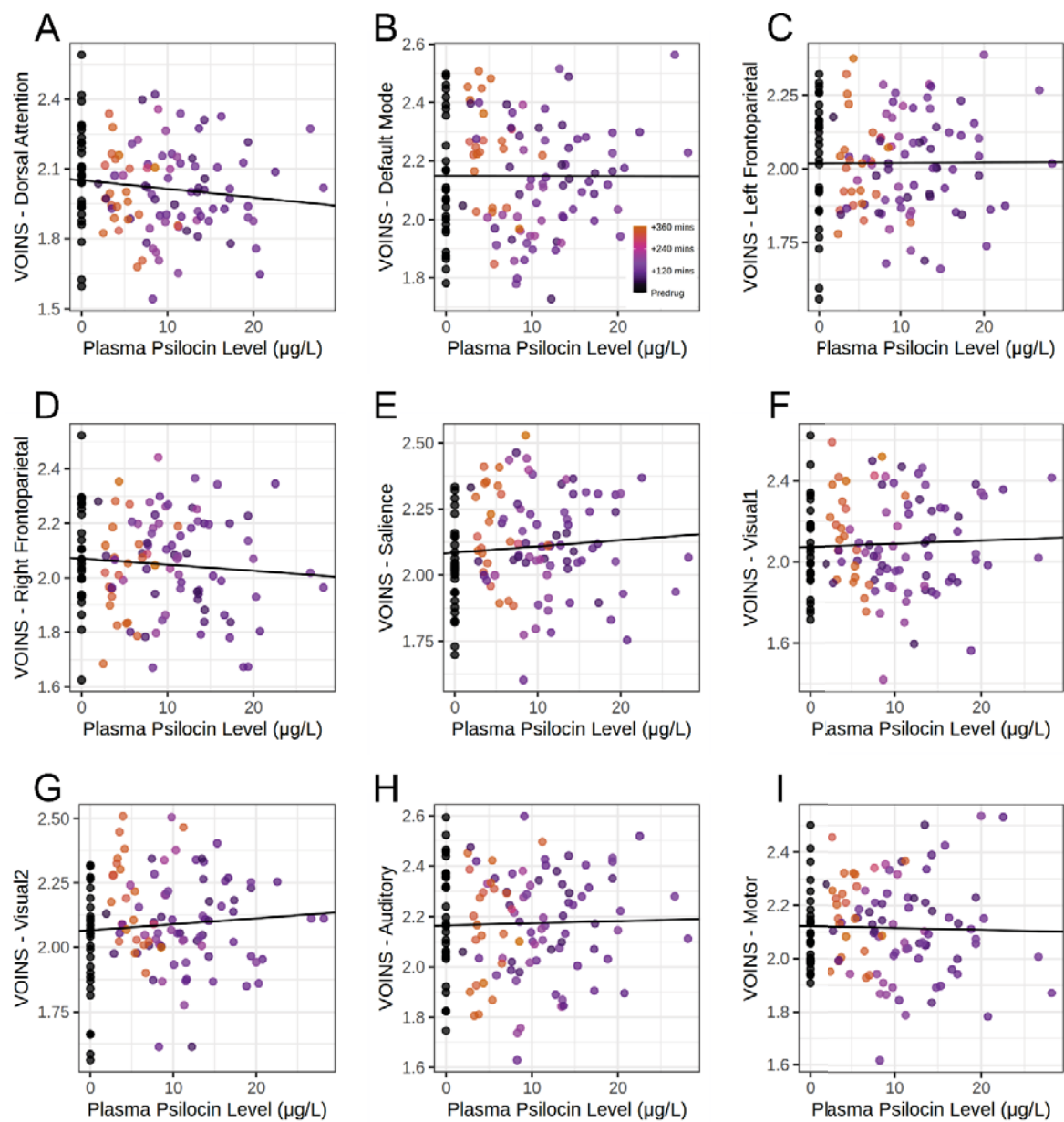


Figure S2: Scatter plots describing the relation between variance of intra-network synchrony (VOINS) of dynamic BOLD activity and plasma psilocin level, for each network. Y-axis values are adjusted for age, sex, MR scanner and motion. All $p_{FWER} > 0.98$.

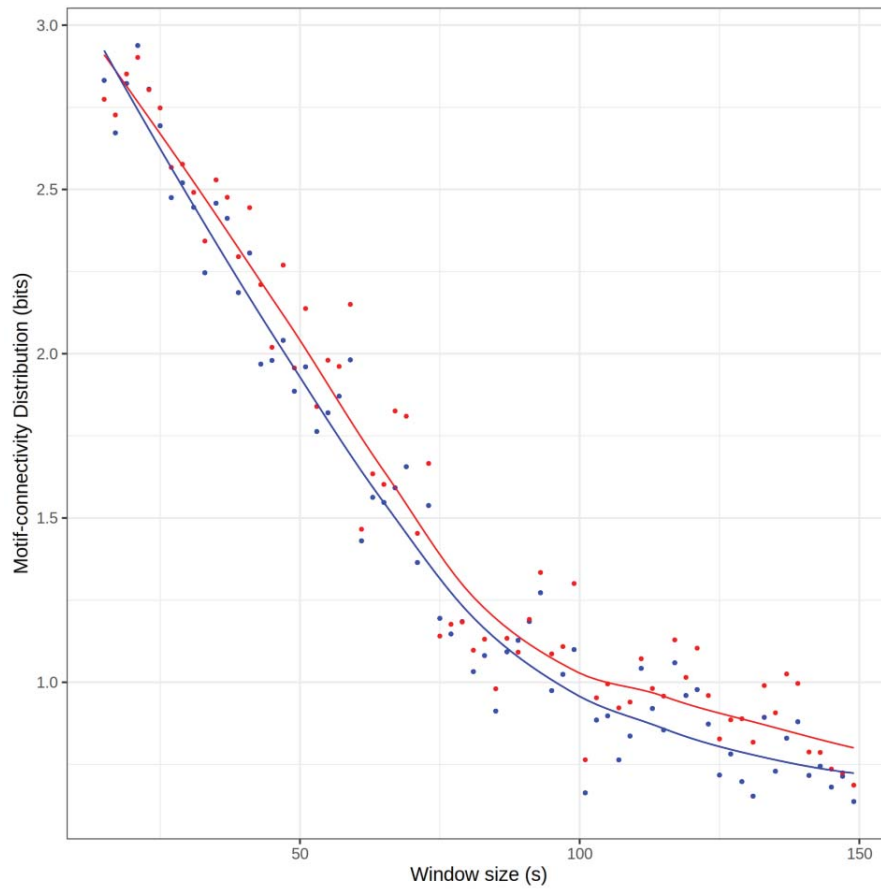


Figure S3: Scatter plot of motif-connectivity distribution entropy with overlaid locally estimated scatter-plot smoothing showing the relation between window-size and entropy derived from the linear model. Blue points and line represent the intercept value from the linear model comparing PPL and entropy (i.e., model estimated entropy when PPL = 0). The red points and line represent model estimated entropy when PPL = 15 $\mu\text{g/L}$, approximately PPL at peak drug effects. Note the discrepancy in y-axis values and that we observed decreasing entropy with increasing window size vis-a-vis Figure 5A from Tagliazucchi et al., 2015.

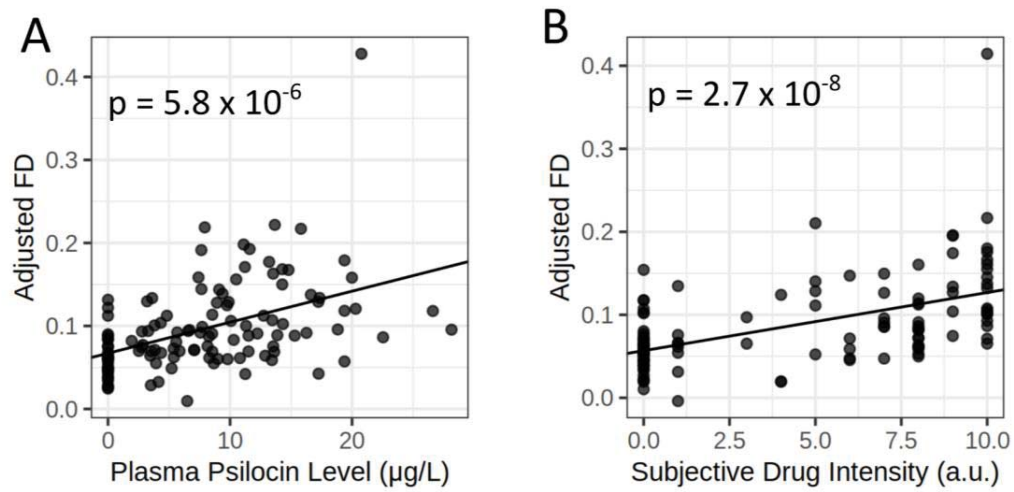


Figure S4: Scatter plots displaying the adjusted linear relation between motion (i.e., framewise displacement, FD) and (A) PPL or (B) SDI. Y-axis values are partial residuals adjusted for covariates, i.e., age, sex, scanner and subject. P-values are uncorrected. Pearson's Rho are 0.33 for PPL and 0.43 for SDI.

References

1. Knudsen, G. M. *et al.* The Center for Integrated Molecular Brain Imaging (Cimbi) database. *NeuroImage* **124**, 1213–1219 (2016).
2. Kolaczynska, K. E., Liechti, M. E. & Duthaler, U. Development and validation of an LC-MS/MS method for the bioanalysis of psilocybin's main metabolites, psilocin and 4-hydroxyindole-3-acetic acid, in human plasma. *J. Chromatogr. B* **1164**, 122486 (2021).
3. Whitfield-Gabrieli, S. & Nieto-Castanon, A. Conn: A Functional Connectivity Toolbox for Correlated and Anticorrelated Brain Networks. *Brain Connect.* (2012) doi:10.1089/brain.2012.0073.
4. Behzadi, Y., Restom, K., Liau, J. & Liu, T. T. A component based noise correction method (CompCor) for BOLD and perfusion based fMRI. *NeuroImage* (2007) doi:10.1016/j.neuroimage.2007.04.042.
5. Tagliazucchi, E., Carhart-Harris, R., Leech, R., Nutt, D. & Chialvo, D. R. Enhanced repertoire of brain dynamical states during the psychedelic experience. *Hum. Brain Mapp.* **35**, 5442–5456 (2014).



DECLARATION OF CO-AUTHORSHIP

The declaration is for PhD students and must be completed for each conjointly authored article. Please note that if a manuscript or published paper has eleven or less authors, all authors must sign a declaration of co-authorship. If it has twelve or more authors, only the PhD student, the corresponding author(s), the senior author, and the principal supervisor need to sign the declaration of co-authorship.


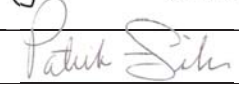
1. Declaration by	
Name of PhD student	Drummond McCulloch
E-mail	Drummond.mcculloch@nru.dk
Name of principal supervisor	Patrick Fisher
Title of the PhD thesis	Pharmacokinetic and pharmacodynamic evaluation of classical psychedelic substances in the human brain

2. The declaration applies to the following article	
Title of article	Molecular, haemodynamic, and functional effects of LSD in the human brain
Article status	
Published <input type="checkbox"/>	Accepted for publication <input type="checkbox"/>
Date: March 2022	Date:
Manuscript submitted <input type="checkbox"/>	Manuscript not submitted <input checked="" type="checkbox"/>
Date:	
If the article is published or accepted for publication, please state the name of journal, year, volume, page and DOI (if you have the information).	

3. The PhD student's contribution to the article (please use the scale A-F as benchmark) <u>Benchmark scale of the PhD-student's contribution to the article</u>	A, B, C, D, E, F
A. Has essentially done all the work (> 90 %) B. Has done most of the work (60-90 %) C. Has contributed considerably (30-60 %) D. Has contributed (10-30 %) E. No or little contribution (<10 %) F. Not relevant	
1. Formulation/identification of the scientific problem	B
2. Development of the key methods	B
3. Planning of the experiments and methodology design and development	B
4. Conducting the experimental work/clinical studies/data collection/obtaining access to data	B

3. The PhD student's contribution to the article (please use the scale A-F as benchmark) <u>Benchmark scale of the PhD-student's contribution to the article</u> A. Has essentially done all the work (> 90 %) B. Has done most of the work (60-90 %) C. Has contributed considerably (30-60 %) D. Has contributed (10-30 %) E. No or little contribution (<10 %) F. Not relevant		A, B, C, D, E, F
5. Conducting the analysis of data	B	
6. Interpretation of the results	B	
7. Writing of the first draft of the manuscript	B	
8. Finalisation of the manuscript and submission	B	
Provide a short description of the PhD student's specific contribution to the article. ⁱ Planned the study, coordinated and performed data collection, formulated the research question, processed the data, performed analyses, made figures, wrote the manuscript.		

4. Material from another thesis / dissertationⁱⁱ	
Does the article contain work which has also formed part of another thesis, e.g. master's thesis, PhD thesis or doctoral dissertation (the PhD student's or another person's)?	Yes: <input type="checkbox"/> No: <input checked="" type="checkbox"/>
If yes, please state name of the author and title of thesis / dissertation.	
If the article is part of another author's academic degree, please describe the PhD student's and the author's contributions to the article so that the individual contributions are clearly distinguishable from one another.	

5. Signatures of the authors incl. the PhD student				
	Date	Name	Title	Signature
1.		Drummond McCulloch	Mr.	
2.		Patrick Fisher	Prof.	
3.				

5. Signatures of the authors incl. the PhD student				
4.				
5.				
6.				
7.				
8.				
9.				
10.				
11.				

6. Signature of the principal supervisor I solemnly declare that the information provided in this declaration is accurate to the best of my knowledge. Date: Principal supervisor: Patrick Fisher

7. Signature of the PhD student I solemnly declare that the information provided in this declaration is accurate to the best of my knowledge. Date: 17-06-2025 PhD student: Drummond McCulloch

Please learn more about responsible conduct of research on the [Faculty of Health and Medical Sciences' website](#).

ⁱ This can be supplemented with an additional letter if needed.

ⁱⁱ Please see Ministerial Order on the PhD Programme at the Universities and Certain Higher Artistic Educational Institutions (PhD Order) § 12 (4):

"Any articles included in the thesis may be written in cooperation with others, provided that each of the co-authors submits a written declaration stating the PhD student's or the author's contribution to the work."

Molecular, haemodynamic, and functional effects of LSD in the human brain

Abstract

In this study, we provide the first study to integrate molecular and functional neuroimaging during psychedelic drug effects in humans. Using simultaneous PET-MRI technology, we describe multiple brain actions of lysergic acid diethylamide (LSD) in healthy volunteers. We quantify the occupancy of LSD at cerebral serotonin 2A receptors and show that LSD increases global cerebral blood flow and internal carotid artery flow without affecting the diameter of the internal carotid artery, opposite effects to those observed following psilocybin. Functional connectivity analyses showed widespread decreases in global connectivity, particularly in visual networks, alongside increases in network-wise sample entropy and spatial complexity. We observed an anticlockwise hysteresis loop between plasma drug levels and subjective effects, suggesting atypical pharmacodynamic mechanisms. By establishing the dose-occupancy relation of LSD in humans, our findings provide critical insights for the clinical development of psychedelic compounds and demonstrate unique neurophysiological effects that distinguish LSD from related psychedelics. Our findings challenge the leading hypotheses of psychedelic brain-action, until now thought to be instrumental for therapeutic efficacy.

Main

Lysergic acid diethylamide (LSD) is a serotonergic psychedelic drug (1). Recent phase 1 and 2a studies have demonstrated that doses of up to 200 µg LSD are safe (2–5), and that a single dose of LSD is associated with symptom reduction in patients with anxiety disorders, up to several months after treatment (6,7). LSD has recently entered three phase 3 trials for the treatment of anxiety and depressive disorders (NCT06941844, NCT06809595, NCT06741228). Intake of LSD changes mood, cognition, and perception from doses as low as 10 µg; the psychoactive effects increase dose-dependently, eliciting extremely intense effects at 100 µg and above (2,4,8). The promising clinical effects highlight the importance of understanding LSD's mechanisms of action in the human brain.

The serotonin 2A receptor (5-HT_{2A}R) is highly expressed in the human neocortex (9) and is the critical target for psychedelic effects, with agonist affinity correlating with potency in inducing subjective effects across psychedelics (10). This is supported by studies showing that ketanserin, a 5-HT_{2A/2C}R antagonist, can block LSD's psychedelic effects (3,4,11), and that selective 5-HT_{2A}R agonists can produce psychedelic effects (12,13). Together, this shows that 5-HT_{2A}R agonism is both necessary and sufficient for the psychedelic effects of LSD. Compared to psilocybin, which produces similar behavioural effects at appropriate doses (2), LSD shows distinct pharmacodynamics, with a reported delay between peak plasma levels and peak subjective effects of up to 1 hour (4,14). A potential explanation for this intriguing observation is based on in vitro crystallography data demonstrating that the binding pocket of LSD requires a conformational change in extracellular loops, which may result in very slow binding and dissociation between LSD and the receptor (15,16).

Understanding LSD's neural effects in humans remains incomplete and has so far mainly been based on blood-oxygen level dependent (BOLD) functional magnetic resonance imaging (fMRI) studies (17). These have identified alterations in global and thalamocortical connectivity, and increases in a range of information-entropy metrics (18), but there has been extremely little replication in the space, and no investigations to date have evaluated relations to target engagement (19). Additionally, the role of the cerebral vasculature, which richly expresses vasoconstriction-mediating 5-HT_{2A}R on vascular smooth muscle cells (20), has largely been neglected. Addressing these gaps around LSD's receptor occupancy and associated systems-level brain function improves our ability to link molecular mechanisms to neural dynamics and therapeutic outcomes.

Leveraging simultaneous PET-MRI technology in healthy volunteers taking an oral dose of LSD, we report for the first time how plasma LSD is associated with in vivo cerebral 5-HT_{2A}R occupancy and subjective drug effects. We present the first comprehensive evaluation of psychedelic effects on brain haemodynamics, revealing that LSD substantially increases internal carotid artery (ICA) flow velocity and cerebral blood flow (CBF), without affecting the ICA diameter. Moreover, when we quantify LSD effects on functional brain activity, we provide evidence for widespread decreases in global connectivity alongside increases in network-wise sample entropy and spatial complexity. These complementary measures provide valuable insights into LSD's neural effects that challenge some widely held beliefs about the acute neural effects of psychedelics.

Results

Baseline multimodal neuroimaging of participants

Eleven healthy participants (2 female; age: mean \pm SD, 31 ± 9 years; weight: 81 ± 12 kg) underwent a multimodal baseline imaging session. See Supplementary Table S1 for demographic details. These included a [^{11}C]Cimbi-36 PET scan to quantify neocortex 5-HT_{2A}R nondisplaceable binding potential (BP_{ND}), multi-band multi-echo fMRI to assess brain activity, and haemodynamic measurements combining ICA angiography, flow quantification with phase contrast mapping (PCM), and CBF measurement with pseudo-continuous arterial spin labelling (pCASL). Baseline 5-HT_{2A}R BP_{ND} showed high binding in the neocortex (mean \pm SD = 1.11 ± 0.26). The preprocessed fMRI data exhibited modular network organisation characteristic of healthy brain function (21), with normalised modularity values averaging 3.65 ± 0.62 (mean \pm SD) times higher than those observed in random networks, confirming community structure in the brain's connectome. CBF estimates (mean \pm SD = 49.2 ± 10.4 ml/100g/min) (22), ICA flow (mean \pm SD = 215.0 ± 57.8 ml/min), and ICA diameter (mean \pm SD = 4.65 ± 0.32 mm, see Table S2) were all within expected ranges (23–25). LSD is metabolised by the CYP2D6 enzyme, which has genetic variations that affect enzymatic function (26). Two participants were intermediate metabolisers ($n = 1$ with activity score 0.5 and $n = 1$ with score 1.0), and the remaining nine participants were normal metabolisers ($n = 4$ with score 1.5, $n = 5$ with score 2.0). The observed relation between peak plasma LSD level (PLL) and dose administered was not clearly modified by *CYP2D6* genotype (Supplementary Figures S1, S2).

LSD pharmacokinetics and acute subjective effects

On a separate day, participants were administered a single oral dose of LSD tartrate (25–200 μg freebase equivalent). See Table 1 for an overview of all occupancies, plasma concentrations, and doses administered at each scan. This dose range was evaluated to estimate the relation to 5-HT_{2A}R occupancy across a clinically relevant range of dose and PLL. In a dose-dependent manner, LSD intake produced psychedelic effects in all participants, without serious adverse effects (Supplementary results). PLL peaked after 96 mins, and subjective drug intensity (SDI) peaked 30 mins later (Figure 1A, B). A clear anticlockwise hysteresis loop emerged when examining the relation between plasma LSD levels and SDI scores over time (Figure 1C); the PLL-SDI curves traced an anticlockwise loop, with lower SDI scores during the ascending phase compared to the descending phase at equivalent PLL. This indicates that for a given PLL, subjective effects were weaker while plasma levels were rising than while they were falling. Seven participants completed PET-MRI scans during peak drug effects, and two completed scans after subjective drug effects had largely subsided. Despite scan sessions lasting over two hours each, all but one participant tolerated the procedure well, reporting feeling calmer, less tired, and less physically uncomfortable than during the baseline scan (Supplementary Figure S3). Only one participant (P10, 150 μg) experienced scanner-related anxiety that necessitated early scan termination; cessation of scanning resolved the anxiety. One participant (P9, 150 μg) experienced severe nausea shortly after drug administration and was not scanned while in the psychedelic state. For two participants (P8, 150 μg and P11, 75 μg), the scanner malfunctioned, and all scan data was lost.

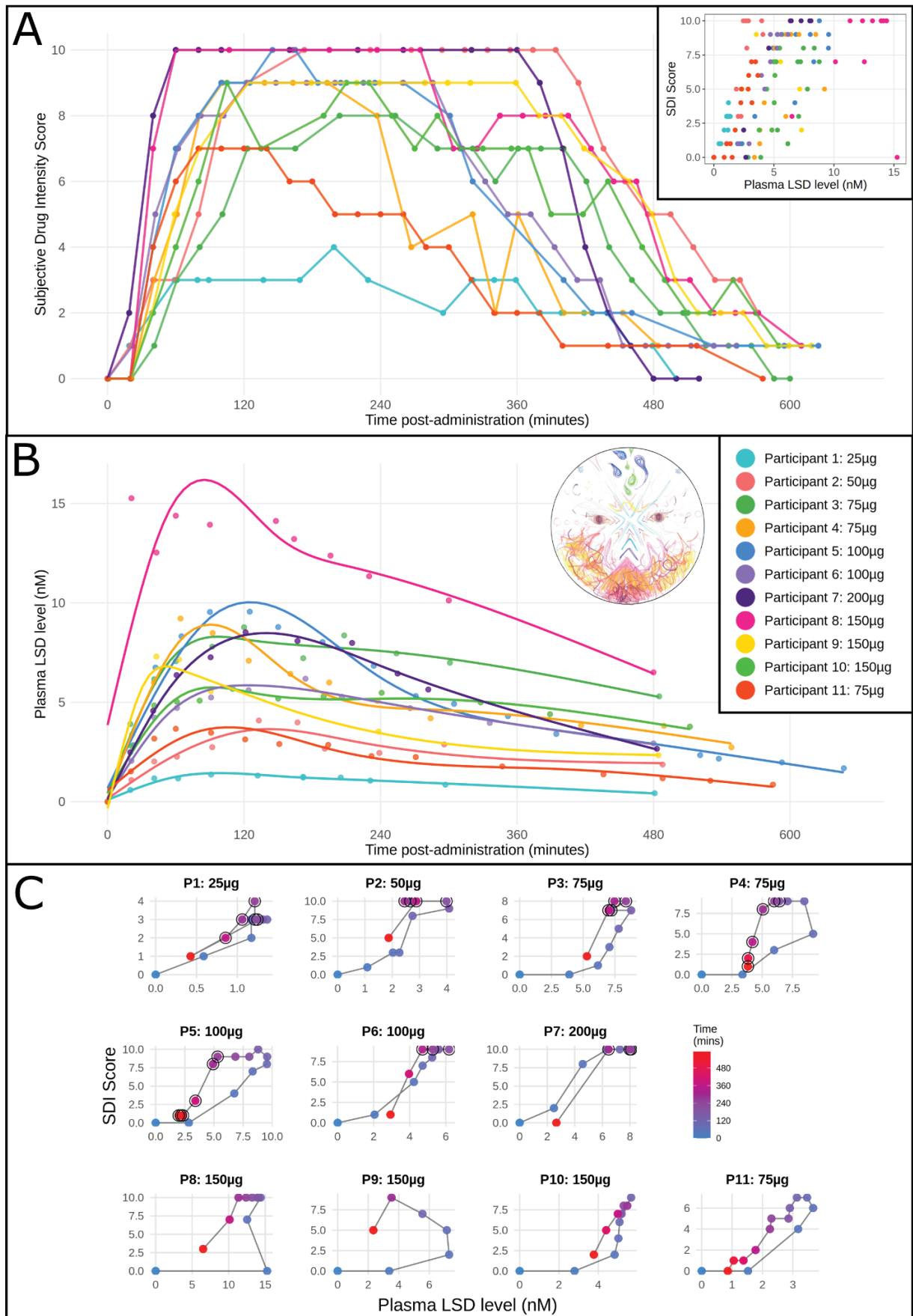


Figure 1 | Subjective and pharmacokinetic effects of LSD intake. A, Time course of subjective drug intensity (SDI) scores (0-10) for each participant following LSD administration (25-200 μ g); insert shows SDI plotted against plasma LSD concentration. B, Plasma LSD concentrations over time post LSD (intake is $t=0$). Curves are fitted with a spline for visualisation only. Subplot includes a representative drawing of the LSD experience by P8 (pink curve). C, Single-subject SDI vs PLL hysteresis plots. Points are chronologically connected by black lines, and points are coloured by time, i.e., the number of minutes post-LSD intake. Black outline circles indicate timepoints during PET scans. P4 and P5 received two PET scans during LSD effects. All but P7 show an anticlockwise hysteresis loop.

Occupancy of LSD at the 5-HT_{2A}R is associated with subjective drug effects

By comparing [¹¹C]Cimbi-36 PET at baseline and after LSD administration (Figure 2A), we calculated neocortical 5-HT_{2A}R LSD occupancy. We fit the occupancy data and PLL measured during the scan to a Hill-Langmuir model ($R^2 = 0.60$) with bootstrapped confidence intervals. This revealed an IC₅₀ of 1.93 nM (95% CI: 0.53-2.79 nM) equivalent to 0.62 ng/ml (CI: 0.17-0.9 ng/ml) and maximum occupancy (Occ_{max}) of 97.4% (95% CI: 75.3-100%) (Figure 2B). A similar relation was observed between LSD dose and occupancy ($R^2 = 0.58$), with an ED₅₀ of 31.1 µg (95% CI: 7.6-46.4 µg) and Occ_{max} of 96.2% (95% CI: 73.5-100%) (Supplementary Figure 4A). When analysing body weight-adjusted LSD dose, we observed a closer relation with occupancy ($R^2 = 0.75$), with an ED₅₀ of 0.41 µg/kg (95% CI: 0.17-0.54 µg/kg) and Occ_{max} of 98.7% (95% CI: 80.3-100%) (Supplementary Figure 4B). Peak occupancy was related to mean within-scan SDI ratings with a sigmoidal fit (Figure 2C, $R^2 = 0.87$).

Additionally, we assessed whether occupancy remained high after PLL had dropped using late-phase scans in two participants. P4 was administered 75 µg. At the peak scan (+161-281 minutes), they showed 84% occupancy and 8.5/10 SDI. At late scan (+420-540 minutes), they showed 74% occupancy, yet only 1.5/10 SDI, suggesting a temporal dissociation between receptor occupancy and subjective drug effects. P5 was administered 100 µg. At peak scan (+271-391 minutes), they showed 67% occupancy and 8.5/10 SDI. At late scan (+522-642 minutes), they showed 12% occupancy and 1/10 SDI, demonstrating that receptor occupancy eventually returns to near-baseline levels.

A

Serotonin 2A Receptor Availability

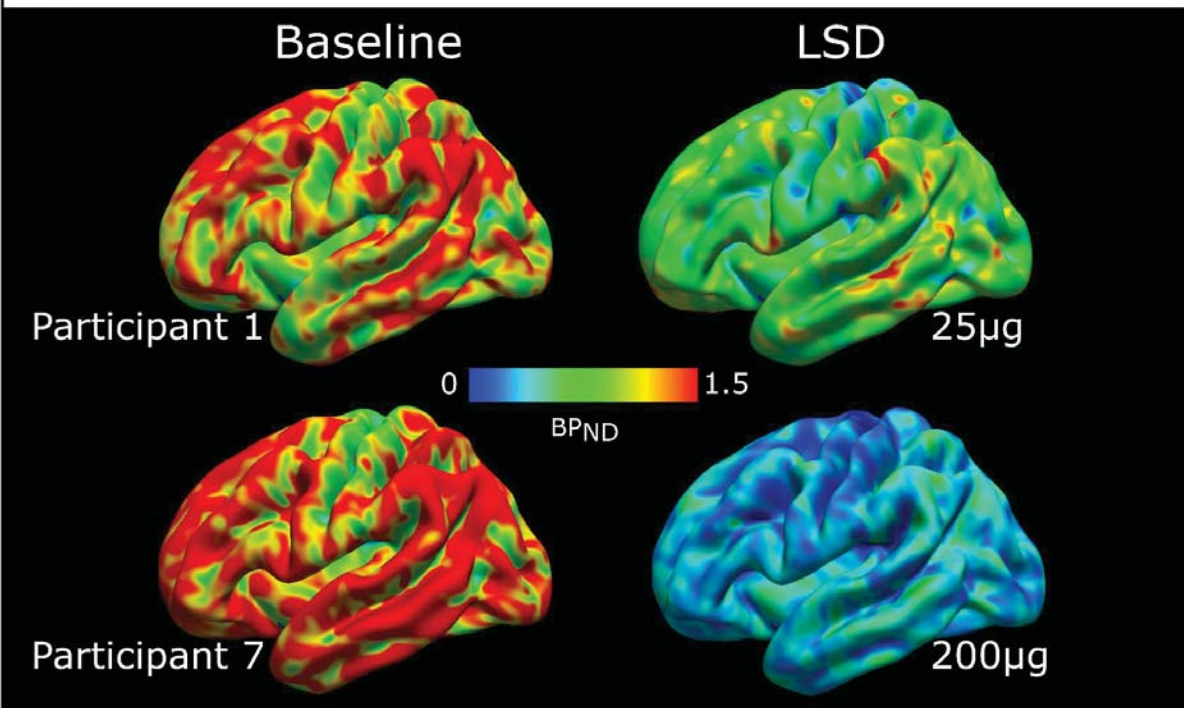
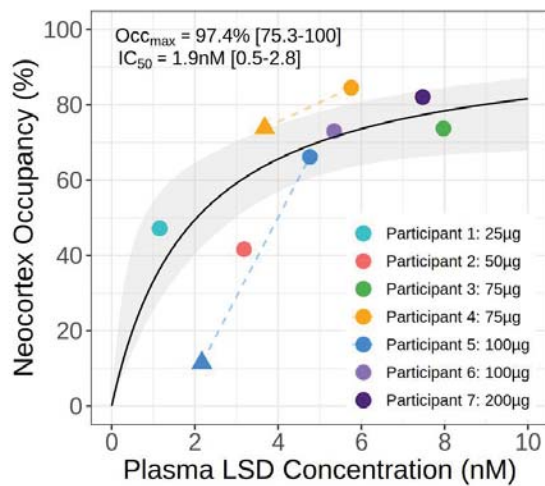
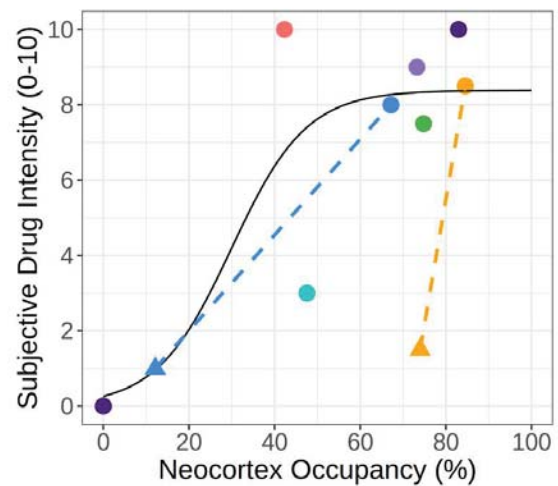
**B****C**

Figure 2 | Serotonin 2A receptor occupancy by LSD measured with [¹¹C]Cimbi-36 PET.

A, Cortical 5-HT_{2A}R nondisplaceable binding potential (BP_{ND}) maps at baseline and peak LSD for participants receiving 25 µg (top) and 200 µg (bottom) doses. The colour scale indicates BP_{ND} values. B, Plasma LSD concentration versus receptor occupancy fitted with Hill-Langmuir model. The solid black line shows the model fit, and bootstrap-derived 95% confidence intervals are shown in grey shading. Circles indicate peak scans; triangles show late scans connected to corresponding peak scans (dotted lines). Model fitting used peak scan data only. C, Receptor occupancy versus subjective drug intensity during PET scanning. The curve is fit with a sigmoid function. Each color represents an individual participant. Model fitting used baseline and peak scan data only (n=7 for peak scans).

	LSD dose µg	Cmax nM	Peak Scan				Late Scan			
			Time post-dose min	[LSD] nM	SDI a.u.	Occupancy	Time post-dose min	[LSD] nM	SDI a.u.	Occupancy
1	25	1.37	175	1.23	3.0	48%				
2	50	4.08	164	3.32	10.0	42%				
3	75	8.77	175	7.22	7.5	75%				
4	75	9.21	161	6.43	8.5	85%	420	3.84	1.5	74%
5	100	9.56	271	5.31	8.0	67%	522	2.25	1.0	12%
6	100	6.19	167	6.19	9.0	73%				
7	200	8.52	168	8.08	10.0	83%				
8	150	15.26								
9	150	7.30								
10	150	5.67								
11	75	3.67								

Table 1 | Pharmacokinetic and receptor occupancy measurements across participants. Overview of LSD doses, peak plasma concentrations (Cmax), timing, and receptor occupancy data from PET scans. The table shows data for each participant including LSD dose (µg, freebase equivalent), maximum observed plasma LSD concentration (nM), timing of PET scans relative to LSD administration (minutes), mean plasma LSD concentration during scan windows (nM), mean subjective drug intensity (SDI) ratings during scans, and measured 5-HT_{2A}R occupancy (%). Data from both peak and late scans are shown where assessed. P8-11 had only baseline PET data collected. SDI was rated on a 0-10 scale, where 0 represents no drug effects and 10 represents the strongest imaginable effects. Receptor occupancy was calculated using [¹¹C]Cimbi-36 PET. Time post-LSD refers to the minutes between LSD administration and radiotracer injection.

LSD increases cerebral blood flow and internal carotid artery flow

Haemodynamic quantification was performed 30-60 minutes after the start of the PET scan. LSD intake produced widespread increases in CBF. Global CBF increased by 19.3% (Cohen's $d_z = 1.20$), with the strongest effects in the occipital cortex (26.4% increase; Cohen's $d_z = 1.85$) and thalamus (19.4% increase; Cohen's $d_z = 1.04$). We observed more modest CBF increases in limbic regions, including the hippocampus (15.1% increase; Cohen's $d_z = 0.88$) and amygdala (10.9% increase; Cohen's $d_z = 0.36$). Convergent with these CBF changes, ICA flow increased by 28% (Cohen's $d_z = 1.30$); yet ICA diameter showed negligible changes (-3.5%; Cohen's $d_z = -0.38$), suggesting the increased blood flow was not driven by macrovascular changes. The correspondence between CBF and ICA flow is shown in Supplementary Figure S5. Full details on regional responses are in Supplementary Table S2 and Figures S6 and S7. Single-subject CBF delta maps (changes in cerebral blood flow following LSD administration) are in Supplementary Figure S8.

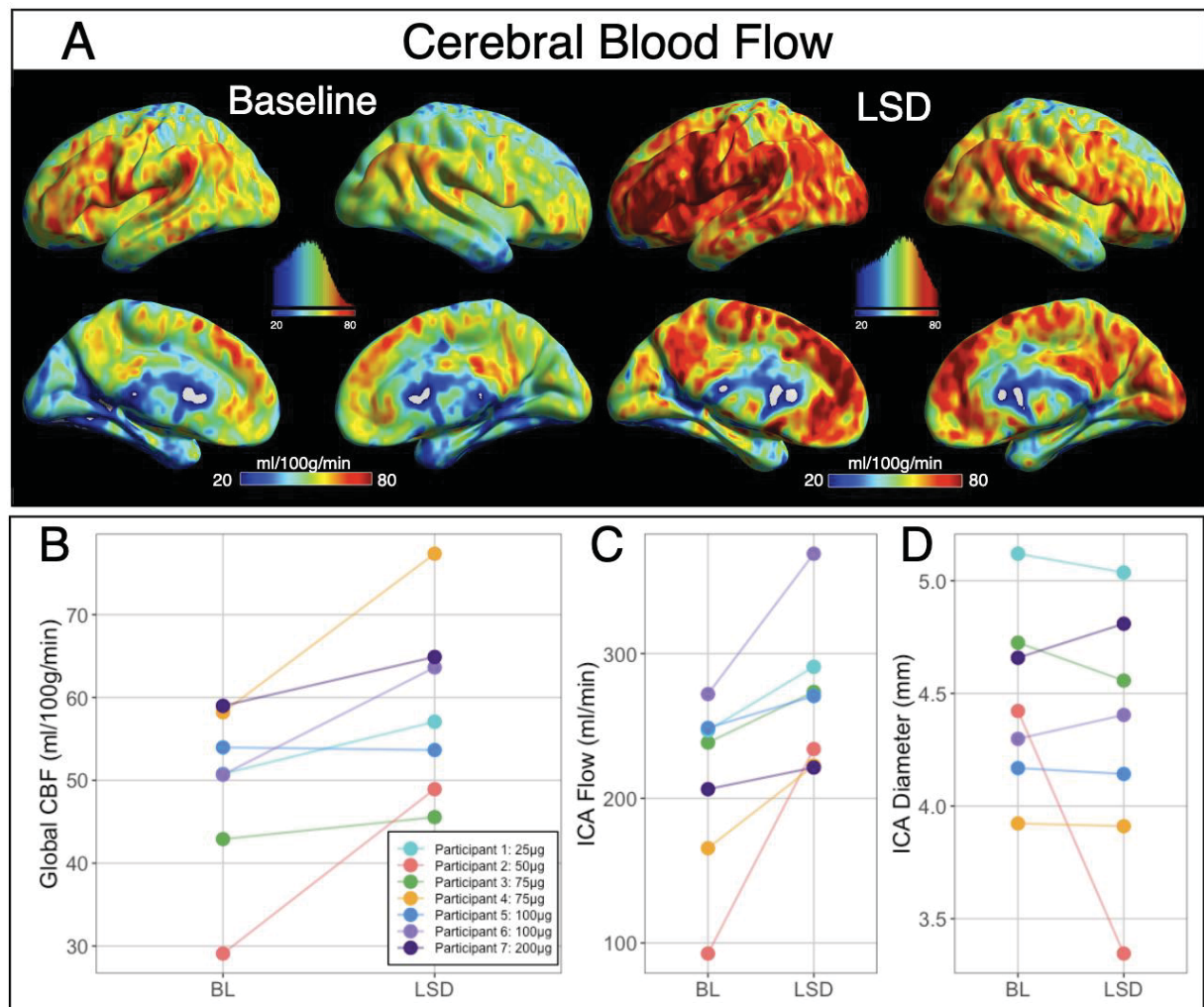


Figure 3 | Changes in cerebral blood flow (CBF) and haemodynamic parameters following LSD administration. A, Group-averaged CBF maps at baseline and after LSD administration, respectively. Color bars indicate CBF values in ml/100g/min. Histograms show distributions of voxel-wise values from the whole brain with the same scale as the colour bar below. B, Global CBF at baseline and post-LSD for individual participants. C, Internal carotid artery (ICA) flow at baseline and post-LSD. D, ICA diameter. In panels B-D, each color represents the same participant across all measurements, with lines connecting baseline (BL) and post-LSD (LSD) values.

LSD decreases global brain connectivity, increases sample entropy, and spatial complexity

fMRI scans were performed 20-40 minutes after the start of the PET scan. LSD decreased global connectivity (i.e., the average correlation across all grey-matter voxels) across most of the cortex, with the largest effect sizes in visual and temporal-parietal network regions (Figure 3A, Supplementary Table S3, Supplementary Figure S9). Effects on thalamocortical connectivity (TCOR) were more spatially restricted, with the most clear effects of increased TCOR with primary somatomotor regions bilaterally (Figure 3B, Supplementary Table S4, Supplementary Figure S10).

LSD also altered the temporal and spatial properties of brain activity. Sample entropy, a measure of regional signal unpredictability, was markedly increased in both visual networks (central: $dz = 1.02$; peripheral: $dz = 0.94$) and control networks (A: $dz = 0.41$; B: $dz = 0.97$; C: $dz = 0.96$) (Figure 3E). Normalised Spatial Complexity, a measure of the signal heterogeneity within a region, showed increases in control A and B ($dz = 0.77/0.72$) and limbic A and B networks ($dz = 0.75/0.67$) (Figure 3F) and a moderate global effect ($dz = 0.55$) (Figure 3G). Network-level analyses showed predominantly decreased connectivity between visual networks and other systems (Figure 3C) with smaller effects on the distribution of dynamic network connectivity (Figure 3D) and the Lempel-Ziv complexity of the signals across the whole brain ($dz = 0.40$). Graph-theory measures such as modularity, small-worldness, and geodesic distribution, a measure of the distribution of connectivity paths across the brain, remained largely unchanged (Figure 3G). For a complete overview of fMRI results, see Supplementary Table S5.

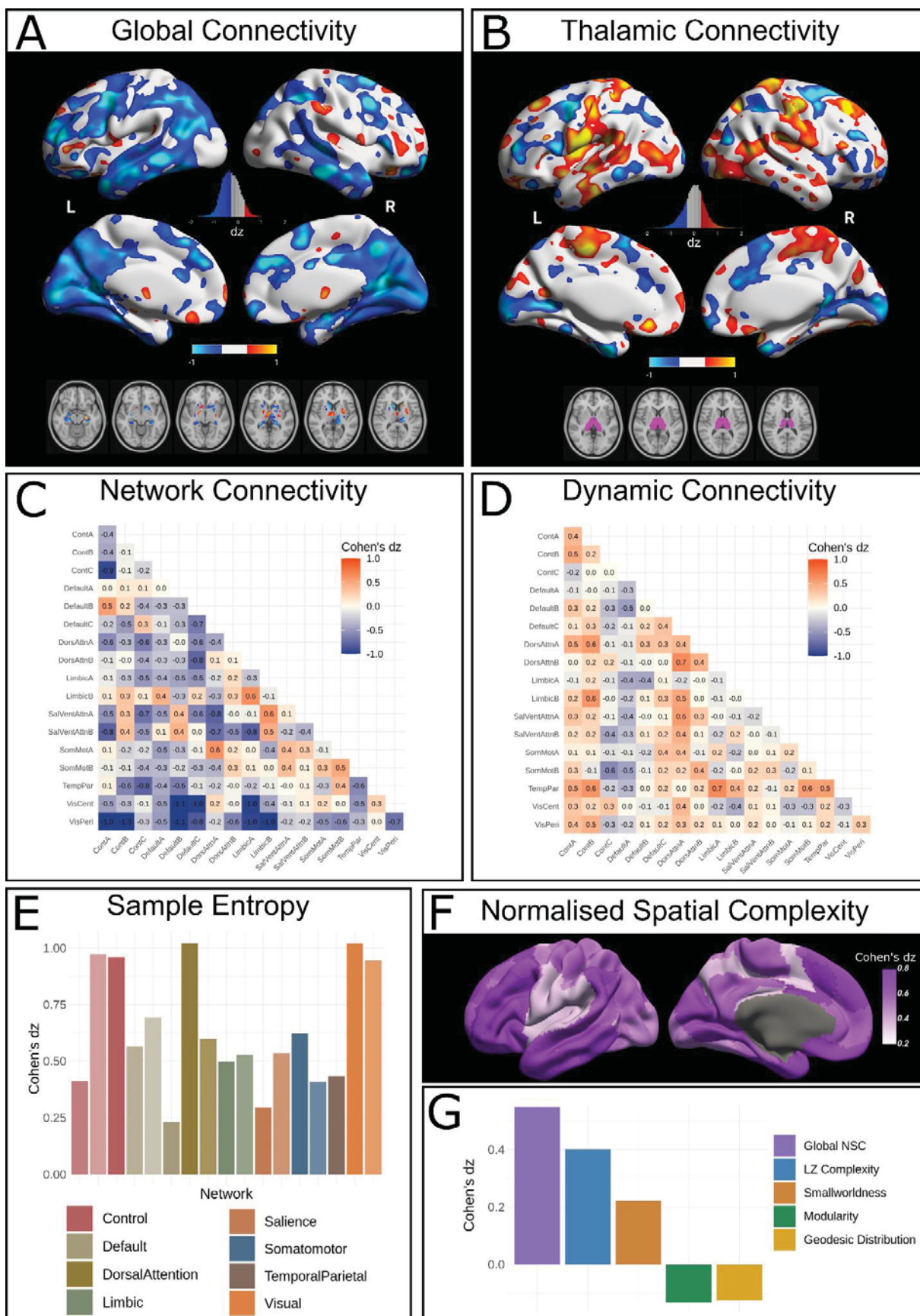


Figure 4 | Functional MRI-measured brain effects of LSD. *A, Whole-brain global connectivity changes shown as Cohen's d_z effect size maps projected onto the cortical surface (colour scale: blue = decreased, orange = increased global connectivity). The lower panel depicts subcortical effects on anatomical slices. B, Thalamic functional connectivity alterations, displayed as surface projections with the corresponding thalamic seed region (pink) shown below. A and B are thresholded at $|\text{Cohen's } d_z| > 0.3$. C, Static functional connectivity matrix showing Cohen's d_z effect sizes for between- and within-network connectivity across Yeo 17 networks. D, Dynamic conditional correlation (DCC) distribution changes between network pairs. E, Sample entropy (a measure of signal unpredictability) alterations across major brain networks and their subdivisions. F, Cortical distribution of Normalized Spatial Complexity changes (a measure of signal heterogeneity within brain regions). G, Effect sizes of global metrics including Normalized Spatial Complexity (NSC), Lempel-Ziv complexity (LZ-complexity, a measure of temporal entropy), small-worldness (measure of network integration and segregation), modularity (degree of network subdivision into communities), and geodesic distribution (distribution of minimum path lengths between brain regions). ($n = 7$); L, left hemisphere; R, right hemisphere.*

Correlations between receptor occupancy and change in cerebral blood flow, and global brain connectivity

To evaluate the relation between each neuroimaging metric, we calculated Spearman's rank correlation coefficients (ρ) between the observed change in CBF, global connectivity across brain regions (GCOR), and neocortical 5-HT_{2A}R occupancy across participants in each of 12 brain regions (Figure 5). GCOR was negatively correlated with neocortical occupancy across almost the entire neocortex, with 11 out of 12 regions showing negative correlations, of which seven were strong ($\rho < -0.5$) (Figure 5A, D). In contrast, change in CBF showed no clear relation with neocortical occupancy, with $|\rho| < 0.2$ in 10 out of 12 regions (Figure 5A, C). The relation between GCOR and CBF was predominantly negative, especially across large cortical regions. (Figure 5A, B).

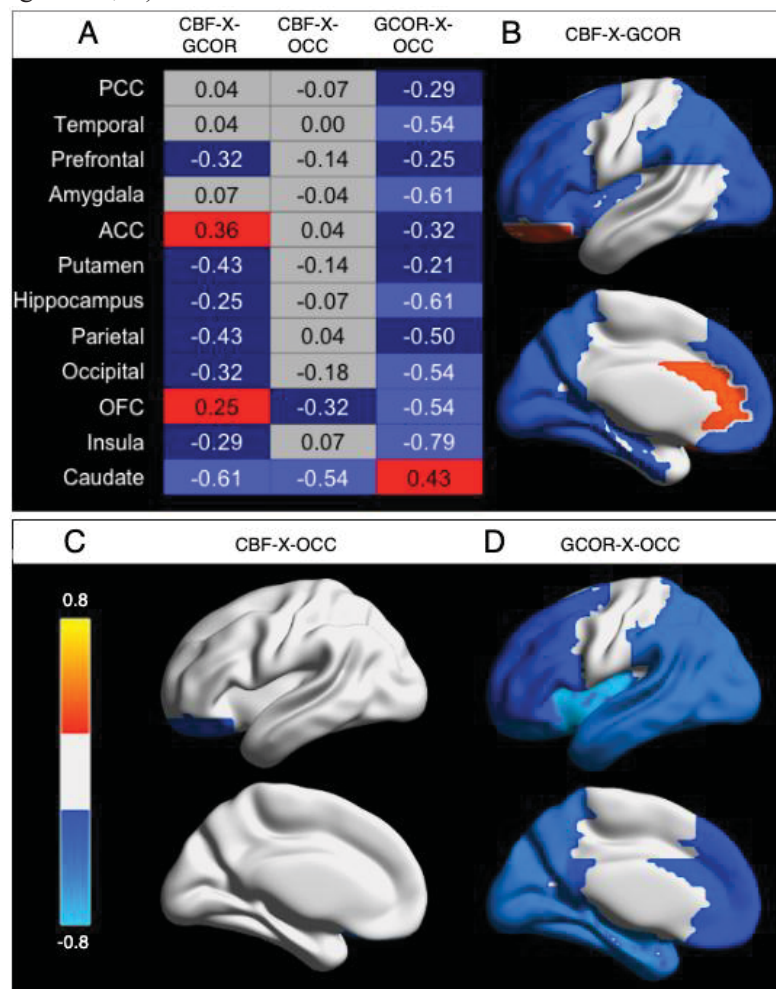


Figure 5 | Correlations between neocortical occupancy (OCC), cerebral blood flow (CBF), and global connectivity across brain regions (GCOR). A, Correlation matrix showing Spearman's rank correlation values for CBF-X-GCOR, CBF-X-OCC, and GCOR-X-OCC across 12 brain regions: posterior cingulate cortex (PCC), temporal, prefrontal, parietal and occipital cortex, anterior cingulate cortex (ACC), orbitofrontal cortex (OFC), amygdala, putamen, hippocampus, insula, and caudate. B-D, BrainNet visualization of correlations in lateral (top) and medial (bottom) views. Brain images and table colouring are thresholded at $|\rho| > 0.2$.

Discussion

In this first human study to administer a psychedelic and acquire simultaneous molecular and functional brain imaging data, we characterised the pharmacodynamic effects of LSD in healthy volunteers, providing *in vivo* cerebral 5-HT_{2A}R occupancy data and quantifying widespread alterations in CBF and functional brain activity. LSD exhibited high-affinity binding to cerebral 5-HT_{2A}R, increased global CBF substantially, and increased flow in the internal carotid arteries without inducing profound changes in the diameter. LSD altered the activity and connectivity of the brain in several ways, including widespread decreases in cortical connectivity, enhanced thalamic coupling with somatomotor regions, and increases in sample entropy and signal complexity across several functional brain networks.

Comparison with *in vitro* work and future applications

Our receptor occupancy results, with an IC₅₀ of 1.9 nM, align well with prior *ex vivo* receptor binding studies conducted on human cortical tissue: specifically, previous work using the antagonist radioligand 3H-spiperone reported an affinity of 4 nM (27) and 3H-ketanserin in 5-HT_{2A}R-expressing NIH-3T3 cells indicated an affinity of 4.2 nM (28). For comparison, clinical data suggest that the EC₅₀ for psychedelic effects is 3–4 nM (29). This convergence across distinct methodologies is reassuring and further validates [¹¹C]Cimbi-36 PET as a tool for evaluating target engagement in humans *in vivo*, relevant for characterising other forthcoming 5-HT_{2A}R-based therapeutics. This is especially important for the Phase 1 testing of prospective non-psychedelic 5-HT_{2A}R agonists, for which target engagement cannot be estimated using behavioural measures. Consistent with our observations assessing psilocybin 5-HT_{2A}R occupancy (30), we observed a generally positive relation between 5-HT_{2A}R occupancy and self-reported subjective drug intensity. However, we observed notable inter- and intra-participant variation across estimates, with one participant receiving only 25 µg LSD rating 10/10 subjective intensity with a corresponding occupancy of 42%, and another rating only 1.5/10 SDI despite having 72% receptor occupancy during a late scan. This positive, yet variable, relation indicates that clear evidence of target engagement requires molecular imaging; it cannot necessarily be derived from subjective effects.

As only the second psychedelic compound after psilocin (30) to have its receptor occupancy profile characterised in humans, this work establishes a framework for evaluating target engagement of emerging compounds. Several classical psychedelics, including 5-MeO-DMT (NCT05800860, NCT05839509) and N,N-DMT (NCT06094907, NCT05553691), are advancing in clinical development without direct occupancy measurements. MDMA has progressed through phase 3 trials (31,32), and some of its clinically relevant effects are known to be blocked by the 5-HT_{2A}R antagonist ketanserin (33). Yet, the degree to which MDMA occupies the 5-HT_{2A}R either directly or via endogenous serotonin release is unresolved, could be resolved using PET, and may be critically relevant for understanding its efficacy and safety.

The relation between dose and occupancy

Our model provides a valuable tool for translating measured plasma LSD concentrations into estimated 5-HT_{2A}R occupancy levels. Mechanistic work based on plasma levels alone overlooks the non-linear relation between drug concentrations and receptor binding. By enabling the conversion from plasma measurements to receptor occupancy estimates, our model offers a more mechanistically sound approach for interpreting

experimental and clinical outcomes in LSD research, potentially improving correlations with biological and clinical endpoints, including physiological biomarkers, subjective experiences, therapeutic outcomes, and neuroimaging measures. Based on typical peak plasma concentrations (4), oral doses of 25 µg, 50 µg, 100 µg, and 200 µg yield approximate receptor occupancies of 43%, 62%, 74%, and 84%, respectively. However, we and others have observed substantial inter-individual variation in peak plasma levels, insufficiently explained by bodyweight or *CYP2D6* genotype (34); occupancy cannot be reliably estimated from dose alone but requires at least blood samples to be measured for drug concentration over time.

Our PET data shows an Occ_{max} of 97% for LSD - notably higher than previously reported values for other 5-HT_{2A}R ligands including psilocin (77%) (30), ketanserin (77%) (35), volinanserin (77%) (36), and pimavanserin (78%) (37). Future work administering high doses of LSD and psilocybin may elucidate whether this observed difference in maximal occupancy is related to consequent differences in downstream behavioural or neural effects. However, the confidence of our Occ_{max} estimate is constrained by limited sampling at high plasma concentrations. The increasing prevalence of adverse effects such as nausea and anxiety at higher doses may pose inherent challenges for future high-dose occupancy studies. Future studies may also wish to account for the concentration of the LSD metabolite nor-LSD, which has been shown to be an agonist at 5-HT_{2A}R with a K_i of approximately 6.1 nM (26).

All but one participant showed a clear anticlockwise hysteresis loop between plasma LSD levels and subjective drug effects, such that SDI peaked approximately half an hour after PLL. This effect is not observed with psilocybin (2,38). Such a delay could be due to slow brain penetrance, post-receptor signalling, or receptor binding. However, LSD has biochemical properties that make slow brain penetrance unlikely (39) and has similar post-receptor signalling properties to psilocybin (40). Structural studies have demonstrated that LSD exhibits unusually slow dissociation kinetics from 5-HT_{2A}R due to unique hydrogen-bond interactions, which may result in the gradual accumulation of 5-HT_{2A}R-bound LSD, thus explaining the observed delay (41). This slow dissociation is not observed with psychedelics from other structural classes (16). This hypothesis could be tested using either radiolabeled LSD or carefully timed [¹¹C]Cimbi-36 scans in the early phase of drug effects. The temporal continuity of our SDI ratings may also be biased by the fact that participants changed from the quiet treatment room to the scanner environment around peak drug effects; however, most participants were already at peak drug effects when transported to the scanner.

We observed one participant who, despite a significant reduction in subjective drug effects at their late-scan, retained high occupancy of 5-HT_{2A}R (in line with their PLL), implying rapid post-receptor tolerance effects, which may be evaluated preclinically. PET cannot distinguish between reductions in available receptor binding sites due to occupancy by cold ligand or by receptor downregulation; therefore, it may be that the observed occupancy is the result of receptor downregulation. However, previous PET work with psilocybin showed no reduction in 5-HT_{2A}R binding one week after a high dose of psilocybin (42), and we show in one participant that BP_{ND} returns almost to baseline after only 8 hours, indicating no substantial rapid receptor downregulation that would positively bias our occupancy estimates. Psilocybin similarly showed a return to baseline BP_{ND} once the drug was cleared (30). We are limited to only qualitatively presenting data from the late scans due to losing three scans because of scanner failures and adverse effects, limiting our capacity to test the lid-hypothesis as described in the preregistration.

Haemodynamic effects of LSD vs psilocybin

Our observation of increased global CBF (19.3%) under LSD stands in marked contrast to the cerebral haemodynamic effects of psilocybin, for which four studies have reported reduced CBF (14,43–45). One study found global CBF reductions of 12% following psilocybin administration, with regional analysis revealing the strongest decreases in parietal (-15%) and occipital regions (-14%), alongside significant ICA constriction (-7%) (45). In contrast, following LSD, we observed widespread CBF *increases*, most pronounced in the occipital (26%) and parietal cortices (18%). These CBF changes were accompanied by increased ICA flow (28%), with ICA diameter remaining relatively stable. The only previous neuroimaging study of LSD's effects on CBF employed 2D time-series acquisition following intravenous LSD administration and reported elevated occipital blood flow. However, the absolute CBF values reported in that study exceeded physiological ranges (>150 ml/100g/min) in both the LSD and placebo conditions, limiting interpretability (14,24).

LSD and psilocybin both produce their psychedelic effects primarily via 5-HT_{2A}R agonism, yet these opposing effects on cerebral haemodynamics suggest distinct downstream or off-target mechanisms. This is supported by our observation that, unlike GCOR effects, 5-HT_{2A}R occupancy was not correlated with changes in CBF. LSD binds with nanomolar affinity to several monoaminergic receptors, including most serotonin, adrenergic alpha 2A and dopamine subtype 2 receptors, whereas psilocybin's receptor binding profile is mostly restricted to the serotonin receptors (46,47). Both psilocybin and LSD are agonists at 5-HT_{2A}R and 5-HT_{1B}R, which induce vasoconstriction (48,49); yet, LSD does not produce vasoconstriction at physiological levels *in vitro*, aligned with our observations here (50). LSD therefore may activate counter-acting vasodilatory pathways, which can be evaluated in future research with selective antagonists. The observed increase in CBF is unlikely to be driven by systemic confounds; although LSD produces increases in blood pressure (4), these are well within the range that is accounted for by autoregulation (51). A [¹⁸F]FDG-PET study has previously shown that psilocybin increases cerebral glucose metabolism despite concurrent reductions in blood flow, implying a functional decoupling between neural activity and perfusion, which may be due to 5-HT_{2A}R-mediated vasoconstriction, as discussed above (52). This hypothesis may be evaluated using a peripherally selective 5-HT_{2A}R antagonist such as sarpogrelate (53). Whether such decoupling also applies to LSD remains unknown, as [¹⁸F]FDG-PET imaging has not yet been performed. Simultaneous [¹⁸F]FDG-PET/MR could directly evaluate this relation between metabolism, blood flow, and neural activity following LSD administration. Previous work with psilocybin has also not yet evaluated ICA flow, which can be measured on all major MRI systems in under two minutes using a phase-contrast mapping sequence.

Effects of LSD on functional brain activity and connectivity

The decreased global connectivity observed across visual networks, attention, and temporal-parietal networks, partially aligns with previous findings, particularly regarding visual cortex connectivity (11,54). However, it diverges from studies reporting widespread increases in frontal and parietal connectivity (55). These decreases in GCOR were strongly correlated with neocortical 5-HT_{2A}R receptor occupancy and are thus likely an on-target effect. Although we find increased thalamic coupling with bilateral somatomotor regions, we did not replicate the more extensive thalamocortical connectivity changes reported in several prior studies (11,54,56). Our entropy analyses provide support for medium-to-large LSD effects on brain signal complexity. We observed large increases in sample entropy across visual and control networks and

medium-to-large increases in normalised spatial complexity, consistent with previous reports (57–59). We did not observe even moderate increases in Lempel-Ziv complexity, geodesic distribution, or dynamic conditional correlation distribution, further supporting the notion that each information-entropy measure represents a distinct phenomenon (59). We did not observe widespread changes in within- and between-network connectivity, which have been widely reported across LSD, psilocybin, and *N,N*-DMT (11,17,60,61) or alterations in graph-theoretical measures such as modularity and small-worldness. Because of the experimental design employing varying doses of LSD and a small sample size, which were chosen based on the occupancy outcomes, we are constrained in our capacity to infer statistically significant effects on functional neural effects. As such, voxel-wise analyses are presented without statistical thresholding, with particular attention to results showing bilateral symmetry. These fMRI findings nevertheless contribute valuable new data to the field, particularly given that most previous analyses of LSD effects have evaluated the same dataset and extremely few studies have evaluated previously investigated methods (19). Presentation of strictly thresholded statistical maps can exaggerate inconsistencies across studies (62); therefore, we report effect sizes from all analyses, which can help establish which neural signatures of LSD are most deserving of continued investigation and facilitate future meta-analyses and cross-study comparisons (63).

We observed that LSD-induced increases in CBF were correlated with decreases in GCOR. The neurovascular coupling model relates increased cerebral metabolic activity with blood flow overcompensation and subsequent increases in the BOLD signal (64,65). By altering CBF, psychedelics may modulate this coupling, as has been reported for, e.g., caffeine (66). Hypercapnia increases CBF without affecting neural activity (67) and has been shown to reduce BOLD correlations, possibly by decreasing signal-to-noise (68), which would also theoretically increase measures of signal complexity, i.e., entropy. Our observations highlight the urgent need for a future study to characterise psychedelic effects on neurovascular coupling by relating cerebral metabolic, blood flow, and BOLD effects. If psychedelics are shown to affect neurovascular coupling, it would substantially affect the interpretation of psychedelic BOLD effects presented in dozens of previous studies, including those presented here.

In summary, this study provides the first *in vivo* pharmacodynamic profile of LSD in humans through simultaneous molecular and functional neuroimaging. We characterise LSD's high-affinity binding to 5-HT_{2A}R and present data suggesting a temporal disconnect between LSD plasma concentrations, receptor occupancy, and subjective drug effects. Our findings of increased cerebral blood flow contrast markedly with psilocybin's CBF-reducing effects, suggesting pharmacological distinctions between these related psychedelics. We observe widespread reductions in global connectivity, which were strongly correlated to receptor occupancy, as well as increases in temporal and spatial complexity. We provide preliminary evidence that such alterations in connectivity and complexity may be confounded by hemodynamic effects, and propose future studies, especially involving direct measurement of the effects of LSD on cerebral metabolism, to help resolve the basis of the observed neural effects. The observations presented here advance our ability to dose LSD in clinical populations and progress our understanding of the neural mechanisms that may underpin their acute and lasting effects.

Methods

Ethics and informed consent

All research procedures were conducted in accordance with the Declaration of Helsinki (69). The study protocol was approved by the ethics committee of the Capital Region of Denmark (H-21060056) and the Danish Medicines Agency (EudraCT no.: 2021-002633-42; CTIS: 2024-519564-41-00). Participants were given information packs including an overview of their rights and the use of their data following telephone screening and before signing the consent forms. The study was preregistered at clinicaltrials.gov (NCT05953038) and aspredicted.com (<https://aspredicted.org/gn3un.pdf>).

Inclusion and exclusion criteria

Inclusion criteria were:

- Healthy individuals 18-75 years old

Exclusion criteria were:

- Current or past history of primary psychiatric illness (DSM-IV axis-I or WHO ICD-10 diagnostic classification)
- Current or past history of primary psychiatric illness (DSM-IV axis-I or WHO ICD-10 diagnostic classification) in a first-degree relative (i.e., parents, siblings)
- Current or past history of neurological disease, significant somatic condition/disease
- Use of medication that could potentially influence results (e.g., drugs that act on relevant components of the serotonin system or may interfere with the metabolism of LSD)
- Non-fluent Danish language skills
- Profound visual or auditory impairments
- Severe learning disability
- Pregnancy on the scan date, verified by a pregnancy test (females, test omitted if confirmed that individual is post-menopausal)
- Breastfeeding (females)
- Contraindications for MRI (e.g., pacemaker, claustrophobia, etc.)
- Contraindications for PET (e.g., claustrophobia, radiation exposure, etc.)
- Current alcohol or drug abuse
- Allergy to administered compounds
- Participant in research study with >10 mSv exposure within the past year or significant occupational exposure to radioactive substances
- Abnormal ECG (i.e., indicating current, previous heart disease or predisposition thereof, e.g., QT prolongation) or use of QT prolonging medication
- Use of psychedelic substances within the preceding six months
- Blood donation up to three months before the study (i.e., more than 500 ml of blood)
- Head injury or concussion resulting in loss of consciousness for more than 2 minutes
- Haemoglobin levels < 7.8 mmol/l for women and 8.4 mmol/l for men
- Ferritin levels outside normal range (12-300 µg/L)

- Body-weight < 50 kg or > 110 kg
- BMI > 35 kg/m²
- Individual assessment by research staff deeming drug administration unsafe due to ethical or psychological circumstances of the participant

Recruitment

Healthy volunteers were recruited from an in-house database of individuals interested in participating in a study involving psychedelics (see CONSORT diagram Supplementary Figure S11). A total of 52 volunteers were contacted via telephone, 32 were excluded at telephone pre-screening, two declined before in-person screening, three were excluded during in-person screening, and 2 dropped out after inclusion but before any study visits. The data presented here are from 11 healthy participants collected between November 2023 and November 2024. Details of recruitment, procedures during the LSD session, ethical approvals, MRI acquisition, and quality control are described in the Supplementary Text. Analyses were pre-registered on the 27th of February 2023 (<https://aspredicted.org/gn3un.pdf>). No statistical methods were used to pre-determine sample sizes.

Study Design

See Supplementary Figure S12 for an overview of scan elements.

Visit 0: Following telephone screening and informed consent, participants underwent a screening battery including evaluation of medical and drug-use history, pregnancy, electrocardiogram, neurological exam, and psychiatric health.

Following inclusion, participants were asked to fill out, online from home, a 2-hour set of state and trait questionnaires.

Visit 1: Whole-blood, plasma, and buffy-coat samples were taken, as well as a urine sample to check for the absence of drugs of abuse and for women to check for pregnancy. Participants then filled out a collection of state questionnaires and underwent a 2-hour simultaneous PET and MRI scan. Music was played via earphones during the entire scan, except when questions were asked. Scan parameters are discussed below.

Visit 2 involved a preparatory conversation with the psychological support staff, typically lasting 60-90 minutes, focused on the LSD intervention process. The conversation addressed both the psychological and physiological effects of the intervention, the role of the support staff, and the participants' expectations for the session. All participants were informed about changes they might experience in perception, emotions, and sense of self, and were provided with techniques to navigate these shifts with openness and acceptance, as well as guidance on managing possible physical effects such as nausea or dizziness. The conversation also explored participants' past experiences with psychoactive substances, and practical matters, including transportation, accommodation arrangements, and post-session support, were addressed to ensure participants had a reliable support network in place. Participants were reminded of the rules and safety measures, including consent for touch and the prohibition of certain behaviours. Additionally, agreements regarding communication during the scanning process were discussed to ensure participants understood

when and how to communicate with the support team. Occasionally, this conversation occurred before the baseline PET scan. Three participants required an additional preparatory session. One was needed because the initial conversation had taken place more than two weeks before the intervention. Another participant required extra preparation to familiarise themselves with the support team, and one participant needed an extra session to integrate talking points from the first preparatory conversation.

Visit 3: 1 week to 1 month later, participants came in for their intervention session. Participants were fitted with two venous catheters, gave blood samples, filled out the same state questionnaires as during baseline scans, and received a dose of LSD tartrate between 25 μg and 200 μg equivalent as LSD freebase. Participants, but not study staff, were blinded to the dose received. Participants were dosed in a comfortable aesthetic room with speakers and in the presence of two trained psychological support staff. Approximately 1 h 45 m following drug administration, participants were transported via wheelchair to the PET-MR scanner. They then underwent the same scan as at visit 1, with injection of radiotracer at approximately 2 h 45 m after LSD administration, such that tracer injection was approximately aligned with peak subjective drug effects. Following the scan, participants returned to the comfortable room via wheelchair. They remained there until their subjective drug effects had diminished. Then they drew a mandala of their experience and were either picked up by a friend or family member and returned home, or were escorted by study staff to the patient hotel at the hospital.

Visit 4: Either the next day or the day after, participants returned for a follow-up conversation with the psychological support staff. From home, participants filled out an online deck of questionnaires describing their acute drug effects. One participant had an extra integrative phone conversation with a member of the psychological support staff.

Three months after intervention, participants were sent a similar online deck of trait and state questionnaires as they filled out at visit 0, which were filled out at home. Participants were instructed to report all adverse effects to the study staff irrespective of whether they deemed them related to the study medication. All staff with participant contact were responsible for the identification of potential adverse effects, which were eventually evaluated by a medical doctor.

PET scanning parameters

PET images were acquired for 120 minutes on one of two identical 3T Siemens Biograph mMR scanners (Siemens Healthcare, Erlangen, Germany) after a bolus injection of [^{11}C]Cimbi-36. Processing of [^{11}C]Cimbi-36 PET data was performed as described by (30). PET data was reconstructed using MR-imaging based attenuation-correction (DeepDixon) (70) and a framing protocol of 6x10s, 6x20s, 6x60s, 8x120s, 19x300s. All frames were aligned to frame 27, with frames 1-12 using the transformation parameters calculated from frame 13's alignment. Segmentation was performed using SPM12MultiSpectral segmentation using session-specific high-resolution T1- and T2-weighted MRI scans. Regions of interest were defined using PVElab (71), a fully automated regional delineation procedure, and regional time-activity curves were extracted for kinetic modeling.

Kinetic modeling was performed using the simplified reference tissue model (SRTM) with neocortex (a volume-weighted average of the below cortical regions) chosen a priori as the region of interest due to the

high expression of 5-HT_{2A}Rs and the beneficial signal-to-noise ratio within this region; cerebellum was chosen as the reference region due to its absence of 5-HT_{2A}R in humans (72).

- Orbital frontal cortex
- Medial inferior frontal gyrus
- Superior temporal gyrus
- Parietal cortex
- Medial inferior temporal gyrus
- Superior frontal gyrus
- Occipital cortex
- Sensorimotor cortex

Nondisplaceable binding potential (BP_{ND}) (73) was the primary outcome measure, with occupancy % calculated as $100 \times ((\text{baseline BP}_{\text{ND}} - \text{LSD scan BP}_{\text{ND}}) / \text{baseline BP}_{\text{ND}})$. The relation between plasma LSD concentration and receptor occupancy was modeled using the single-site binding model, the Hill-Langmuir equation:

$$\text{Occupancy} = (\text{Occ}_{\text{max}} \times [\text{LSD}]) / (\text{IC}_{50} + [\text{LSD}])$$

where Occ_{max} represents maximum achievable occupancy and IC₅₀ represents the plasma concentration producing 50% occupancy, and [LSD] was the average concentration of LSD from blood samples taken during the PET scan (one at injection, two during the scan, and one at scan cessation).

The Hill-Langmuir equation parameters were estimated using nonlinear least squares regression via the `stats::nls` function (version 4.3.1) in R with the 'port' algorithm, which ensures physically meaningful parameter estimates through constrained optimisation (i.e., Occ_{max} bounded between 0-100%, IC₅₀ constrained to positive values). To assess uncertainty in these estimates, we performed a residual bootstrap with 10,000 iterations. For each iteration, residuals from the observed model were randomly resampled with sign flips and added to the fitted values to generate new synthetic datasets preserving the underlying relation. The model was fit to each synthetic dataset using the same constrained optimisation approach. This procedure provides robust confidence intervals that respect the physical constraints of receptor binding while accounting for the uncertainty in our limited sample size. Bootstrap estimates were calculated using the median of the bootstrap distribution, with 95% confidence intervals defined by the 2.5th and 97.5th percentiles.

Surface maps of 5-HT_{2A}R BP_{ND} (Figure 2) were generated in PETSURFER using MRTM2, where k₂' was estimated with neocortex as the high-binding region and cerebellum as the reference region (74). These maps are used only for data visualisation. All other reported BP_{ND} or occupancy estimates are from SRTM-derived BP_{ND} values.

MRI scanning parameters

During the entire baseline and first post-intervention PET-MRI scan, participants listened to the following playlist: <https://open.spotify.com/playlist/5yT9nTRdgoPIb2f0h5QuKg?si=b6374a44413a485b>;

participants who completed a second PET-MRI scan after LSD administration listened to the following playlist: <https://open.spotify.com/playlist/0UW0wjkE14sXIjwqlmKf5Y?si=74ad7745384244c5>.

During the 120-minute PET scan, we acquired the following MR scans using a 32-channel head coil:

High-resolution T1-weighted structural images with a 3D magnetization-prepared rapid gradient-echo (MPRAGE) sequence with the following parameters: repetition time (TR) = 2300 ms, echo time (TE) = 2.26 ms, inversion time (TI) = 900 ms, flip angle = 8°, field of view (FOV) = 256 x 256 mm², matrix size = 256 x 256, voxel size = 1 x 1 x 1 mm³, 176 sagittal slices, and GRAPPA parallel imaging with an acceleration factor of 3.

High-resolution T2-weighted structural images were acquired using a 3D turbo spin-echo sequence (SPACE) sequence with the following parameters: repetition time (TR) = 3200 ms, echo time (TE) = 407 ms, variable flip angle with a nominal value of 120°, field of view = 230 x 230 mm², matrix size = 256 x 256, 0.9 mm isotropic voxels, 256 sagittal slices, GRAPPA in-plane acceleration factor = 2, partial Fourier sampling, echo-train length = 254, receiver bandwidth = 725 Hz/pixel; images were reconstructed to a 512 x 512 matrix.

We acquired field maps using the vendor-provided gradient echo field mapping sequence with the following parameters: TR = 500 ms; TE1/TE2 = 6.16/8.62 ms; flip angle = 60°; FOV = 100% phase FOV; matrix size = 68 × 68; slice thickness = 3 mm with 3 mm spacing; phase encoding direction = anterior-posterior (j-). The sequence produced three images: magnitude images at both echo times and a phase difference map calculated between the two echoes.

These were then followed by either two or three functional imaging blocks, time permitting, consisting of the following scans:

Pseudo-continuous arterial spin labelling (pCASL) images were acquired using a five post-label delay 3D turbo gradient spin echo sequence with the following parameters: scan time = 7 min 11 sec, label/control pairs = 12, native voxel size = 3 x 3 x 3 mm, image matrix = 96 × 96, number of slices = 40, label duration = 1508 ms, post-label delays = [500, 500, 1000, 1000, 1500, 1500, 2000, 2000, 2000, 2500, 2500, 2500] ms, echo time = 3.78 ms, repetition time = 4100 ms, flip angle = 120°, two background suppression pulses optimised for each PLD. The acquisition included an M0 scan with which to calibrate the pCASL signal without any background suppression.

Time of Flight (TOF) angiography images were acquired using a 3D gradient recalled (GR) sequence with the following parameters: scan time = 6 min 30 s, slice thickness = 0.8 mm, echo time = 4.79 ms, repetition time = 27 ms, flip angle = 18°, acquisition matrix = 482x640 covering a 150x200 mm² field-of-view.

Phase Contrast Mapping (PCM) images were acquired using a 2D sequence with the following parameters: scan time = 8.36 s, slice thickness = 8 mm, echo time = 7.5 ms, repetition time = 100.4 ms, flip angle = 10°, VENC = 100 cm/s, acquisition matrix = 320x320 matrix covering a 240x240 mm² field-of-view.

BOLD functional images were acquired using a multi-echo, multi-band echo-planar imaging (EPI) sequence with the following parameters: TR = 1117 ms, TEs = 15.0/33.68/52.36 ms, flip angle = 70°, FOV = 204 x 204 mm, matrix size = 68 x 68, voxel size = 3 x 3 x 3 mm, axial slices = 42, multi-band acceleration factor = 3, in-plane acceleration (GRAPPA) acceleration factor = 2, and phase-encoding direction = anterior-to-posterior (j-).

Investigational medicinal product

The study medication was produced by Apotheke Dr. Hysek, Biel, Switzerland, in accordance with Good Manufacturing Practice (GMP). LSD was prepared as drinking solutions containing 36.5 µg or 146 µg of GMP-grade LSD tartrate (Lipomed AG, Arlesheim, Switzerland), corresponding to 25 or 100 µg of LSD base, dissolved in 1 mL of 20% alcohol solution (v/v). Participants were blinded to dose by affixing opaque stickers to the bottles before being given to the participants. Participants were not blinded to the fact that they would receive LSD. The investigational medicinal product was stored in a locked safe within a fridge kept at 4-6°C, and doses were prepared on the actual dosing day.

Behavioural effects

Before each EPI scan, participants were asked to listen to the music. Immediately following each scan, the participants were first asked if they had fallen asleep, and then to rate the following questions on a scale from 0 to 10, where 0 was *not at all* and 10 was *very much*: How calm do you feel? How much claustrophobia are you experiencing? How tired do you feel? How much physical discomfort are you in? Participants were then asked to evaluate the effect of the music they listened to during that scan on the following emotions from the Geneva Emotional Music Scale (GEMS): wonder, transcendence, tenderness, nostalgia, powerfulness, happiness, peacefulness, sadness, and tension.

On the dosing day, participants were asked to rate how intense their LSD experience was on a scale from 0 to 10 approximately every 20 minutes from ingestion of the drug until they were considered sober by study staff. During scans, these were less frequent, aligning with blood samples.

Cerebral blood flow quantification

The preprocessing pipeline of pCASL consisted of several steps. First, label/control difference images were realigned for each post-label delay (PLD). The high-resolution T1-weighted structural image was then co-registered with the M0 image. Absolute CBF quantification was performed using BASIL (part of FSL - FMRIB software library) on all pCASL images (75). This process involved label/control image subtraction and signal calibration to absolute CBF (ml/100g/min), incorporating M0 scan data and employing a single, well-mixed tissue compartment model for tracer kinetics modeling. Standard parameters were applied for the quantitative modeling process (76). The structural image underwent segmentation using SPM12 to generate probability maps for grey matter, white matter, and cerebrospinal fluid. Subsequently, the calibrated pCASL image was transformed into MNI standard space using warps estimated during the segmentation step. Finally, the normalized pCASL images were smoothed spatially using a 3D Gaussian kernel (8 mm full-width half-maximum (FWHM)).

For regional analyses, we used the Anatomical Automatic Labelling atlas version 3 (AAL3) (77), which provides detailed cortical and subcortical parcellation in MNI space. We combined anatomically adjacent regions to create larger, functionally relevant regions of interest (ROIs). This resulted in 13 bilateral regions: prefrontal cortex, temporal cortex, parietal cortex, occipital cortex, anterior and posterior cingulate cortices, thalamus, amygdala, putamen, caudate nucleus, hippocampus, insula, and orbitofrontal cortex. Regional CBF values were calculated using grey-matter weighted averaging based on subject-specific segmentation maps. The specific composition of these compound ROIs followed the same approach as previously described (45), with full details provided in the Supplemental Table S6.

Internal carotid artery diameter quantification

We quantified ICA diameter using publicly available in-house software (<https://github.com/kristian1801/ica-segmentation-tool>). Through this software's pipeline, the TOF images were automatically processed with background subtraction, anisotropic diffusion filtering, and top-hat filtering to enhance vascular structures. The software's graphical interface allowed manual selection of the ICA, which was then automatically segmented using a 2D region-growing algorithm with dynamic intensity thresholding across axial slices. The software then reconstructed a 3D model of the segmented ICA and calculated vessel diameter using the median of measurements from each slice. All images were visually inspected to ensure the quality of the estimates.

Internal carotid artery flow quantification

We quantified ICA flow using previously developed PCMCALCULATOR software (78,79) (software available at <https://github.com/MarkVestergaard/PCMCALCULATOR>). Through this software's pipeline, PCM images were processed to measure through-plane flow. The software's graphical interface allowed manual selection of the ICA, which was then automatically analysed to calculate the flow rate. The methodology has been previously validated for both 3T Philips and 3T Siemens MR systems.

pCASL data quality control

pCASL and fMRI quality control are graphically described in Supplementary Figure S13.

1. Initial Data Collection and Exclusions

The dataset included multiple pCASL runs from baseline and LSD intervention sessions. Early quality assessment identified systematic signal dropout issues in runs 2 and 3, and 11 runs from 6 participants were excluded due to shimming-related signal dropouts.

2. Registration Quality Control

All pCASL images underwent visual inspection before and after transformation to MNI space.

Registration quality was assessed by:

- Alignment with participant structural images
- Correspondence with standard atlas landmarks
- Verification of anatomical boundaries and key structures.

3. Final Dataset Construction

7 participants met all quality criteria for both baseline and LSD sessions

Baseline CBF maps were constructed by averaging:

- * 3 runs for 3 participants

- * 2 runs for 4 participants

- LSD session analysis used only the first run from each participant's session.

Functional MRI preprocessing and denoising

Functional and anatomical preprocessing was performed using Configurable Pipeline for the Analysis of Connectomes (C-PAC version 1.8.7. Dev1). The .yaml file containing all settings used is available on the project GitHub (<https://github.com/Pneumaethylamine/dOccLS>). T1-weighted anatomical images underwent brain extraction using FSL's Brain Extraction Tool with the “robust” setting. Tissue segmentation using FSL's FAST and segmentation masks were made using a probability threshold of 0.9. Functional preprocessing steps included slice-timing correction, motion correction using AFNI's 3dvolreg, and distortion correction using a phase difference field map. Functional images were masked using AFNI and intensity-normalised. For spatial normalisation, anatomical images were registered to the MNI152 template using Advanced Normalization Tools (ANTs). Functional images were co-registered to the anatomical image using FSL's FLIRT with boundary-based registration, and subsequently transformed to MNI space. Nuisance regression was performed in each subject's native space. We applied ICA-AROMA (non-aggressive). Additional nuisance regressors included 24 motion parameters (6 motion parameters, their derivatives, squared terms, and squared derivatives), the first 5 principal components from white matter and cerebrospinal fluid, mean CSF signal, and linear and quadratic trends. A bandpass filter (0.01-0.1 Hz) was applied. Global-signal regression was not applied.

Preprocessed data were visually inspected at each step; following visual inspection, it was deemed that brain extraction was superior for one participant using the non-robust FSL BET setting, all other preprocessing steps remained the same. Post-processing steps included spatial smoothing using a 4mm FWHM Gaussian kernel, normalisation, and demeaning.

Functional MRI data quality control

1. Initial Data Exclusions

- Early quality assessment revealed systematic signal dropout issues in runs 2 and 3 of several sessions related to erroneous shim settings
- 4 runs from 3 participants were excluded due to these shimming-related signal dropouts.

2. Preprocessing Quality Control

- Standard preprocessing was applied to all remaining runs
- During ICA-AROMA denoising, one run was classified as containing >90% noise components
- Visual inspection of this run confirmed severe artifacts throughout the timeseries
- This run was excluded from further analysis.

3. Motion Assessment

- Mean framewise displacement (FD) was calculated using Power's method

- A threshold of 0.2 mm mean FD was set as the initial screening criterion
- All runs exceeding this threshold underwent comprehensive visual inspection, including:
 - * Temporal plots of 6 motion parameters and their derivatives
 - * DVARS timeseries
 - * Functional time series for key regions of interest
 - * Seed-based connectivity matrices
 - * Raw EPI data and preprocessed BOLD timeseries
- Based on this assessment, 2 runs showing excessive motion-related artifacts were excluded.

4. Final Dataset Construction

- 7 participants met all quality criteria for both baseline and LSD sessions
- Baseline maps were constructed by averaging:
 - * 3 runs for 4 participants
 - * 2 runs for 3 participants
- LSD session analysis used only the first run from each participant's session, none of which were excluded as described above.

fMRI correlation metrics

Scripts for transforming C-PAC outputs to the appropriate input format and for performing each fMRI analysis are publicly available (<https://github.com/Pneumaethylamine/dOccLS>).

Atlas and region selection

Unless otherwise stated, all measures were calculated using a combined atlas of the Schaefer 200-region parcellation and the 32-region S2 Tian subcortical atlas (80). For network connectivity, graph theory, and information-entropy analyses, we extracted time series data using the Schaefer 200-parcel atlas, and correlations were estimated using Nilearn in C-PAC (81). Each Schaefer 200-region region was assigned to one of seventeen networks as described in the Yeo-17 network parcellation, which was used for estimating network-connectivity scores (82). These networks include: Control (A, B, C), Default Mode (A, B, C), Dorsal Attention (A, B), Limbic (A, B), Salience/Ventral Attention (A, B), Somatomotor (A, B), Temporal Parietal, Visual Central, and Visual Peripheral. Thalamo-cortical correlation was calculated using merged thalamic regions from the S2 Tian subcortex atlas as a single seed (available on GitHub), and all voxels from the Schaefer-200 atlas as regions of interest (80,83). Normalised Spatial Complexity and Sample Entropy used Yeo-17 Networks as seeds.

Global correlation (GCOR)

The correlation between the time series for each voxel and every other voxel in a mask was calculated, and the median scores were considered as the GCOR score for that voxel. The resultant GCOR maps were then smoothed with a 3 mm FWHM kernel to limit variance due to inter-individual anatomical differences and enhance the spatial alignment of features across participants.

Thalamo-cortical correlation (TCOR)

The correlation between the timeseries for the thalamus seed and every other voxel in the mask was calculated, and the median scores were considered the TCOR score for that voxel. The resultant TCOR maps were then smoothed with a 3 mm FWHM kernel.

Surface projections of GCOR and TCOR analyses were generated using BrainNetViewer (84), with effects thresholded at absolute Cohen's $d_z > 0.3$ to delineate regions exhibiting at least small modulation of connectivity.

Atlas-based network connectivity

Network connectivity was quantified for both between-network and within-network connections. Let $C(r_a, r_b)$ denote the functional connectivity score between regions r_a and r_b . The connectivity A_{ij} between networks N_i and N_j was computed as: $A_{ij} = \text{median}(C(r_a, r_b))$ for all $r_a \in N_i$ and $r_b \in N_j$ when $r_a \neq r_b$.

fMRI information entropy metrics

Information-entropy metrics were calculated using the in-house developed Copenhagen Brain Entropy (CopBET) toolbox, available on GitHub <https://github.com/anders-s-olsen/CopBET>. For more detailed

methods, please see (59). Each applied metric is summarised briefly below. The measures Geodesic distribution entropy, Dynamic Conditional Correlation and Normalised Global Spatial Complexity apply a Shannon entropy quantification $H(X) = -\sum_{x \in X} p(x) \cdot \log_2 p(x)$ where $H(X)$ refers to the Shannon entropy of probability mass function X containing bins (x) with height (p).

Geodesic distribution entropy

Geodesic distribution entropy is a measure of the entropy of static connectivity given by the matrix of Pearson correlation coefficients, R , calculated as described above (85). Degree refers to the number of non-zero elements in any given row of a thresholded matrix. ROI-specific degrees are computed based on R , with $N=200$, using absolute correlation values. The goal of the thresholding for this analysis is to reach a pre-specified mean degree across rows. To achieve this, a threshold below which all absolute values are set to 0 is gradually increased until the mean number of non-zero elements is at the desired level. Here, we applied a scan-specific threshold that produced a mean degree range of 20-40. We report in the main text only the results from a mean degree of 40, as this aligns with a threshold applied in the previous literature. This means that each scan may have a different absolute threshold value, but nearly identical mean degree. The matrix was then binarised, setting all non-zero elements to 1. The "shortest path length" was then computed as the fewest edges one must traverse to go from one node to another using the MATLAB function "distances". The Shannon entropy of the distribution of path lengths from each node to all other nodes was then calculated.

Dynamic conditional correlation entropy

Windowless framewise correlation coefficients were calculated for all edges using the Dynamic Conditional Correlation (DCC) toolbox (86,87). Subsequently, the probability distribution over each ROI-to-ROI DCC time series was established, and the Shannon entropy was calculated. Each ROI was assigned to one of the Yeo-17 networks. Each ROI-to-ROI pair was then assigned to its respective network-to-network association (e.g., motor-motor, default mode-motor, etc.); the mean entropy of each network-to-network association was calculated.

Normalised spatial complexity (NSC)

NSC entropy was calculated using principal component analysis (PCA) of the voxelwise fMRI time series across the whole cortex or each Yeo-17 Network separately (58). This yields a set of eigenvalues. Let $\lambda_1, \lambda_2, \dots, \lambda_m$ be the eigenvalues obtained from the PCA, where m is the total number of eigenvalues. These eigenvalues are first normalised by dividing each by the sum of all eigenvalues: $\lambda_i' = \lambda_i / \sum_{i=1}^m \lambda_i$, where λ_i' is the normalised eigenvalue and the sum is taken over all i from 1 to m . The NSC entropy is then computed as: $NSC = -\sum_{i=1}^m (\lambda_i' * \log(\lambda_i')) / \ln(m)$, where the sum is taken over all i from 1 to m . The division by $\ln(m)$ serves to normalise the entropy value, ensuring it falls between 0 and 1. This calculation is performed both on the whole-brain level and for each region of interest defined by the atlas, resulting in a global NSC entropy value and a set of regional NSC entropy values for each fMRI session.

Multi-scale sample entropy

Sample entropy is defined as the negative logarithm of the conditional probability that if two vectors with length m (set to 2) are dissimilar below a threshold distance r (set as 0.3), then vector pairs with length $m+1$

will also have distance below the threshold. Sample entropy for scales 1-5 was evaluated for each network, meaning that each time-series was split into non-overlapping windows of length (scale) s volumes and the means of each window were concatenated to form a condensed time-series upon which sample entropy was calculated (88). Sample entropy was calculated for each voxel in the Yeo-17 networks and then averaged across voxels to return a score for each scale for each network. Scale 1 (i.e., no downsampling) is reported in the main text; all scales are reported in the Supplementary Table S5.

Lempel-Ziv complexity

The BOLD time series for each ROI were first Hilbert-transformed. The amplitude of the Hilbert series was then binarised around the mean amplitude for that region, i.e., assigned as 1 if greater than the mean and 0 if less. These binarised time series were combined into a $T \times N$ matrix, where T is the number of time points and $N = 232$ is the number of regions. This matrix was collapsed into a single vector to compute the Lempel-Ziv complexity over time (LZct, LZ78 algorithm) wherein regional time series were concatenated. LZct represents a calculation of the temporal entropy of each ROI (89,90).

fMRI graph theory metrics

Graph theory metrics used functions from the Brain Connectivity Toolbox (2019 March version) (91).

Modularity

Modularity was calculated by applying the `community_louvain` function from the Brain Connectivity Toolbox (BCT) (91) with $\gamma = 1$ and asymmetric treatment of negative weights to the weighted, undirected Pearson's correlation matrix for each scan individually. This was repeated 100 times, and the maximum value was saved as the absolute modularity. Subsequently, 100 null graphs were created using the `null_model_und_sign` function in BCT; for each null graph, the same procedure for calculating modularity was applied, i.e., taking the maximum of 100 repetitions of applying the `community_louvain` function. The observed modularity was normalised with respect to the mean modularity of these null models, i.e., $\text{normalised_modularity} = \text{absolute_modularity} / \text{null_modularity}$.

Small-worldness

A positive-only matrix was used by removing all negative correlations because small-worldness stems from calculating path-length, which is ill-described for graphs with negative correlations. Further, we did not consider it sensible to take the absolute values, as negative correlations represent distinct neural phenomena from positive correlations, and there is no consensus strategy for how to account for these in the estimation of small-worldness (92).

First, the mean clustering coefficient (C) across all regions was calculated using the BCT function `clustering_coef_wu`. The average path length (L) was calculated using the BCT function `distance_wei_floyd('log')` as the mean of the non-infinite, non-zero path lengths. We generated 100 null graphs using the BCT function `null_model_und_sign` on the unthresholded matrix, which was then thresholded to include only positive edges. C and L were calculated for each null graph, and observed small-

worldness was normalised as $SM_{\text{norm}} = (C / \text{mean}(C_{\text{null}})) / (L / \text{mean}(L_{\text{null}}))$, where C_{null} and L_{null} are C and L , respectively, calculated on null graphs.

Multimodal analysis

Registration and regional alignment

To enable cross-modal comparisons between CBF and BOLD fMRI (GCOR), we quantified both modalities within the same set of brain regions defined by the AAL3 atlas (93). CBF data were already processed within the AAL regions. To ensure spatial correspondence, individual GCOR maps were transformed into AAL3 space, and regional mean values were extracted from the same atlas-defined regions. For PET data, we used previously computed neocortical 5-HT_{2A}R occupancy estimates for each participant.

Cross-modality correlation analysis

We used Spearman's rank correlation (ρ) to assess the relation between neocortical 5-HT_{2A}R occupancy and changes in regional CBF, between occupancy and changes in regional GCOR, and between changes in CBF and GCOR. Changes for CBF and GCOR scores were calculated as LSD minus baseline. Correlations were run across participants for each region to identify spatial variability in how receptor occupancy relates to functional brain changes.

Statistics

Given the densely sampled but limited cohort ($n = 7$) and heterogeneous dosing regimens, we prioritised effect size analyses to characterize LSD-induced hemodynamic and functional connectivity alterations. Effect sizes provide meaningful information about the magnitude and practical meaningfulness of the observed changes, particularly valuable in studies with smaller samples (94). While we initially explored linear mixed-effect models to account for repeated measures, these often failed to converge or produced singular fits. Therefore, to ensure consistent modeling across measures, we averaged across densely sampled baseline runs to calculate participant- and session-specific maps, considering only the first scans during LSD sessions. We computed Cohen's d_z values as the mean difference between conditions (LSD - baseline) divided by the standard deviation of those differences. For CBF regional effects, we supplemented the effect size analyses with a step-down permutation procedure that leveraged all possible permutations of our dataset to control for multiple comparisons (see Supplementary Figure S7 and Supplementary Table S2 for details).

For the relation between average subjective drug intensity and occupancy, a sigmoid function was fit where the parameters a, b, and c were estimated using nonlinear least squares regression on the model data. The sigmoid model was implemented in R (v4.3.1) using the following code:

```
sigmoid_model <- stats::nls(avg_score ~ a / (1 + exp(-b * (OCCUPANCY - c))),  
  data = model_data,  
  start = list(a = 5, b = 0.1, c = 50))
```

Plasma LSD quantification

Plasma samples (100 μ L) were spiked with 20 μ L internal standard (LSD-d3) and protein precipitated with acetonitrile (700 μ L) using a fully automated robotic system. The supernatant (700 μ L) was acidified with 50 μ L 10% formic acid in acetonitrile, evaporated, and reconstituted in 100 μ L 12.5% methanol:12.5% acetonitrile in 0.05% formic acid.

LSD was quantified by ultra-high-performance liquid chromatography–tandem mass spectrometry (UHPLC–MS/MS) using a Kinetex Biphenyl column (2.6 μ m, 2.1 x 50 mm), and gradient elution of A: 1 mM ammonium formate in 0.1% formic acid and B: 1:1 methanol:acetonitrile with 0.1% formic acid. The column temperature was held constant at 50°C, the flow rate was 0.50 mL/min, and the total run time was 3.9 min. The injection volume was 2 μ L. The quantification was performed using multiple reaction monitoring (MRM) in positive ionization mode. The two MRM transitions used for LSD were m/z 324 \rightarrow 223 and 324 \rightarrow 207. The MRM transition used for the internal standard LSD-d3 was m/z 327 \rightarrow 226.

Five calibrators in plasma were freshly prepared for each series, and two quality control (QC) samples in plasma were included in each series in duplicates. The measurement range was 0.0001–0.01 mg/kg (0.28 – 28.5 nM) using a linear calibration model and a weighting factor of 1/x. The method showed acceptable accuracy and precision for the QCs according to international guidelines.

Concentrations were quantified in mcg of LSD per kg blood, which were converted to nanomolar values using an estimated plasma density of 1.02 g/ml and the molecular weight of LSD of 323.43 g/mol.

CYP2D6 genotyping

CYP2D6 genotyping was performed according to established methods at the Danish Epilepsy Centre Laboratory Unit using validated real-time PCR assays (For detailed methodology, see Jensen et al.) (95).

Code availability

The code used for analyses are available on Github <https://github.com/Pneumaethylamine/dOccLS>.

Data availability

Data from this study are available through the Center for Integrated Molecular Brain Imaging (Cimbi) Database and Biobank at Rigshospitalet, Copenhagen (96). Researchers can request access to the dataset by completing a standardised application form available at the Cimbi website (<https://nru.dk/index.php/research-menu/research-groups/115-the-cimbi-database-and-biobank>) (96)

Funding

This project was funded by Savværksejerfonden and Novo Nordisk Fonden (NNF23OC0082288). DEM's salary was supported by an unrestricted grant from COMPASS Pathways PLC, which had no input in the study design or manuscript preparation. KL's salary was supported by Rigshospitalet Research Fund (R259-

A11532). KHRJ's salary was funded by The Lundbeck Foundation as part of the BrainDrugs study (R279-2018-1145). FH was supported by the Swiss National Science Foundation (grant no. P500PM_210867)

Author contributions

D.E.W.M. and K.L. contributed equally to this work as co-first authors. D.E.W.M. designed the study, developed protocols, collected data, performed data analysis, created visualizations, and wrote the manuscript. K.L. collected data, performed data analysis, created visualizations, and wrote the manuscript. A.J., K.H.R.J., and C.H.N. provided medical supervision throughout study implementation. F.H. provided supervision and assisted with regulatory submissions. N.F., V.N., E.S., P.S.A., and A.S. recruited and screened participants and assisted with data collection. M.G. and P.P.R. provided psychological support during the psychedelic sessions. P.S.J. managed the database and data organization. V.S. performed radiochemistry for the PET tracers. S.S.J. and M.K.K.N. conducted quantification of plasma drug levels. T.L.A. supervised PET and MRI scanning procedures. D.S.S. provided psychology supervision and guidance. C.S. supervised PET data analysis. P.M.F. and G.M.K. contributed equally to this work as co-senior authors. They designed the study, supervised the project implementation, provided resources, and contributed to manuscript writing and revision. All authors reviewed and approved the final version of the manuscript.

Acknowledgements

We would like to thank Dr. Cedric Hysek and Dr. Matthias Liechti for supplying LSD for the study, Lone Freyr and Emilie Henriksen for facilitating and planning all of the scans. Dorthe Givard for her endlessly patient administrative support. Prof. Brice Ozenne for patient statistical advice. Dr. Maja Marstrand-Jørgensen for helping with setting up the scan parameters and REDcap databases, and for looking after our baby daughter during the long scan days. The John and Birthe Meyer Foundation is gratefully acknowledged for the donation of the Cyclotron and PET-MRI scanner.

Conflicts of interest

DEM salary is supported by an unrestricted grant from COMPASS Pathways Ltd, which had no input on study design or manuscript preparation. The authors declare that the research was conducted in the absence of any commercial, non-financial, or financial relationships that could be construed as a potential conflict of interest.

Bibliography

1. Nichols DE. Psychedelics. *Pharmacol Rev*. 2016;
2. Holze F, Ley L, Müller F, Becker AM, Straumann I, Vizeli P, et al. Direct comparison of the acute effects of lysergic acid diethylamide and psilocybin in a double-blind placebo-controlled study in healthy subjects. *Neuropsychopharmacology*. 2022 May 25;47(6):1180–7.
3. Becker AM, Klaiber A, Holze F, Istampoulouoglou I, Duthaler U, Varghese N, et al. Ketanserin Reverses the Acute Response to LSD in a Randomized, Double-Blind, Placebo-Controlled, Crossover Study in Healthy Participants. *Int J Neuropsychopharmacol*. 2023 Feb 14;26(2):97–106.
4. Holze F, Vizeli P, Ley L, Müller F, Dolder P, Stocker M, et al. Acute dose-dependent effects of lysergic acid diethylamide in a double-blind placebo-controlled study in healthy subjects. *Neuropsychopharmacology*. 2021;
5. Becker AM, Holze F, Grandinetti T, Klaiber A, Toedtli VE, Kolaczynska KE, et al. Acute Effects of Psilocybin After Escitalopram or Placebo Pretreatment in a Randomized, Double-Blind, Placebo-Controlled, Crossover Study in Healthy Subjects. *Clin Pharmacol Ther*. 2022 Apr;111(4):886–95.
6. Gasser P, Kirchner K, Passie T. LSD-assisted psychotherapy for anxiety associated with a life-threatening disease: A qualitative study of acute and sustained subjective effects. *J Psychopharmacol (Oxf)*. 2015 Jan 11;29(1):57–68.
7. Holze F, Gasser P, Müller F, Dolder PC, Liechti ME. Lysergic Acid Diethylamide–Assisted Therapy in Patients With Anxiety With and Without a Life-Threatening Illness: A Randomized, Double-Blind, Placebo-Controlled Phase II Study. *Biol Psychiatry [Internet]*. 2022 Sep; Available from: <https://linkinghub.elsevier.com/retrieve/pii/S0006322322015530>
8. Murphy RJ, Sumner R, Evans W, Ponton R, Ram S, Godfrey K, et al. Acute Mood-Elevating Properties of Microdosed Lysergic Acid Diethylamide in Healthy Volunteers: A Home-Administered Randomized Controlled Trial. *Biol Psychiatry*. 2023 Sep 15;94(6):511–21.
9. Beliveau V, Ganz M, Feng L, Ozenne B, Højgaard L, Fisher PM, et al. A High-Resolution In Vivo Atlas of the Human Brain's Serotonin System. *J Neurosci*. 2017;
10. Glennon RA, Titeler M, McKenney JD. Evidence for 5-HT₂ involvement in the mechanism of action of hallucinogenic agents. *Life Sci*. 1984 Dec;35(25):2505–11.
11. Preller KH, Burt JB, Ji JL, Schleifer CH, Adkinson BD, Stämpfli P, et al. Changes in global and thalamic brain connectivity in LSD-induced altered states of consciousness are attributable to the 5-HT_{2A} receptor. *eLife*. 2018;7:1–31.
12. Buchborn T, Lyons T, Knöpfel T. Tolerance and Tachyphylaxis to Head Twitches Induced by the 5-HT_{2A} Agonist 25CN-NBOH in Mice. *Front Pharmacol*. 2018 Feb 6;9:17.
13. Fantegrossi WE, Gray BW, Bailey JM, Smith D, Hansen M, Kristensen JL. Hallucinogen-like effects of 2-([2-(4-cyano-2,5-dimethoxyphenyl) ethylamino]methyl)phenol (25CN-NBOH), a novel N-benzylphenethylamine with 100-fold selectivity for 5-HT_{2A} receptors, in mice. *Psychopharmacology (Berl)*. 2015 Mar;232(6):1039–47.
14. Carhart-Harris RL, Muthukumaraswamy S, Roseman L, Kaelen M, Droog W, Murphy K, et al. Neural correlates of the LSD experience revealed by multimodal neuroimaging. *Proc Natl Acad Sci*. 2016

Apr 26;113(17):4853–8.

15. Kim K, Che T, Panova O, DiBerto JF, Lyu J, Krumm BE, et al. Structure of a Hallucinogen-Activated Gq-Coupled 5-HT_{2A} Serotonin Receptor. *Cell*. 2020 Sep;182(6):1574-1588.e19.
16. Gumpfer RH, Jain MK, Kim K, Sun R, Sun N, Xu Z, et al. The structural diversity of psychedelic drug actions revealed. *Nat Commun*. 2025 Mar 19;16(1):2734.
17. McCulloch DEW, Knudsen GM, Barrett FS, Doss MK, Carhart-Harris RL, Rosas FE, et al. Psychedelic resting-state neuroimaging: A review and perspective on balancing replication and novel analyses. *Neurosci Biobehav Rev*. 2022 Jul;138:104689.
18. Doss MK, Madden MB, Gaddis A, Nebel MB, Griffiths RR, Mathur BN, et al. Models of psychedelic drug action: modulation of cortical-subcortical circuits. *Brain* [Internet]. 2021 Dec 13; Available from: <https://academic.oup.com/brain/advance-article/doi/10.1093/brain/awab406/6460325>
19. McCulloch DEW, Lopez JP, Dalla C, Castrén E, Erritzoe D, Frokjaer VG, et al. Knowledge gaps in psychedelic medicalisation: Preclinical and neuroimaging mechanisms. *Neurosci Appl*. 2023 Dec 15;103929.
20. Machida T, Iizuka K, Hirafuji M. 5-hydroxytryptamine and its receptors in systemic vascular walls. *Biol Pharm Bull*. 2013;36(9):1416–9.
21. Sporns O, Betzel RF. Modular Brain Networks. *Annu Rev Psychol*. 2016 Jan 4;67(1):613–40.
22. Hasselbalch SG, Madsen PL, Knudsen GM, Holm S, Paulson OB. Calculation of the FDG lumped constant by simultaneous measurements of global glucose and FDG metabolism in humans. *J Cereb Blood Flow Metab Off J Int Soc Cereb Blood Flow Metab*. 1998 Feb;18(2):154–60.
23. Krejza J, Arkuszewski M, Kasner SE, Weigle J, Ustymowicz A, Hurst RW, et al. Carotid Artery Diameter in Men and Women and the Relation to Body and Neck Size. *Stroke*. 2006 Apr;37(4):1103–5.
24. Alsop DC, Detre JA, Golay X, Günther M, Hendrikse J, Hernandez-Garcia L, et al. Recommended implementation of arterial spin-labeled perfusion MRI for clinical applications: A consensus of the ISMRM perfusion study group and the European consortium for ASL in dementia. *Magn Reson Med*. 2015;73(1):102–16.
25. Zarrinkoob L, Ambarki K, Wåhlin A, Birgander R, Eklund A, Malm J. Blood flow distribution in cerebral arteries. *J Cereb Blood Flow Metab Off J Int Soc Cereb Blood Flow Metab*. 2015 Mar 31;35(4):648–54.
26. Luethi D, Hoener MC, Krähenbühl S, Liechti ME, Duthaler U. Cytochrome P450 enzymes contribute to the metabolism of LSD to nor-LSD and 2-oxo-3-hydroxy-LSD: Implications for clinical LSD use. *Biochem Pharmacol*. 2019 Jun;164:129–38.
27. Pierce PA, Peroutka SJ. Hallucinogenic drug interactions with neurotransmitter receptor binding sites in human cortex. *Psychopharmacology (Berl)*. 1989 Jan 1;97(1):118–22.
28. Rickli A, Luethi D, Reinisch J, Buchy D, Hoener MC, Liechti ME. Receptor interaction profiles of novel N-2-methoxybenzyl (NBOMe) derivatives of 2,5-dimethoxy-substituted phenethylamines (2C drugs). *Neuropharmacology*. 2015 Dec;99:546–53.
29. Dolder PC, Schmid Y, Haschke M, Rentsch KM, Liechti ME. Pharmacokinetics and Concentration-Effect Relationship of Oral LSD in Humans. *Int J Neuropsychopharmacol*. 2015 Jun 24;19(1):pyv072.

30. Madsen MK, Fisher PM, Burmester D, Dyssegaard A, Stenbæk DS, Kristiansen S, et al. Psychedelic effects of psilocybin correlate with serotonin 2A receptor occupancy and plasma psilocin levels. *Neuropsychopharmacology*. 2019;44(7):1328–34.
31. Mitchell JM, Ot'alora G. M, van der Kolk B, Shannon S, Bogenschutz M, Gelfand Y, et al. MDMA-assisted therapy for moderate to severe PTSD: a randomized, placebo-controlled phase 3 trial. *Nat Med*. 2023 Oct;29(10):2473–80.
32. Mitchell JM, Bogenschutz M, Lilienstein A, Harrison C, Kleiman S, Parker-Guilbert K, et al. MDMA-assisted therapy for severe PTSD: a randomized, double-blind, placebo-controlled phase 3 study. *Nat Med*. 2021 Jun;27(6):1025–33.
33. Liechti ME, Saur MR, Gamma A, Hell D, Vollenweider FX. Psychological and physiological effects of MDMA ('Ecstasy') after pretreatment with the 5-HT₂ antagonist ketanserin in healthy humans. *Neuropsychopharmacology*. 2000;23(4):396–404.
34. Vizeli P, Studerus E, Holze F, Schmid Y, Dolder PC, Ley L, et al. Pharmacological and non-pharmacological predictors of the LSD experience in healthy participants. *Transl Psychiatry*. 2024 Sep 4;14(1):1–8.
35. Holze F, Madsen MK, Svarer C, Gillings N, Stenbaek DS, Rudin D, et al. Ketanserin exhibits dose- and concentration-proportional serotonin 2A receptor occupancy in healthy individuals: Relevance for psychedelic research. *Eur Neuropsychopharmacol J Eur Coll Neuropsychopharmacol*. 2024 Nov;88:43–8.
36. Gründer G, Yokoi F, Offord SJ, Ravert HT, Dannals RF, Salzmänn JK, et al. Time course of 5-HT_{2A} receptor occupancy in the human brain after a single oral dose of the putative antipsychotic drug MDL 100,907 measured by positron emission tomography. *Neuropsychopharmacol Off Publ Am Coll Neuropsychopharmacol*. 1997 Sep;17(3):175–85.
37. Nordstrom AL, Mansson M, Jovanovic H, Karlsson P, Halldin C, Farde L, et al. PET analysis of the 5-HT_{2A} receptor inverse agonist ACP-103 in human brain. *Int J Neuropsychopharmacol*. 2008;11(2):163–71.
38. Madsen MK, Stenbæk DS, Arvidsson A, Armand S, Marstrand-Joergensen MR, Johansen SS, et al. Psilocybin-induced changes in brain network integrity and segregation correlate with plasma psilocin level and psychedelic experience. *Eur Neuropsychopharmacol J Eur Coll Neuropsychopharmacol*. 2021 Sep;50:121–32.
39. Kim S, Chen J, Cheng T, Gindulyte A, He J, He S, et al. PubChem in 2021: new data content and improved web interfaces. *Nucleic Acids Res*. 2021 Jan 8;49(D1):D1388–95.
40. Wallach J, Cao AB, Calkins MM, Heim AJ, Lanham JK, Bonniwell EM, et al. Identification of 5-HT_{2A} receptor signaling pathways associated with psychedelic potential. *Nat Commun*. 2023 Dec 15;14(1):8221.
41. Kim K, Che T, Panova O, DiBerto JF, Lyu J, Krumm BE, et al. Structure of a Hallucinogen-Activated Gq-Coupled 5-HT_{2A} Serotonin Receptor. *Cell*. 2020 Sep 17;182(6):1574–1588.e19.
42. Madsen MK, Fisher PM, Stenbæk DS, Kristiansen S, Burmester D, Lehel S, et al. A single psilocybin dose is associated with long-term increased mindfulness, preceded by a proportional change in neocortical 5-HT_{2A} receptor binding. *Eur Neuropsychopharmacol*. 2020;33:71–80.
43. Lewis CR, Preller KH, Kraehenmann R, Michels L, Staempfli P, Vollenweider FX. Two dose investigation of the 5-HT-agonist psilocybin on relative and global cerebral blood flow. *NeuroImage*.

2017;159(July):70–8.

44. Rieser NM, Gubser LP, Moujaes F, Duerler P, Lewis CR, Michels L, et al. Psilocybin-induced changes in cerebral blood flow are associated with acute and baseline inter-individual differences. *Sci Rep*. 2023 Oct 14;13(1):17475.
45. Larsen K, Lindberg U, Ozenne B, McCulloch DE, Armand S, Madsen MK, et al. Acute psilocybin and ketanserin effects on cerebral blood flow: 5-HT_{2A}R neuromodulation in healthy humans. *J Cereb Blood Flow Metab*. 2025 Feb 26;0271678X251323364.
46. Rickli A, Luethi D, Reinisch J, Buchy D, Hoener MC, Liechti ME. Receptor interaction profiles of novel N-2-methoxybenzyl (NBOMe) derivatives of 2,5-dimethoxy-substituted phenethylamines (2C drugs). *Neuropharmacology*. 2015 Dec;99:546–53.
47. Janowsky A, Eshleman AJ, Johnson RA, Wolfrum KM, Hinrichs DJ, Yang J, et al. Mefloquine and psychotomimetics share neurotransmitter receptor and transporter interactions in vitro. *Psychopharmacology (Berl)*. 2014 Jul;231(14):2771–83.
48. Golino P, Piscione F, Willerson JT, Cappelli-Bigazzi M, Focaccio A, Villari B, et al. Divergent Effects of Serotonin on Coronary-Artery Dimensions and Blood Flow in Patients with Coronary Atherosclerosis and Control Patients. *N Engl J Med*. 1991 Mar 7;324(10):641–8.
49. Tepper SJ, Rapoport AM, Sheftell FD. Mechanisms of Action of the 5-HT_{1B/1D} Receptor Agonists. *Arch Neurol*. 2002 Jul 1;59(7):1084–8.
50. Klotz JL, Bush LP, Smith DL, Shafer WD, Smith LL, Vevoda AC, et al. Assessment of vasoconstrictive potential of D-lysergic acid using an isolated bovine lateral saphenous vein bioassay. *J Anim Sci*. 2006 Nov;84(11):3167–75.
51. Lassen NA. Cerebral Blood Flow and Oxygen Consumption in Man. *Physiol Rev*. 1959 Apr;39(2):183–238.
52. Vollenweider FX, Leenders KL, Scharfetter C, Maguire P, Stadelmann O, Angst J. Positron emission tomography and fluorodeoxyglucose studies of metabolic hyperfrontality and psychopathology in the psilocybin model of psychosis. *Neuropsychopharmacology*. 1997;16(5):357–72.
53. Saini HK, Takeda N, Goyal RK, Kumamoto H, Arneja AS, Dhalla NS. Therapeutic potentials of sarpogrelate in cardiovascular disease. *Cardiovasc Drug Rev*. 2004;22(1):27–54.
54. Avram M, Fortea L, Wollner L, Coenen R, Korda A, Rogg H, et al. Large-scale brain connectivity changes following the administration of lysergic acid diethylamide, d-amphetamine, and 3,4-methylenedioxymphetamine. *Mol Psychiatry*. 2024 Sep 11;1–11.
55. Tagliazucchi E, Roseman L, Kaelen M, Orban C, Muthukumaraswamy SD, Murphy K, et al. Increased Global Functional Connectivity Correlates with LSD-Induced Ego Dissolution. *Curr Biol*. 2016;26(8):1043–50.
56. Müller F, Lenz C, Dolder P, Lang U, Schmidt A, Liechti M, et al. Increased thalamic resting-state connectivity as a core driver of LSD-induced hallucinations. *Acta Psychiatr Scand*. 2017 Dec;136(6):648–57.
57. Lebedev AV, Kaelen M, Lövdén M, Nilsson J, Feilding A, Nutt DJ, et al. LSD-induced entropic brain activity predicts subsequent personality change. *Hum Brain Mapp*. 2016;37(9):3203–13.
58. Siegel JS, Subramanian S, Perry D, Kay BP, Gordon EM, Laumann TO, et al. Psilocybin

desynchronizes the human brain. *Nature*. 2024 Aug;632(8023):131–8.

59. McCulloch DEW, Olsen AS, Ozenne B, Stenbæk DS, Armand S, Madsen MK, et al. Navigating the chaos of psychedelic neuroimaging: A multi-metric evaluation of acute psilocybin effects on brain entropy [Internet]. *medRxiv*; 2023 [cited 2024 Mar 11]. p. 2023.07.03.23292164. Available from: <https://www.medrxiv.org/content/10.1101/2023.07.03.23292164v1>
60. Timmermann C, Roseman L, Haridas S, Rosas FE, Luan L, Kettner H, et al. Human brain effects of DMT assessed via EEG-fMRI. *Proc Natl Acad Sci*. 2023 Mar 28;120(13):e2218949120.
61. Preller KH, Duerler P, Burt JB, Ji JL, Adkinson B, Stämpfli P, et al. Psilocybin Induces Time-Dependent Changes in Global Functional Connectivity. *Biol Psychiatry*. 2020;
62. Botvinik-Nezer R, Holzmeister F, Camerer CF, Dreber A, Huber J, Johannesson M, et al. Variability in the analysis of a single neuroimaging dataset by many teams. *Nature*. 2020 Jun;582(7810):84–8.
63. Taylor PA, Aggarwal H, Bandettini PA, Barilari M, Bright MG, Caballero-Gaudes C, et al. Go Figure: Transparency in neuroscience images preserves context and clarifies interpretation. *ArXiv*. 2025 Apr 10;arXiv:2504.07824v1.
64. Drew PJ. Vascular and neural basis of the BOLD signal. *Curr Opin Neurobiol*. 2019 Oct;58:61–9.
65. Paulson OB, Hasselbalch SG, Rostrup E, Knudsen GM, Pelligrino D. Cerebral Blood Flow Response to Functional Activation. *J Cereb Blood Flow Metab*. 2010 Jan 1;30(1):2–14.
66. Perthen JE, Lansing AE, Liao J, Liu TT, Buxton RB. Caffeine-induced uncoupling of cerebral blood flow and oxygen metabolism: A calibrated BOLD fMRI study. *NeuroImage*. 2008 Mar 1;40(1):237–47.
67. Biswal B, Hudetz AG, Yetkin FZ, Haughton VM, Hyde JS. Hypercapnia reversibly suppresses low-frequency fluctuations in the human motor cortex during rest using echo-planar MRI. *J Cereb Blood Flow Metab Off J Int Soc Cereb Blood Flow Metab*. 1997 Mar;17(3):301–8.
68. Liu TT. Neurovascular factors in resting-state functional MRI. *NeuroImage*. 2013 Oct 15;80:339–48.
69. World Medical Association. World Medical Association Declaration of Helsinki: Ethical Principles for Medical Research Involving Human Participants. *JAMA*. 2025 Jan 7;333(1):71–4.
70. Gong K, Yang J, Kim K, El Fakhri G, Seo Y, Li Q. Attenuation correction for brain PET imaging using deep neural network based on Dixon and ZTE MR images. *Phys Med Biol*. 2018 Jun 13;63(12):125011.
71. Svarer C, Madsen K, Hasselbalch SG, Pinborg LH, Haugbøl S, Frøkjær VG, et al. MR-based automatic delineation of volumes of interest in human brain PET images using probability maps. *NeuroImage*. 2005 Feb 15;24(4):969–79.
72. Ettrup A, da Cunha-Bang S, McMahon B, Lehel S, Dyssegaard A, Skibsted AW, et al. Serotonin 2A receptor agonist binding in the human brain with [¹¹C]Cimbi-36. *J Cereb Blood Flow Metab Off J Int Soc Cereb Blood Flow Metab*. 2014 Jul;34(7):1188–96.
73. Innis RB, Cunningham VJ, Delforge J, Fujita M, Gjedde A, Gunn RN, et al. Consensus nomenclature for in vivo imaging of reversibly binding radioligands. *J Cereb Blood Flow Metab*. 2007;
74. Greve DN, Svarer C, Fisher PM, Feng L, Hansen AE, Baare W, et al. Cortical surface-based analysis reduces bias and variance in kinetic modeling of brain PET data. *NeuroImage*. 2014 May 15;92:225–36.

75. Chappell MA, Groves AR, Whitcher B, Woolrich MW. Variational Bayesian Inference for a Nonlinear Forward Model. *IEEE Trans Signal Process*. 2009 Jan;57(1):223–36.
76. Alsop DC, Detre JA, Golay X, Günther M, Hendrikse J, Hernandez-Garcia L, et al. Recommended Implementation of Arterial Spin Labeled Perfusion MRI for Clinical Applications: A consensus of the ISMRM Perfusion Study Group and the European Consortium for ASL in Dementia. *Magn Reson Med*. 2015 Jan;73(1):102–16.
77. Rolls ET, Huang CC, Lin CP, Feng J, Joliot M. Automated anatomical labelling atlas 3. *NeuroImage*. 2020 Feb 1;206:116189.
78. Vestergaard MB, Ghanizada H, Lindberg U, Arngrim N, Paulson OB, Gjedde A, et al. Human Cerebral Perfusion, Oxygen Consumption, and Lactate Production in Response to Hypoxic Exposure. *Cereb Cortex*. 2022 Mar 15;32(6):1295–306.
79. Vestergaard MB, Larsson HB. Cerebral metabolism and vascular reactivity during breath-hold and hypoxic challenge in freedivers and healthy controls. *J Cereb Blood Flow Metab Off J Int Soc Cereb Blood Flow Metab*. 2019 May;39(5):834–48.
80. Tian Y, Margulies DS, Breakspear M, Zalesky A. Topographic organization of the human subcortex unveiled with functional connectivity gradients. *Nat Neurosci*. 2020;
81. Abraham A, Pedregosa F, Eickenberg M, Gervais P, Mueller A, Kossaifi J, et al. Machine learning for neuroimaging with scikit-learn. *Front Neuroinformatics* [Internet]. 2014 Feb 21 [cited 2025 Jan 27];8. Available from: <https://www.frontiersin.org/journals/neuroinformatics/articles/10.3389/fninf.2014.00014/full>
82. Yeo BT, Krienen FM, Sepulcre J, Sabuncu MR, Lashkari D, Hollinshead M, et al. The organization of the human cerebral cortex estimated by intrinsic functional connectivity. *J Neurophysiol*. 2011;
83. Schaefer A, Kong R, Gordon EM, Laumann TO, Zuo XN, Holmes AJ, et al. Local-Global Parcellation of the Human Cerebral Cortex from Intrinsic Functional Connectivity MRI. *Cereb Cortex*. 2018;
84. Xia M, Wang J, He Y. BrainNet Viewer: A Network Visualization Tool for Human Brain Connectomics. *PLOS ONE*. 2013 Jul 4;8(7):e68910.
85. Viol A, Palhano-Fontes F, Onias H, de Araujo DB, Hövel P, Viswanathan GM. Characterizing Complex Networks Using Entropy-Degree Diagrams: Unveiling Changes in Functional Brain Connectivity Induced by Ayahuasca. *Entropy* 2019 Vol 21 Page 128. 2019 Jan 30;21(2):128.
86. Lindquist MA, Xu Y, Nebel MB, Caffo BS. Evaluating Dynamic Bivariate Correlations in Resting-state fMRI: A comparison study and a new approach. *NeuroImage*. 2014 Nov 1;101:531–46.
87. Barrett FS, Doss MK, Sepeda ND, Pekar JJ, Griffiths RR. Emotions and brain function are altered up to one month after a single high dose of psilocybin. *Sci Rep*. 2020;10(1):1–14.
88. Delgado-Bonal A, Marshak A. Approximate Entropy and Sample Entropy: A Comprehensive Tutorial. *Entropy*. 2019 Jun;21(6):541.
89. Schartner MM, Carhart-Harris RL, Barrett AB, Seth AK, Muthukumaraswamy SD. Increased spontaneous MEG signal diversity for psychoactive doses of ketamine, LSD and psilocybin. *Sci Rep*. 2017 Apr 19;7(1):46421.
90. Varley TF, Carhart-Harris R, Roseman L, Menon DK, Stamatakis EA. Serotonergic psychedelics LSD & psilocybin increase the fractal dimension of cortical brain activity in spatial and temporal domains.

NeuroImage. 2020 Oct;220:117049.

91. Rubinov M, Sporns O. Complex network measures of brain connectivity: Uses and interpretations. *NeuroImage*. 2010 Sep;52(3):1059–69.
92. Zhan L, Jenkins LM, Wolfson OE, GadElkarim JJ, Nocito K, Thompson PM, et al. The significance of negative correlations in brain connectivity. *J Comp Neurol*. 2017 Oct 15;525(15):3251–65.
93. Rolls ET, Huang CC, Lin CP, Feng J, Joliot M. Automated anatomical labelling atlas 3. *NeuroImage*. 2020 Feb;206:116189.
94. Lakens D. Calculating and reporting effect sizes to facilitate cumulative science: a practical primer for t-tests and ANOVAs. *Front Psychol* [Internet]. 2013 Nov 26 [cited 2025 Jan 27];4. Available from: <https://www.frontiersin.org/journals/psychology/articles/10.3389/fpsyg.2013.00863/full>
95. Larsen JB, Rasmussen JB. Pharmacogenetic testing revisited: 5' nuclease real-time polymerase chain reaction test panels for genotyping CYP2D6 and CYP2C19. *Pharmacogenomics Pers Med*. 2017;10:115–28.
96. Knudsen GM, Jensen PS, Erritzoe D, Baaré WFC, Ettrup A, Fisher PM, et al. The Center for Integrated Molecular Brain Imaging (Cimbi) database. *NeuroImage*. 2016 Jan 1;124(Pt B):1213–9.

Supplementary materials

Supplementary Results

- Adverse effects
- LSD effects on emotional response to music

Supplementary Figures

- S1. Relation between CYP2D6 metabolizer status and LSD plasma levels
- S2. Relation between weight-adjusted LSD dose and peak plasma concentrations
- S3. In-scanner comfort ratings during scans
- S4. Dose-occupancy relation for LSD
- S5. LSD-induced changes in cerebral blood flow and internal carotid artery flow
- S6. Regional cerebral blood flow measurements at baseline and after LSD administration
- S7. Distribution of t-statistics for LSD effects on cerebral blood flow across brain regions
- S8. Individual changes in cerebral blood flow following LSD administration.
- S9. Individual changes in global brain connectivity following LSD administration
- S10. Individual changes in thalamo-cortical connectivity following LSD administration
- S11. Study protocol overview and participant flow (CONSORT diagram)
- S12. Quality control pipeline across imaging modalities
- S13. Music-evoked emotional responses measured by the Geneva Emotional Music Scale (GEMS)

Supplementary Tables

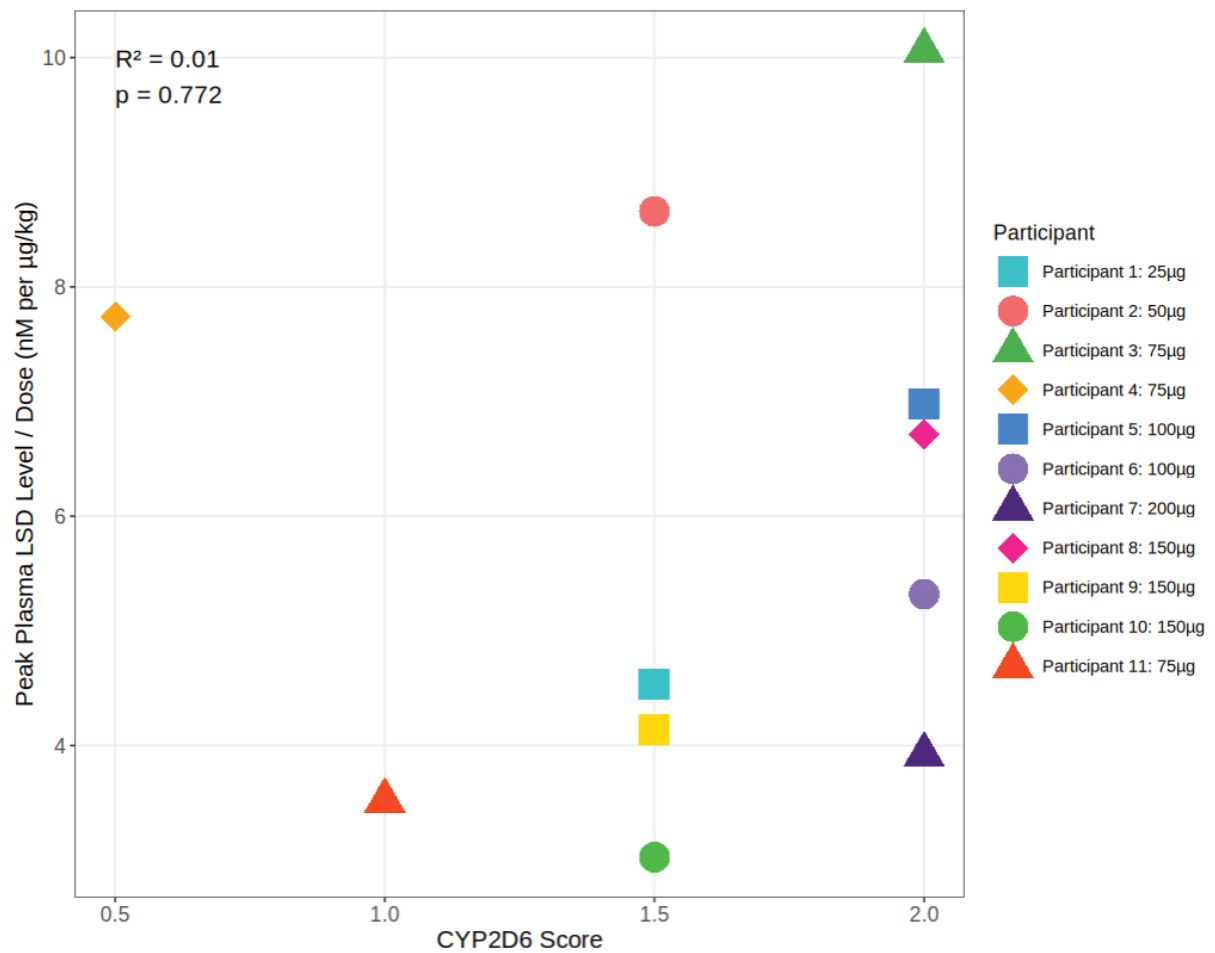
- S1. Participant characteristics and PET scan parameters across study phases
- S2. Regional cerebral blood flow, internal carotid artery diameter, and flow measures
- S3. Global correlation (GCOR) regional effects
- S4. Thalamo-cortical correlation (TCOR) regional effects
- S5. Functional MRI results and effect sizes
- S6. AAL3 regions combined to create regions of interest

Adverse effects

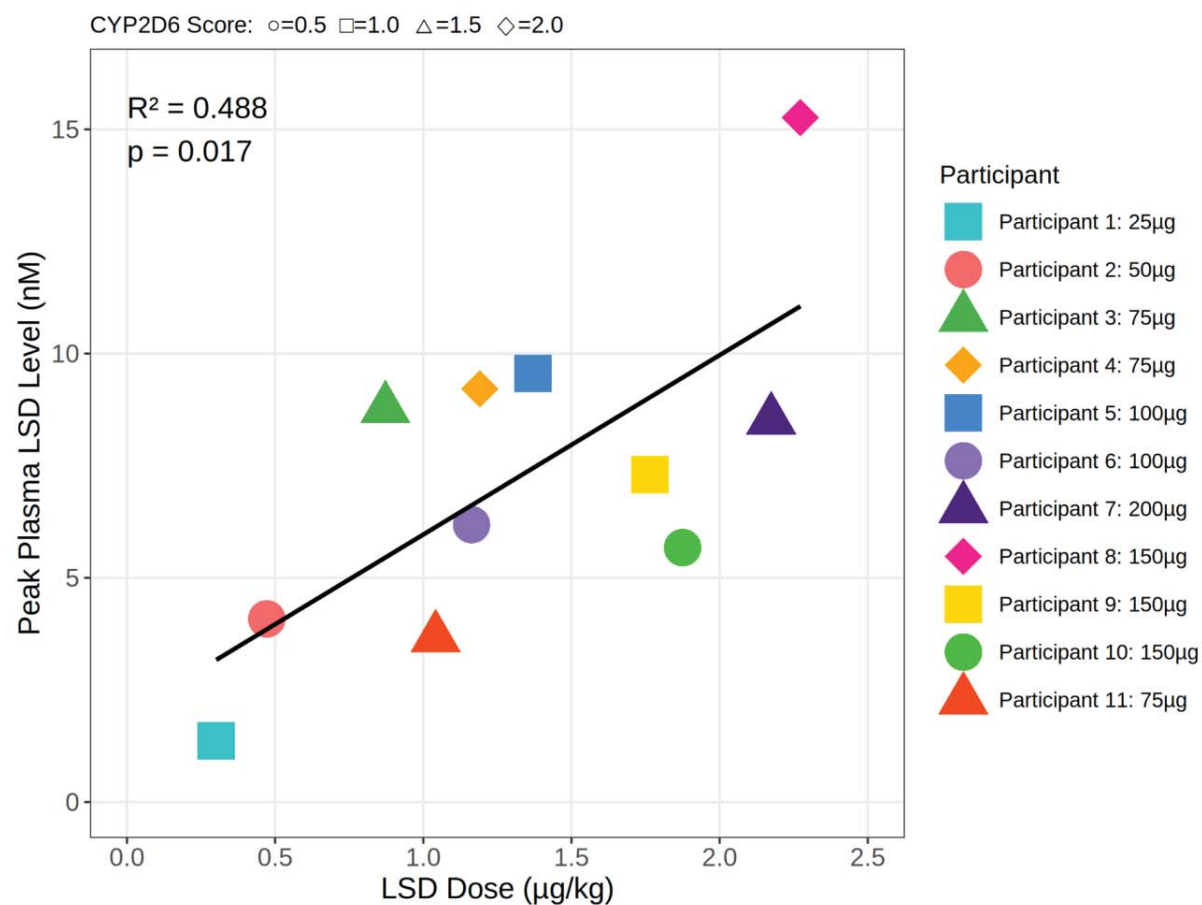
Three participants experienced transient adverse events. One participant reported mild nausea, dizziness, and moderate anxiety with ego dissolution, which resolved concurrently with the acute drug effects. Another participant experienced severe emesis and nausea that resolved with drug clearance, followed by temporary difficulty with distance visual accommodation that spontaneously resolved within 72 hours. A third participant reported acute anxiety associated with the scanner environment that dissipated upon exiting the scanner, and mild sleep disturbances lasting approximately one week post-administration, with spontaneous resolution. No serious adverse events occurred, and no medical intervention was required for any participant.

LSD effects on emotional response to music

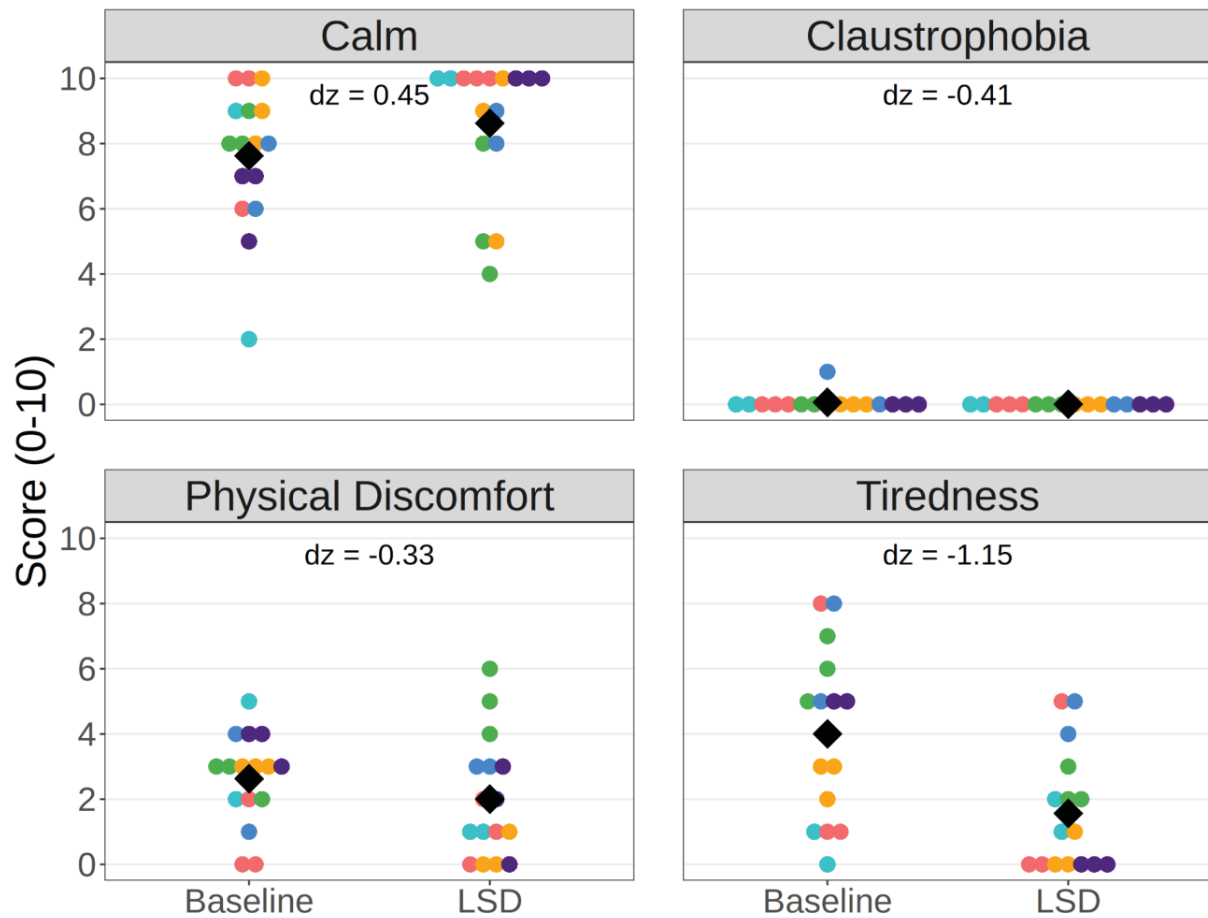
LSD enhanced emotional responses to music during the scan compared to the baseline scan (Supplementary Figure S14). The most pronounced effect was observed in the item 'Transcendence', showing a large increase ($d_z = 1.63$) under LSD compared to baseline. Moderate increases were also observed in Strength ($d_z = 0.89$) and Joy ($d_z = 0.71$). Smaller but notable effects were seen in Wonder ($d_z = 0.55$), Tension ($d_z = 0.47$), and Tenderness ($d_z = 0.46$). Sadness showed a modest increase ($d_z = 0.40$), whereas Nostalgia and Peacefulness demonstrated the smallest effects (both $d_z = 0.26$).



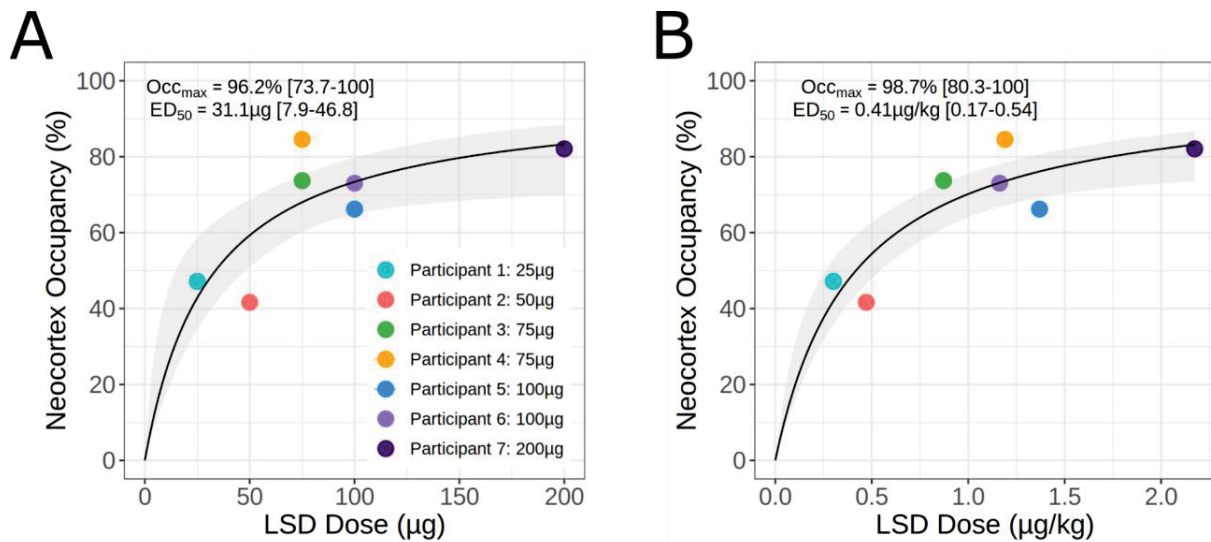
Supplementary Figure S1 | Relation between CYP2D6 metabolizer status and LSD plasma levels. Peak plasma LSD concentrations normalised by body weight-adjusted dose (nM per µg/kg) plotted against CYP2D6 metabolizer scores for all participants (n=11). Each point represents an individual participant, with different shapes and colors identifying unique participants. *CYP2D6* scores range from 0.5 (poor metabolizer) to 2.0 (normal metabolizer).



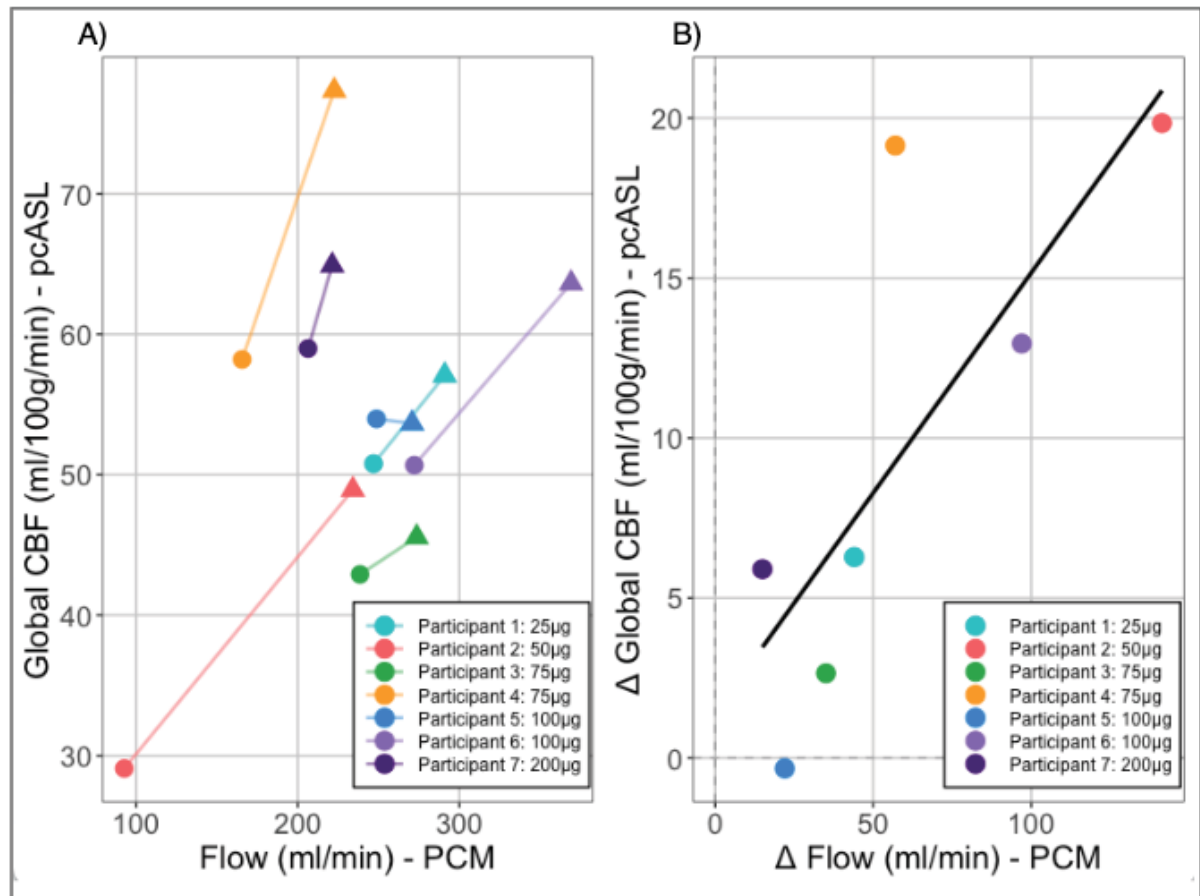
Supplementary Figure S2 | Relation between weight-adjusted LSD dose and peak plasma concentrations. Peak plasma LSD concentrations plotted against body weight-adjusted dose (µg/kg) across study participants (n=11). Individual CYP2D6 metaboliser scores are indicated by marker shapes (circle=0.5, square=1.0, triangle=1.5, diamond=2.0), reflecting varying metabolic capacity. The black line shows the linear regression ($R^2=0.49$, $p=0.017$), demonstrating a significant positive correlation between administered dose and peak plasma levels. Peak weight-adjusted plasma LSD levels showed little correlation with CYP2D6 metabolizer status ($R^2 = 0.01$, $P = 0.78$).



Supplementary Figure S3 | In-scanner comfort ratings during scans. Self-reports during baseline and LSD conditions ($n=6$). Effect sizes (Cohen's dz) show reduced Tiredness ($dz = 1.3$) with minimal changes in Calm, Claustrophobia, and Physical Discomfort ratings. Each color represents a unique participant receiving doses ranging from 25-200 μg of LSD. Ratings were collected immediately following each scanning sequence during peak drug effects, approximately 2-3 hours post-administration.

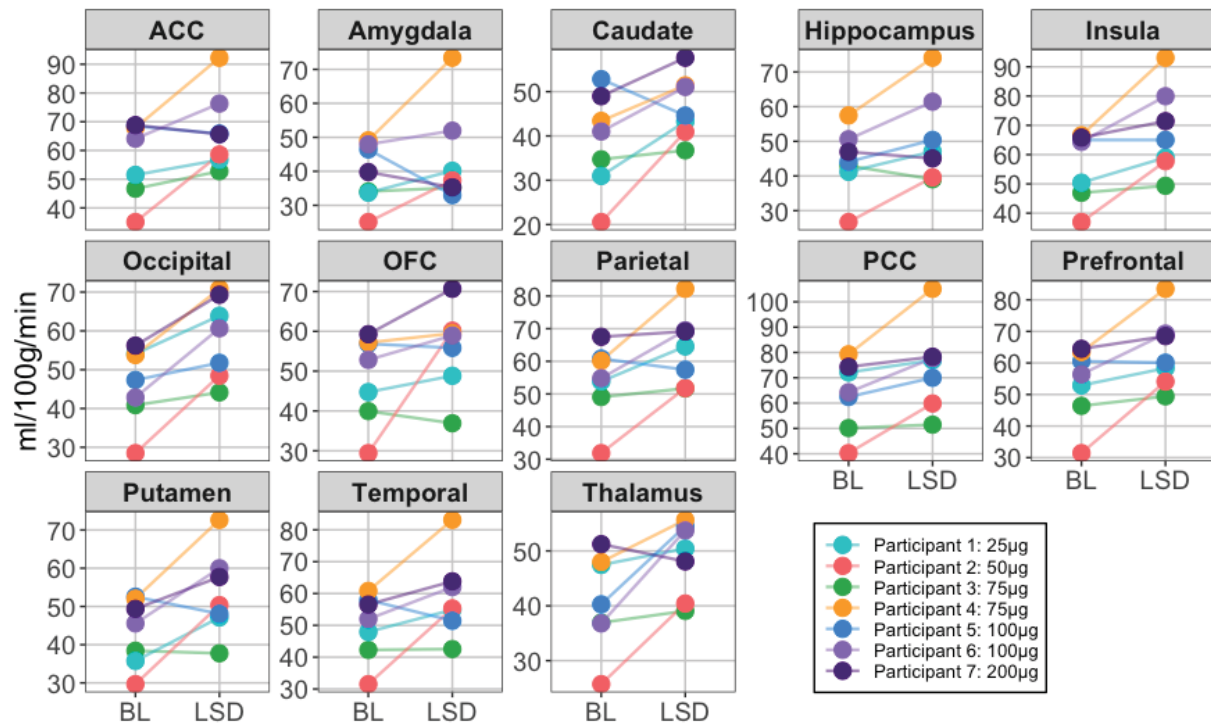


Supplementary Figure S4 | Dose-occupancy relation for LSD. A: LSD dose (μg) versus receptor occupancy fitted with Hill-Langmuir model. The solid black line shows the model fit, and bootstrap-derived 95% confidence intervals are shown in grey shading. Model estimates from the original fit with bootstrap confidence intervals indicate maximum occupancy of 96.2% [73.5-100%] and ED₅₀ of 31.1 μg [7.6-46.4 μg]. **B:** Body weight-adjusted LSD dose (μg/kg) versus receptor occupancy fitted with Hill-Langmuir model. The solid black line shows the model fit with bootstrap-derived 95% confidence intervals in grey shading. Model estimates indicate maximum occupancy of 98.7% [80.3-100%] and ED₅₀ of 0.41 μg/kg [0.17-0.54 μg/kg]. The improved coefficient of determination ($R^2 = 0.75$ versus $R^2 = 0.58$ for unadjusted dose) suggests that body weight adjustment better predicts receptor occupancy.

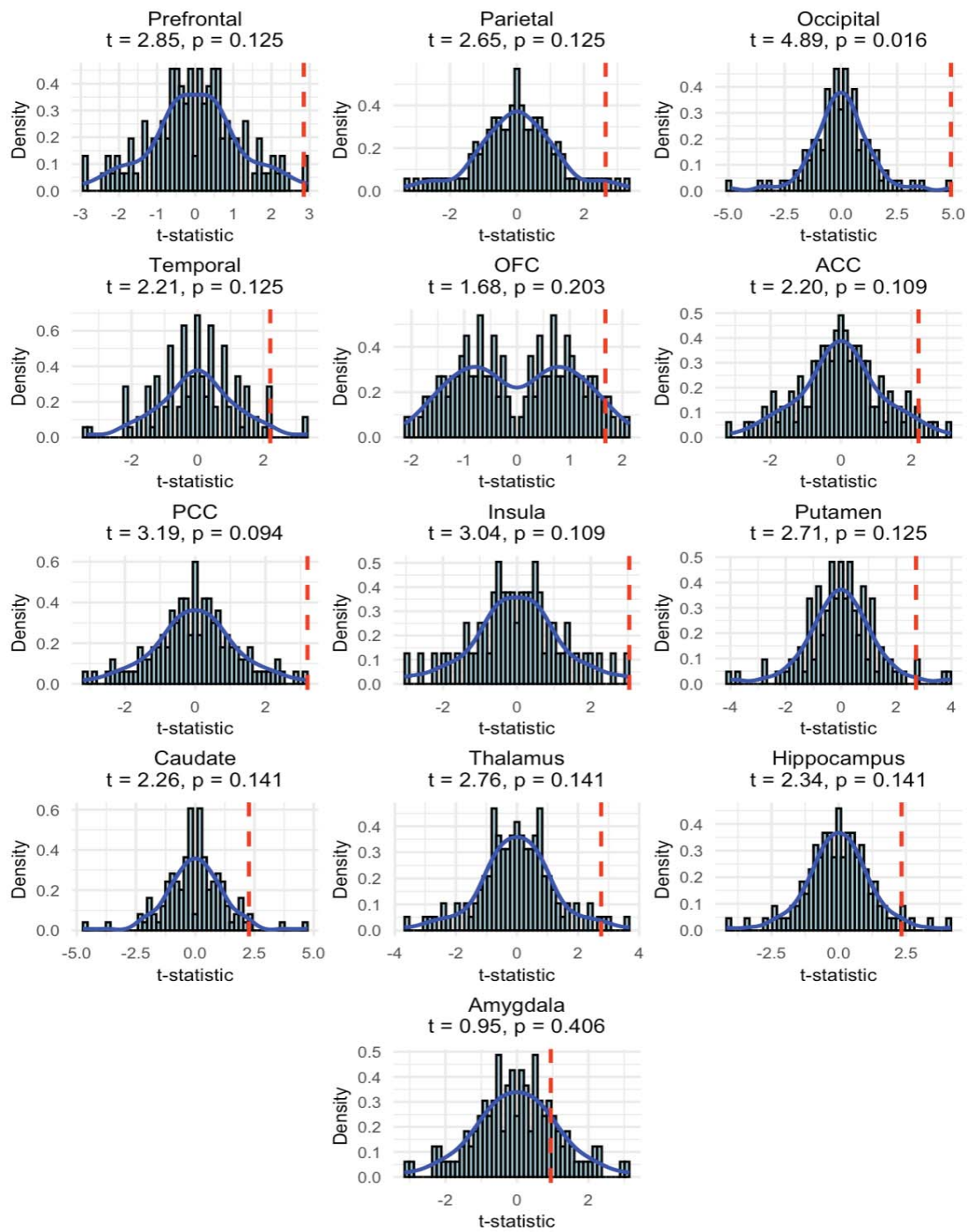


Supplementary Figure S5 | LSD-induced change in cerebral blood flow and internal carotid artery flow. A) Global cerebral blood flow (CBF) measured using pseudo-continuous Arterial Spin Labeling (pCASL) plotted against internal carotid artery flow measured with Phase Contrast Mapping (PCM), with circles representing baseline measurements and triangles representing post-LSD administration for seven participants at varying doses (25-200μg). B) Relation between LSD-induced changes (Δ) in global CBF and changes in internal carotid artery flow, showing a significant positive correlation ($r = 0.786$, $p = 0.036$).

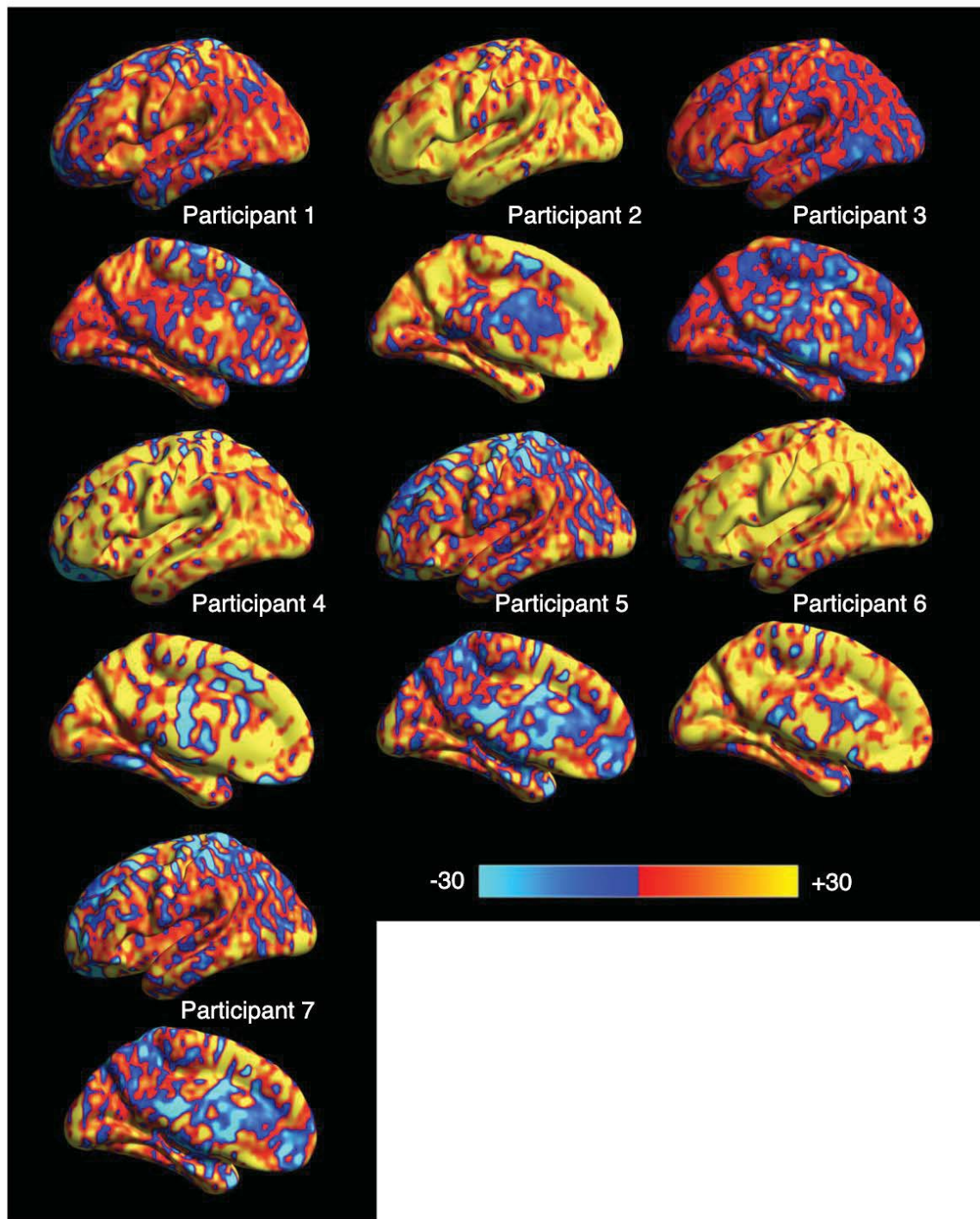
Regional ASL effects



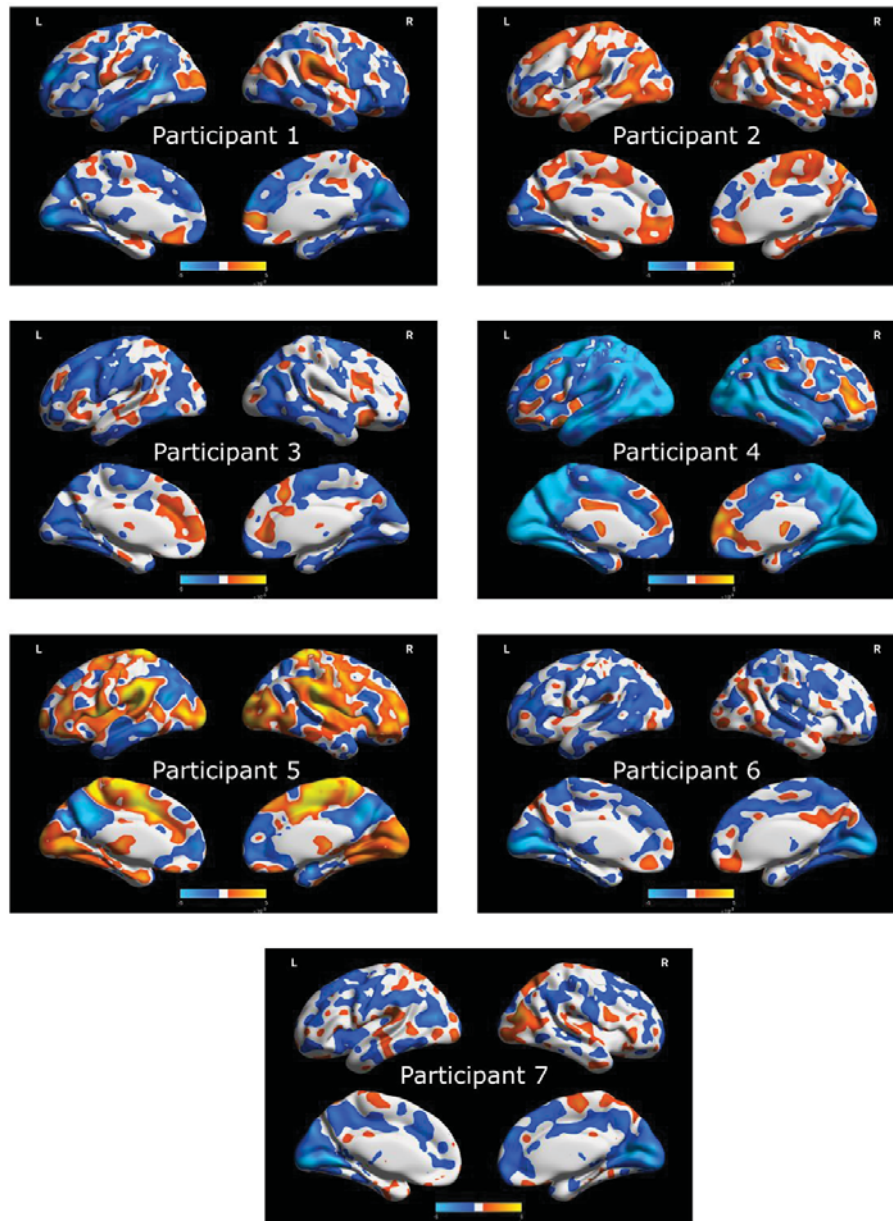
Supplementary Figure S6 | Regional cerebral blood flow (CBF) measurements at baseline (BL) and after LSD administration across 13 brain regions. Each colored line represents a different participant who received varying doses of LSD (25-200µg), with measurements shown in ml/100g/min. Brain regions analysed include the anterior cingulate cortex (ACC), amygdala, caudate, hippocampus, insula, occipital cortex, orbitofrontal cortex (OFC), parietal cortex, posterior cingulate cortex (PCC), prefrontal cortex, putamen, temporal cortex, and thalamus.



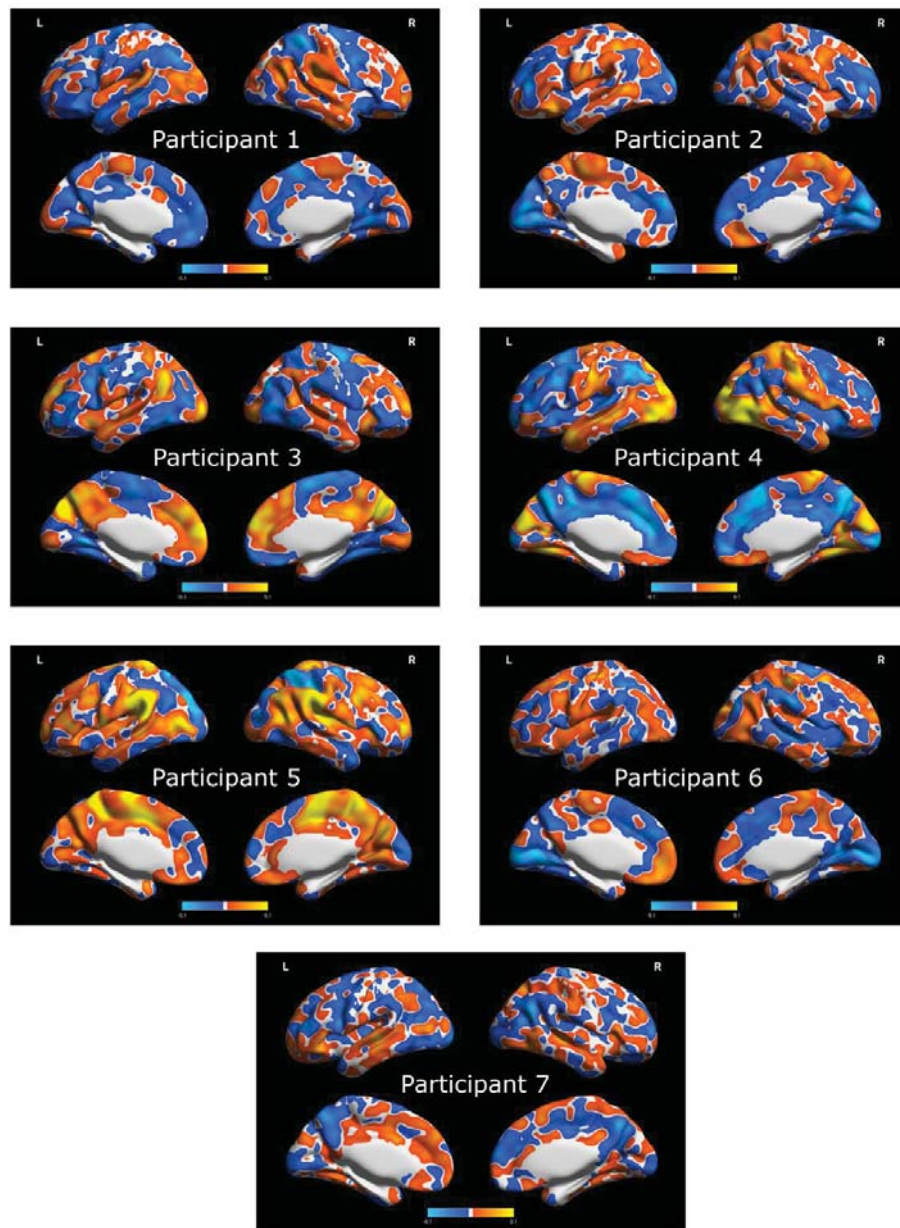
Supplementary Figure S7 | Distribution of t-statistics for the LSD effect on cerebral blood flow across 13 brain regions. Each subplot shows the null distribution of t-statistics generated from permutation testing, represented by histograms (light blue bars) with overlaid density curves (blue lines). The observed t-statistic for each region is indicated by a vertical red dashed line. The test statistics (t-value) and stepdown-adjusted p-values are shown above each plot. The Occipital region shows the strongest effect ($t = 4.89$, $p = 0.016$), whereas the Amygdala shows the weakest effect ($t = 0.95$, $p = 0.406$).



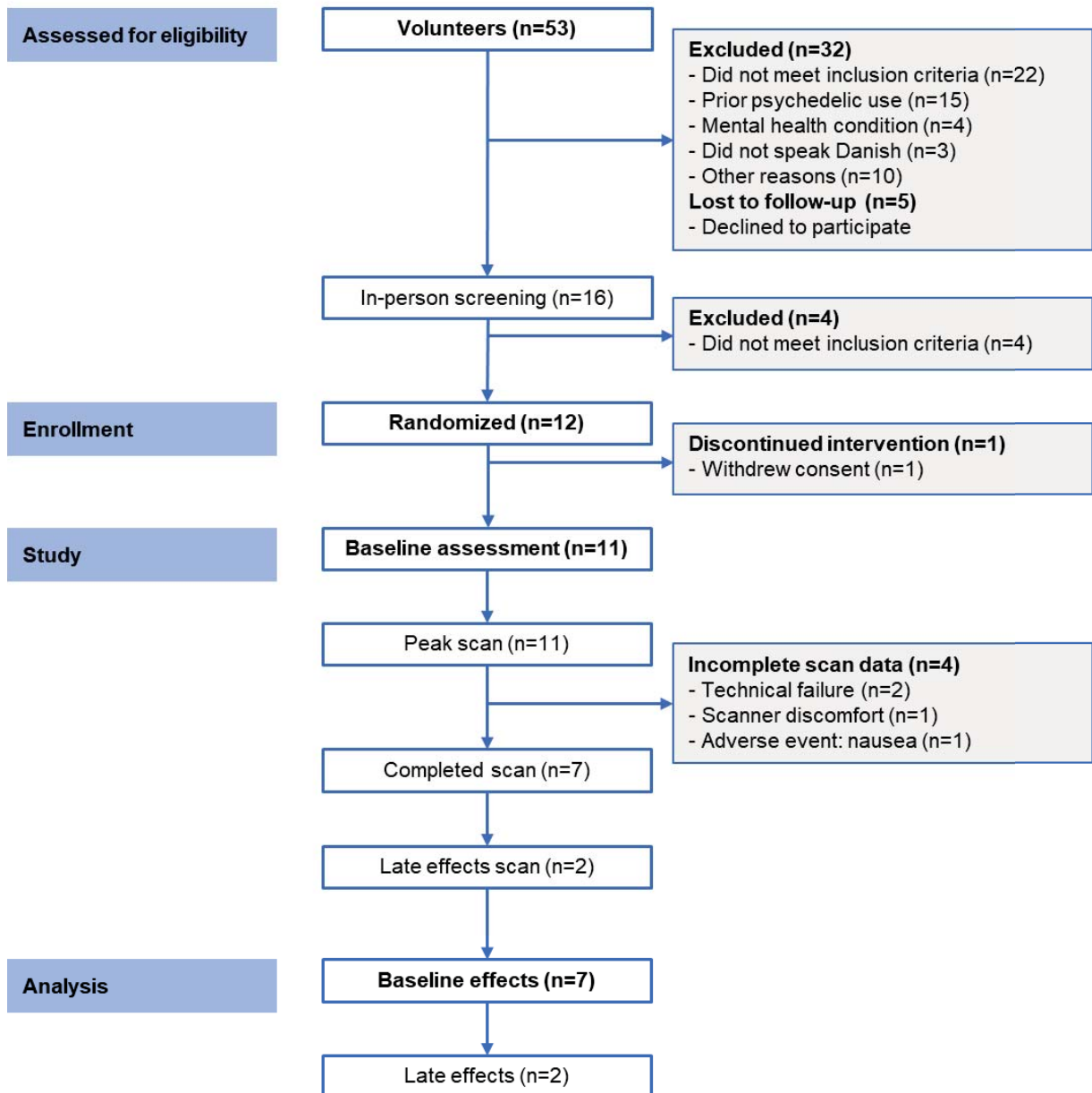
Supplementary Figure S8 | Individual changes in cerebral blood flow following LSD administration. Changes in cerebral blood flow (CBF) for each participant following LSD administration compared to baseline, shown on inflated cortical surfaces. The color scale indicates CBF changes from -30 to +30 ml/100g/min, with red-yellow showing increases and blue showing decreases. Made using BrainNetViewer.



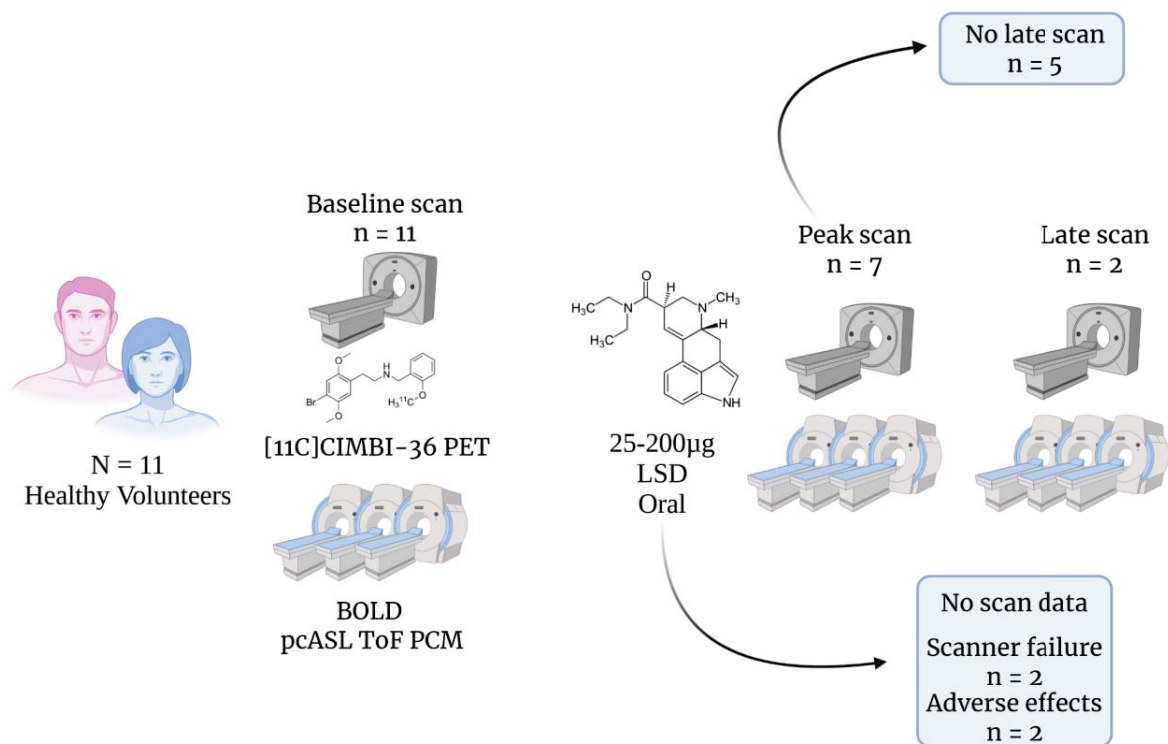
Supplementary Figure S9 | Individual changes in global brain connectivity following LSD administration. Brain surface renderings showing changes in global functional connectivity for each of the seven participants included in the final analysis. Each panel displays lateral and medial views of both hemispheres (L: left, R: right) with changes in connectivity represented on inflated cortical surfaces. Orange-yellow colours indicate increases in global connectivity, whereas blue colours indicate decreases relative to baseline. Colour intensity corresponds to the magnitude of connectivity change, thresholded at an absolute delta correlation coefficient (R) of $5e-4$. All maps were generated using BrainNetViewer. Consistent patterns of decreased connectivity (blue) can be observed across visual and attention networks in most subjects, aligning with the group-level findings reported in the main text.



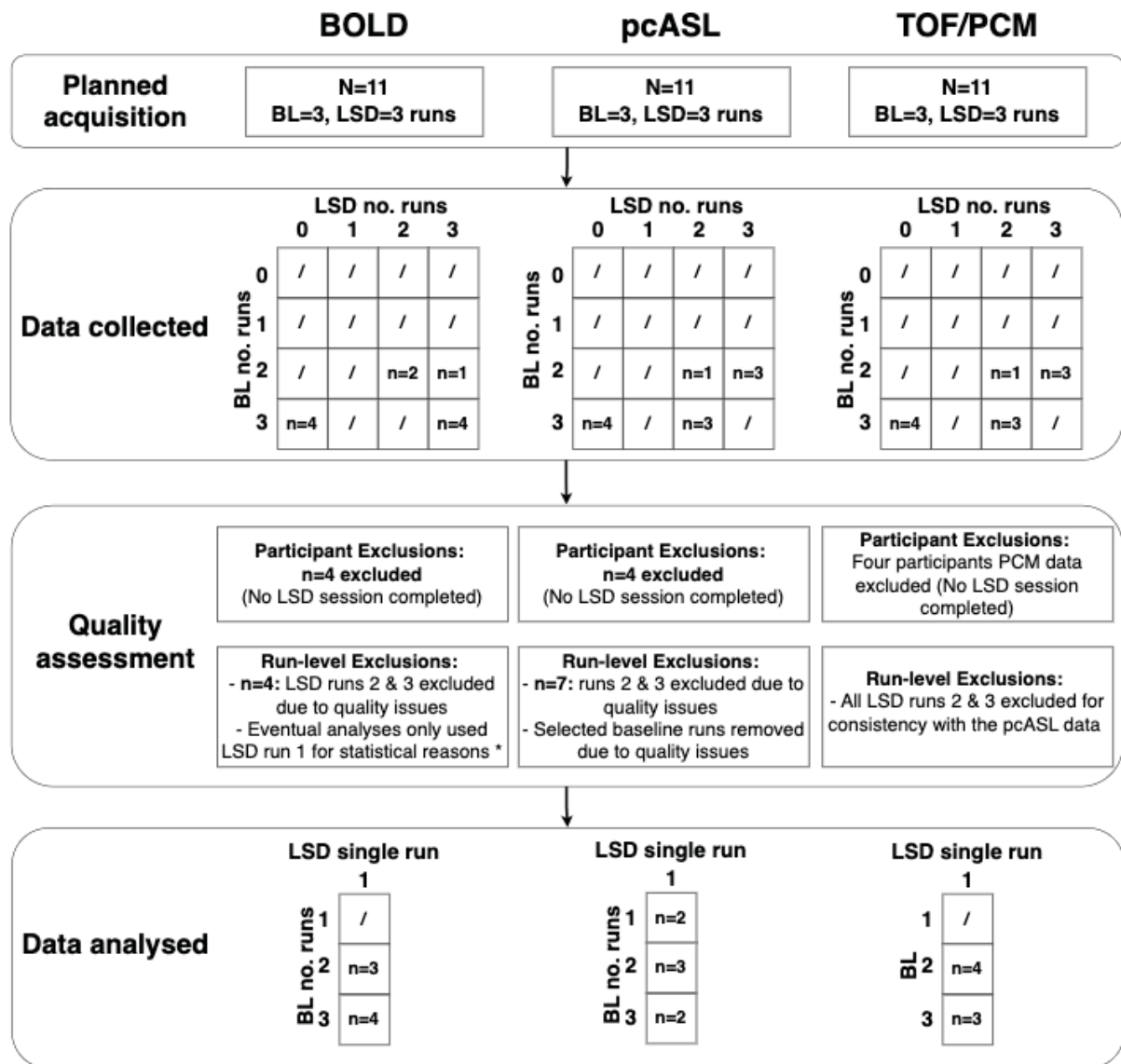
Supplementary Figure S10 | Individual changes in thalamo-cortical connectivity following LSD administration. Brain surface renderings showing changes in functional connectivity between the thalamus and cortex for each of the seven participants included in the final analysis. Each panel displays lateral and medial views of both hemispheres (L: left, R: right) with changes in connectivity represented on inflated cortical surfaces. Orange-yellow colours indicate increased thalamo-cortical connectivity while blue colours indicate decreased connectivity relative to baseline. Colour intensity corresponds to the magnitude of connectivity change, thresholded at an absolute delta correlation coefficient (R) of $5e-3$. All maps were generated using BrainNetViewer.



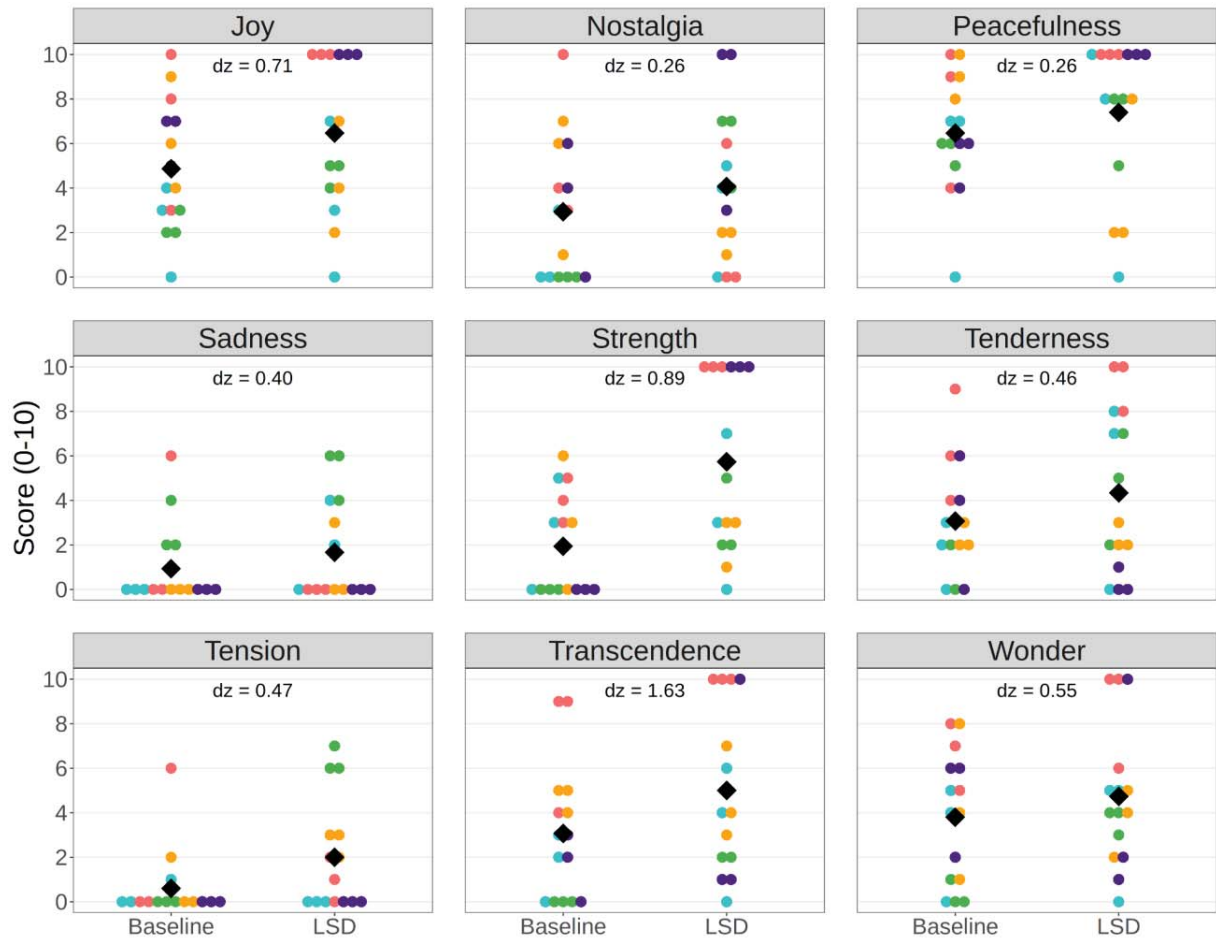
Supplementary Figure S11 | CONSORT flow diagram showing participant recruitment and retention through the study.



Supplementary Figure S12 | Schematic illustration of the study design and participant progression through different scanning phases. All participants (n=11) underwent a baseline scan including [¹¹C]CIMBI-36 PET imaging and multimodal MRI (multi-band multi-echo BOLD, pseudo-continuous arterial spin labeling, time-of-flight angiography, and phase contrast mapping). Following LSD administration (25-200µg oral), participants completed peak scans (n=7), and two of them also completed late scans. Four participants did not complete LSD scans due to scanner failure (n=2) or adverse effects (n=2). Of the seven completing peak scans, two completed late scans.



Supplementary Figure S13 | Quality control pipeline across imaging modalities. The figure illustrates the quality control and data processing pipeline across the MRI modalities: BOLD, pcASL, and TOF/PCM. The planned acquisition for all modalities included BL=3 (Baseline) and LSD=3 runs. The "Data collected" matrices show the distribution of participants according to the number of baseline runs (y-axis, 0-3) and LSD runs (x-axis, 0-3) that were successfully collected. Forward slashes (/) indicate that no participants had that particular combination of runs. The "Data analysed" panel shows the final distribution of included runs for each modality.



Supplementary Figure S14 | Music-evoked emotional responses to LSD measured by Geneva Emotional Music Scale (GEMS). Music-evoked emotions that were measured within-scan using the GEMS at baseline and after LSD administration. The figure shows nine emotional dimensions: Joy, Nostalgia, Peacefulness, Sadness, Strength, Tenderness, Tension, Transcendence, and Wonder. Scores range from 0-10 on each dimension. Individual participant responses are shown as colored dots, while black diamonds represent group means. Effect sizes between conditions are indicated by Cohen's d (dz) values for each emotional dimension.

Measure	Baseline	Peak Scan	Late Scan
n	11	7	2
Age	31 ± 9[23-55]	29 ± 6[23-41]	28*
Sex (M/F)	9 M / 2 F	6 M / 1 F	1 M / 1 F
Weight (kg)	81 ± 12[63-106]	84 ± 14[63-106]	68*
Height (cm)	184 ± 9[167-195]	184 ± 8[170-192]	175*
Injected dose (MBq)	361 ± 117[147-501]	334 ± 81[207-427]	417, 436
Injected mass (µg)	0.21 ± 0.16[0.033-0.63]	0.20 ± 0.11 [0.02-0.31]	0.31, 0.38
Previous psychedelic uses	18 ± 43[0-146]	8 ± 9[0-20]	0, 1

Supplementary Table S1 | Participant characteristics and PET scan parameters across study phases. Demographics, physical characteristics, and study parameters for participants in baseline (n=11), peak LSD (n=7), and late LSD (n=2) scanning sessions. Data are presented as mean ± standard deviation with [minimum-maximum] ranges. Measures include age (years), sex distribution (Male/Female), weight (kg), height (cm), radiotracer parameters (injected dose in MBq and mass in µg), and number of previous psychedelic uses. * Only means are presented in Late Scan column to avoid reporting single-subject demographic information.

MEASURE	Baseline			LSD			Change		Statistics			
	$\mu \pm \sigma$	M	range	$\mu \pm \sigma$	M	range	Δ	$\Delta\%$	t-stat	p-value	p-stepdown	cohen's dz
gCBF	49.2 ± 10.4	50.8	29.1 - 59.0	58.7 ± 10.9	57.1	45.6 - 77.4	6.3	19.3	3.16	0.020	NA	1.20
Prefrontal	53.7 ± 11.7	56.4	31.4 - 64.5	63.3 ± 11.4	60.1	49.4 - 83.5	3.7	18.0	2.85	0.029	0.125	1.08
Parietal	54.0 ± 11.4	54.8	31.9 - 67.5	63.8 ± 11.0	64.6	51.7 - 82.2	9.8	18.0	2.65	0.038	0.125	1.00
Temporal	49.9 ± 10.3	52.0	31.5 - 60.8	59.0 ± 12.7	55.3	42.5 - 83.1	3.4	18.4	2.21	0.069	0.125	0.84
Occipital	46.2 ± 9.8	47.3	28.5 - 56.2	58.4 ± 10.5	60.7	44.1 - 70.8	13.3	26.4	4.89	0.003	0.016	1.85
OFC	48.6 ± 11.0	52.8	29.4 - 59.3	55.8 ± 10.6	59.0	36.9 - 70.7	6.1	14.9	1.68	0.144	0.203	0.63
ACC	57.5 ± 13.3	64.1	35.1 - 68.8	66.9 ± 13.6	65.7	52.8 - 92.3	1.6	16.3	2.20	0.070	0.109	0.83
PCC	63.3 ± 13.9	64.3	40.3 - 79.3	74.2 ± 17.0	76.9	51.5 - 105.1	12.7	17.3	3.19	0.019	0.094	1.21
Insula	56.6 ± 11.8	64.4	37.0 - 66.6	67.9 ± 14.9	65.0	49.3 - 93.1	0.6	20.1	3.04	0.023	0.109	1.15
Hippocampus	44.3 ± 9.5	44.1	26.7 - 57.5	51.0 ± 12.7	47.1	39.0 - 74.1	3.0	15.1	2.34	0.058	0.141	0.88
Amygdala	39.5 ± 9.0	39.8	25.1 - 49.1	43.8 ± 14.5	37.3	33.0 - 73.4	-2.4	10.9	0.95	0.380	0.406	0.36
Thalamus	40.9 ± 8.8	40.3	25.7 - 51.2	48.8 ± 6.7	50.4	39.1 - 55.7	10.2	19.4	2.76	0.033	0.141	1.04
Caudate	38.9 ± 11.1	41.0	20.6 - 52.8	46.5 ± 7.2	44.6	36.7 - 57.7	3.6	19.5	2.26	0.064	0.141	0.86
Putamen	43.3 ± 8.9	45.6	29.7 - 52.5	53.4 ± 11.2	50.3	37.7 - 72.6	4.8	23.2	2.71	0.035	0.125	1.03
ICA Diameter (mm)	4.5 ± 0.4	4.4	3.9 - 5.1	4.3 ± 0.6	4.4	3.3 - 5.0	0.0	-3.5	1.00	0.356	NA	-0.38
ICA Flow (ml/min)	210.1 ± 62.3	238.5	92.6 - 272.1	268.9 ± 51.9	270.7	221.3 - 369.1	32.2	28.0	-3.43	0.014	NA	1.30

Supplementary Table S2 | Regional cerebral blood flow (ml/100g/min), internal carotid artery (ICA) diameter (mm), and blood flow (ml/min) measures at baseline and after LSD administration. Values are presented as means (μ) with standard deviations (σ), medians (M), and ranges [.,], along with numerical (Δ) and percentage ($\Delta\%$) changes, t-statistics, p-values (uncorrected and step-down corrected), and effect sizes (Cohen's dz).

Additional supplementary tables

The following supplementary Tables are available as Excel workbooks.

Supplementary Table S3 | Global correlation (GCOR) changes following LSD administration.

Regional changes in global functional connectivity organized by brain region and network. The table includes baseline and LSD condition means, absolute and percentage changes, effect sizes (Cohen's d_z), and statistical results for each brain region analyzed. Values are reported for both hemispheres where applicable, with regions sorted by network membership according to the Schaefer 200-parcel atlas.

Supplementary Table S4 | Thalamo-cortical correlation (TCOR) changes following LSD

administration. Detailed results showing changes in functional connectivity between the thalamus and cortical regions. For each cortical region, the table presents baseline and LSD condition means, changes in connectivity strength, effect sizes (Cohen's d_z), and corresponding statistical tests. Results are organized by anatomical location and network membership to facilitate interpretation of the spatial patterns of connectivity changes.

Supplementary Table S5 | Functional MRI results. Detailed results from analyses of network-level functional connectivity measures, including static and dynamic network connectivity, sample entropy at multiple scales, normalized spatial complexity, and global brain organization metrics (modularity, small-worldness, etc.). For each metric, the table presents mean values at baseline and under LSD conditions, absolute and percentage changes, effect sizes (Cohen's d_z), and both uncorrected and corrected p-values.

Supplementary Table S6 | AAL3 regions of interest. Description of how we combined regions from the Automated Anatomical Labeling 3 (AAL3) atlas into 13 broader anatomical regions of interest (ROIs). Each row represents one of these ROIs, with the corresponding AAL3 subregions that were combined to create it. All regions include both left and right hemispheric components.